MOLECULAR DYNAMIC CALCULATIONS OF THE EFFECT OF POLARITY ON THE PROPERTIES OF LIQUIDS CONSISTING OF SMALL LINEAR MOLECULES

by

Keith F. Carter

A thesis submitted in part fulfilment of the requirements for the degree of Doctor of Philosophy in the Faculty of Science of the University of London.

Department of Chemistry,
Royal Holloway College,
Egham Hill,
Egham,
Surrey TW20 OEX.

1983.

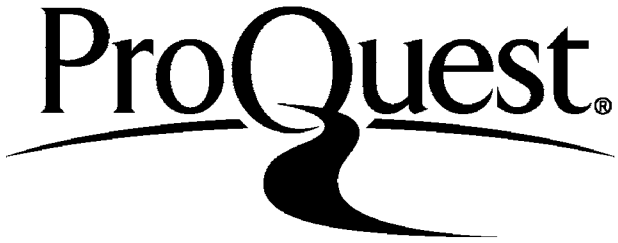

ACKNOWLEDGEMENTS.

I am deeply grateful to Professor K. Singer for the help and guidance he has given me. I should like to thank the other members of the research group for their invaluable assistance with numerous technical problems, in particular Murthy, Eveline Adams and Alan Taylor. My thanks also goes to Mrs. K. Hales for kindly typing the manuscript.

Finally I should like to thank my mother and Aunt Dooly, my family and friends for their continued support and encouragement, and my father for his guidance, inspiration and example.

Abstract.

The effects of quadrupolar interactions on the thermodynamics, statics and dynamics of linear molecules consisting of two Lennard-Jones centres is studied for the liquid phase. This is illustrated by using nitrogen, chlorine and carbon dioxide molecules as representative of the differing bond lengths that can arise in these systems. The changes due to the magnitude of the quadrupole moment are investigated for the chlorine system. Calculations of the structure of two-Lennard-Jones centre fluids is also carried out using the RISM method.

CONTENTS.

continued...

CHAPTER I.

Introduction.

The study of liquid systems by computer simulation is a relatively new technique. The Monte Carlo method was first devised by Metropolis et al(1) as a method of sampling the configurational phase space of the partition function. The molecular dynamics method suggested by Alder and Wainwright(2) sampled the entire phase space of the system by calculating the dynamical trajectories of an ensemble of particles interacting with a given classical Hamiltonian. This technique allows both the static and dynamic properties of the ensemble to be calculated and is used in the present work. A review of computer simulation techniques applied to simple single particle fluids is given by McDonald and Singer(3).

The molecular dynamics study of fluids of linear molecules with Lennard-Jones interactions has been previously undertaken in depth by Singer, Taylor and Singer(4,5,6), for their thermodynamic, static and dynamic properties. While the interaction potential used by Singer et al. should reasonably accurately account for the repulsive and dispersive forces between molecules, no account is taken of the multipolar forces also known to be present in the interactions of these molecules, the most significant of which being their quadrupole moments.

The specific aim of the present work is to examine the effects of additional multipolar interactions on ensembles of these linear molecules using the molecular dynamics technique. Three particular systems were chosen for investigation: nitrogen, chlorine and carbon dioxide, representing small, medium and large elongation molecules respectively. The quadrupole moments of nitrogen and carbon dioxide are well known, but for chlorine no satisfactory single value could be found. This enabled the study of the effects of variation in magnitude of the quadrupole moment to be undertaken with the chlorine system, by choosing three widely differing values of the quadrupole moment. In this way

the present work studies the effects of quadrupolar interactions throughout the range of possible elongations, and studies the effect of quadrupole moment magnitude for a system of moderate elongation.

In Chapter II, the details of the interaction potential are discussed and the molecular dynamics technique explained. The thermodynamic results of the molecular dynamics calculation are presented in Chapter III together with a discussion of the applicability of the principle of corresponding states to quadrupolar fluids illustrated by the use of thermodynamic perturbation theory applied to a simplified model of these fluids. The static properties calculated from the molecular dynamics simulation are given in Chapter IV, with particular reference to their angular properties.

A comparison of the static results of Singer et al. to those calculated by integral equation methods, in particular the RISM method developed by Chandler and Anderson(7) is undertaken in Chapter V. Unfortunately no adequate way of representing multipolar interactions in these calculations could be found, thus the angular dependence of the pair correlation function is investigated for hard-core and Lennard-Jones interacting fluids only.

The dynamical results of the molecular dynamics calculation are presented in Chapter VI, showing the variation of the auto-correlation functions with changes in the system parameters. These results are further analysed in Chapter VII using the memory function formalism to parametarize the decay constants of the correlation functions. A comparison of the memory function formalism and random frequency modulation theory is also made.

A review of the general trends found in the present work is given in Chapter VIII, illustrating the effects of quadrupolar interactions on ensembles of linear molecules in the liquid phase.

REFERENCES FOR CHAPTER I.

1. Metropolis, Rosenbluth, Rosenbluth, Teller and Teller, J.Chem.Phys., 1953, 21, 1087.
2. B.J. Alder and T.W. Wainwright, J.Chem.Phys., 1959, 31, 459.
3. I.R. McDonald and K. Singer, Quart.Rev.Chem.Soc., 1970, 24, 238.
4. K. Singer, A. Taylor and J.V.L. Singer, Mol.Phys., 1977, 33, 1757.
5. K. Singer, J.V.L. Singer and A. Taylor, Mol.Phys., 1979, 37, 1239.
6. E. Detyna, K. Singer, J.V.L. Singer and A.J. Taylor, Mol.Phys., 1980, 41, 31.
7. D. Chandler and H.C. Andersen, J.Chem.Phys., 1972, 57, 1918, Ibid, 1972, 57, 1930.

CHAPTER II.

Part 1 - The Pair Potential.

The Pair Potential used for molecular dynamics calculations chosen to be a basic two-centre Lennard-Jones potential, has already been investigated by Barojas, Levesque and Quentrec(1), Cheung and Powles(2) for nitrogen systems and by Singer et al.(3) for fluorine, chlorine, bromine and carbon dioxide systems. To study the effects of polarity in these systems, a dipole or quadrupole interaction was added to this basic potential.

Lennard-Jones Part.

The basic Lennard-Jones potential sites were chosen

$$\phi_{LJ}(r) = 4\varepsilon\{(\frac{\sigma}{r})^{12} - (\frac{\sigma}{r})^{6}\} \qquad \text{(II-1)}$$

to coincide with the nuclei of the molecule. This may be expressed

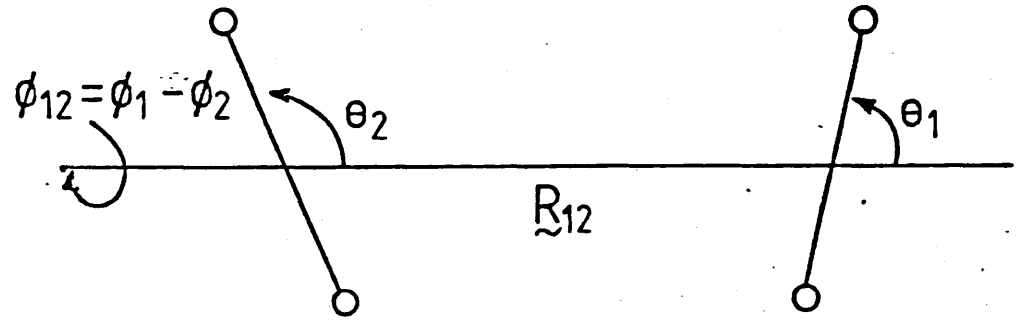

FIGURE (II-1)

as an intermolecular potential

$$\phi_{ij}(R) = \sum_{m=1}^{2}\sum_{n=1}^{2} \phi_{LJ}(\underset{\sim}{R}_{ij} + (-1)^m.\underset{\sim}{s}_i + (-1)^n.\underset{\sim}{s}_j) \qquad \text{(II-2)}$$

where $\underset{\sim}{R}_{ij} = \underset{\sim}{R}_i - \underset{\sim}{R}_j$, $R = |\underset{\sim}{R}|$ and $L = 2|\underset{\sim}{s}|$. $\underset{\sim}{R}_i$ is the coordinate of the centre of mass of the i^{th} molecule and $\underset{\sim}{s}_i$ is its bond orientation vector, where L is the bond length of the molecule. Taking the binomial expansion of this potential, and neglecting terms beyond $(L/R)^4$ gives for the repulsive R^{12} part

$$\phi_{ij}^{rep}(R) = 16\varepsilon\{(\frac{\sigma}{R})^{12}[1 + RT1 + RT2 + RT3]\} \qquad \text{(II-3)}$$

where

$$RT1 = 3(\frac{L}{R})^2(7Cos^2\theta_1 + 7Cos^2\theta_2 - 1)$$

$$RT2 = \frac{21}{8}(\frac{L}{R})^4[1 - 16Cos^2\theta_1 - 16Cos^2\theta_2 + 288Cos^2\theta_1Cos^2\theta_2$$

$$+ 2(Cos\theta_1Cos\theta_2 + Sin\theta_1Sin\theta_2Cos\phi_{12})^2$$

$$- 64Cos\theta_1Cos\theta_2(Cos\theta_1Cos\theta_2 + Sin\theta_1Sin\theta_2Cos\phi_{12})]$$

$$RT3 = \frac{21}{8}(\frac{L}{R})^4(1 - 16Cos^2\theta_1 - 16Cos^2\theta_2 + 48Cos^4\theta_1 + 48Cos^4\theta_2)$$

using the coordinate system shown in Figure (II-1). This expansion has been previously shown by Kohin(4) up to the RT2 term, and extended to the RT3 term by Goodings and Henkelman(5) who tested the convergence of the angular expansion for the α-nitrogen lattice and found that it was within 2% of the value calculated directly. Note - the expansion will be convergent only in the region of space where R>L. The angular expansion of the attractive R^6 term gives

$$\phi_{ij}^{Att}(R) = -16\epsilon\{(\frac{\sigma}{R})^6 |1 + AT1 + AT2 + AT3|\} \qquad (II-4)$$

where

$$AT1 = \frac{3}{2}(\frac{L}{R})^2 (4Cos^2\theta_1 + 4Cos^2\theta_2 - 1)$$

$$AT2 = \frac{3}{4}(\frac{L}{R})^4 [1-10Cos^2\theta_1 - 10Cos^2\theta_2 + 120Cos^2\theta_1 Cos^2\theta_2$$

$$+ 2(Cos\theta_1 Cos\theta_2 + Sin\theta_1 Sin\theta_2 Cos\phi_{12})^2$$

$$- 40Cos\theta_1 Cos\theta_2 (Cos\theta_1 Cos\theta_2 + Sin\theta_1 Sin\theta_2 Cos\phi_{12})]$$

$$AT3 = \frac{3}{4}(\frac{L}{R})^4 (1-10Cos^2\theta_1 - 10Cos^2\theta_2 + 20Cos^4\theta_1 + 20Cos^4\theta_2)$$

This can be compared with the attractive dispersion potential of DeBoer(6), where the angular expansion is in terms of the anisotropy factor of the polarizability. Although the Lennard-Jones attractive potential makes no use of any information about the polarizability of the molecule, the angular expansions bear close similarity. The convergence of this angular expansion was tested, term by term, for a liquid chlorine configuration using the chlorine (LJ+HQ) potential parameter given in Table (II-2). The results of the convergence test are given in Table (II-1). The spherical harmonics of the basic 2-centre Lennard-Jones potential and the angular expansion are shown in Figures (II-2) and (II-3) respectively, for this system. This shows that the potential is well reproduced by the expansion for large R (i.e. $R \geq 3L$). However, as R approaches L the convergence becomes progressively worse, causing the repulsive interactions to be poorly represented, this having a significant effect on the position and depth of the potential minimum.

While the siting of the repulsive centres at the nuclei seems to

	T1	T2	T3	T4	T5	T6
P1	4.95	-0.33584	.78508E+05	.48384E-38	.38852E-18	-
P2	3.73	-1.00009	-.27355E+05	.46141E-39	-.27310E-20	200,220,221,222, 400
P3	4.24	-0.70221	-.23769E+05	.57758E-39	.13831E-18	220,221,222,400
P4	4.50	-0.53559	-.17335E+05	.12416E-38	.10982E-18	400
P5	4.596	-0.4871	-.99681E+04	.13842E-38	.21204E-18	-

N.B. All results include quadrupolar contributions.

P1 Normal 2-Centre Lennard-Jones potential

P2 Angular expansion - RT1=RT2=RT3=0.0, AT1=AT2=AT3=0.0

P3 Angular expansion - RT2=RT3=0.0, AT2=AT3=0.0

P4 Angular expansion - RT3=0.0, AT3=0.0

P5 Full angular expansion

T1 Position of minimum of the 000 spherical harmonic of the potential ($\mathring{A}$)

T2 Depth of minimum ($U/4\epsilon$)

T3 Internal Energy (U) (J/M)

T4 Mean Squared Torque (J^2)

T5 Mean Squared Force (N^2)

T6 Spherical Harmonics neglected in angular expansion (only terms up to 400 considered)

TABLE (II-1).

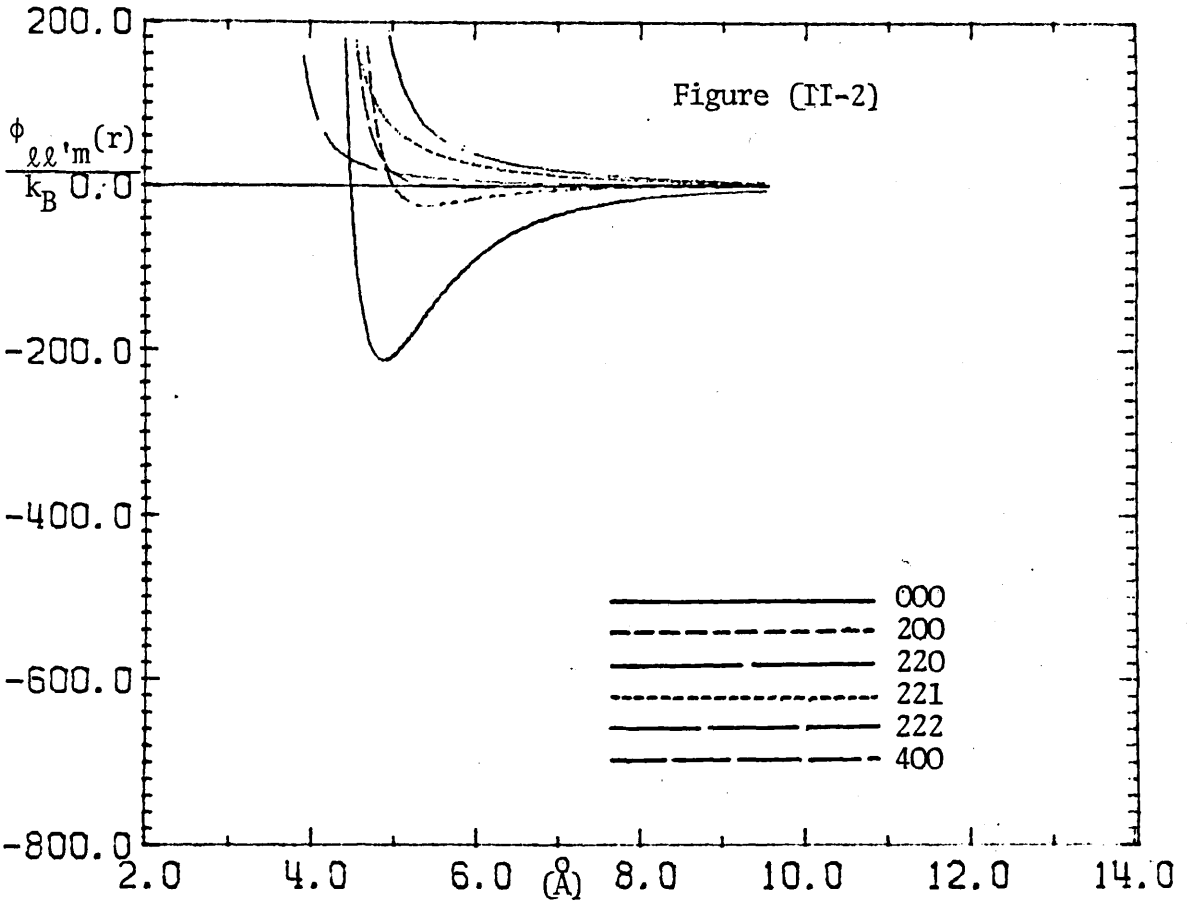

Figure (II-2)

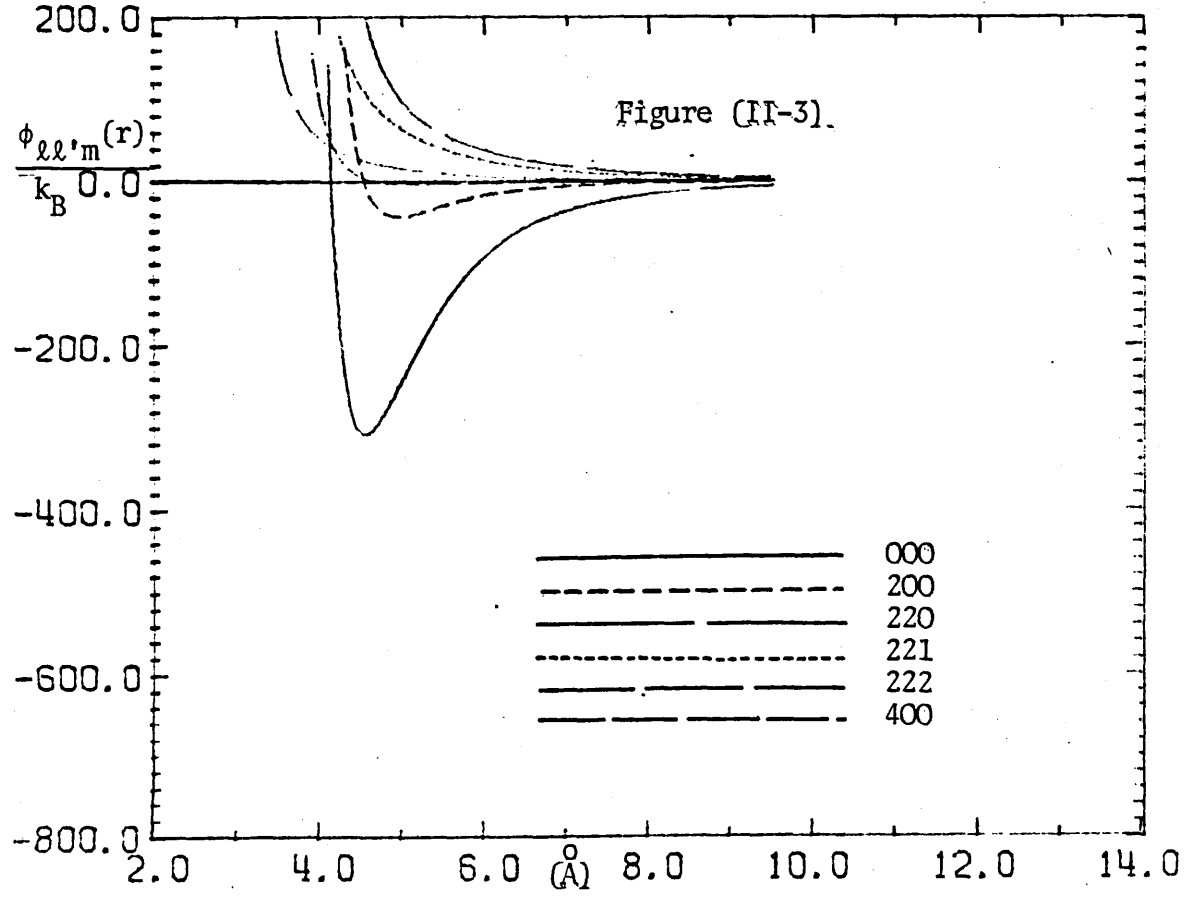

Figure (II-3)

be a reasonable assumption in terms of the electron density distributions, the siting of the dispersive centres in the same positions seems arbitrary, since information on the apparent centres of polarizability within the molecule is not available. It may be that while the 2-centre Lennard-Jones potential adequately represents the repulsive potential, the dispersive potential is not so well described in terms of intermolecular interactions.

The effective 'angle averaged' 2-centre Lennard-Jones potential, which corresponds to the (000) harmonic in the spherical harmonic expansion of the angular expansion of the potential is

$$\frac{1}{16\pi^2}\iint \left[\phi_{ij}^{rep}(R) + \phi_{ij}^{Att}(R)\right] d\omega_i d\omega_j = \bar{\phi}_{ij}^{(1)}(R)$$

$$= 16\varepsilon \left\{\left(\frac{\sigma}{R}\right)^{12}\left[1 + 11\left(\frac{L}{R}\right)^2 + 66.733\left(\frac{L}{R}\right)^4\right]\right.$$

$$\left. - \left(\frac{\sigma}{R}\right)^{6}\left[1 + 2.5\left(\frac{L}{R}\right)^2 + 4.666\left(\frac{L}{R}\right)^4\right]\right\} \qquad \text{(II-5)}$$

This shows the basic dependence of the potential on the bond length L. Further expanding of the potential in the dilute gas ensemble in terms of powers 1/kT, to find the effective temperature-dependence as shown by Hirschfelder(7). The effective potential is

$$\bar{\phi}_{ij}^{(2)}(R) = \bar{\phi}_{ij}^{(1)}(R) - \frac{256\varepsilon^2}{kT}\left\{\left(\frac{\sigma}{R}\right)^{24}\left[78.4\left(\frac{L}{R}\right)^4 + 1642.6\left(\frac{L}{R}\right)^6 + 12017.3122\left(\frac{L}{R}\right)^8\right]\right.$$

$$- 2\left(\frac{\sigma}{R}\right)^{18}\left[22.4\left(\frac{L}{R}\right)^4 + 301.3\left(\frac{L}{R}\right)^6 + 1092.317\left(\frac{L}{R}\right)^8\right]$$

$$\left. + \left(\frac{\sigma}{R}\right)^{12}\left[6.4\left(\frac{L}{R}\right)^4 + 38.0956\left(\frac{L}{R}\right)^6 + 103.414\left(\frac{L}{R}\right)^8\right]\right\} \qquad \text{(II-6)}$$

The temperature dependent part is completely a function of L, containing no isotropic part unlike the simple angle averaged potential.

This expansion is only valid at large R such that the difference between the maximum and minimum values of the potential is very much less than kT. However, the expansion is useful for consideration of the thermodynamic properties of the system using effective potential methods, within the framework of thermodynamic perturbation theory.

Multipolar Part.

The dipole or quadrupole was represented by point charges, sited at the diatomic nuclei for dipoles, with quadrupoles having an additional site at the centre of mass of the molecule, such that

$$\mu = \sum_i q_i z_i \qquad \text{(II-7)}$$

$$Q = \sum_i q_i z_i^2 \qquad \text{(II-8)}$$

and

$$\sum_i q_i = 0$$

where μ is the dipole moment, Q-the quadrupole moment, q_i is the i^{th} charge situate at a distance z_i from the origin, of a linear molecule, defined as in Stogryn and Stogryn(8). The charges interact by Coulomb Law

$$\phi^c_{mn}(r) = \frac{Z_m Z_n}{4\pi\varepsilon_0 r_{mn}} \qquad \text{(II-9)}$$

The binomial angular expansion of this potential gives the point dipole and quadrupole interactions which are given by

$$\phi_{\mu\mu}(R) = \frac{\mu^2}{R^3}\left(\mathrm{Sin}\theta_1\mathrm{Sin}\theta_2\mathrm{Cos}\phi_{12} - 2\mathrm{Cos}\theta_1\mathrm{Cos}\theta_2\right) \qquad \text{(II-10)}$$

$$\phi_{QQ}(R) = \frac{3Q^2}{4R^5}\,(1 - 5\mathrm{Cos}^2\theta_1 - 5\mathrm{Cos}^2\theta_2 + 17\mathrm{Cos}^2\theta_1\mathrm{Cos}^2\theta_2$$

$$+ 2\mathrm{Sin}^2\theta_1\mathrm{Sin}^2\theta_2\mathrm{Cos}^2\phi_{12} - 16\mathrm{Sin}\theta_1\mathrm{Sin}\theta_2\mathrm{Cos}\theta_1\mathrm{Cos}\theta_2\mathrm{Cos}\phi_{12}) \qquad \text{(II-11)}$$

using the coordinate system of Figure (II-1). Comparison between the discrete charge models of dipoles and quadrupoles and the idealized point dipole and quadrupole interactions, has been made by Streett and Gubbins(9); by studying the energies of particular configurations for the case $L^* = (L/\sigma) = 0.5471$, $Q^* = (Q/(\varepsilon\sigma^5)^{\frac{1}{2}}) = 2$ and $L^* = 0.5471$ and $\mu^* = 2 = (\mu/(\varepsilon\sigma^3)^{\frac{1}{2}})$ where ε and σ are the site-site Lennard-Jones parameters. The agreement for the quadrupolar potential is good, whereas for dipoles it is only fair. The factors involved in the convergence of the point-multipolar interactions are charge density, size of multipole moment and bond length.

For dipolar fluids the direct summation method has been tested for convergence of the forces and energy with a system of 256 nitrogen molecules, in a liquid configuration. Comparison of the contribution from successive radial shells to the forces and energy was used to test convergence. The contribution at large distances ($R \geq 10\text{Å}$) should be small. The error between summation over all 256 molecules in the cube, and a cut-off sphere of radius half side of the cube was found to be approximately 8.5% in the coulombic forces, as compared with 0.05% in the Lennard-Jones forces and approximately 5% in the coulombic energy as compared to 1% in the Lennard-Jones energy. The percentage error in the energy and forces is independent of the magnitude of the dipole moment or ε, although the absolute error is a function of their magnitude. The energy and forces also fluctuate which depends on the configuration of the molecules taken.

Thus, if the criterion for satisfactory convergence is that the absolute error in the total forces must be less than approximately 1%;

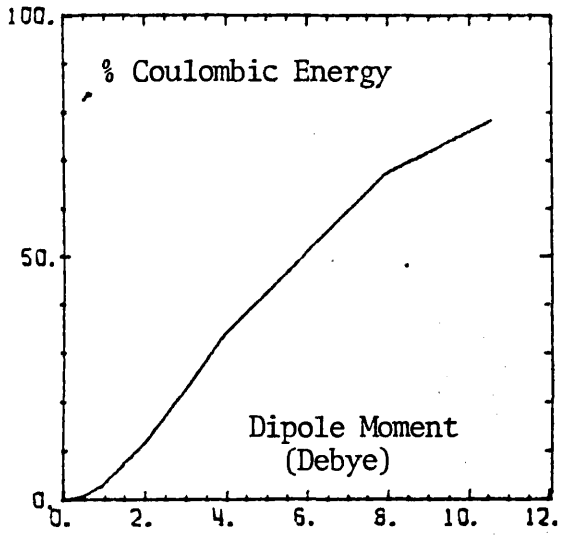

Figure (II-4)

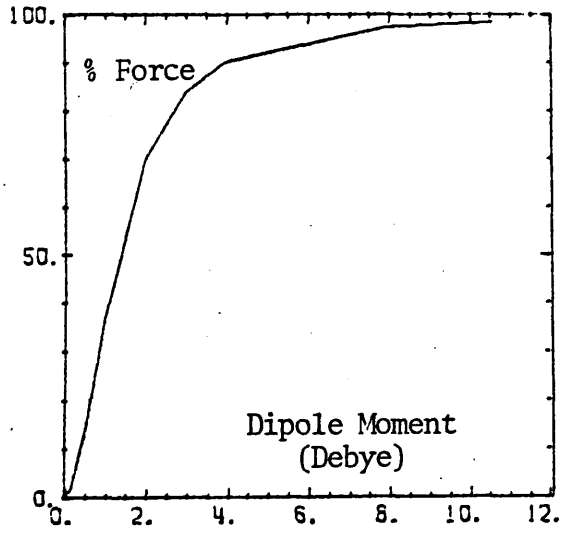

Figure (II-5)

then the coulombic force must be less than 15% of the total force. Similar restrictions apply for the coulombic energy. The percentage coulombic energy and force variation with increasing dipole moment is shown in Figures (II-4) and (II-5) respectively. It can be seen that the direct summation of the discrete charge model requires the dipole moment to be restricted to approximately 0.5 Debye, for satisfactory convergence of the total forces. Overall the convergence behaves as R^{-3} for dipoles and R^{-5} for quadrupoles, which is at least an order of magnitude better. This can be seen from the spherical harmonic expansion of the point-dipole and quadrupole potentials where the only non-zero terms are

$$\phi^{\mu\mu}_{(110)}(R) = \frac{-2\mu^2}{R^3} \quad : \quad \phi^{\mu\mu}_{(111)}(R) = \frac{2\mu^2}{R^3} \qquad \text{(II-12)}$$

$$\phi^{QQ}_{(220)}(R) = \frac{6Q^2}{5R^5} \quad : \quad \phi^{QQ}_{(221)}(R) = \frac{-8Q^2}{5R^5}$$

$$\phi^{QQ}_{(222)}(R) = \frac{2Q^2}{5R^5} \qquad \text{(II-13)}$$

The spherical harmonics of the quadrupolar interaction decay almost as fast as the basic Lennard-Jones attractive term. The convergence is thus good, particularly as the (220), (221) and (222) harmonics of the orientational radial distribution function decay to zero within approximately 10Å. Thus the spherical harmonic expansion for the internal energy, mean square torques and forces are converged in the same range.

A two dimensional molecular dynamics simulation of the effects of coulombic versus multipolar intermolecular potential for a fluid was also carried out by Occelli, Quantrec and Brot(10).

Potential Parameters.

The potential parameters chosen for the basic 2-centre Lennard-Jones system were those of Quantrec(1) for nitrogen, Jelinek, Slutsky and Karo(11) for chlorine and Singer et al.(3) for carbon dioxide. To this a dipole or quadrupole was added. In the case of dipoles, the error in the discrete charge summation was limited by using a dipole moment of 0.5 Debye. For the quadrupole moment, the values given in Stogryn and Stogryn(8) were used for nitrogen and carbon dioxide, where the recommended value had been determined from a variety of methods which gave consistent results. For chlorine the value given by Stogryn and Stogryn based only on a quantum mechanical calculation differed markedly from an experimental determination by Jao et al.(12). Both these values were used, as well as a third value taken to be the mean of the other two. This enables the effects of increasing quadrupole moment to be studied.

The full list of potential parameters is given in Table (II-2).

TABLE (II-2)

System	L (Å)	ε/k (K)	σ (Å)	L/σ	μ (Debye)	Q (10^{-26}esu cm^2)
N_2(LJ)	1.0975	43.95	3.341	0.3285	-	-
N_2(LJ+Q)	1.0975	41.75	3.341	0.3285	-	-1.52[A]
Cl_2(LJ)	2.02	205.5	3.32	0.608	-	-
Cl_2(LJ+D)	2.02	205.5	3.32	0.608	0.5	-
Cl_2(LJ+LQ)	2.02	198.72	3.32	0.608	-	+2.46[B]
Cl_2(LJ+MQ)	2.02	190.13	3.331	0.6064	-	+4.30
Cl_2(LJ+HQ)	2.02	157.54	3.341	0.6046	-	+6.14[A]
CO_2(LJ)	2.37	163.6	2.989	0.793	-	-
CO_2(LJ+Q)	2.37	135.09	2.992	0.792	-	-4.3[A]

A - from Stogryn and Stogryn(8)

B - from Jao et al.(12)

For dipoles, the change in the thermodynamic quantities of the system was small and thus no compensating adjustment of the Lennard-Jones parameters ε and σ was required. However in all but one quadrupolar case, it was found that ε and σ needed to be reduced to compensate for the increased cohesiveness of the quadrupolar potential. This was accomplished by fitting ε to a known point on the phase diagram of energy E, (calculated using the 2-centre Lennard-Jones potential without quadrupolar interactions) and adjusting the molar volume (effective adjustment of σ) to obtain the correct pressure. The adjusted potentials were then examined in terms of lattice energies and second virial coefficients.

Lattice Energies.

The lattice energies were calculated for α-nitrogen and carbon dioxide solids, on the basis of a cubic (T_A^6-Pa3) structure given by Schnepp and Jacobi(13). The summation over whole numbers of unit cells was carried out to (29,29,29) in terms of the lattice indices. This is sufficient to ensure convergence for the discrete charge model. The results are given in Table (II-3).

TABLE (II-3).

α-nitrogen	Lattice Parameter a_o (Å)	Lattice Energy (Kcal/mole)
Expt.†	4.00	1.925
LJ only	3.965	2.17
(LJ+Q) PQ	3.924	2.43
(LJ+Q) DC	3.926	2.41
Carbon dioxide.		
Expt.‡	3.925	6.83
LJ only	3.997	5.54
(LJ+Q) PQ	3.881	7.57
(LJ+Q) DC	3.906	6.97

† Reference (14)
‡ Reference (15)
PQ - Evaluated using point quadrupole potential
DC - Evaluated using discrete charge model.

For nitrogen the agreement with the experimental values is reasonable for the Lennard-Jones potential only, however the addition of the quadrupole moment makes the agreement worse. In this case the two quadrupole potentials give almost the same result. For carbon dioxide the reverse is true. The Lennard-Jones potential only gives a poor

lattice energy, which on inclusion of the quadrupolar term increases considerably to give better agreement. These results suggest that the quadrupole moment is too large in this case. However it might be that further improvement could be made by including higher multipolar terms and polarizability in the potential. There is also a marked difference in the results of the two quadrupolar potentials for carbon dioxide. This is possible due to the divergence of the point quadrupole potential at small distances, which is dependent on the magnitude of the bond length.

Second Virial Coefficients.

The second virial coefficients were calculated from

$$B(T) = \frac{-2\pi N_A}{2V_m} \int_0^{\infty} \int_0^{2\pi} \int_0^{\pi} \int_0^{\pi} f(R,\theta_1,\theta_2,\phi_{12}) \sin\theta_1 \sin\theta_2 d\theta_1 d\theta_2 d\phi_{12} \qquad \text{(II-14)}$$

where

$$f(R,\theta_1,\theta_2,\phi_{12}) = -1 + \exp[-(R,\theta_1,\theta_2,\phi_{12})/kT] \qquad \text{(II-15)}$$

The evaluation of these angular integrals has been discussed by Thompson et al.(16). It was decided to use 20-point Gauss-Legendre quadrature for each of the angular integrals, to ensure equal weighting. The integral in R was evaluated by taking 6 ranges of 20-point Gauss-Legendre integration, arranged such that the interval became shortest at the region of maximum change in the function. The range 0.0→2.0Å was evaluated analytically as the function is -1.0 throughout. Thus the error in the calculated second virial coefficient was not more than ±1.0, when the number of integration ranges was reduced.

The second virial coefficients for nitrogen, chlorine and carbon dioxide are given in Tables (II-4), (II-5) and (II-6) respectively.

TABLE (II-4).

Nitrogen.

T/K	75	110	200	300	400	500	
	274±5	132±2	35.2±1	4.2±0.5	-9.0±0.5	-16.9±0.5	Expt (17)
	281	135	37.5	5.7	-8.9	-16.7	LJ only(2) (Cheung and Powles)
$\frac{-B(T)}{cm^3 mol^{-1}}$	249	123	31.9	2.1	-11.4	-18.6	(LJ+Q) (18) (Cheung and Powles)
	258	129	35.5	4.4	-9.6	-17.3	(LJ+Q) (19) (MacRury et al.)
	371	184	56.9	16.4	-1.7	-11.6	LJ only
	358	174	52.2	13.4	-3.8	-13.3	(LJ+Q)

TABLE (II-5).

Chlorine.

T/K	175	200	250	300	400	500	600	
	1126	810.1	497.0	344.9	198.1	127.3	85.9	LJ only
$\frac{-B(T)}{cm^3 mol^{-1}}$	1031	750.3	465.5	324.5	186.6	119.5	80.0	(LJ+LQ)
	1049	755.6	462.7	319.9	181.8	115.2	76.2	(LJ+MQ)
	1112	760.2	436.5	289.8	155.5	93.5	58.0	(LJ+HQ)

TABLE (II-6).

Carbon Dioxide.

T/K	210	260	300	400	500	600	
	300	166.8	121.5	60.2	30.0	12.4	Expt. (20) and (21)
$\frac{-B(T)}{cm^3 mol^{-1}}$	275	179.9	135.1	72.4	39.9	20.2	LJ only
	284	159.2	115.9	57.2	27.7	10.1	(LJ+Q)

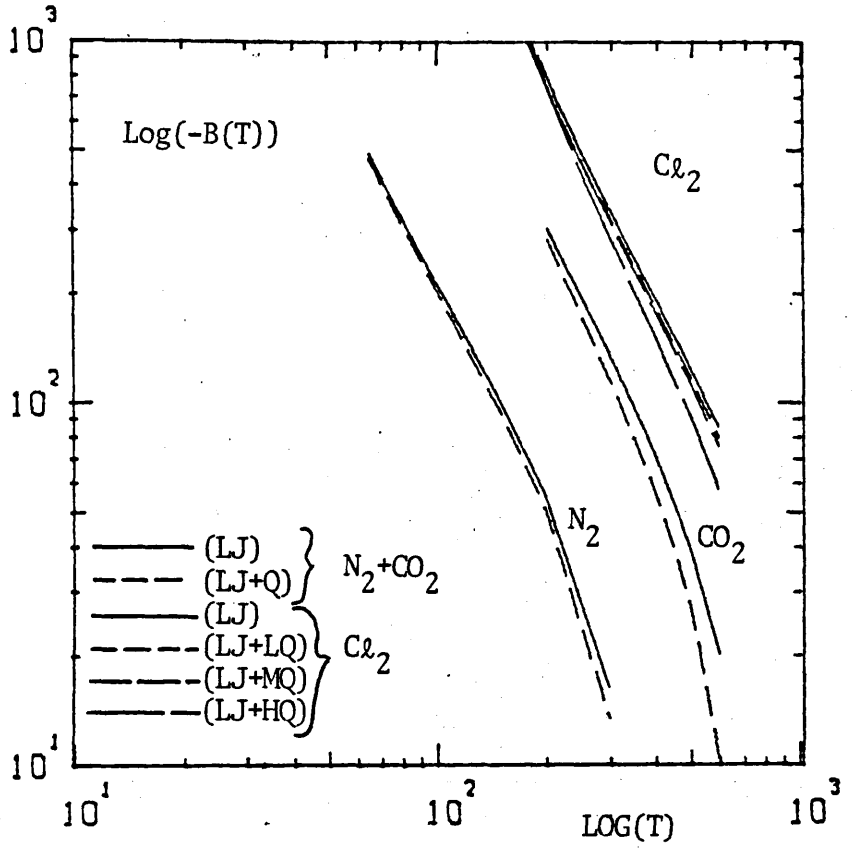

Figure (II-6)

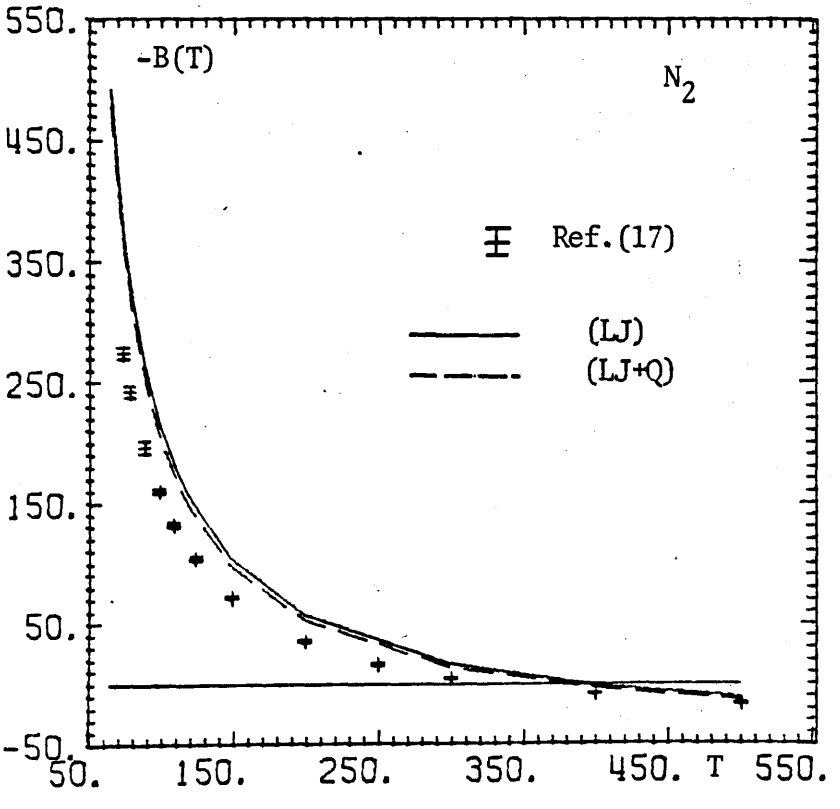

Figure (II-7)

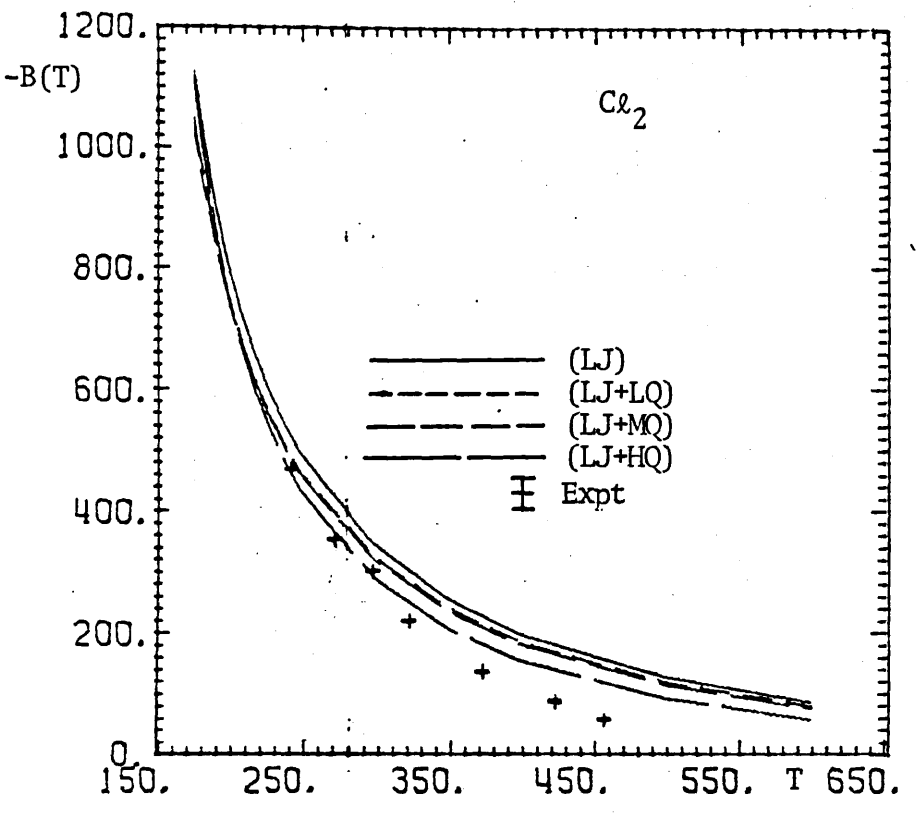

Figure (II-8)

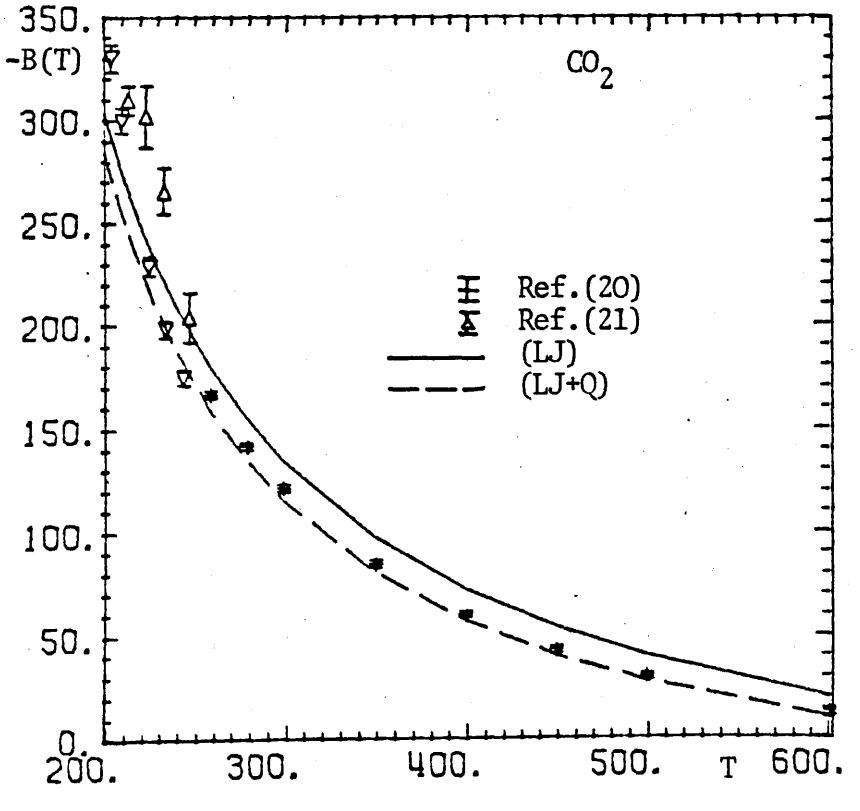

Figure (II-9)

The results are also graphed in Figures (II-6) to (II-9).

The primary effect of the quadrupole moment is a lowering in magnitude of the virial coefficients throughout the temperature range. This is shown in the case of chlorine (LJ+LQ) for which the Lennard-Jones ε and σ are not reduced to compensate for the quadrupole. The reduction of ε and σ decreases the expected effect from the quadrupole. A secondary effect is that the quadrupole slightly increases the slope of B(T), particularly at low temperatures.

The variation of the basic 2-centre Lennard-Jones potential second virial coefficient has been discussed by Sweet and Steele(22), who tabulated the variation of the second virial coefficient with temperature and bond length (anisotropy). The effect of increasing anisotropy, in terms of bond length and quadrupole moment has also been discussed by MacRury et al. (19), who found the same decrease in magnitude of the virial coefficients with increasing quadrupole moment. This lowing is due to the increased cohesive (negative) energy contribution of the quadrupole. Using the angle averaged Lennard-Jones potential of equations (II-5) and (II-6) as well as the angle averaged quadrupolar potential of equation (II-45) it can be seen that the form of the total potential is

$$\phi = \phi_{LJ}^{(1)}(\varepsilon,\sigma,L) + \phi_{LJ}^{(2)}(\varepsilon,\sigma,L)/kT + \phi_{Q}^{(1)}(Q)/kT + \phi_{Q}^{(2)}(Q)/(kT)^2$$

$$\text{where } Q = f(q,L) \qquad \text{(II-16)}$$

From this, the addition of the quadrupolar terms will increase the temperature and bond length dependence of the total potential, and thus will have an effect on the slope of the second virial coefficient.

The virial coefficients of nitrogen, both for Quantrec's potential(1) and for the (LJ+Q) potential seem poor, especially in comparison with the potentials of Cheung and Powles(2,18) and MacRury et al. (19), although the addition of the quadrupolar term does improve agreement with the experimental values slightly.

The lack of experimental data for chlorine makes testing of the potential difficult, although the second virial coefficients seem reasonable. There is strong variation in the coefficients with changes in the size of the quadrupole moment.

The carbon dioxide potential, based on the fitted potential of Singer et al.(3), was in good agreement with the experimental values, both for the lattice energy and the virial coefficients. In both instances the addition of the quadrupolar term increased agreement with experimental values.

It should be pointed out however that the parameters of the basic 2-centre Lennard-Jones potentials have been fitted to experimental data, and as such have been optimized in the absence of a quadrupole moment. Thus these parameters compensate for the lack of a quadrupole. However, when a quadrupole moment is included in the potential, the Lennard-Jones parameters must be adjusted so that the potential does not become too cohesive for the simulation of real liquids.

CHAPTER II.

Part 2. Molecular Dynamics Simulation Method.

The molecular dynamics simulation method was conceived by Alder and Wainwright(23). This work was then applied and extended by Rahman(24) and Verlet(25), to simple one-centre Lennard-Jones potentials. The technique was further extended to diatomic molecules by Berne and Harp(26). The basic methods employed here remain the same.

The system consists of a cube of side L, determined by the required density and contains N (108 or 256) molecules. In order to represent the fluid extending to infinity, the cube is surrounded by periodic images of itself. The interaction potential between molecules i and j is

$$\phi_{ij}(\underset{\sim}{r}_{ij}) = 4\varepsilon \sum_{\substack{m=1 \\ m\neq 2}}^{3} \sum_{\substack{n=1 \\ n\neq 2}}^{3} \left\{ \left(\frac{\sigma}{|\underset{\sim}{r}_{im} - \underset{\sim}{r}_{jn}|} \right)^{12} - \left(\frac{\sigma}{|\underset{\sim}{r}_{im} - \underset{\sim}{r}_{jn}|} \right)^{6} \right\}$$

$$+ \sum_{m=1}^{3} \sum_{n=1}^{3} \frac{Z_m Z_n}{4\pi\varepsilon_0 |\underset{\sim}{r}_{im} - \underset{\sim}{r}_{jn}|} \qquad \text{(II-17)}$$

where m and n denote the interaction sites of the molecule. (m=1,3 - atom sites : m=2 - centre of mass). The molecules are assumed to be rigid such that $|\underset{\sim}{r}_{i1} - \underset{\sim}{r}_{i3}| = L$, although it is not a necessary requirement that the interaction sites are distributed in this manner. Throughout the calculation of these interactions the 'minimum-image convention' was employed, so that a particle in the primary cube is only allowed to interact with the (N-1) other particles in the primary cube, or the nearest images of these particles in adjacent cubes. Thus each particle is always at the centre of a cube, composed of primary cube molecules or nearest images. This convention must be applied on a molecular basis, rather than an atomic basis to preserve molecular charge distribution. The instantaneous potential energy is then given by

$$\Phi = \sum_{i=1}^{(N-1)} \sum_{j>i}^{N} \phi_{ij}(r_{ij}) + \Phi_{LR} \qquad \text{(II-18)}$$

the virial by

$$\Psi = \sum_{i=1}^{(N-1)} \sum_{j>i}^{N} \sum_{m=1}^{3} \sum_{n=1}^{3} \frac{d\phi(|\underset{\sim}{r}_{im}-\underset{\sim}{r}_{jn}|)}{d(|\underset{\sim}{r}_{im}-\underset{\sim}{r}_{jn}|)} \cdot \frac{(|\underset{\sim}{r}_{im}-\underset{\sim}{r}_{jn}|).R_{ij}}{R_{ij}} + \Psi_{LR} \qquad \text{(II-19)}$$

where $\underset{\sim}{R}_{ij} = (|\underset{\sim}{r}_{i2}-\underset{\sim}{r}_{j2}|)$

Φ_{LR} and Ψ_{LR} are long range correction terms. However for ease of evaluation the virial sum (II-19) is replaced by

$$\Psi = \sum_{i=1}^{(N-1)} \sum_{j>i}^{N} \sum_{m=1}^{3} \sum_{n=1}^{3} \left(\frac{d\phi(|\underset{\sim}{r}_{im}-\underset{\sim}{r}_{jn}|)}{d(|\underset{\sim}{r}_{im}-\underset{\sim}{r}_{jn}|)} \cdot (|\underset{\sim}{r}_{im}-\underset{\sim}{r}_{jn}|)\right) + \sum_{i=1}^{N} \underset{\sim}{\ell}_i.\underset{\sim}{F}_i^D + \Psi_{LR}$$

(II-20)

where $\underset{\sim}{\ell}_i$ = Bond vector and $\underset{\sim}{F}_i^D = \frac{1}{2}(\underset{\sim}{F}_{i1}-\underset{\sim}{F}_{i3})$.
The force on each interaction site is also calculated

$$\underset{\sim}{F}_{im} = - \sum_{\substack{j=1 \\ (j\neq i)}}^{N} \sum_{n=1}^{3} \frac{d\phi(|\underset{\sim}{r}_{im}-\underset{\sim}{r}_{jn}|)}{d(|\underset{\sim}{r}_{im}-\underset{\sim}{r}_{jn}|)} \cdot \frac{(\underset{\sim}{r}_{im}-\underset{\sim}{r}_{jn})}{(|\underset{\sim}{r}_{im}-\underset{\sim}{r}_{jn}|)} \qquad \text{(II-21)}$$

Equations of Motion.

The equations of motion are solved for each molecule over a very short time step Δt. The motion is assumed to be CLASSICAL. The centre of mass $\underset{\sim}{R}_i$ and the bond vector $\underset{\sim}{\ell}_i$ of the i^{th} molecule are defined by

$$\underset{\sim}{R}_i = \sum_{k=1}^{3} m_{ik}\underset{\sim}{r}_{ik} \Big/ \sum_{k=1}^{3} m_{ik} \qquad \text{(II-22)}$$

$$\underset{\sim}{\ell}_i = \underset{\sim}{r}_{i1} - \underset{\sim}{r}_{i3} \qquad \text{(II-23)}$$

These then obey the classical equations of motion

$$M_i \ddot{\underset{\sim}{R}}_i = \sum_{k=1}^{3} \underset{\sim}{F}_{ik} \qquad \text{(Translational)} \qquad \text{(II-24)}$$

$$\mu_i \ddot{\underset{\sim}{\ell}}_i = \frac{m_{i3}}{M_i} \underset{\sim}{F}_{i1} - \frac{m_{i1}}{M_i} \underset{\sim}{F}_{i3} = \underset{\sim}{F}_i^D \qquad \text{(Rotational)} \qquad \text{(II-25)}$$

where $M_i = \sum_{k=1}^{3} m_{ik}$ and $\mu_i = (m_{i1} \cdot m_{i3})/(m_{i1} + m_{i3})$.
For homonuclear diatomics $m_{i1} = m_{i3}$ and $m_{i2} = 0$.

Translation.

The translational equation (II-24) is solved by expanding $\ddot{\underset{\sim}{R}}_i$ giving

$$\underset{\sim}{R}_i(t+\Delta t) = 2\underset{\sim}{R}_i(t) - \underset{\sim}{R}_i(t-\Delta t) + \left(\sum_{k=1}^{3} \underset{\sim}{F}_{ik}\right)\Delta t^2 / M_i \qquad \text{(II-26)}$$

This is known as Verlet's leap-frog algorithm(25), which is a first order expansion of $\ddot{\underset{\sim}{R}}_i$. More accurate higher order expansions may be used, but have the disadvantage that they require the particle coordinates to be stored for a higher number of previous configurations. The problem is exactly analogous to that of numerical integration of equidistantly spaced points. Verlet's algorithm can be though of as equivalent to the trapezoid rule integration. The accuracy of solution of the equations of motion is determined by the size of the integration step Δt.

Rotation.

The rotational equation is more involved and is approximately solved in a trigonometric manner by a second order predictor-corrector type algorithm. The rigid molecule gives the condition $|\ell|^2$ constant, implying

$$\underset{\sim}{\ell}_i \cdot \ddot{\underset{\sim}{\ell}}_i = -\dot{\underset{\sim}{\ell}}_i \cdot \dot{\underset{\sim}{\ell}}_i \tag{II-27}$$

thus the force component parallel to $\underset{\sim}{\ell}$ is removed,

$$\underset{\sim}{F}_i'' = (\underset{\sim}{F}_i^D \cdot \frac{\underset{\sim}{\ell}_i}{|\ell|}) \cdot \frac{\underset{\sim}{\ell}_i}{|\ell|} \tag{II-28}$$

giving

$$\mu \ddot{\underset{\sim}{\ell}}_i - \mu(\ddot{\underset{\sim}{\ell}}_i \cdot \underset{\sim}{\ell}_i) \cdot \underset{\sim}{\ell}_i / \ell^2 = \underset{\sim}{F}_i^D - \underset{\sim}{F}_i'' = \underset{\sim}{F}_i^{\perp} \tag{II-29}$$

Thus equation (II-25) for the rotational motion, using (II-27) becomes

$$\mu \ddot{\underset{\sim}{\ell}}_i = \underset{\sim}{F}_i^{\perp} - \mu |\dot{\underset{\sim}{\ell}}_i|^2 \cdot \underset{\sim}{\ell}_i / \ell^2 \tag{II-30}$$

The algorithm for solving (II-30) was developed by Singer and Taylor(3). In this algorithm the last term of (II-30) which keeps the value of $|\underset{\sim}{\ell}_i|$ constant, is replaced by an equivalent kinematic restriction, as it is difficult to evaluate $|\dot{\underset{\sim}{\ell}}_i^2|$ accurately. The equation is solved by constraining the trajectory to the surface of a sphere; instead of on a tangential plane which is the effect of solving (II-30) neglecting the last term.

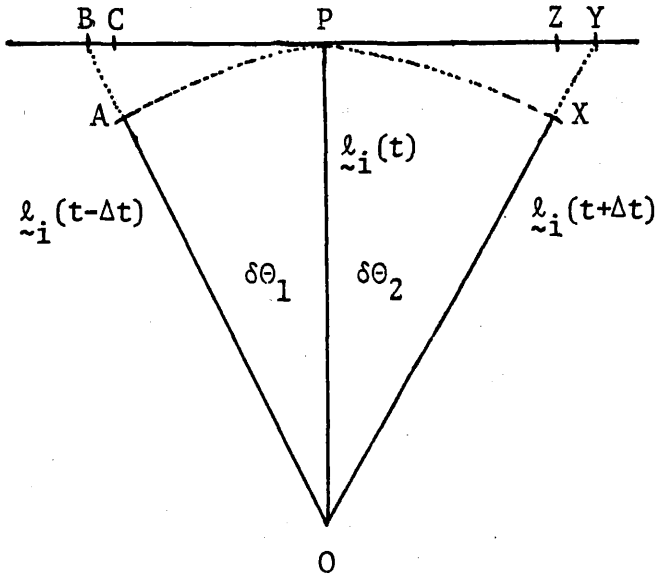

Figure (II-10)

In Figure (II-10) $\underset{\sim}{OA}$, $\underset{\sim}{OP}$ and $\underset{\sim}{OX}$ are vectors representing $\underset{\sim}{\ell}_i(t-\Delta t)$, $\underset{\sim}{\ell}_i(t)$ and $\underset{\sim}{\ell}_i(t+\Delta t)$ respectively. Thus the angles $\delta\Theta_1$ and $\delta\Theta_2$ are given by

$$\delta\Theta_1 = \text{Cos}^{-1}((\underset{\sim}{\ell}_i(t).\underset{\sim}{\ell}_i(t-\Delta t))/\ell^2)$$

$$\delta\Theta_2 = \text{Cos}^{-1}((\underset{\sim}{\ell}_i(t).\underset{\sim}{\ell}_i(t+\Delta t))/\ell^2) \qquad \text{(II-31)}$$

$\underset{\sim}{OB}$ gives the projection of the vector $\underset{\sim}{\ell}_i(t-\Delta t)$ or $\underset{\sim}{OA}$ on to the plane tangential to the vector $\underset{\sim}{\ell}_i(t)$ at $|\underset{\sim}{\ell}_i| = \ell$

$$\underset{\sim}{OB} = \underset{\sim}{\ell}_i^T(t-\Delta t) = \underset{\sim}{\ell}_i(t-\Delta t).\frac{|\underset{\sim}{\ell}_i(t)|^2}{(\underset{\sim}{\ell}_i(t-\Delta t).\underset{\sim}{\ell}_i(t))} \qquad \text{(II-32)}$$

Correcting $\underset{\sim}{BP} = \ell\tan\delta\Theta_1$ to the length of the arc $\underset{\sim}{AP} = 1\delta\Theta_1$ without altering its direction gives $\underset{\sim}{CP}$ which defines the shortened vector $\underset{\sim}{\ell}_i^S(t-\Delta t)$

$$\underset{\sim}{\ell}_i(t)-\underset{\sim}{\ell}_i^S(t-\Delta t) = \frac{\ell\delta\Theta_1}{\ell\tan\Theta_1}.(\underset{\sim}{\ell}_i(t)-\underset{\sim}{\ell}_i^T(t-\Delta t)) \qquad \text{(II-33)}$$

$\underset{\sim}{OZ} = \underset{\sim}{\ell}_i^S(t+\Delta t)$ is determined by

$$\underset{\sim}{\ell}_i^S(t+\Delta t) = 2\underset{\sim}{\ell}_i(t)-\underset{\sim}{\ell}_i^S(t-\Delta t) + \underset{\sim}{F}_i^{\perp}.\Delta t^2/\mu \qquad \text{(II.34)}$$

The reverse of the $\underset{\sim}{\ell}_i(t-\Delta t)$ corrected projection is carried out to give the resultant $\underset{\sim}{\ell}_i(t+\Delta t)$ using $\underset{\sim}{PZ} = \underset{\sim}{PX} = \ell\delta\Theta_2$

$$\underset{\sim}{\ell}_i^T(t+\Delta t) = \underset{\sim}{\ell}_i(t) + \frac{\tan\delta\Theta_2}{\delta\Theta_2}.(\underset{\sim}{\ell}_i^S(t+\Delta t)-\underset{\sim}{\ell}_i(t)) \qquad \text{(II-35)}$$

and

$$\underset{\sim}{\ell}_i(t+\Delta t) = \frac{|\underset{\sim}{\ell}_i(t)|}{|\underset{\sim}{\ell}_i(t+\Delta t)|} \cdot \underset{\sim}{\ell}_i^{\mathrm{T}}(t+\Delta t) \qquad \text{(II-36)}$$

This rotational algorithm, as pointed out by Singer, has the advantage that derivatives of the forces, which fluctuate very rapidly and thus are difficult to evaluate, are not needed. The stability of this algorithm is dependent on the angles $\delta\Theta_1$ and $\delta\Theta_2$ (which are a function of $|F^{\perp}|/\mu$ and Δt) being small.

Averages.

Having solved the equations of motion, averages and sub-averages of various thermodynamic quantities are calculated, in particular

$$E = \frac{N_A}{N} \left\langle \tfrac{1}{2} \left(\sum_{i=1}^{N} M_i |\dot{\underset{\sim}{R}}_i|^2 + \mu_i |\dot{\underset{\sim}{\ell}}_i|^2 \right) + \sum_{i=1}^{N} \Phi(\underset{\sim}{R}_i, \underset{\sim}{\ell}_i) \right\rangle \qquad \text{(II-37)}$$

$$T = \frac{1}{5Nk} \left\langle \left(\sum_{i=1}^{N} M_i |\dot{\underset{\sim}{R}}_i|^2 + \mu_i |\dot{\underset{\sim}{\ell}}_i|^2 \right) \right\rangle \qquad \text{(II-38)}$$

$$P = \frac{1}{V} \left(N_A kT - \frac{N_A}{3N} \langle \Psi \rangle \right) \qquad \text{(II-39)}$$

where the virial is defined in equation (II-19). The mean-square torque and force are calculated by Cheung's method(27).

$$\langle F^2 \rangle = \frac{N_A}{N} \left\langle \left(\sum_{i=1}^{N} \underset{\sim}{F}_i^{\,2} \right) \right\rangle \qquad \text{(II-40)}$$

$$\langle \tau^2 \rangle = \frac{N_A}{N} \left\langle \sum_{i=1}^{N} \left(\frac{|\ddot{\underset{\sim}{\ell}}_i \times \underset{\sim}{\ell}_i|^2}{\ell^2} \right) \right\rangle \qquad \text{(II-41)}$$

The specific heat at constant volume is also calculated from the fluctuations of the averaged potential, translational and rotational energies, by another of Cheung's methods(28), which is an extension

of the work of Lebowitz et al.(29) for monatomic systems.

$$C_v = n_Q R\{1 - N<(\delta Q)^2>/n_Q k^2 T^2\}^{-1} \qquad \text{(II-42)}$$

where $<(\delta Q)^2> = (<Q^2>-<Q>^2)$, the fluctuation in the Q energy. It is assumed that $<Q> = n_Q kT$ where n_Q is the number of degrees of freedom of energy Q. It can be seen from Cheung's paper that this is not an accurate means of calculating C_v, but it does serve as a rough estimate for the specific heat at the given simulation point.

Long-Range corrections.

The long-range corrections are evaluated on the basis that the Lennard-Jones centre distribution at long ranges is uniform and can be approximated on an atomic basis giving

$$\Phi_{LJ} = \frac{32\pi N_A^2}{V} \varepsilon\sigma^3 \{\frac{1}{9}(\frac{\sigma}{R_c})^9 - \frac{1}{3}(\frac{\sigma}{R_c})^3\} \qquad \text{(II-43)}$$

$$\Psi_{LJ} = \frac{64\pi N_A^2}{V} \varepsilon\sigma^3 \{-\frac{2}{3}(\frac{\sigma}{R_c})^9 + (\frac{\sigma}{R_c})^3\} \qquad \text{(II-44)}$$

where R_c is the cut-off applied to the Lennard-Jones potential. The quadrupole potential was summed over the entire molecular dynamics cube. The long-range quadrupolar corrections were calculated numerically assuming the orientations of the molecules to have become angle-averaged. The energy correction in the quadrupolar case was found to be approximately 1Joule and the pressure correction less than 1 atmosphere for a system of 108 chlorine molecules. As this was less than the statistical error, these terms were neglected. This can also be seen from the angle-averaged quadrupolar potential of Stell et al.(30),

$$\overline{\phi}^{QQ}(r) = -\frac{7}{5kT}\left(\frac{Q^4}{r^{10}}\right) + \frac{72}{245k^2T^2}\left(\frac{Q^6}{r^{15}}\right) \qquad \text{(II-45)}$$

which is very small at large ranges. It is also a function of Q^4 and Q^6 and is temperature dependent.

General Aspects of Simulation.

The molecules are moved over the time step Δt, and the process repeated until sufficient statistics for the various analyses has been accumulated. This is typically $5000\Delta t$ for N=108 and $2500\Delta t$ for N=256 molecules. In the systems studied, due to the large anisotropic forces, it was necessary to keep $\Delta t = 4.0 \times 10^{-15}$ which is comparatively small. This gave fluctuations in the total energy of approximately 5 in 10^4-10^5 Joules over $5 \times 10^3 \Delta t$ for the most anisotropic (highest quadrupolar) case, and was less for all other cases. No drifting in the energy was observed.

For each simulation run the centre of mass positions and bond vectors of each molecule were written on magnetic tape at every Δt for subsequent analysis.

Prior to the final run the system must be brought to equilibrium at the required temperature and volume. This is done by scaling the velocities, if necessary, at every $20\Delta t$. The scaling is equivalent to adjusting the total energy of the system until it corresponds to the required temperature in the equilibrated system. The system is taken to be at equilibrium when a) the translational and rotational temperatures are within 5 K of each other, b) the temperature is consistantly within 5 K of the specified temperature and c) the fluctuations in the pressure become less than ± 100 atmospheres.

Although these criteria are somewhat arbitrary they do serve well as a test of equilibrium. Other methods where the system is only equilibrated for a brief interval ($\approx 500\Delta t$) so that the positions

of the particles have been substantially changed, must be regarded as unsatisfactory. This is because equilibrium is obtained only when the fluctuations in the translational, rotational and potential energies are small and there is no drift of energy between any pair of energies. The total energy should also correspond to the required temperature.

It was found that this process of temperature scaling needed to be carried out for $7500\Delta t$ for N=108 molecules to ensure the correct equilibrium. After this period a further $2500\Delta t$ was needed for the system to settle completely to equilibrium after the temperature scaling, before the final production run was made.

The initial starting configuration was usually a similar liquid configuation. If this was not available a face-centred cubic lattice was used, together with arbitary velocity assignment, such that the net velocity in the system was zero. The lack of structure (i.e. deviation from the crystal lattice) was monitored by Verlet's order parameter(25).

An indication of the computer time used is that on the University of London CDC7600 one Δt required 0.4 seconds for N=108 and 2.5 seconds for N=256.

Sources of Error.

Sources of error in the simulation are varies and not easily quantifiable. They are a) the effect of the periodic boundary conditions which introduces artificial periodicity and hence correlations, b) the minimum-image convention perhaps produces angle-averaging at the edges of the molecular dynamics cell, c) the finite cut-off of the potential, d) the size of the time step t and e) the statistical averaging, however good, could always be better, given a larger sample of molecules and a greater number of time steps.

These result in an approximate error in the pressure of ± 50 atmospheres and in the temperature of ± 2 K. The error is determined from studying the fluctuations in these quantities with the number of time steps of simulation. The 'error' in the simulation of real liquids is due to the exact form of the potential with its higher order terms is unknown.

The simulation is classical mechanical. This is justified by the smallness of the translational and rotational quantum steps for the masses of the molecules considered here. Work on quantum corrected molecular dynamics simulation is being undertaken for systems of rare gas atoms by Singer et al.(31). The quantum correction formulae show that the effective potential is velocity dependent. The velocity distribution also differs from the classical Maxwellian distribution. It may be that these effects, particularly on the dynamics of the system, are not negligable, even if they are small.

REFERENCES FOR CHAPTER II.

1. J. Barojas, D. Levesque and B. Quentrec - Phys.Rev., 1973, A7, 1092.
2. P.S.Y. Cheung and J.G. Powles - Mol.Phys., 1975, 30, 921.
3. K. Singer, A. Taylor and J.V.L. Singer - Mol.Phys., 1977, 33, 1757.
4. B.C. Kohin - J.Chem.Phys., 1970, 33, 882.
5. D.A. Goodings and M. Henkelman - Can.J.Phys., 1971, 49, 2898.
6. J. de Boer - Physica, 1942, 9, 363.
7. J.O. Hirschfelder, D.F. Curtiss and R.B. Bird - 'Molecular Theory of Gases and Liquids', (Wiley, New York, 1964).
8. D.E. Stogryn and A.P. Stogryn - Mol.Phys., 1966, 11, 371.
9. W.B. Streett and K.E. Gubbins - Ann.Rev.Phys.Chem., 1977, 28, 373.
10. R. Occelli, B. Quentrec and C. Brot - Mol.Phys., 1978, 36, 257.
11. G.E. Jelinek, L.J. Slutsky and A.M. Karo - J.Phys.Chem.Solids, 1972, 33, 1279.
12. T.C. Jao, N.H.F. Beebe, W.B. Person and J.R. Sabin - Chem.Phys. Lett., 1974, 26, 474.
13. O. Schnepp and N. Jacobi - Adv.Chem.Phys., 1972, 22, 205.
14. T.A. Scott - Phys.Rep. 1976, 27, 89.
15. C.S. Murthy and K. Singer - Private communication.
16. S.M. Thompson, D.J. Tildesley and W.B. Streett - Mol.Phys. 1976, 32, 711.
17. J.H. Dymond and E.B. Smith - The Virial Coefficients of Gases - A Critical Compilation, (Clarendon Press, 1969).
18. P.S.Y. Cheung and J.G. Powles - Mol.Phys., 1976, 32, 1383.
19. T.B. Macrury, W.A. Steele and B.J. Berne - J.Chem.Phys., 1976, 64, 1288.
20. K. Schafer - Z.Phys.Chem., 1937, B36, 85.

21. J.M.H. Levelt Sengers, M. Klein and J.S. Gallagher - Pressure - Volume - Temperature Relationships of Gases Virial Coefficients. Heat Division, National Bureau of Standards (USA) - March 1971.

22. J.R. Sweet and W.A. Steele - J.Chem.Phys., 1967, 47, 3029.

23. B.J. Alder and T.E. Wainwright - J.Chem.Phys., 1959, 31, 459.

24. A. Rahman - Phys.Rev., 1964, 136A, 405.

25. L. Verlet - Phys.Rev., 1968, 165, 21/Ibid 1967, 159, 98.

26. G.D. Harp and B.J. Berne - Adv.Chem.Phys., 1970, 17, 63.

27. P.S.Y. Cheung - Chem.Phys.Lett., 1976, 40, 19.

28. P.S.Y. Cheung - Mol.Phys., 1977, 33, 519.

29. J.L. Lebowitz, J.K. Percus and L. Verlet - Phys.Rev., 1967, 153, 250.

30. J.C. Rasaiah, B. Larsen and G. Stell - J.Chem.Phys., 1975, 63, 722.

31. K. Singer, R. Renaud and N. Corbin - Private communication.

CHAPTER III.

Thermodynamics.

1. Introduction.

The equilibrium properties of classical fluids can be expressed in terms of their partition function, which is the integral over the Hamiltonian of the system for a given volume and temperature thus

$$Q_N(V,T) = \frac{1}{N!h^{3N}} \iint \exp\left[-H(r^N,p^N)/kT\right] dr^N dp^N \ldots \qquad \text{(III-1)}$$

This partition function is them related to the Helmholtz free energy of the system A by

$$Q_N(V,T) = \exp\left[-A_N(V,T)/kT\right] \qquad \text{(III-2)}$$

Standard thermodynamic relationships can now be used to obtain quantities such as the energy, pressure or entropy of the system.

However, the Hamiltonian contains both kinetic and potential energy terms which at equilibrium allow the integral (III-1) to be separated such that

$$Q_N(V,T) = \frac{1}{N!h^{3N}} \left[2\pi mkt\right]^{3N/2} Z_N(V,T) \qquad \text{(III-3)}$$

where $Z_N(V,T)$ is the configurational integral

$$Z_N(V,T) = \int \exp\left[-U_N(r^N)/kT\right] dr^N \qquad \text{(III-4)}$$

and $U_N(r^N)$ is the potential energy term of the Hamiltonian.

In the ideal gas limit where $U_N(r^N) = 0$ then the configurational integral is simply V^N. This allows the partition function to be separated into "ideal" and "excess" contributions

$$Q_N(V,T) = Q_N^{id}(V,T) \left\{\frac{Z_N(V,T)}{V^N}\right\} \qquad \text{(III-5)}$$

which enables the Helmholtz free energy to be similarly separated into ideal and excess terms

$$A = A^{id} + A^{ex} \qquad \text{(III-6)}$$

where A^{ex} can then be expressed in terms of the configurational integral alone

$$A^{ex} = -kT \ln \left\{\frac{Z_N(V,T)}{V^N}\right\} \qquad \text{(III-7)}$$

All other thermodynamic quantities which can be obtained from the Helmholtz free energy can now be written in terms of ideal and excess quantities. Thus the thermodynamics of a system with non-trivial interactions between the particles is dependent on the evaluation of the configurational integral. Both methods of computer simulation, Monte-Carlo and Molecular Dynamics may be regarded as methods of accurate evaluation of the associated configurational averages.

The systems to be investigated were chosen to be molecular liquids represented by two-centre Lennard-Jones potentials, previously investigated by Singer et al. (1), to which an additional quadrupole term has been added. This enables a better representation of the strongly anisotropic nature of the intermolecular potentials to be made, particularly in the case of Chlorine and Carbon Dioxide which are known to have large quadrupole moments. As discussed in Chapter II, suitable

adjustments have been made to the Lennard-Jones parameters σ and ε to compensate for the inclusion of the quadrupole. It can then be expected that if other multipolar terms in the potential are small, then the two-centre Lennard-Jones and quadrupole should be a very adequate representation of the total intermolecular potential, particularly when the quadrupole is distributed in the form of fractional charges, giving a more strongly angle-dependent potential at small interaction distances.

2. Molecular Dynamics Simulation.

The methods of calculating the thermodynamic quantities from a simulation have been discussed in Chapter II. In particular equations (II-37) to (II-39) are used to evaluate the basic quantities of energy, temperature and pressure.

In order to study the full range of adjustable parameters in the intermolecular potential, namely σ, ε, L and Q, three molecules were chosen, Nitrogen, Chlorine and Carbon Dioxide representing small, medium and large values of the bond length L within physically meaningful bounds. Reliable values for quandrupole moment of Nitrogen and Carbon Dioxide are available and have been used, while for Chlorine values range from small to large. This gave an opportunity to study the effect of changing quadrupole moment on a system with a moderate bond length. Three values of the quadrupole moment were chosen for Chlorine spanning the range of physically possible values. These values are given in Chapter II.

These systems were then investigated by choosing two isochores along which a simulation was performed at three well separated temperatures, the lowest of which approximated zero pressure, and the highest 1000 atmospheres pressure. This enables derivative properties such as the specific heat to be calculated.

These results have been tabulated using the usual reduced quantities

$$T^* = kT/\varepsilon \quad : \quad \rho^* = \rho N_A \sigma^3$$

$$E^* = E/N_A\varepsilon \quad : \quad p^* = p\sigma^3/\varepsilon$$

$$L^* = L/\sigma \quad : \quad Q^* = Q/(\varepsilon\sigma^5)^{\frac{1}{2}} \qquad \text{(III-8)}$$

although care should be taken in comparison with results without quadrupoles as the parameter T* only reflects the contribution from the Lennard-Jones part of the potential and thus cannot be used as a guide to the temperature of the system or the relationship of the phase point to the critical and triple points. However, alteration of ε will give different values of both T* and Q* enabling ε to be regarded as a common factor in all terms of the potential energy function.

The isochores have been chosen for easy comparison with the work of Singer et al. (1) in the case of Chlorine and Carbon Dioxide and Quentrec et al. (2) for nitrogen. The variation of E* and p* as a function of T* along each isochore is given in Table (III-1). As there are only typically three points per isochore, only linear dependence can be safely deduced. The energy and pressure isochores have been plotted in Figures (III-1) and (III-2) respectively for the Chlorine system with varying quadrupole moments, including the comparable isochores of the Lennard-Jones only system taken from the results of Singer et al. (1). The basic behaviour of the systems, is the same as the Lennard-Jones only system, with the slopes of the energy isochores (C_V) increasing slowly with density. The quadrupole moment is seen to increase the slope of the function as well as making the intercept substantially more negative. The same effect is obzerved for the pressure isochores except that the effect is very much more pronounced as would be expected for systems with increasing

TABLE (III-1)

ρ^*	$E^* = A+BT^*$ A	B	$P^* = a+bT^*$ a	b
$L^* = 0.328$ $Q^* = 0.0$ (N_2) (2)				
0.696	-20.718	3.740	-8.578	5.967
0.622	-18.294	3.418	-8.972	4.250
$L^* = 0.328$ $Q^* = 0.0$ (N_2) (33)				
0.696	-20.925	3.816	-9.292	6.167
0.622	-18.277	3.411	-9.158	4.315
$L^* = 0.328$ $Q^* = 1.159$ (N_2)				
0.700	-23.220	4.262	-11.518	6.899
0.626	-19.795	3.621	-10.157	4.477
$L^* = 0.608$ $Q^* = 0.0$ (Cl_2) (1)				
0.541	-15.671	3.956	-6.301	5.784
0.485	-13.700	3.522	-5.607	3.793
$L^* = 0.608$ $Q^* = 0.739$ (Cl_2)				
0.541	-15.836	4.006	-6.040	5.658
0.485	-13.959	3.624	-5.730	3.838
$L^* = 0.608$ $Q^* = 1.321$ (Cl_2)				
0.546	-17.842	4.570	-7.348	6.289
0.490	-15.582	4.050	-6.294	4.066
$L^* = 0.608$ $Q^* = 2.073$ (Cl_2)				
0.551	-23.456	5.397	-10.013	6.474
0.494	-20.771	4.947	-9.377	4.854
$L^* = 0.793$ $Q^* = 0.0$ (CO_2) (1)				
0.459	-13.062	3.741	-4.436	4.282
0.393	-10.843	3.333	-3.791	2.591
$L^* = 0.793$ $Q^* = 2.039$ (CO_2)				
0.423	-15.906	4.226	-5.355	3.233
0.381	-14.039	3.953	-4.492	2.386

anisotropy, on the basis that the higher the anisotropy the greater the effective volume of a molecule is. The magnitude of the quadrupolar perturbation is comparable in magnitude to substantial changes in the bond length.

The values of the energy isochore intercept (E_0^*) as a function of density are plotted in Figure (III-3). These no longer show the commonality between systems exhibited by the Lennard-Jones only potentials of Singer et al. (1). The quadrupole moment causes a non-linear decrease in E_0^* which is most clearly shown in the case of chlorine, where variation with increasing quadrupole moment is shown. The values for carbon dioxide ($Q^* = 2.039$) and chlorine ($Q^* = 2.073$) which have approximately equal quadrupoles do not appear to retain the linear relationship of E_0^* as a function of ρ^* for a given Q^*, previously observed for $Q^* = 0$. This suggests that the changes in quadrupolar systems are a function of Q^* and L^*, such that the two variables are interdependent.

Similar behaviour is exhibited by the intercepts of the pressure isochores P_0^*, illustrated in Figure (III-4). However, the behaviour of the Lennard-Jones only nitrogen system, abstracted from the calculation of Quentrec et al. (2) is clearly anomolous, showning a positive gradient with density. It should also be noted that the pressure calculation has a higher statistical error in the molecular dynamics calculation and thus these results have a rather higher scatter. This is also evident from the crossing of the chlorine ($Q^* = 0$) and ($Q^* = 0.793$) lines. The trend of substantial decrease in P_0^* with increasing quadrupole moment remains clear and has the same proportion as for E_0^*.

The effect of the quadrupole moment on the specific heat of the systems (C_V) is shown in Figure (III-5) where the reduced unit equivalent $(\partial E^*/\partial T^*)_{\rho^*}$ is plotted against density ρ^* for various values of the quadrupole moment. The quadrupole increases C_V in a strongly non-linear manner, but does not significantly alter the variation of C_V with

ρ^*, within the small range of densities studied. The effect of increasing the quadrupole moment can be regarded as increasing the effective anisotropy of the system, in a manner similar to an increase in bond length at a given density. The curves for chlorine ($Q^* = 2.073$) and carbon dioxide appear to lie close to the same line dispite differing values of the bond length, which suggests that the quadrupole, when large, dominates bond length effects.

The variation of $(\partial P^*/\partial T^*)_{\rho^*}$ with ρ^* is illustrated in Figure (III-6), which is similar to that of $(\partial E^*/\partial T^*)_{\rho^*}$ except that the change with increasing quadrupole moment is an order of magnitude smaller. This is probably because while the quadrupole increases the anisotropy of the potential, there is also a corresponding increase in the cohesiveness which minimized changes in the pressure gradient.

From the isochores, energy and density isobars may be deduced, which are linear as there are only two isochores per system. Equations for the isobars at $p^* = 0$ are given in Table (III-2) including values for non-quadrupolar systems (1,2). The energy isobars are plotted in Figure (III-7) and show strongly non-linear decrease in energy with increasing quadrupole moment. The shift to higher T^* is due to the reduction in ε previously discussed. The specific heat (C_p) also increases as a function of quadrupolar strength. The same type of qualitative behaviour can be seen in the density isobars illustrated in Figure (III-8), where the intercepts becomes progressively more negative as the gradient $(\partial\rho^*/\partial T^*)_{p^*}$ becomes larger with increasing Q^*. Equations for the isobars at $p^* = 0.5$ are given in Table (III-3). Comparison with Table (III-2) shows that the behaviour with increasing p^* is qualitatively the same as the Lennard-Jones only systems, in that the magnitudes of the constant terms and the gradients decrease with p^*.

Throughout the study of these thermodynamic quantities the effect of the quadrupole moment has been consistantly non-linear in every case studied, such that the small quadrupole ($Q^* = 0.739$) produced only a marginal deviation from Lennard-Jones only behaviour, and must be

TABLE (III-2)

$\rho^*=0$	$E^* = A+BT^*$ A	B	$\rho^* = a+bT^*$ a	b
$L^* = 0.328$ $Q^* = 0.0$ (N_2)*				
	-24.254	6.242	0.854	-.110
$L^* = 0.328$ $Q^* = 0.0$ (N_2) ●				
	-25.306	6.724	0.877	-.120
$L^* = 0.328$ $Q^* = 1.159$ (N_2)				
	-28.713	7.554	0.906	-.124
$L^* = 0.608$ Q^* 0.0 (Cl_2)				
	† -19.387	7.370	0.698	-.144
	‡ (-19.38)	(7.38)	(0.704)	(-.150)
$L^* = 0.608$ $Q^* = 0.739$ (Cl_2)				
	-19.107	7.073	0.681	-.131
$L^* = 0.608$ $Q^* = 1.321$ (Cl_2)				
	-22.305	8.392	0.718	-.147
$L^* = 0.608$ $Q^* = 2.073$ (Cl_2)				
	-30.769	10.122	0.780	-.148
$L^* = 0.793$ $Q^* = 0.0$ (CO_2)				
	† -16.998	7.54	0.619	-.155
	‡ (-17.46)	(7.95)	(0.635)	(-.170)
$L^* = 0.793$ $Q^* = 2.039$ (CO_2)				
	-25.834	10.221	0.731	-.186

* Extracted from data of Quantrec et al. (2)
● Extracted from data of Cheung and Powles (33)
† Extracted from data of Singer et al. (1) in same range of density values as quadrupolar cases.
‡ Overall fit to data given by Singer et al. (1)

TABLE (III-3).

P^*=0.5	$E^* = A+BT^*$ A	B	$\rho^* = a+bT^*$ a	b
L^* = 0.328 Q^* = 0.0 (N_2) *				
	-24.377	6.147	0.855	-.105
L+ = 0.328 Q^* = 0.0 (N_2) ●				
	-25.180	6.495	0.877	-.114
L^* = 0.328 Q^* = 1.159 (N_2)				
	-28.410	7.241	0.902	-.116
L^* = 0.608 Q^* = 0.0 (Cl_2)				
	† -19.121	6.889	0.693	-.129
	‡ (-18.90)	(6.73)		
L^* = 0.608 Q^* = 0.759 (Cl_2)				
	-18.954	6.702	0.680	-.120
L^* = 0.608 Q^* = 1.321 (Cl_2)				
	-21.946	7.858	0.711	-.132
L^* = 0.608 Q^* = 2.073 (Cl_2)				
	-30.446	9.701	0.776	-.139
L^* = 0.793 Q^* = 0.0 (CO_2)				
	† -16.606	6.813	0.610	-.131
	‡ (-16.76)	(6.90)		
L^* = 0.793 Q^* = 2.039 (CO_2)				
	-24.262	8.840	0.694	-.149

*, ●, † and ‡ as for Table (III-2)

regarded as a very weak effect, whereas the larger quadrupoles ($Q^* \approx 1.2$) produces significant perturbations, and in the largest case ($Q^* \approx 2.0$) the quadrupole effects tend to dominate over bond length effects. This behaviour cannot be fitted to any simple power law from such as $\Delta = CQ^{*\alpha}$, which suggests that as the quadrupole increases, significant changes occur in the radial distribution function, particularly with regard to types of preferred molecular configurations, such that for the larger quadrupole systems, the thermodynamic results cannot be regarded as perturbations to the Lennard-Jones only systems.

No attempt has been made to fit the molecular dynamics results to any thermodynamically consistant equations of state as the number of adjustable parameters required would be too large for the number of available data points.

3. Comparison with Real Liquids.

In general the calculated properties of the molecular dynamics simulation do not lie in the vacinity of the experimental curves, as the potentials used cannot be expected to be a good representation in all phases, particularly those calculated by matching to the lattice properties. It is therefore necessary to scale the properties of the simulated fluid to the same range of the experimental ones to facilitate a true comparison between the fluids.

This is accomplished using the principle of Corresponding States(3), whereby any fluid whose interaction potential can be written as

$$u(r) = \varepsilon F(\sigma/r) \qquad \text{(III-9)}$$

where ε is an energy and σ is a distance and F denotes some functional form of the potential, can be shown to be equivalent to a second fluid characterized by the parameters ε' and σ' at a corresponding volume (σ'^3/σ^3) and temperature $(T\varepsilon'/\varepsilon)$. Thus, for each configuration in the first assembly there is a corresponding configuration in the second (assuming the same number of particles), which enables the two partition

functions given by equation (III-1) to be related

$$Q(V,T) = (\sigma'/\sigma)^{-3N} Q'(V\sigma'^3/\sigma^3,\ T\varepsilon'/\varepsilon) \qquad \text{(III-10)}$$

As seen before, the thermodynamic properties of the ensemble can then be deduced from the partition function. This gives for the configurational free energy

$$A'(V,T) = (\varepsilon/\varepsilon')A(V\sigma'^3/\sigma^3, T\varepsilon'/\varepsilon) - 3NkT \ln|\sigma/\sigma'| \qquad \text{(III-11)}$$

and similarly for the pressure

$$P'(V,T) = (\varepsilon/\varepsilon')(\sigma'^3/\sigma^3)P(V\sigma'^3/\sigma^3, T\varepsilon'/\varepsilon) \qquad \text{(III-12)}$$

Then if the equation of state of the reference fluid is

$$\phi(P,V,T) = 0 \qquad \text{(III-13)}$$

then that of the conformal substance is

$$\phi(P(\varepsilon'/\varepsilon)(\sigma/\sigma')^3, V(\sigma'/\sigma)^3, T(\varepsilon'/\varepsilon)) = \phi'(P,V,T) = 0 \qquad \text{(III-14)}$$

which is an expression of the principle of corresponding states. This form of dimensional analysis can only apply if

1) the partition function can be factorized into a dynamic and a configurational part.
2) the configurational integral may be treated by the methods of classical statistical mechanics, and
3) the substances have strictly conformal potentials.

Unfortunately in the case of anisotropic potentials the occupation of configurational sites, which act as local minima, is dependent on the kinetic energy available, and thus condition 3) is not fulfilled. Further as seen in Chapter II the angle averaged potentials themselves may be expressed as a Taylor series in powers of (1/kT), which in the case of the quadrupolar part has no zero order term. However, the radial distribution function may be regarded as unchanged for small changes in the parameters ε and σ, enabling the principle of corresponding states to be applied.

The procedure to find a match to the experimental data is as follows. The experimental liquid-vapour coexistance line is chosen, along which the pressures are nearly always less than 10 atm. and generally less than 1 atm. These pressures enable comparison with the molecular dynamics zero pressure isobar, as the error in the calculated pressures is approximately ± 100 atm. A point is then chosen in the middle of the data range, and the principle of corresponding states used to produce agreement between calculated and experimental at that point, by suitable adjustment of the parameters ε and σ. Specifically the energy, temperature and density were matched at that point to give the appropriate scaling factors $f = (\varepsilon'/\varepsilon)$ and $g = (\sigma'/\sigma)$.

The full interaction potential between two molecules may be written as the sum of four Lennard-Jones interactions and nine fractional charge interactions representing the quadrupole, the interaction between molecules i and j being given by

$$\phi_{ij} = \varepsilon f\left[\frac{\underset{\sim}{r}_{ij}\pm\underset{\sim}{\ell}_i\pm\underset{\sim}{\ell}_j}{\sigma}\right] + \frac{4C^2}{4\pi\varepsilon_o\sigma}\left[\frac{\sigma}{\underset{\sim}{r}_{ij}}\right]$$

$$- \frac{2C^2}{4\pi\varepsilon_o\sigma}\left[\frac{\sigma}{\underset{\sim}{r}_{ij}\pm\underset{\sim}{\ell}_i} + \frac{\sigma}{\underset{\sim}{r}_{ij}\pm\underset{\sim}{\ell}_j}\right] + \frac{C^2}{4\pi\varepsilon_o\sigma}\left[\frac{\sigma}{\underset{\sim}{r}_{ij}\pm\underset{\sim}{\ell}_i\pm\underset{\sim}{\ell}_j}\right] \qquad \text{(III-15)}$$

Hence on scaling the energies by a factor λ

$\varepsilon \to \lambda\varepsilon = \varepsilon' : C^2 \to \lambda C^2 = C'^2$ and scaling the distances by a factor μ

$\sigma \to \mu\sigma = \sigma' : \ell \to \mu\ell = \ell'$

Thus scaling the energies and distances produces a change in the quadrupole moment

$$Q = \sum_i C_i \ell_i^2 = Q'/(\sqrt{\lambda}\mu^2)$$

when calculated from the fractional charge distribution.

Throughout the comparisons with real liquids the vibrational energies have been subtracted from the experimental energies by assuming an undisturbed harmonic oscillator giving

$$E_{vit} = gN_o k\Theta_v (\exp[\Theta_v/T]-1)^{-1} \qquad \text{(III-16)}$$

where the values of g and Θ_v are given by Rosen(6) as

N_2: g=1, Θ_v=3371: Cl_2: g=1: Θ_v=810 and CO_2: g=2: Θ_v=954.

It should also be remembered that the comparisons are based on a few points on two isochores and must not be expected to agree closely over the entire range of experimental values. There was not enough data points to evaluate α_p, C_p and K_T for comparison with the experimental values.

3-A. Nitrogen.

The experimental data for nitrogen is taken from Rowlinson(4), and references cited therein, and Van Itterbeek(5). Results of the comparison are given in Table (III-4) and Table (III-5). Also included in these tables is the data of Quantrec et al.(2) to which the principle of corresponding states has also been applied. Both sets of data are in reasonable agreement with the experimental values, although the present quadrupolar simulation leads to better values of the energy and molar volume, particularly at higher temperatures.

TABLE (III-4).

T/K	V_m/cm^3mol^{-1}			$-E/kJmol^{-1}$		
	Exp	LJ	LJ+Q	Exp	LJ	LJ+Q
63.148	32.28	32.38	32.06	4.207	4.156	4.285
70	33.32	33.41	33.26	3.825	3.800	3.855
80	35.18	35.03	35.19	3.247	3.281	3.227
90	37.55	36.82	37.36	2.669	2.762	2.599
100	40.68	38.79	39.81	2.061	2.244	1.971
110	45.2	40.99	42.60	1.404	1.724	1.343
120	53.3	43.46	45.81	.636	1.206	.715

TABLE (III-5)

T/K	$\beta_V=(\partial P/\partial T)_{vm}/barK^{-1}$			$C_V=(\partial E/\partial T)_{vm}/Jmol^{-1}K^{-1}$		
	Exp	LJ	LJ+Q	Exp	LJ	LJ+Q
63.148	23.5	22.8	26.4	35.6	31.0	35.5
70	20.7	21.0	23.5	33.0	30.3	33.8
80	16.6	18.3	18.8	29.9	29.2	31.1
90	13.1	15.2	13.5	27.8	27.9	28.0
100	9.8	11.8	7.5	26.8	26.5	24.6
110	7.0	8.0	0.7	26.6	25.0	20.7
120	-	3.7	-	-	23.3	16.1

For C_v the quadrupole gives better agreement except at higher temperatures, but for β_v the quadrupolar case is poor, the experimental data being much better represented by the Lennard-Jones only potential. However, care should be taken not to place too much emphasis on these comparisons as they are based on a few points on just two isochores for both systems. This does not allow the evaluation of α_p, C_p or K_T. Both systems were matched to the experimental data at 75^o K, the corresponding states parameters for the Lennard-Jones system of Quentrec being .

$(T'/T) = .8388$: $(\sigma'/\sigma) = .986362$

$\varepsilon/k = 36.86$: $\sigma = 3.295 \times 10^{-10}$m

The quadrupolar case is very similar

$(T'/T) = .8279$: $(\sigma'/\sigma) = .989866$

$\varepsilon/k = 34.56$: $\sigma = 3.307 \times 10^{-10}$m : $Q = -1.355 \times 10^{-26}$ esu cm^2

3-B. Chlorine.

For chlorine the experimental data was taken from Wagenbrath(7) and Gmelin(8) as presented by Singer. The comparison is given in Tables (III-6) and (III-7). The results of the small quadrupolar system are slightly worse than the Lennard-Jones system of Singer et al. This must be regarded as due to insufficient data points as it is against the trend with increasing quadrupole moment, that is increasing specific heats and β_v. In general it is seen that the best comparison with the experimental values is close to the 'medium' quadrupole case. The large quadrupole has the effect of giving too strong variation of the thermodynamic quantitites with temperature and producing too large values

TABLE (III-6).

T/K	V_m/cm^3mol^{-1}				$-E/kJmol^{-1}$			
	Exp	LJ+SQ	LJ+MQ	LJ+HQ	Exp	LJ+SQ	LJ+MQ	LJ+HQ
173.1	41.29	41.26	40.56	39.62	17.71	17.33	18.05	18.98
203.1	42.84	43.04	42.62	42.06	15.77	15.57	15.95	16.46
238.1	45.31	45.31	45.31	45.31	13.51	13.51	13.51	13.51
273.1	48.31	47.84	48.36	49.10	11.24	11.45	11.07	10.56
293.1	50.33	49.41	50.29	51.57	9.97	10.28	9.67	8.88
313.1	52.71	51.10	52.39	54.30	8.71	9.10	8.28	7.20
333.1	55.59	52.90	54.66	57.33	7.44	7.92	6.88	5.52

TABLE (III-7).

	$\beta_V=(\partial P/\partial T)_V/bar\,K^{-1}$				$C_V=(\partial E/\partial T)_V/Jmol^{-1}K^{-1}$			
	Exp	LJ+SQ	LJ+MQ	LJ+HQ	Exp	LJ+SQ	LJ+MQ	LJ+HQ
173.1	28.4	20.0	22.6	23.7	39.4	33.0	37.8	45.2
203.1	25.9	17.5	19.0	20.6	30.3	31.7	35.9	43.2
238.1	19.2	14.2	14.3	16.5	27.3	30.2	33.4	40.6
273.1	12.7	10.7	8.9	11.8	31.6	28.5	30.5	37.5
293.1	10.6	8.4	5.5	8.7	30.5	27.4	28.7	35.5
313.1	9.4	6.0	1.8	5.2	26.6	26.3	26.7	33.3
333.1	7.9	3.5	-	1.4	27.4	25.1	24.6	30.8

TABLE (III-8).

System	(T'/T)	(σ'/σ)
LJ+SQ	.8715	1.009849
LJ+MQ	.8543	1.010940
LJ+LQ	.8324	1.016781

Corresponding States Parameters

System	ε/k	$\sigma \times 10^{-10}$ m	$Q(\times 10^{-26}$ esu cm$^2)$
LJ+SQ	173.18	3,353	2.34
LJ+MQ	162.43	3.356	4.06
LJ+LQ	131.13	3.376	5.79

for the specific heats. These systems were matched to experiment at 238.9° K and the corresponding states parameters are given in Table (III-8). The correspondence with those parameters obtained by Singer for the Lennard-Jones system are strikingly close to those obtained here for the small quadrupole case. It seems that quadrupoles of this size are too small to have a significant effect on the thermodynamics of the liquid. It should be remembered that the effect of a quadrupole varies as roughly the square of its magnitude.

3-C. Carbon Dioxide.

In this case the PVT data comes from the equation of state of Altunin and Gadetski(9) and the heat capacities and other data is from Newitt et al.(10). The comparisons are given in Table (III-9) and Table (III-10) in which the results of Singer et al. have been included for comparison. Here the effect of the quadrupole moment is most marked, bringing close agreement with the experimental data in all cases except for β_V, which is the reverse of the Lennard-Jones system. It must therefore be presumed that the quadrupole plays a major role in determining the thermodynamics of Carbon Dioxide. The system was matched to the experimental data at 233° K giving

$$(T'/T) = .9784 \quad : \quad (\sigma'/\sigma) = .996363$$

$$\varepsilon/k = 132.18 \quad : \quad \sigma = 2.978\times10^{-10} \quad : \quad Q = -4.22\times10^{-26} \text{esu cm}^2$$

It should be noted that the renormalization parameters (T'/T) and (σ'/σ) are both very close to unity, justifying the validity of the transformation in this case.

4. Thermodynamic Perturbation Theory.

The use of the principle of corresponding states in the determination of the properties of the associated real fluids relies on the three conditions previously stated. It was seen for angle-dependent

TABLE (III-9).

T/K	V_m/cm^3mol^{-1}			$-E/kJmol^{-1}$		
	Exp	LJ	LJ+Q	Exp	LJ	LJ+Q
218	37.55	38.79	37.50	9.73	9.61	9.86
233	39.46	40.44	39.46	8.59	8.59	8.59
253	42.72	43.03	42.42	6.99	7.14	6.89
273	47.35	46.19	45.86	5.27	5.61	5.19
293	-	-	49.91	3.12	3.74	3.49

TABLE (III-10).

T/K	$\beta_v=(\partial P/\partial T)_{vm}/v_{ar}K^{-1}$			$C_v=(\partial E/\partial T)_{vm}/Jmol^{-1}K^{-1}$		
	Exp	LJ	LJ+Q	Exp	LJ	LJ+Q
218	14.4	15.3	17.4	-	28.6	35.4
233	12.5	14.0	15.4	31.7	28.3	34.4
253	10.1	12.2	12.2	37.1	27.6	32.8
273	8.1	9.0	8.6	37.3	26.0	30.9
293	-	-	4.3	-	22.5	28.7

potentials, these conditions were only fulfilled for small changes in the parameters. However, in the cases of Nitrogen and Chlorine the scaling, particularly of the energy is not small.

As has been seen in Chapter II both the Lennard-Jones and the Quadrupolar potentials can be expressed as angle dependent potentials which can then be angle-averaged to give "effective" single-centre temperature dependent potentials. These potentials can then be used to study the expected variation of the thermodynamic quantities of these systems using thermodynamic perturbation theory, and the way these quantities change when the parameters of the system are scaled.

The subject of thermodynamic perturbation theory has been extensively reviewed, in particular by Smith(11), Rowlinson(4), Streett and Gubbins(12) and Barker and Henderson(13,14). Here the λ-expansion method of Zwanzig(15) and Barker and Henderson(16) will be used. This relies on rewriting the interparticle potential as the sum of two terms; the first a reference potential $u_o(r)$, which characterizes a system whose properties have already been established and a perturbing potential $u_1(r)$, giving

$$U(r) = U_o(r) + \lambda u_1(r) \qquad \text{(III-17)}$$

where the parameter λ varies from 0 to 1 enabling the perturbing potential to be gradually switched on. The perturbation expansion of the free energy can be written as a Taylor series about $\lambda=0$ (in the thermodynamic limit)

$$A = A_o + \lambda\left(\frac{\partial A}{\partial \lambda}\right)_{\lambda=0} + \frac{\lambda^2}{2}\left(\frac{\partial^2 A}{\partial \lambda^2}\right)_{\lambda=0} + \ldots \qquad \text{(III-18)}$$

Now substituting equation (III-17) into the expression for the configurational integral equation (III-4) then using equation (III-7) the first term in the series is found as

$$\left(\frac{\partial A}{\partial \lambda}\right)_N = \frac{\int \ldots \int \exp(-U/kT).U_1.d\underset{\sim}{r}_1.d\underset{\sim}{r}_2 \ldots d\underset{\sim}{r}_N}{Z_N} \qquad \text{(III-19)}$$

This can be rewritten as the sum of $N(N-1)/2$ identical terms giving

$$\left(\frac{\partial A}{\partial \lambda}\right)_N = \frac{\frac{1}{2}\int U(r_{12}) \left[N(N-1) \int \ldots \int \exp(-U/kT) d\underset{\sim}{r}_3 \ldots d\underset{\sim}{r}_N\right] d\underset{\sim}{r}_1 d\underset{\sim}{r}_2}{Z_N} \qquad \text{(III-20)}$$

where the definition of the two particle distribution function is

$$\rho_N^{\lambda}(r_{12}) = \left[N(N-1) \int \ldots \int \exp(-U/kT) d\underset{\sim}{r}_3 \ldots d\underset{\sim}{r}_N\right] \qquad \text{(III-21)}$$

which is simply related to the radial distribution function in the thermodynamic limit (i.e. $N \to \infty$) by

$$\rho^{\lambda}(r_{12}) = \rho^2 g^{\lambda}(r_{12}) \qquad \text{(III-22)}$$

where ρ is simply the number density of the system N/V. Thus the first term in the expansion is

$$\left(\frac{\partial A}{\partial \lambda}\right) = \frac{N\rho}{2} \int u_1(r_{12}) g^{\lambda}(r_{12}) dr_{12} \qquad \text{(III-23)}$$

The second term in the series is derived in a similar manner, but results in a much more complicated expression, which in the thermodynamic limit is given by

$$(kT)\left(\frac{\partial^2 A}{\partial \lambda^2}\right) = -\frac{1}{2}\int\int \rho^{\lambda}(12)\left[u_1(12)\right]^2 d\underset{\sim}{r}_1 d\underset{\sim}{r}_2$$

$$-\int\int\int \rho^{\lambda}(123) u_1(12) u_1(23) d\underset{\sim}{r}_1 d\underset{\sim}{r}_2 d\underset{\sim}{r}_3$$

$$-\frac{1}{4}\int\int\int\int \left[\rho^{\lambda}(1234) - \rho^{\lambda}(12)\rho^{\lambda}(34)\right] u_1(12) u_1(34) d\underset{\sim}{r}_1 d\underset{\sim}{r}_2 d\underset{\sim}{r}_3 d\underset{\sim}{r}_4$$

$$+\rho^2 \frac{kT}{4N}\left(\frac{\partial \rho}{\partial p}\right)_T^{\lambda}\left[\int\int \left(\frac{d\rho^{\lambda}(12)}{d\rho}\right) u_1(12) d\underset{\sim}{r}_1 d\underset{\sim}{r}_2\right]^2 \qquad \text{(III-24)}$$

The required derivatives are given in both cases by the limit $\lambda \to 0$, at which g^{λ} becomes the distribution function of the reference system g_o.

The only reference system whose properties have been very extensively investigated is the hard-sphere system. Thus perturbation theory is dependent on relating the properties of the system of interest to those of an equivalent hard-sphere fluid with a perturbation applied to it. Fortunately nearly all interatomic potentials can be expressed as the sum of a steeply repulsive short range term and a long range attractive term that is slowly varying. It is then possible to treat the short range repulsive part as a reference potential, which may be related to an equivalent hard sphere system. This can be accomplished using the method of Barker and Henderson(17), in which the total interatomic potential is written as

$$u(r) = u_o(r) + u_1(r) \qquad \text{(III-25)}$$

where

$$u_o(r) = u(r) \quad : \quad u_1(r) = 0. \qquad r < \delta$$

$$u_o(r) = 0 \quad : \quad u_1(r) = u(r) \qquad r > \delta \qquad \text{(III-26)}$$

where δ can be chosen either as the minimum or the first zero of the potential. The correspondence between the two systems is then made using a Taylor series expansion, setting

$$\exp[-u(r)/kT] = 1-\Theta(d+(r-d)/\alpha-\delta)\exp[-U_o(d+(r-d)/\alpha)/kT]$$

$$+ \Theta(d+(r-d)/\alpha-\delta) \qquad \text{(III-27)}$$

where $\Theta(x)$ is the Heaviside unit step function. Substitution of this form into the configurational integral and then using equation (III-7) and expanding about $\alpha=0$ gives

$$A_o = A_{HS}-\alpha 2\pi N\rho kT\, d^2 g_{HS}(d)\{d-\int_o^\infty [1-\exp(-U_o(z)/kT]dz\} + O(\alpha^2) \qquad \text{(III-28)}$$

Thus the equivalent hard sphere system is simply chosen by annuling the first order term in α, i.e. choosing d such that

$$d = \int_o^\delta [1-\exp(-u_o(r)/kT)]dr \qquad \text{(III-29)}$$

This gives good results for dense fluids but fails to account for any density dependence of the system, being a function of temperature only.

Density dependence of the reference system was introduced by Weeks, Chandler and Andersen(18) and independently by Gubbins et al.(19), both of whom separate the potential using equation (III-25) but choose different separation criterion, such that the division is about the minimum of the potential R_{min}, whose depth is ε_{min} enabling purely repulsive and attractive potentials to be defined

$$U_o(r) = u(r) + \varepsilon_{min} \quad : \quad U_1(r) = -\varepsilon_{min} \qquad r < R_{min}$$

$$U_o(r) = 0 \qquad : \quad U_1(r) = U(r) \qquad r > R_{min} \qquad \text{(III-30)}$$

The equivalent hard-sphere system may now be found by the expansion of $\exp[-u_o(r)/kT]$ about that of the hard sphere system, where the expansion parameter α can take a value between 0 and 1. Thus

$$\exp[-u(r)/kT] = \exp[-u_{HS}(r)/kT]$$

$$+ \alpha\{\exp[-u_o(r)/kT] - \exp[-u_{HS}(r)/kT]\} \qquad \text{(III-31)}$$

Substitution into the configurational integral and expansion about α=0 gives

$$A = A_{HS} - \tfrac{1}{2}N\rho\alpha\int\Delta f(r)y_{HS}(r)\,d\underset{\sim}{r} + O(\alpha^2) \qquad \text{(III-32)}$$

where

$$\Delta f(r) = \exp[-u_o(r)/kT] - \exp[-u_{HS}(r)/kT] \qquad \text{(III-33)}$$

and

$$y_{HS}(r) = \exp[u_{HS}(r)/kT]g_{HS}(r) \qquad \text{(III-34)}$$

The diameter is then found by annuling the first order term in α, as before, giving a non-linear equation for d

$$\int\Delta f(r)y_{HS}(r)d\underset{\sim}{r} = 0 \qquad \text{(III-35)}$$

The hard sphere diameter obtained from this is both density and temperature dependent.

The thermodynamic properties of a system characterised by a potential u(r) are then approximately given by a hard-sphere fluid whose diameter d is chosen from equation (III-35), and a perturbation term given to first order by equation (III-23), where the reference distribution function used is the hard-sphere system.

It is now possible to generalize the above to the case of non-spherical molecules, the simplest form of which consists of an anisotropic perturbation to a spherical core. Thus the λ-expansion is rewritten as

$$u(r,\omega_1,\omega_2) = u_o(r) + \lambda u_1(r,\omega_1,\omega_2) \qquad \text{(III-36)}$$

which may be treated in exactly the same manner as before to give

$$\left(\frac{\partial A}{\partial \lambda}\right) = \tfrac{1}{2}N\rho\iiint g_{HS}(r)u_1(r,\omega_1,\omega_2)\, d\omega_1 d\omega_2 d\underset{\sim}{r} \qquad \text{(III-37)}$$

The second order term is also analogous to equation (III-24) with the substitution of $u_1(r,\omega_1,\omega_2)$ for $u_1(r)$ and the addition of the integrals $d\omega_1$ and $d\omega_2$ in each case. The evaluation of these integrals is often carried out by expanding the perturbing potential into spherical harmonics

$$u_1(r,\omega_1,\omega_2) = \sum_{\ell=0}^{\infty}\sum_{\ell'=0}^{\infty}\sum_{m=0}^{\infty} u^1_{\ell\ell'm}(r)\, S_{\ell m}(\Theta,\phi)S_{\ell' m}(\Theta',\phi') \qquad \text{(III-38)}$$

where Θ,ϕ and Θ',ϕ' specify the orientation of the two molecules relative to a line, length r, joining their centres of mass, and

$$S_{\ell m}(\Theta,\phi) = \left[(2\ell+\ell)\,\frac{(\ell-|m|)}{(\ell+|m|)}\right]^{\frac{1}{2}} P_\ell^{|m|}(\cos\Theta)e^{im\phi} \qquad \text{(III-39)}$$

with the following restrictions $\ell,\ell' \geq 0$, $|m| \leq \min(\ell,\ell')$. P_ℓ^m is the associated Legendre polynomial. Simplification of the above procedure can be achieved by suitable choice of reference and perturbing potentials i.e.

$$u_o(r) = \int u(r,\omega_1,\omega_2)\, d\omega_1 d\omega_2 \qquad \text{(III-40)}$$

and

$$u_1(r,\omega_1,\omega_2) = U(r,\omega_1,\omega_2) - U_o(r)$$

which automatically sets the angle-average of $u_1(r,\omega_1,\omega_2)$ to zero, such that the first order term in the expansion of the free energy is zero.

$$\left(\frac{\partial A}{\partial \lambda}\right) = \tfrac{1}{2}N\rho \int g_{HS}(r) \left[\iint u_1(r,\omega_1,\omega_2) d\omega_1 d\omega_2\right] d\underset{\sim}{r} = 0 \qquad \text{(III-41)}$$

The second order term can also be simplified and expressed as

$$kT\left(\frac{\partial^2 A}{\partial \lambda^2}\right) = -\tfrac{1}{2}N\rho \sum_{\ell\neq\ell'\neq m}^{\infty\ \infty\ \infty} \int u^1_{\ell\ell'm}(r) g_o(r)\, d\underset{\sim}{r}$$

$$-N\rho^2 \sum_{\ell=0}^{\infty} \int u^1_{\ell 00}(r_{12}) u^1_{\ell 00}(r_{23}) P(\cos\Theta_{23}) d\underset{\sim}{r}_{12} d\underset{\sim}{r}_{23} \qquad \text{(III-42)}$$

where Θ_{23} is the angle between $\underset{\sim}{r}_{12}$ and $\underset{\sim}{r}_{23}$. Multipolar perturbations such as dipole and quadrupole interactions have no terms of order $u^1_{\ell 00}(r)$ in the spherical harmonic expansion of the potential, and thus the second integral in equation (III-42) vanishes. A similar simplification takes place for the third order term in the λ-expansion(20), giving

$$(kT)^2 \left(\frac{\partial^3 A}{\partial \lambda^3}\right) = \rho^3 \int\ldots\int g_o(123) u_1(r_{12},\omega_1,\omega_2) u_1(r_{13},\omega_1,\omega_3)$$

$$+ U_1(r_{23},\omega_2,\omega_3) d\underset{\sim}{r}_1 d\underset{\sim}{r}_2 d\underset{\sim}{r}_3 d\omega_1 d\omega_2 d\omega_3 \qquad \text{(III-43)}$$

This λ-expansion technique may also be used to calculate the radial distribution function $g(r,\omega_1,\omega_2)$ for which the general result corresponding to equation (III-42) is

$$g(r_{12},\omega_1,\omega_2) = g_o(r_{12}) - (1/kT) u_1(r_{12},\omega_1,\omega_2) g_o(r_{12})$$

$$-(\rho/kT) \int \left[u_1(r_{13},\omega_1,\omega_3) + u_1(r_{23},\omega_2,\omega_3)\right] g_o(123) d\underset{\sim}{r}_3 d\omega_3 \qquad \text{(III-44)}$$

For multipolar potentials the integral in equation (III-44) vanishes. This method has been used to second order by Gubbins and Gray(21) to investigate single-centre Lennard-Jones fluids with weak quadrupole moments.

The above method is only valid for systems whose repulsive core interactions are either spherical, or for systems in which the bond length of the molecule is small compared with the atomic repulsive core diameter, enabling a spherical molecular core approximation to be made. This would be valid in the cases of Fluorine, Nitrogen and Methane for example.

Systems which do not have approximately spherical cores must be treated in a different manner. This is usually accomplished by choosing a reference fluid which itself has non-spherical cores of approximately the same shape, such as systems of hard elipsoids or hard dumbells. The properties of these systems have been established using computer simulation or integral equation techniques, which are fully discussed in Chapter V. Perturbation theory for the attractive part of the potential may now be applied in a similar manner to the above using the spherical harmonic expansion of the radial distribution function of the

reference fluid. This technique was developed by Sandler(22), and has been applied to liquid chlorine using a hard-core interaction site reference fluid by Tildesley(23).

5. Simple Method for Non-Spherical Molecules.

In order to establish the way in which the properties of molecular fluids might be expected to scale on the application of the principle of corresponding states, a very simple model of the thermodynamics of molecular fluids is being proposed. This consists of relating the properties of the system to a reference fluid of hard dumbells whose properties have been established by computer simulation.

The molecular fluids studied consist of two-Lennard-Jones centres together with a quadrupole moment represented by fractional charges. In this case only the two Lennard-Jones centres provide strongly repulsive interactions, which enables the molecular core to be represented as a hard dumbell. However, the effective diameters of the atomic cores which make up the dumbell must be determined on an atom/atom interaction basis. This is done by calculating the effective site diameter using the Andersen, Weeks and Chandler (AWC) method described earlier, following the method of application of Verlet and Weis (24) in which the diameter d is given in terms of the Barker-Henderson diameter d_{BH} calculated from equation (III-29) but using the AWC potential separation given by equation (III-30). Thus the diameter d is written as

$$d = d_{BH}(1 + \Psi\delta) \qquad \text{(III-45)}$$

where the term $\Psi\delta$ results from the approximate solution of the non-linear equation (III-35). Verlet and Weis show that these terms can be expressed as

$$\delta = \int_0^\infty (r/d_{BH} - 1)^2 \delta u_o(r) dr \qquad \text{(III-46)}$$

where

$$\delta u_o(r) = d/dr \exp[-u_o(r)/kT] \qquad \text{(III-47)}$$

and

$$\Psi = \sigma_1/2\sigma_o$$

σ_1 and σ_2 have been derived from the Carnahan and Stirling equation of state(25) for hard sphere systems, by finding the Taylor series expansion of y_{HS} for a given distance $x = r/d$ as a function of its packing fraction η, thus

$$x^2 y_{HS}(x,\eta) = \sigma_o + \sigma_1(x-1) + \sigma_2/2(x-1)^2 + \ldots \qquad \text{(III-48)}$$

and the derivatives σ_i are given by

$$\sigma_o = (1-\tfrac{1}{2}\eta)(1-\eta)^{-3}$$

$$\sigma_1 = (2-7.5\eta+\tfrac{1}{2}\eta^2-5.7865\eta^3-1.51\eta^4)(1-\eta)^{-4} \qquad \text{(III-49)}$$

In this case the packing fraction used for the calculation of the correction term Ψ is the generalized packing fraction $\eta = \rho V_m$, where V_m is the volume of the molecule

$$V_m = (\pi/6)(d^3 + 1.5Ld^2 - 0.5L^3) \qquad \text{(III-50)}$$

The atomic site diameter calculated in this way is then a function of both density and temperature.

The properties of the equivalent hard-core reference system can now be calculated from the equation of state of a hard dumbell fluid established from computer simulation by Tildesley and Street(25) who expressed the equation of state in the form

$$\frac{PV}{NkT} = \frac{1+(1+u\ell^*+V\ell^{*3})\eta+(1+w\ell^*+X\ell^{*3})\eta^2-(1+y\ell^*+Z\ell^{*3})\eta^3}{(1-\eta)^3} \qquad \text{(III-51)}$$

where

$$\ell^* = L/\sigma \quad : \quad \eta = \rho Vm$$

and

$$U = 0.37836 \quad : \quad V = 1.07860 \quad : \quad W = 1.30376$$

$$X = 1.80010 \quad : \quad Y = 2.39803 \quad : \quad Z = 0.35700$$

The corresponding free energy is given by

$$\frac{A_{ex}}{NkT} = \frac{[4+A\ell^*+B\ell^{*3}]\eta-[3+C\ell^*+D\ell^{*3}]\eta^2}{(1-\eta)^2+(Y\ell^*+Z\ell^{*3})\ell n(1-\eta)} \qquad \text{(III-52)}$$

where

$$A = (U+Y) \quad : \quad B = (Z+V)$$

$$C = \tfrac{1}{2}(U-W+3Y) \quad : \quad D = \tfrac{1}{2}(V-X+3Z)$$

The attractive part of the potential may now be calculated using the angle averaged potential discussed in Chapter II. This allows the perturbation to be treated as spherically symmetric. The excess free energy can now be calculated using equations (III-23) and (III-24), for an effectively spherical system, whose diameter d_{sph} is defined as equivalent to the effective volume of the hard dumbell particle. This

is achieved by finding the excluded volume of the hard dumbell molecule (i.e. the volume of a given dumbell particle into which no other dumbell particle of the same size can penetrate). This excluded volume V_{ex} has been exactly expressed by Isihara(26) as a complicated function of diameter and bond length. The diameter d_{sph} is then given by

$$d_{sph} = \sqrt[3]{6V_{ex}/\pi} \qquad \text{(III-53)}$$

Here d_{sph} is also a function of temperature and density, as the atomic site diameter d is involved in the determination of V_{ex}.

Thermodynamic perturbation theory for potentials of multipolar symmetry has been extensively discussed by Stell et al.(27,28,29), in the context of effective angle-averaged multipolar potentials, which is in keeping with the present treatment. They show that the free energy of a system with quadrupolar interactions, using the λ-expansion method, may be written as

$$A = A_o + A_2^Q + (A_{2,2}^Q + A_3^Q) \qquad \text{(III-53)}$$

where

$$A_2^Q = \frac{\rho}{2kT} \int g_{HS}(r)\, \bar{u}_Q^{(2)} d\underset{\sim}{r}$$

$$A_{2,2}^Q = \frac{\rho}{2(kT)^2} \int g_{HS}(r)\, \bar{u}_Q^{(3)}\, d\underset{\sim}{r} \qquad \text{(III-54)}$$

and

$$A_3^Q = \left(\frac{\rho}{kT}\right)^2 \int g_{HS}(r_{12},r_{13},r_{23})\, \bar{u}_{TQ}^{(3)} d\underset{\sim}{r}_2 d\underset{\sim}{r}_3$$

The first order term A_1 vanishes as the angle-average of the quadrupole potential is zero. If the three body term A_3^Q is neglected then the contribution to the free energy of the system from the quadrupolar interactions, to second order can be expressed as the sum of the A_2 and $A_{2,2}$ terms. This corresponds to the use of an effective temperature dependent potential(27) $(u_Q^{(2)}(r) + u_Q^{(3)}(r))$, given by

$$\bar{u}_Q^{(2)}(r) = -\frac{7}{5kT}\frac{Q^4}{r^{10}}$$

$$\bar{u}_Q^{(3)}(r) = \frac{72}{245(kT)^2}\frac{Q^6}{r^{15}} \qquad \text{(III-55)}$$

which can also be obtained by the average over all angles of the square and cube of the quadrupolar potential respectively.

The quadrupolar contribution to the free energy can now be expressed in terms of the reduced variables $x = \rho d_{sph}^3$: $y = r/d_{sph}$ and $t = kTd_{sph}^5/Q^2$ as

$$A_2^Q = -\frac{14x\pi I_{10}^{HS}(x)}{5\,t^2} \qquad \text{(III-56)}$$

and

$$A_{2,2}^Q = \frac{144x\pi I_{15}^{HS}(x)}{245\,t^2} \qquad \text{(III-57)}$$

where $I_n^{HS}(x)$ represents the integral over the hard sphere radial distribution function for a potential of the form r^{-n}.

$$I_n^{HS}(x) = \int_1^\infty g_{HS}(y,x)y^{2-n}dy \qquad \text{(III-58)}$$

This integral may be evaluated for all values of n, greater than 3, as a polynomial in x, by expanding the hard sphere radial distribution function in powers of the density(30)

$$g(r) = \exp(-u_{HS}(r)/kT)\left[1+\rho g_1(r) + \rho^2 g_2(r)+\ldots\right] \qquad \text{(III-59)}$$

and using the following form

$$I_n^{HS}(x) = \frac{1}{n-3} + \sum_{m=1}^{\infty} x^m J_{mn}$$

$$J_{mn} = \int_1^{\infty} g_m(y)\, y^{2-n}\, dy \qquad \text{(III-60)}$$

where the numerical values of $g_1(y)$, $g_2(y)$ and $g_3(y)$ can be found in Kirkwood(30), Nijboer and Van Hove(31), and Ree, Keeler and McCarthy(32). This series is rapidly convergent and was terminated at m=3.

The Lennard-Jones part of the potential is also treated by the λ-expansion method for the attractive part using the effective angle-averaged potentials discussed in Chapter II. Thus we have

$$A = A_o + A_1^{LJ} + A_2^{LJ} \qquad \text{(III-61)}$$

where as before

$$A_1^{LJ} = \tfrac{1}{2}N\rho\int g_{HS}(r)\, u_{LJ}(r)\, d\underset{\sim}{r} \qquad \text{(III-62)}$$

and

$$A_2^{LJ} = -N\rho/2kT\int g_{HS}(r)\left[u_{LJ}(r)\right]^2 d\underset{\sim}{r} \qquad \text{(III-63)}$$

This result for A_2^{LJ} is only valid when 3 and higher body terms are neglected. It should be noted that the A_1 term does not vanish as in the case of potentials with multipolar symmetry. This corresponds to the use of an effective temperature dependent potential for the Lennard-Jones part given by

$$\bar{u}_{LJ}(r) = 16\varepsilon\{(\tfrac{\sigma}{r})^{12}[1 + 11(\tfrac{L}{r})^2] - (\tfrac{\sigma}{r})^6[1 + 2.5(\tfrac{L}{r})^2]\}$$

$$- \frac{256\varepsilon^2}{kT}\{(\tfrac{L}{r})^4[78.4\,(\tfrac{\sigma}{r})^{24} - 44.8\,(\tfrac{\sigma}{r})^{18} + 6.4\,(\tfrac{\sigma}{r})^{12}\} \qquad \text{(III-64)}$$

where terms of the order of $(L/r)^4$ and greater have been neglected. This can then be used to give the free energy in terms of the integrals $I_n^{HS}(x)$, where x in this case, due to the AWC separation of the potential is given by the minimum of the potential. Thus

$$A_1^{LJ} = 32\pi\varepsilon x z^6[z^6\{I_{12}^{HS}(x) + 11\ell^2 I_{14}^{HS}(x)\}$$

$$- \{I_6^{HS}(x) + 2.5\ell^2 I_8^{HS}(x)\}] \qquad \text{(III-65)}$$

where $x = \rho R_{min}^3$: $z = \sigma/R_{min}$: $\ell = L/R_{min}$. A similar expression can be written for A_2^{LJ}.

The total free energy of the system is now the sum of all these contributions

$$A = A_{id} + A_{ex}$$

$$= A_{id} + A_{HDB} + A_1^{LJ} + A_2^{LJ} + A_2^{Q} + A_{2,2}^{Q} \qquad \text{(III-66)}$$

where the ideal gas contribution A_{id} is given by

$$A_{id} = NkT\ell n\rho - NkT - 3/2NkT\ell n[2\pi mkT/h^2] \qquad \text{(III-67)}$$

The internal energy and pressure of the system can now be obtained by appropriate differentiation of the free energy

$$U = \left(\frac{\partial(A/kT)}{\partial(1/kT)}\right)_V \qquad \text{(III-68)}$$

$$P = -\left(\frac{\partial A}{\partial V}\right)_T \qquad \text{(III-69)}$$

The polynomial expansion of $I_n^{HS}(x)$ enables analytic differentiation of the free energy although the resultant expressions are rather complicated.

The results for nitrogen are shown in Figures (III-9,10), for chlorine (Q^*=0.739) in Figures (III-11,12), chlorine (Q^*=1.321) in Figures (III-13,14), chlorine (Q^*=2.073) in Figures (III-15,16) and Carbon Dioxide in Figures (III-17,18).

It can be seen from these figures that the slopes of the curves i.e. C_V and β_V are in very good agreement with the molecular dynamics calculations, the PVT points of which are also shown. However, the variation of energy with density, although changing in the correct direction is far too large. The variation of pressure with density also shows inconsistancies. In general though, given the grossness of the approximation to the attractive part of the potential, the results are remarkably good. Further terms added to the potential are divergent rather than convergent unless resummed in the manner of a suitable Padé approximant, which is beyond the scope of the present work.

This approximate method gives reasonable results over the whole range of bond lengths, whereas other perturbation methods can only handle small bond length molecules such as nitrogen. This is probably

because other methods(21) rely on the calculation of an equivalent hard-sphere fluid whose diameter is defined by $\bar{d} = \langle d \rangle_{\omega_1\omega_2}$. However, the calculation of $\bar{d}$ is very difficult and the properties of the resultant hard-sphere reference system are generally a poor representataion of the actual system. The method of Quirke et al.(34) is based on a spherically averaged reference fluid, and thus the effects of shape of the molecules can only be included through the perturbation term. Similar methods using an effective potential to find a better spherical reference fluid(35) fail for the same reasons. The method of Kohler et al.(36) using a hard dumbell reference fluid together with an effective potential is similar to the present work except in the method of choosing the diameter of the hard-dumbell fluid is based on the effective intermolecular potential matched to an effective angle averaged hard-dumbell potential. The correct choice of the diameter is crucial to determining the properties of the reference fluid. The present method based on site-site diameters is simpler and more physical as it allows direct correspondence between the system and the reference fluid to be made. Tildesley's method(23) amounts to a full solution of the RISM equations for the associated hard-dumbell fluid together with a softening of this fluid, and cannot be regarded as a true perturbation theory. This method is the same as the RISM(HTA) method of Chapter V, but does not include the effects of the attractive parts of the potential. The change in structure and thermodynamics due to this have been calculated in Chapter V. The consistancy of the present method is due to the use of the hard dumbell reference fluid which gives a better representation of the properties of the system particularly as it is based on site-site density dependent diameters. The effects of attractive and multipolar interactions can also be included in a simple way enabling the thermodynamics, but not the structure of these fluids to be determined.

The salient feature of the above calculation is the increasing non-linearity of the variation of energy and pressure with temperature as a function of increasing quadrupole moment. This is due to the increasing significance of the temperature-dependent effective quadrupole potential. It can then be deduced that the principle of corresponding states cannot be applied to these fluids except for small perturbations about a given point. Large scalings of the properties of strongly quadrupolar fluids cannot be valid under the corresponding states principle.

REFERENCES.

1. K. Singer, A. Taylor and J.V.L. Singer, Mol.Phys., 1977, 33, 1757.
2. J. Barojas, D. Levesque and B. Quentrec, Phys.Rev., 1973, A7, 1092.
3. K.S. Pitzer, J.Chem.Phys., 1939, 7, 583.
4. J.S. Rowlinson and F.L. Swinton, "Liquids and Liquid Mixtures" 3rd. Ed. (Butterworth Scientific, London, 1982).
5. A. Van Itterbeek and O. Verbeke, Physica, 1960, 26, 931.
6. B. Rosen (Ed.), International Tables of Selected Constants 17, Spectroscopic Data relative to Diatomic Molecules (Pergamon Press, London, 1970).
7. H. Wagenbreth, P.T.B.Mitteil, 1968, 78, 91.
8. Gmelin's Hanb.Anorg.Chem., 1968, Suppl. Vol.B, 1.
9. V.A. Altunin and O.G. Gadetski, Thermla Engng., 1971, 18, 120.
10. D.M. Newitt, M.U. Pai, N.R. Kuloor, and J.A.W. Huggins, in "Thermoldynamic Functions of Gases", (Ed. F.Din, Butterworths, London, 1956).
11. W.R. Smith, in Chemical Society S.P.R., Statistical Mechanics Vol.1 (Ed. K. Singer, Chemical Society, London, 1973).
12. W.B. Streett and K.E. Gubbins, Am.Rev.Phys.Chem., 1977, 28, 373.
13. J.A. Barker and D. Henderson, Ann.Rev.Phys.Chem., 1972, 23. 439.
14. J.A. Barker and D. Henderson, Rev.Mod.Phys., 1976, 48, 587.
15. R.W. Zwanzig, J.Chem.Phys., 1954, 22, 1420.
16. J.A. Barker and D. Henderson, J.Chem.Phys., 1967, 47, 2856.
17. J.A. Barker and D. Henderson, in "Physical Chemistry, An Advanced Treatise", Vol.8A (Ed. H. Eyring, D. Henderson and W. Tort) (Academic Press, New York, 1971).
18. J.D. Weeks, D. Chandler and H.C. Anderson, J.Chem.Phys., 1971, 54, 5237.

19. K.E. Gubbins, W.R. Smith, M.K. Tham and E.W. Tiepel, Mol.Phys. 1971, 22, 1089.

20. G. Stell, J. Rasaiah and H. Narang, Mol.Phys., 1972, 23, 393.

21. K.E. Gubbins and C.G. Gray, Mol.Phys., 1972, 23, 187.

22. S.I. Sandler, Mol.Phys., 1974, 28, 1207.

23. D.J. Tildesley, Mol.Phys., 1980, 41, 341.

24. L. Verlet and J-J. Weis, Mol.Phys., 1972, 24, 1013.

25. D.J. Tildesley and W.B. Streett, Mol.Phys., 1980, 41, 85.

26. A. Isihara, J.Chem.Phys., 1951, 19, 397.

27. G. Stell, J.C. Rasaiah and H. Narang, Mol.Phys., 1972, 23, 393.

28. G. Stell, J.C. Rasaiah and H. Narang, Mol.Phys., 1974, 27, 1393.

29. J.C. Rasaiah, B. Larsen and G. Stell, J.Chem.Phys., 1975, 63, 722.

30. J.G. Kirkwood, J.Chem.Phys., 1935, 3, 300.

31. B.R.A. Nijboer and L. van Hove, Phys.Rev., 1952, 85, 777.

32. F.H. Ree, R.N. Keeler and S.L. McCarthy, J.Chem.Phys., 1966, 44, 3407.

33. P.S.Y. Cheung and J.G. Powles, Mol.Phys., 1975, 30, 921.

34. N. Quirke, J.W. Perram and G. Jacucci, Mol.Phys., 1980, 39, 1311.

35. F. Kohler, W. Marius, N. Quirke, J.W. Perram, C. Hoheisel and H. Breitenfelder-Manske, Mol.Phys., 1979, 38, 2057.

36. F. Kohler, N. Quirke and J.W. Perram, J.Chem.Phys., 1979, 71, 4128.

FIGURES.

(III-1) E^* vs. T^* for $L^* = 0.608$

Key: $S \equiv Q^* = 0.739$, $M \equiv Q^* = 1.321$, $L \equiv Q^* = 2.073$

Solid line $\rho^* = 0.55$: Dashed line $\rho^* = 0.48$

(III-2) P^* vs. T^* for $L^* = 0.608$ - Key as for (III-1)

(III-3) E_o^* vs. ρ^*

Solid lines

N : $Q^* = 1.159$, $L^* = 0.328$

S : $Q^* = 0.739$, $L^* = 0.608$

M : $Q^* = 1.321$, $L^* = 0.608$

L : $Q^* = 2.073$, $L^* = 0.608$

C : $Q^* = 2.039$, $L^* = 0.793$

Dashed Lines - Results of Singer et al.(1) for N_2, Cl_2 and CO_2

(III-4) P_o^* vs. ρ^* - Key as for (III-3)

(III-5) $(\partial E^*/\partial T^*)\rho^*$ vs. ρ^* - Key as for (III-3)

(III-6) $(\partial P^*/\partial T^*)\rho^*$ vs. ρ^* - Key as for (III-3)

(III-7) $E^*(p^*=0)$ vs. T^* - Key for (III-3)

(III-8) $\rho^*(p^*=0)$ vs. T^* - Key as for (III-3)

(III-9) P(atm) vs. T(K) for N_2($L^* = 0.328$, $Q^* = 1.159$)

Lines - Theory from Equation (III-66)

Points - MD simulation

(III-10) U(J/mol) vs. T(K) for N_2 ($L^* = 0.328$, $Q^* = 1.159$)

Key as for (III-9)

(III-11) P(atm) vs. T(K) for Cl_2($L^* = 0.608$, $Q^* = 0.739$)

Key as for (III-9)

(III-12) U(J/mol) vs. T(K) for Cl_2 ($L^* = 0.608$, $Q^* = 0.739$)

Key as for (III-9)

(III-13) P(atm) vs. T(K) for Cl_2 ($L^* = 0.608$, $Q^* = 1.321$)

Key as for (III-9)

(III-14) U(J/mol) vs. T(K) for Cl_2 (L* = 0.608, Q* = 1.321)

Key as for (III-9)

(III-15) P(atm) vs. T(K) for Cl_2 (L* = 0.608, Q* = 2.073)

Key as for (III-9)

(III-16) U(J/mol) vs. T(K) for Cl_2 (L* = 0.608, Q* = 2.073)

Key as for (III-9)

(III-17) P(atm) vs. T(K) for CO_2 (L* = 0.793, Q* = 2.039)

Key as for (III-9)

(III-18) U(J/mol) vs. T(K) for CO_2 (L* = 0.793, Q* = 2.039)

Key as for (III-9)

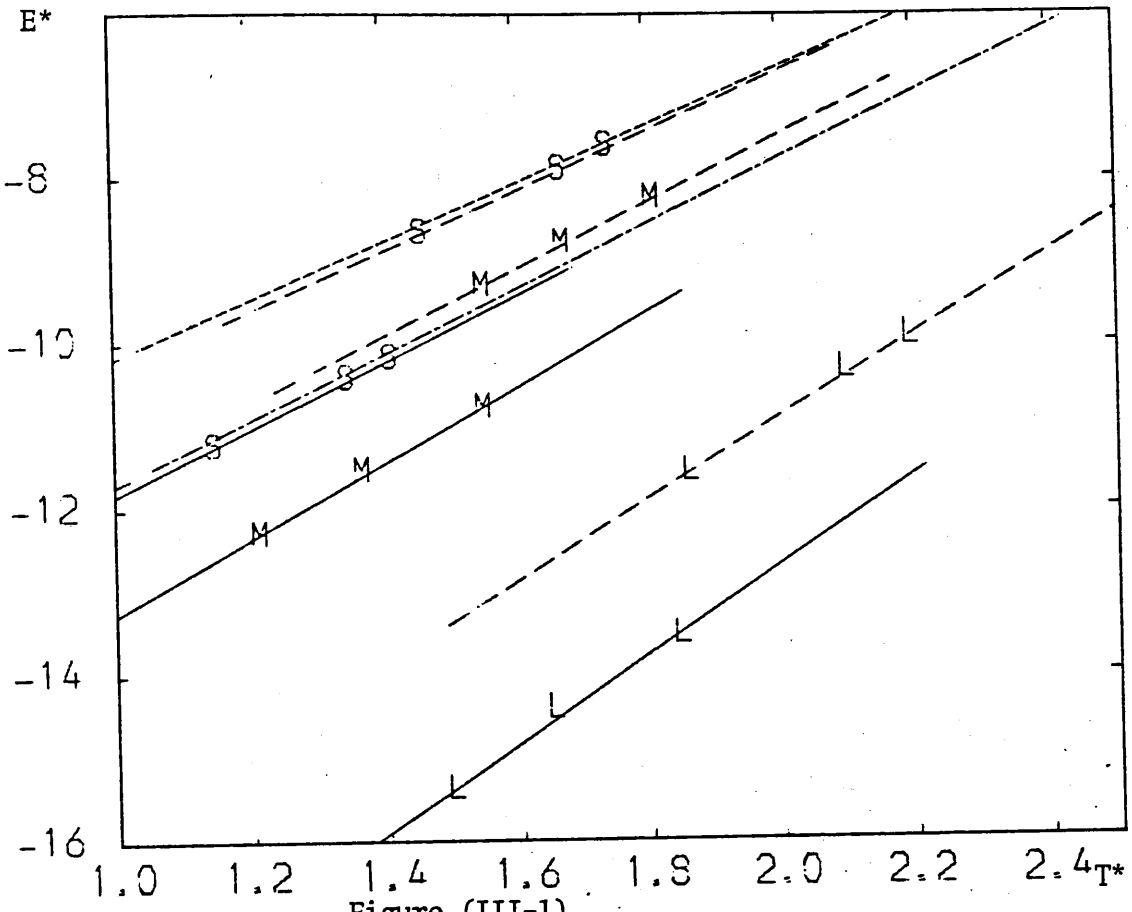

Figure (III-1)

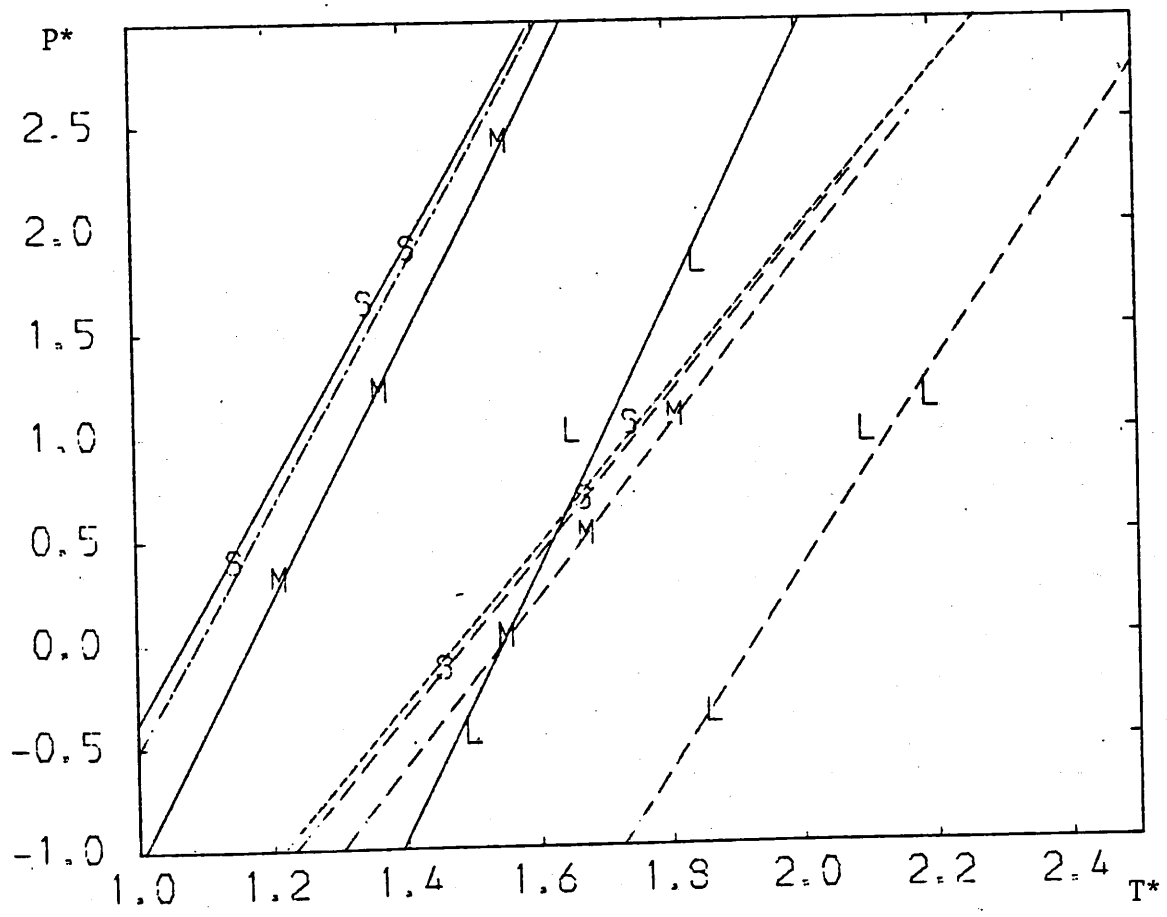

Figure (III-2)

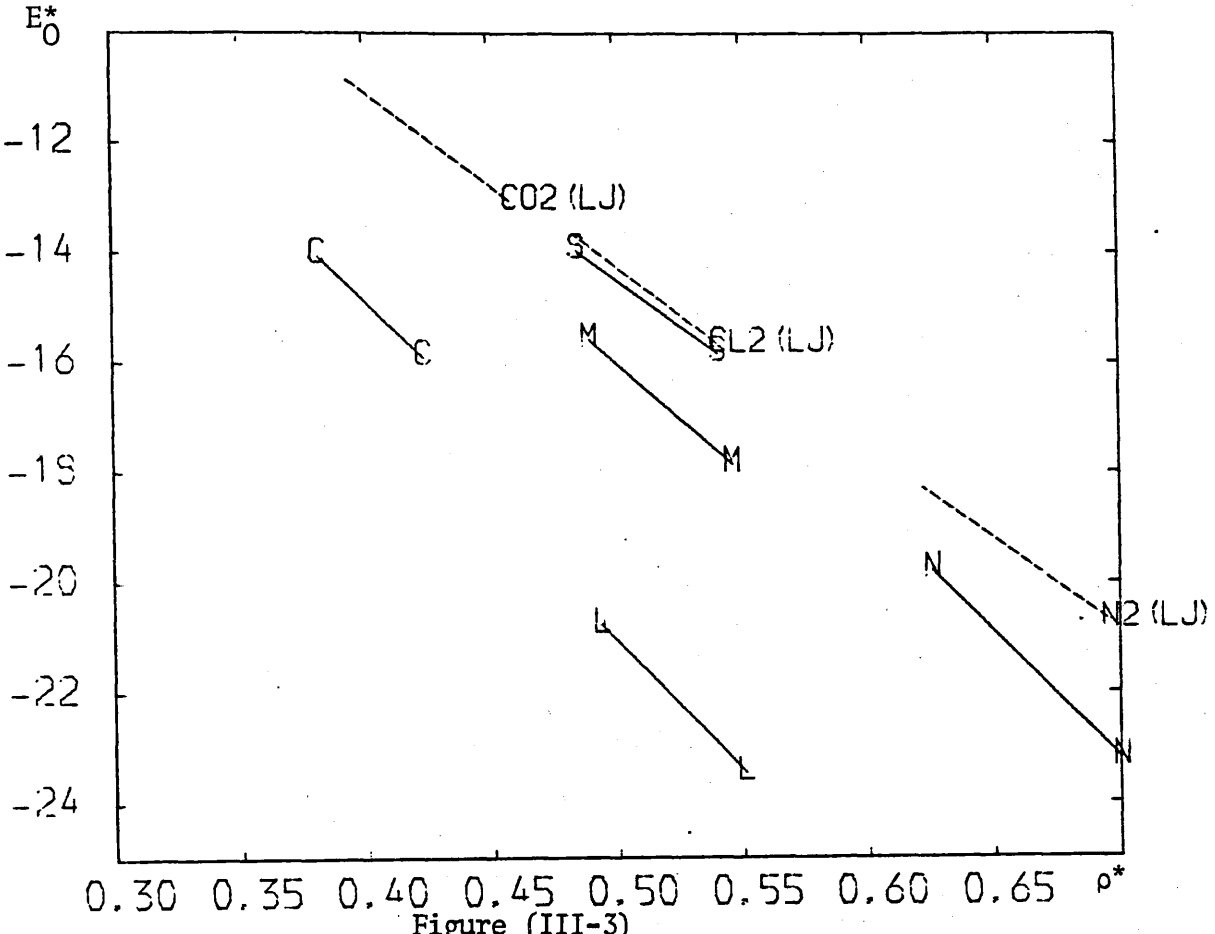

Figure (III-3)

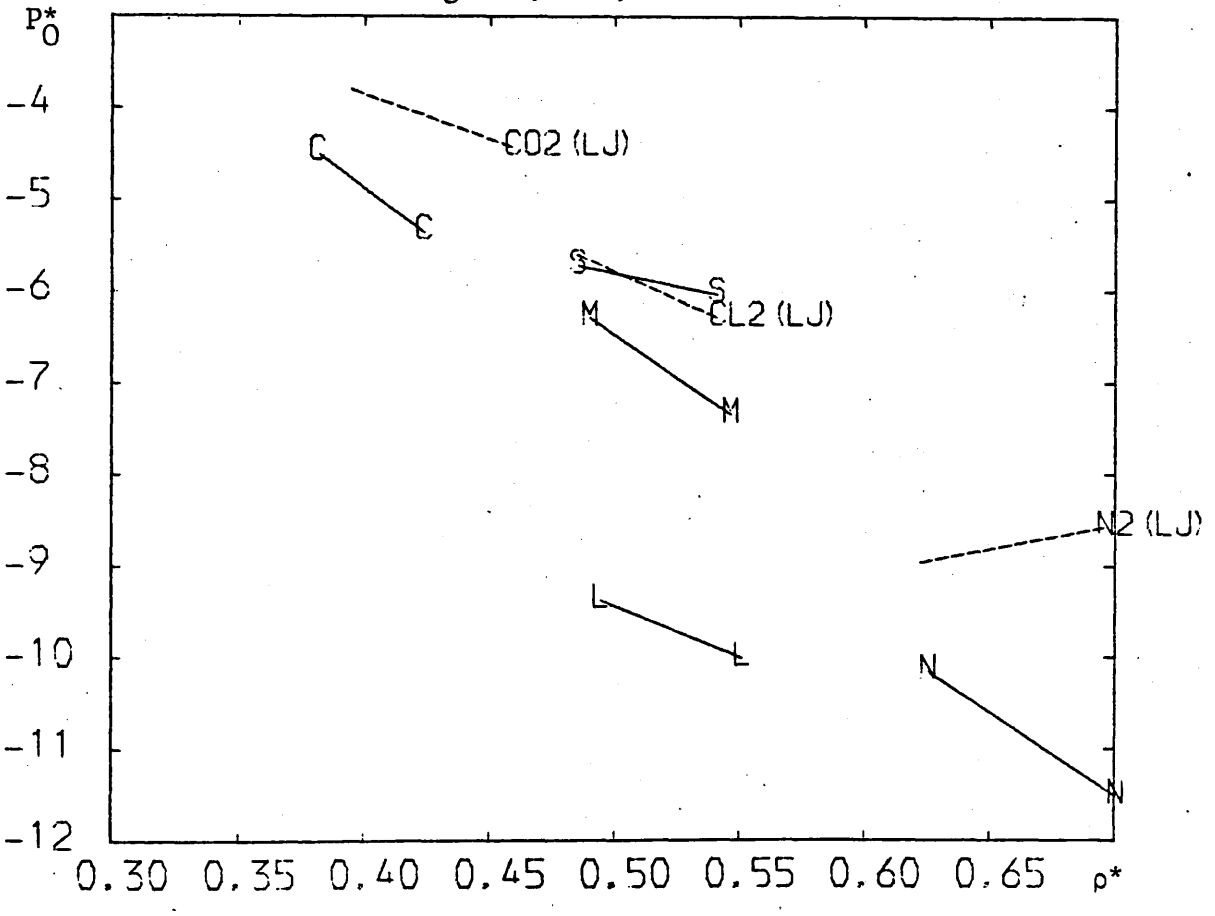

Figure (III-4)

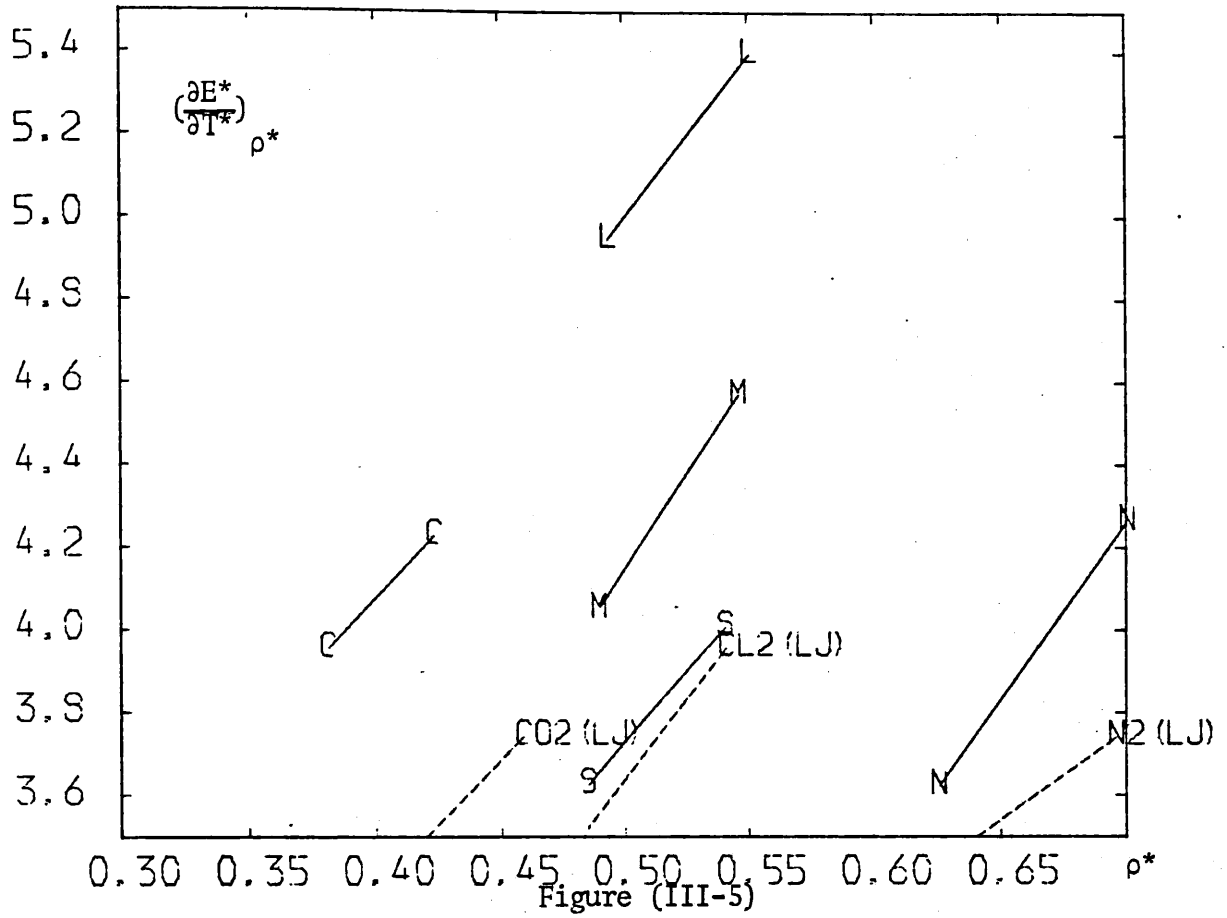

Figure (III-5)

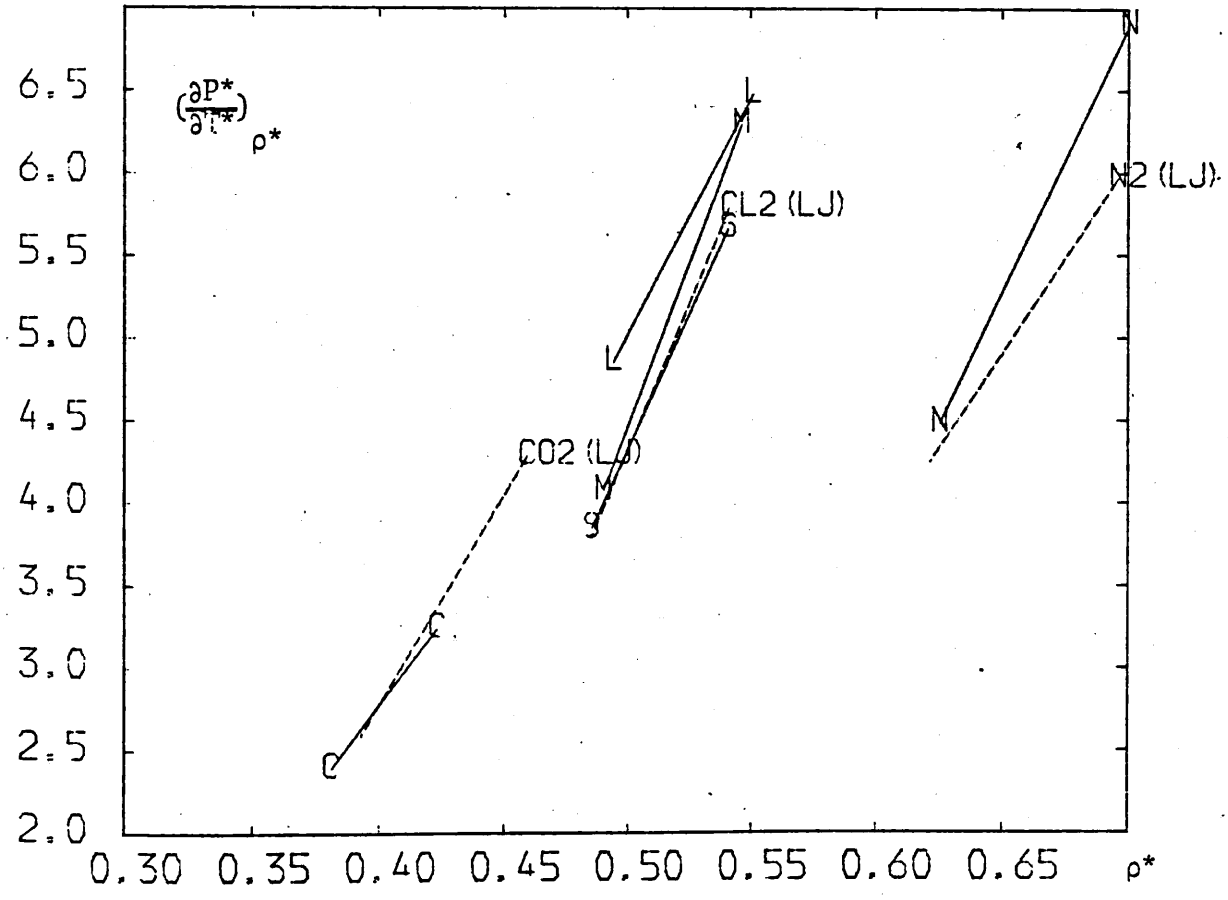

Figure (III-6)

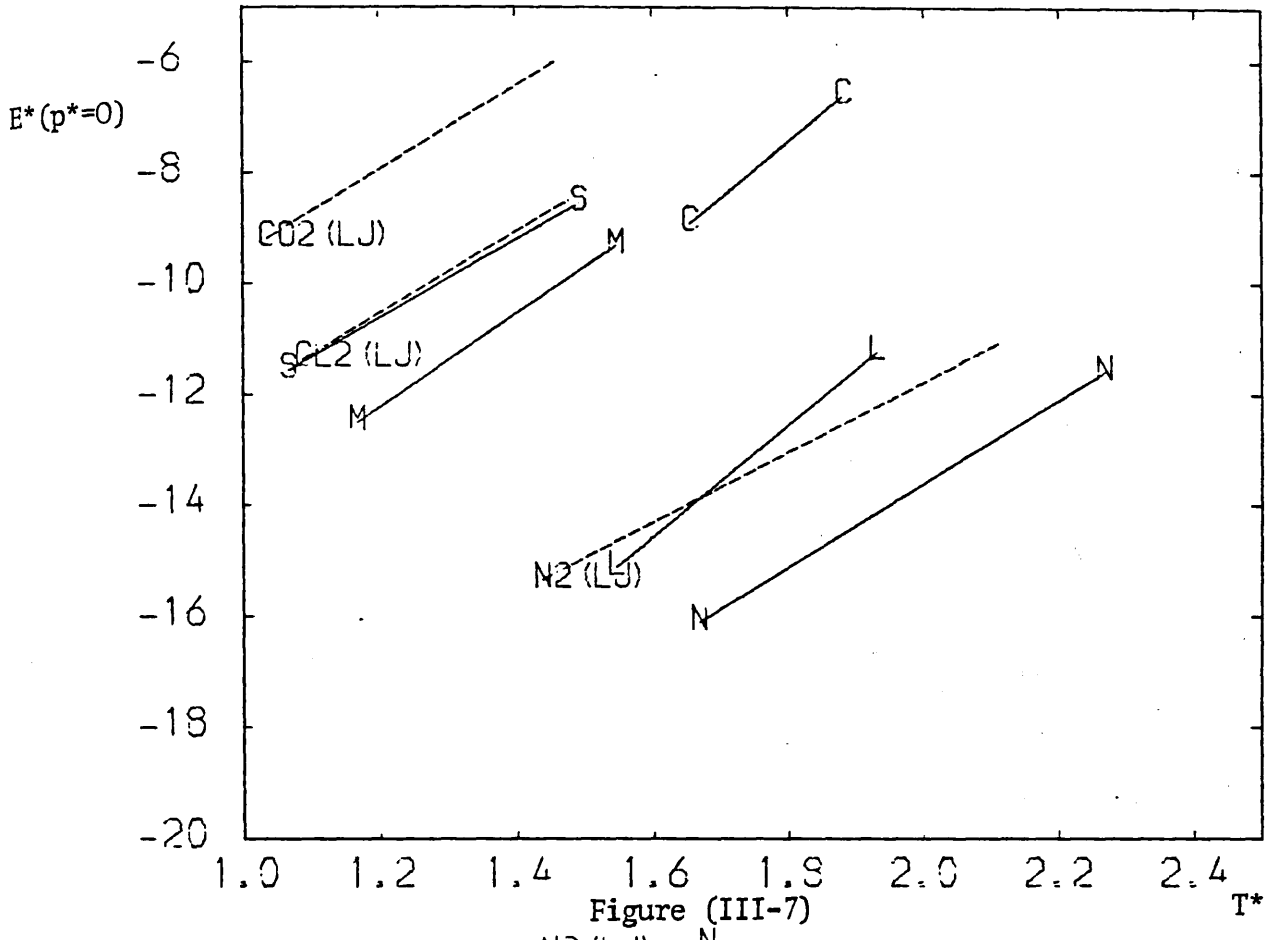

Figure (III-7)

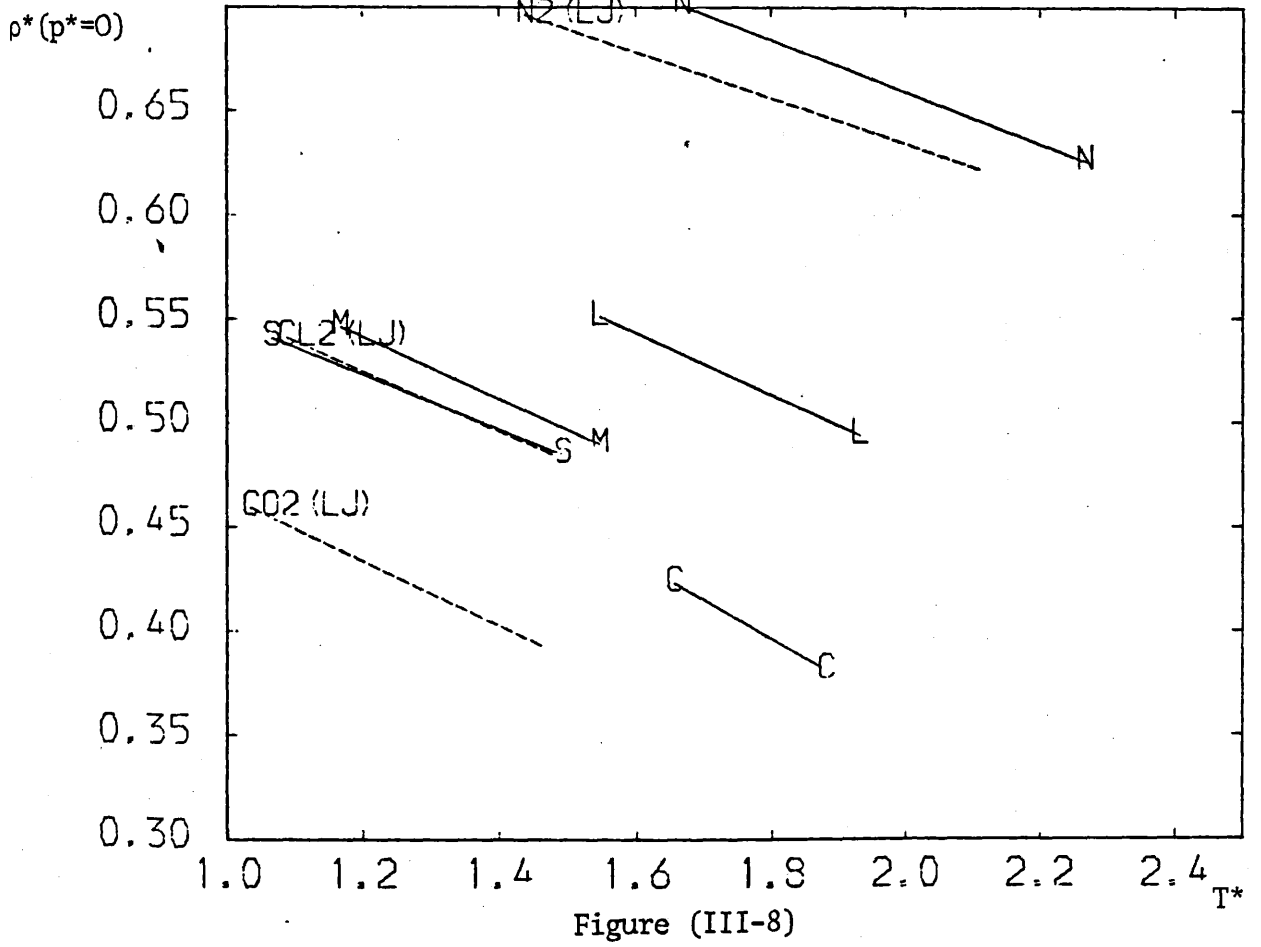

Figure (III-8)

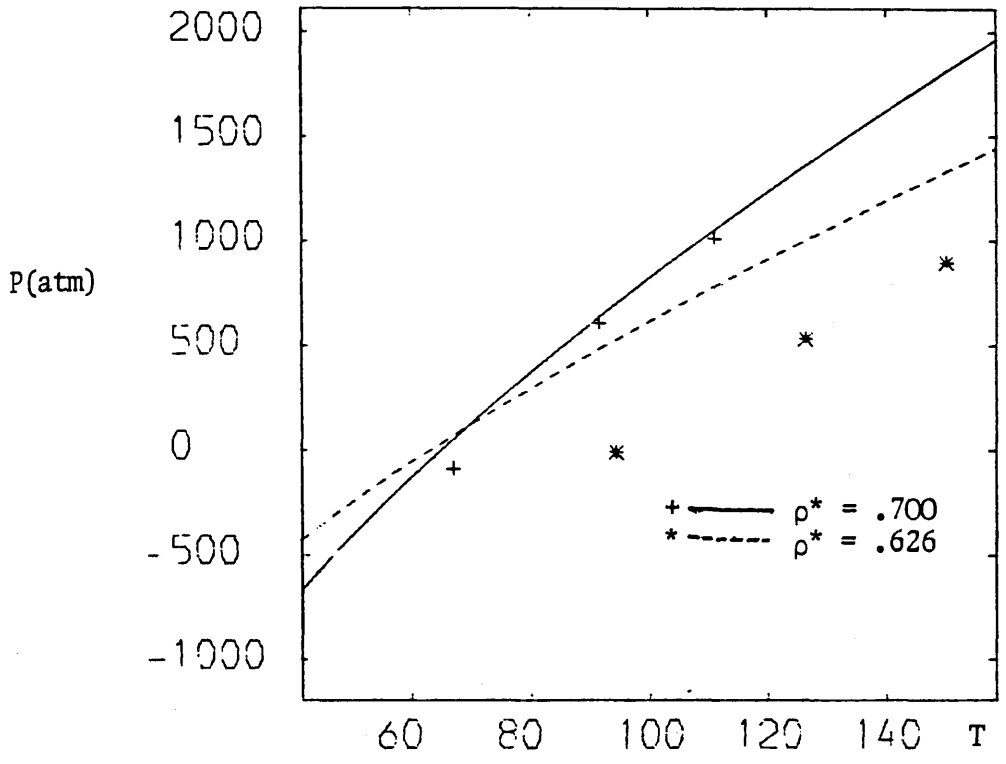

N_2(Q* = 1.159)

Figure (III-9)

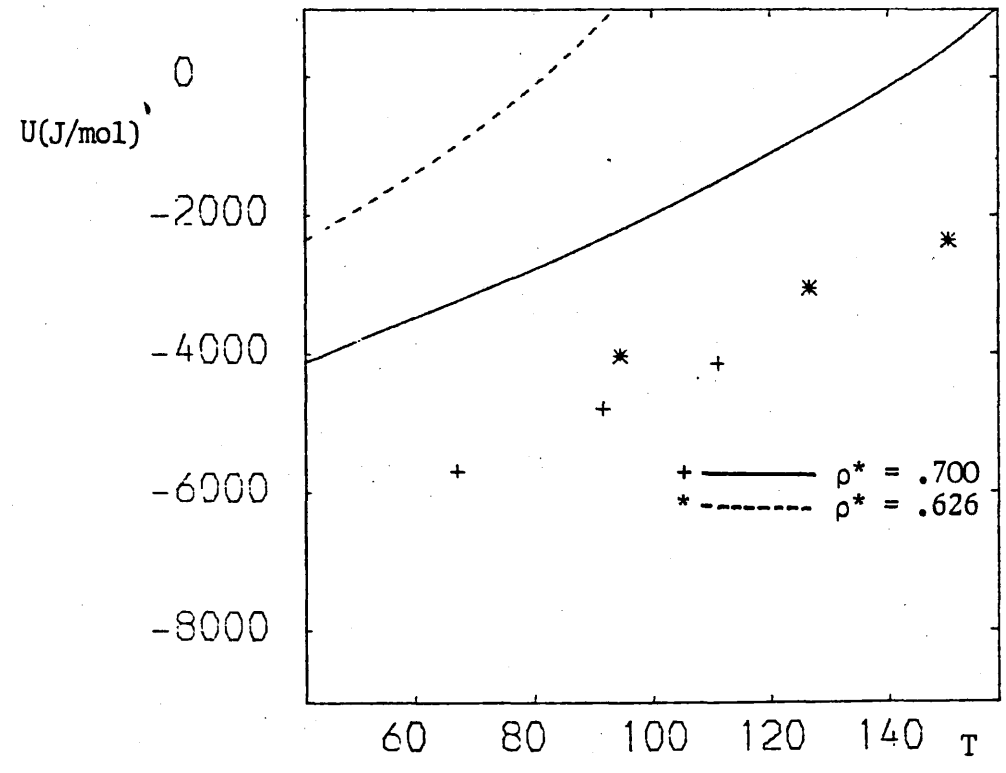

Lines - Theory
Points - MD

Figure (III-10)

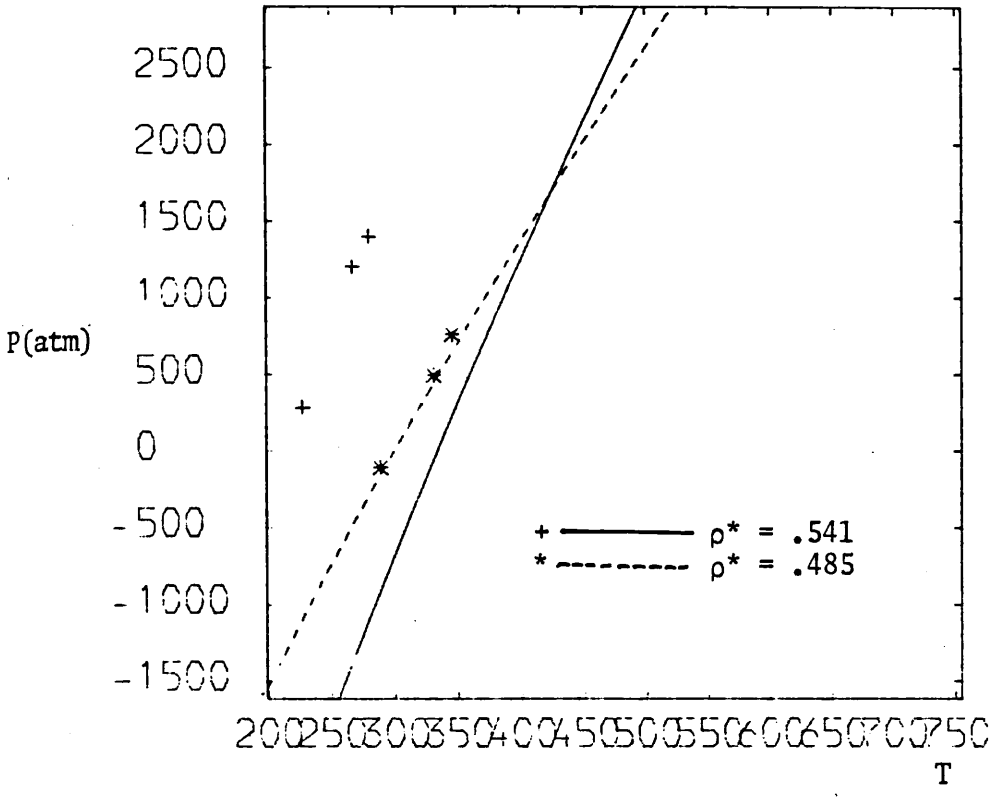

Cl_2(Q* = 0.739)

Figure (III-11)

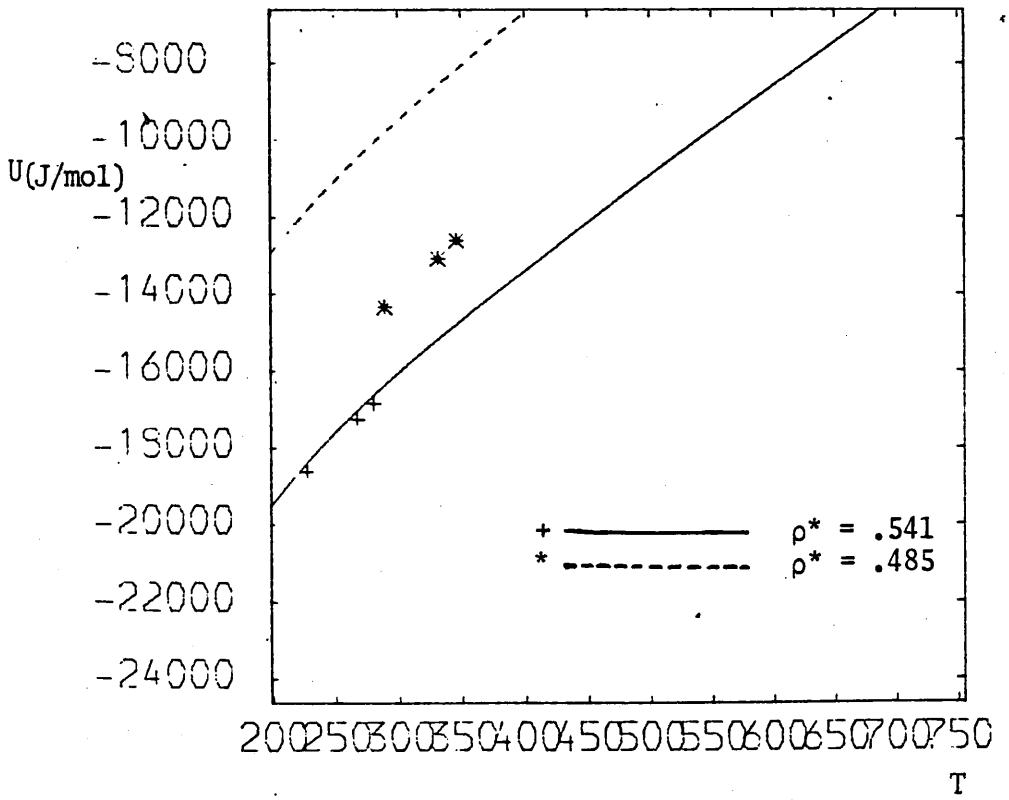

Figure (III-12)

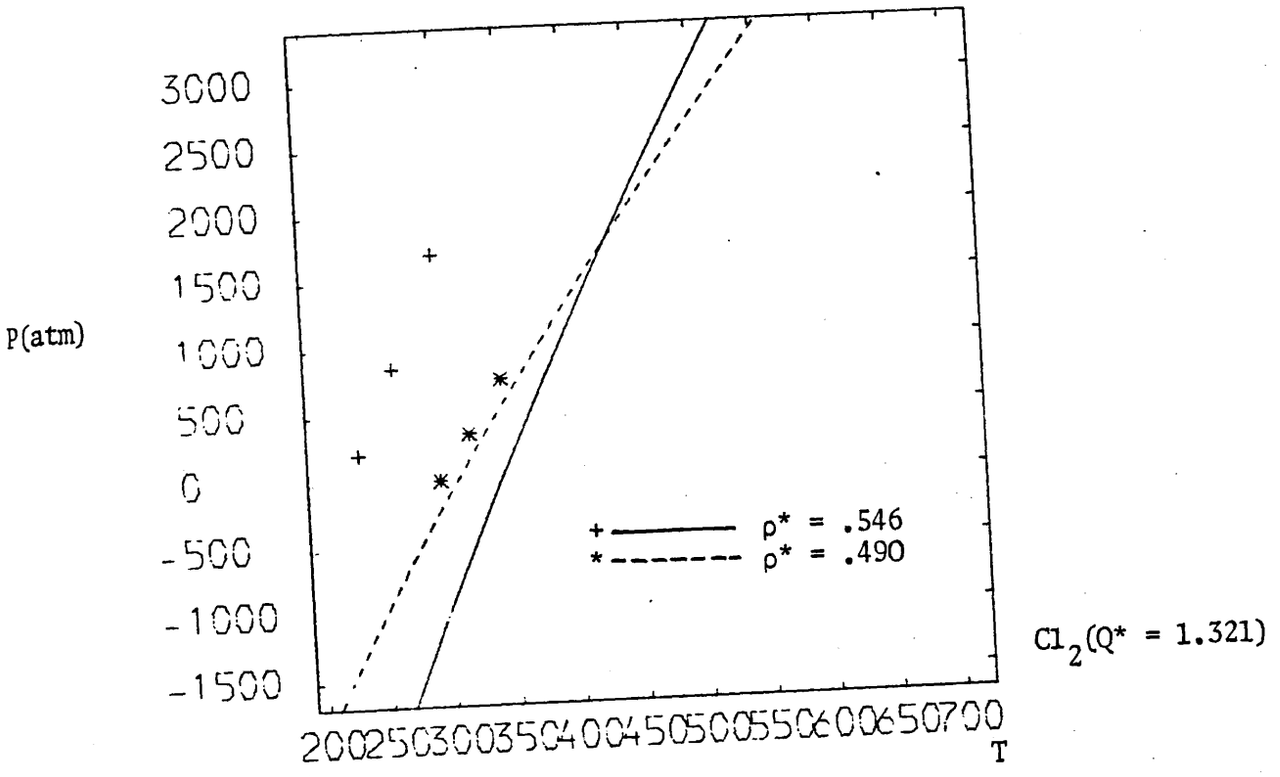

Figure (III-13)

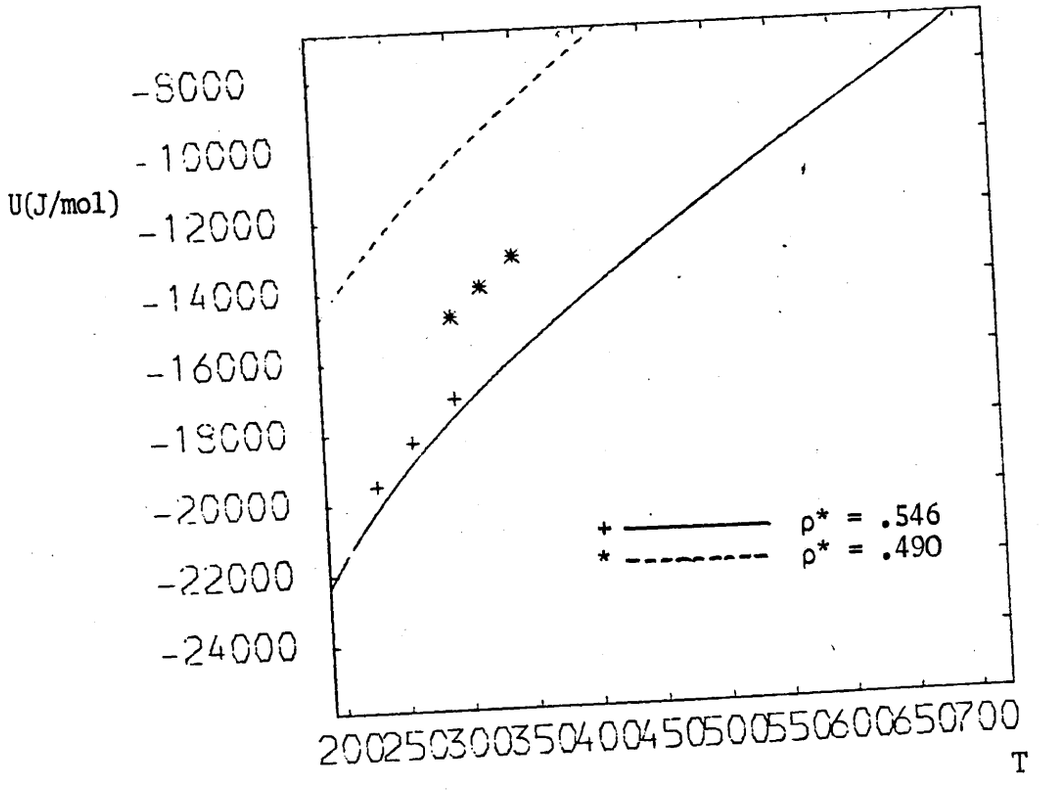

Figure (III-14)

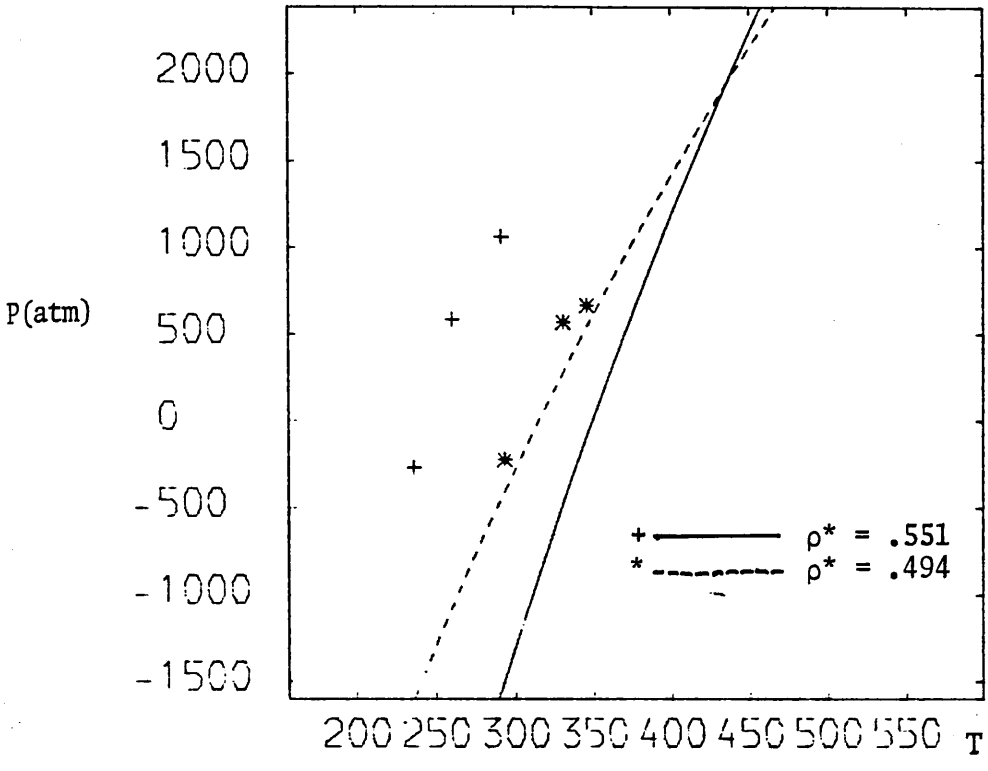

Figure (III-15)

Cl_2 (Q* = 2.073)

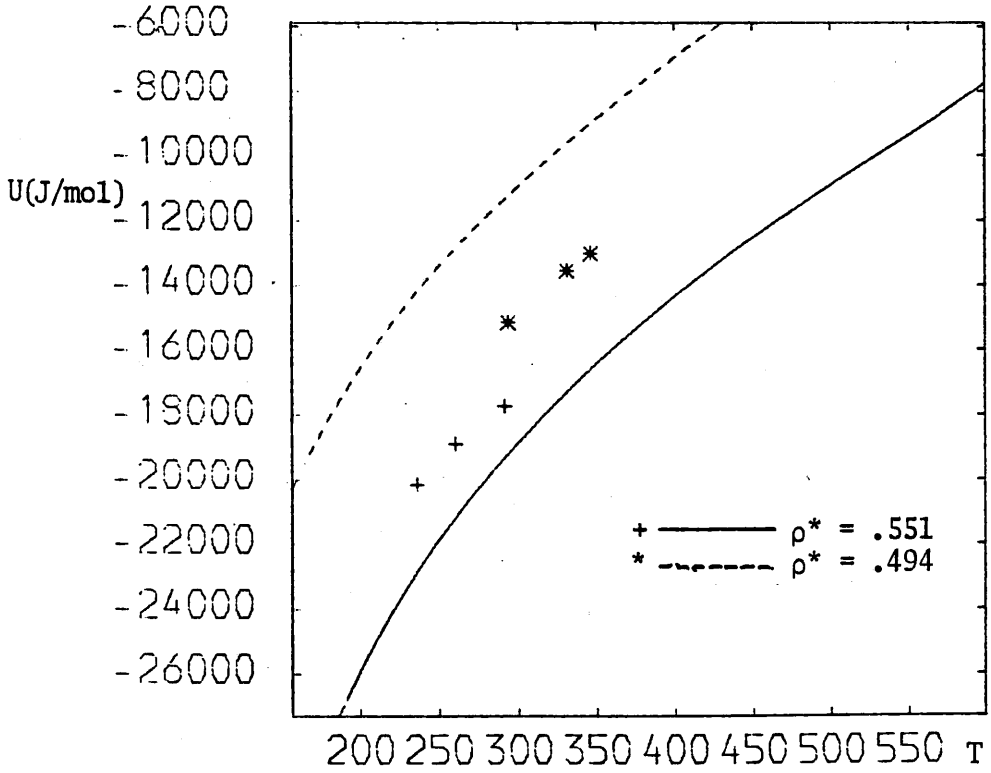

Figure (III-16)

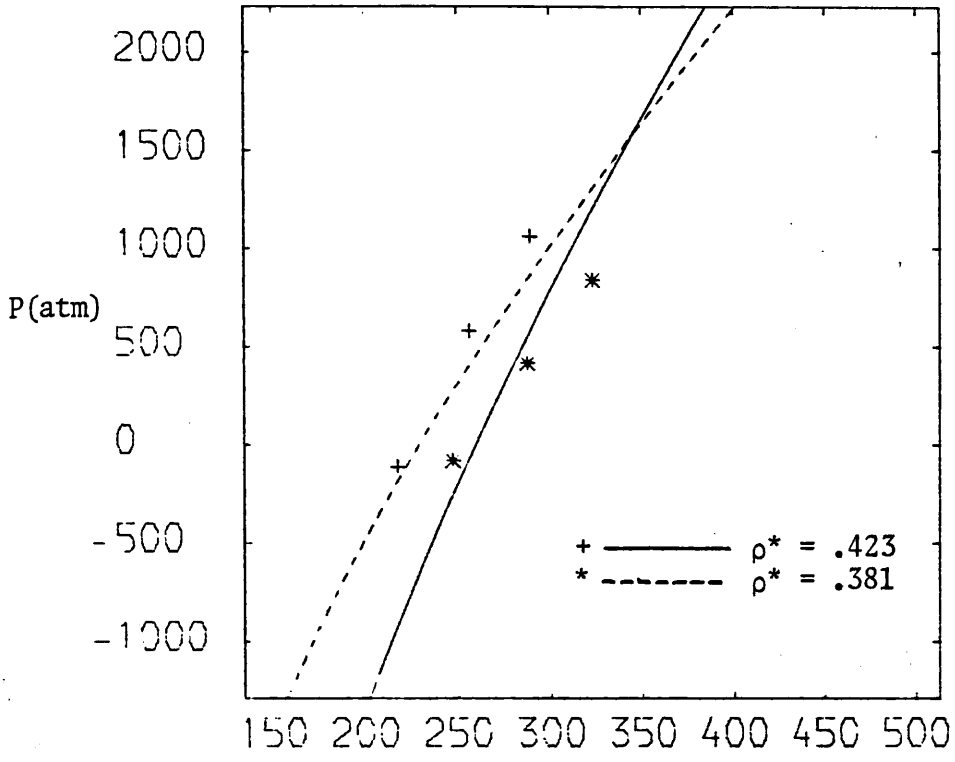

Figure (III-17)

CO_2 ($Q^* = 2.039$)

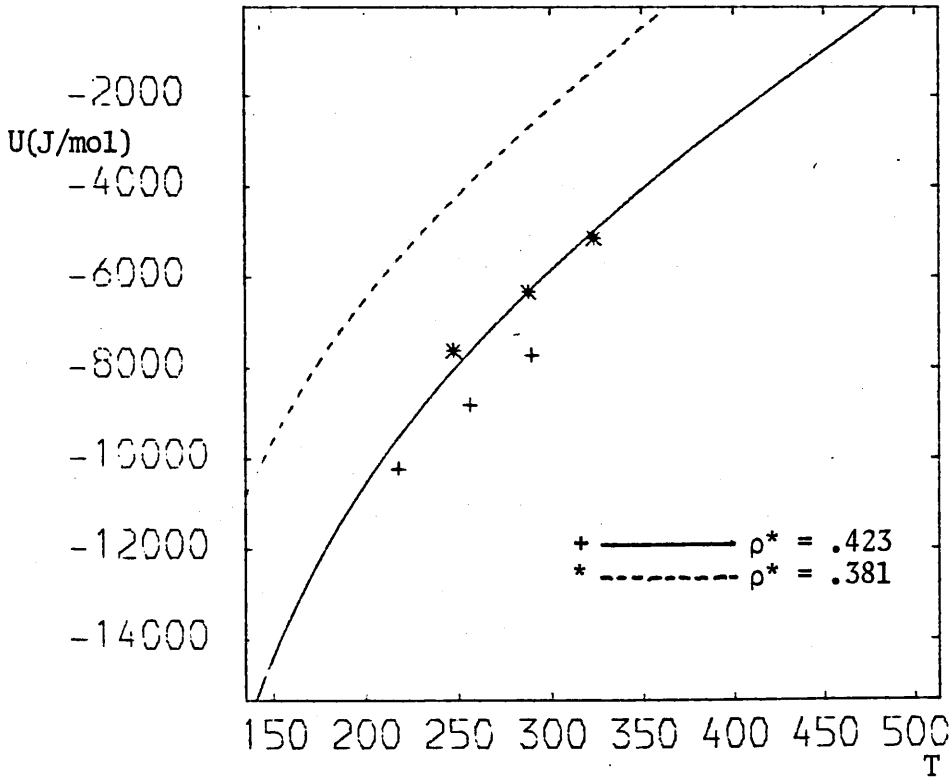

Figure (III-18)

CHAPTER IV.

Statics.

1. Introduction.

The radial distribution function, otherwise known as the pair correlation function is defined as the average number of particles n(r) situated at a distance between r and (r + Δr) from a reference particle in the limit of Δr going to zero

$$g(r) = \lim_{\Delta r \to 0} \left[n(r+\Delta r)/4\pi r^2 \rho \Delta r \right] \qquad \text{(IV-1)}$$

where ρ is the number density of the fluid.

Alternatively the angular pair correlation function may be defined in terms of a canonical ensemble of N particles whose centre of mass positions are $\underset{\sim}{r}^N \equiv \underset{\sim}{r}_1 \ldots \underset{\sim}{r}_N$ and orientations $\omega^N \equiv \omega_1 \ldots \omega_N$ and the potential energy of the system is written $U(\underset{\sim}{r}^N, \omega^N)$. The pair correlation function is then

$$g(r_{12},\omega_1,\omega_2) = \frac{\Omega^2}{\rho^2 (N-2)!} \int \frac{\exp(U/kT)\, d\underset{\sim}{r}_3 \ldots d\underset{\sim}{r}_N d\omega_3 \ldots d\omega_N}{Z_c} \qquad \text{(IV-2)}$$

where Ω has the value 4π for linear molecules. Z_c is the configuration integral given by

$$Z_c = \frac{1}{N!} \int \exp(U/kT)\; d\underset{\sim}{r}^N d\omega^N \qquad \text{(V-3)}$$

This angular function $g(r,\omega_1,\omega_2)$ is then simply related to the angle independent function by

$$g(r) = \langle g(r,\omega_1,\omega_2) \rangle_{\omega_1 \omega_2} \qquad \text{(IV-4)}$$

Site-site distribution functions may also be defined analogously to equation (IV-1), or may be expressed in terms of the angular distribution

function using the appropriate centre of mass to site vectors $\underset{\sim}{r}_{c\alpha}$ on each molecule

$$g\alpha\beta(r) = \langle g(\underset{\sim}{r}-\underset{\sim}{r}_{c1\alpha} + \underset{\sim}{r}_{c2\beta},\omega_1,\omega_2)\rangle_{\omega_1,\omega_2} \qquad \text{(IV-5)}$$

where $\underset{\sim}{r}_{c1\alpha}$ is the position of site α on molecule 1 relative to the centre of mass. The reverse process of generating the orientational spherical harmonics of the pair correlation function from the product of the site-site distribution functions is discussed in Chapter V. Reviews of the properties of pair correlation functions are given by Gray and Egelstaff, Gray and Gubbins(2).

The bulk phase thermodynamic properties can now be obtained from the configurational integral Z_c by way of the Helmholtz free energy

$$A^c = -kT\ln[Z_c] \qquad \text{(IV-6)}$$

This expression can then be differentiated to give the configurational energy and pressure of the system

$$U^c = \left(\frac{\partial(A^c/kT)}{\partial(1/kT)}\right)_V = \frac{1}{2}\rho N\int d\underset{\sim}{r}\langle g(r,\omega_1,\omega_2)U(\underset{\sim}{r},\omega_1,\omega_2)\rangle_{\omega_1,\omega_2} \qquad \text{(IV-7)}$$

$$P = -\left(\frac{\partial A}{\partial V}\right)_T = \rho kT - \frac{\rho^2}{6}\int d\underset{\sim}{r}.\underset{\sim}{r}.\langle g(r,\omega_1,\omega_2)\frac{\partial u(r,\omega_1,\omega_2)}{\partial r}\rangle_{\omega_1,\omega_2} \qquad \text{(IV-8)}$$

Other properties can also be calculated from the pair correlation function, such as the isothermal compressibility $\chi = \rho^{-1}(\partial\rho/\partial P)_T$ which is the first term in a series of equations known as the compressibility heirarchy that have been derived from the canonical ensemble by Buckingham and Graham(3)

$$\rho kT\chi = 1 + \rho\int d\underset{\sim}{r}\langle g(r,\omega_1,\omega_2)-1\rangle_{\omega_1\omega_2} \qquad \text{(IV-9)}$$

These integrals can be rewritten in terms of spherical harmonics. This is accomplished by expanding the individual angle dependent function into a series of harmonic functions(4,5,6,7,8). If the orientation of a pair of linear molecules is given by the Euler angles ω_1 and ω_2 respectively, then any function of their mutual orientation $X(r,\omega_1,\omega_2)$ can be expressed in terms of a sum over their spherical harmonics.

$$X(r,\omega_1,\omega_2) = 4\pi \sum_{\ell\ell'm} X_{\ell\ell'm}(r) Y_{\ell m}(\omega_1) Y_{\ell' -m}(\omega_2) \qquad \text{(IV-10)}$$

where the normalized spherical harmonic functions are given by

$$Y_{\ell m}(\Theta,\phi) = i^{|m|-m} \sqrt{\frac{(2\ell+1)(\ell-|m|)!}{4\pi(\ell+|m|)!}}\ P_\ell^m(\cos\Theta) e^{im\phi} \qquad \text{(IV-11)}$$

using ordinary Legendre polynomials $P_\ell^m(x)$ the properties of which are well known. The spherical harmonic functions are orthonormal

$$\int Y_{\ell m}(\omega) Y_{\ell' m'}(\omega) d\omega = \delta_{\ell\ell'} \delta_{mm'} \qquad \text{(IV-12)}$$

and the sign of the normalization factor gives the relation

$$Y_{\ell m}(\omega) = (-1)^m Y^*_{\ell -m}(\omega) \qquad \text{(IV-13)}$$

which may be used for simplification of expressions. The molecules under consideration in the present work are linear and have a centre of symmetry. This produces a type of selection rule for the indices of the spherical harmonic functions: ℓ and ℓ' must be EVEN and $|m| \leq$ Minimum of (ℓ,ℓ'). Using the orthonormal properties both sides of equation (IV-10) may be multiplied by the complex conjugate of the harmonic of any rank. and the resultant expression integrated over all angular space to give

$$X_{\ell\ell'm}(r) = (1/4\pi)\iint X(r,\omega_1,\omega_2)Y^*_{\ell m}(\omega_1)Y^*_{\ell',-m}(\omega_2)d\omega_1 d\omega_2 \qquad \text{(IV-14)}$$

Integrals with indices $\ell\ell'm$, for linear molecules, which do not obey the above 'selection rule' will be zero. It should be noted that on changing from Euler angles to the orientation angles illustrated in Figure (II-1) of Chapter II, a factor 2π is needed due to the contraction $d\phi_1 d\phi_2 \equiv 2\pi d\phi_{12}$

$$\frac{1}{4\pi}\int d\omega_1 d\omega_2 \equiv 1/2 \int_0^{2\pi} d\phi_{12} \int_0^{\pi} d\theta_1 \sin\theta_1 \int_0^{\pi} d\theta_2 \sin\theta_2 \qquad \text{(IV-15)}$$

Equation (IV-14) can now be used as the formal definition of the ensemble average of the product $Y^*_{\ell m}(\omega_1)Y^*_{\ell',-m}(\omega_2)$ with suitable normalization from

$$16\pi^2 X_{ooo}(r) = \iint X(r,\omega_1,\omega_2)d\omega_1 d\omega_2 \qquad \text{(IV-16)}$$

Thus the harmonic expansion functions are given by

$$X_{\ell\ell'm}(r) = 4\pi X_{ooo}(r)\langle Y^*_{\ell m}(\omega_1)Y^*_{\ell',-m}(\omega_2)\rangle_{\omega_1,\omega_2} \qquad \text{(IV-17)}$$

This may then be used in conjunction with equation (IV-1) for the evaluation of the spherical harmonics of the pair distribution function within a spherical shell of thickness Δr from the computer simulation. The ensemble average in equation (IV-17) may be rewritten in terms of the orientational angles(8) shown in Figure (II-1) to give

$$\langle Y_{\ell\ell'm}(\theta_1,\theta_2,\phi_{12})\rangle_{\theta_1,\theta_2,\phi_{12}} \equiv \langle Y^*_{\ell m}(\omega_1)Y^*_{\ell',-m}(\omega_2)\rangle_{\omega_1\omega_2}$$

and

$$Y_{000} = 1/4\pi$$
$$Y_{200} = \sqrt{5}/8\pi(3q_1^2-1)$$
$$Y_{220} = 5/16\pi(3q_1^2-1)(3q_2^2-1)$$
$$Y_{221} = -15/8\pi(q_1q_2p_1p_2S)$$
$$Y_{222} = 15/32\pi p_1^2p_s^2(2S^2-1)$$
$$Y_{400} = 3/32\pi(35q_1^4-30q_1^2+3) \qquad \text{(IV-18)}$$

where

$$q_1 = \cos\Theta_1 \quad : \quad q_2 = \cos\Theta_2$$
$$p_1 = \sin\Theta_1 \quad : \quad p_2 = \sin\Theta_2$$
$$S = \cos\phi_{12}$$

Only terms up to 400 are used in the present work although further terms in this series are given by Streett and Tildesley(8) who also discuss the series convergence.

Experimentally the structure of a fluid is determined by X-ray or Neutron Diffraction, from which the structure factor S(k) can be deduced. A general treatment of this is given by Steele and Pecora(10), while a detailed discussion of neutron diffraction from molecular fluids is given by Gubbins et al.(11). Here the discussion will be confined to neutron diffraction, as X-ray scattering methods are less sensitive to angular correlations between molecules(12), due to the electron density distribution of many molecules being nearly spherical.

In the static approximation the differential cross-section for all nuclei in the sample $d\sigma/d\Omega$ is the sum of the coherent and incoherent parts (Coherent scattering is usually elastic giving rise to diffraction, while the incoherent part, due to a number of processes, is essentially structureless and angle independent.

$$\frac{d\sigma}{d\Omega} = \sum_{ij\alpha\beta} \langle b_{i\alpha} b_{j\beta} \exp(i\underset{\sim}{k}.\underset{\sim}{r}_{i\alpha j\beta})\rangle = \left(\frac{\partial\sigma}{\partial\Omega}\right)_{con} + \left(\frac{\partial\sigma}{\partial\Omega}\right)_{inc} \qquad \text{(IV-19)}$$

where $\underset{\sim}{r}_{i\alpha j\beta} = \underset{\sim}{r}_{i\alpha} - \underset{\sim}{r}_{j\beta}$ is the distance between a pair of scattering sites (atomic nuclei) α and β on molecules i and j respectively. The individual terms are

$$\left(\frac{\partial\sigma}{\partial\Omega}\right)_{inc} = N_a \sum_{\alpha} \left[(\bar{b}_{\alpha})^2 - b_{\alpha}^2\right]$$

$$\left(\frac{\partial\sigma}{\partial\Omega}\right)_{con} = \sum_{ij} \sum_{\alpha\beta} b_{\alpha} b_{\beta} \langle \exp(i\underset{\sim}{k}.\underset{\sim}{r}_{i\alpha j\beta})\rangle = N_a (\Sigma b_{\alpha})^2 S(k) \qquad \text{(IV-20)}$$

where b_{α} is the coherent scattering length of nucleus α and the bar denotes the average scattering length. Values of the scattering lengths and X-ray scattering amplitudes are given by Bacon(13). The frequency dependent structure factor $S(k,\omega)$ can also be obtained by studying the energy dependence of the scattered neutrons as a function of scattering angle giving $\partial^2\sigma/\partial\Omega\partial E \propto S(k,\omega)$. This can be performed using a pulsed neutron source (spallation source) and measuring the time of flight of the neutrons. Returning to the frequency independent structure factor S(k), the coherent term can be rewritten using

$$\underset{\sim}{r}_{i\alpha j\beta} = \underset{\sim}{R}_{ij} + (\underset{\sim}{r}_{ci\alpha} - \underset{\sim}{r}_{cj\beta}) \qquad \text{(IV-21)}$$

using the notation of equation (IV-5), enabling separation of the structure factor into self (intra) and distinct (inter) terms

$$S(k) = S_{inter}(k) + S_{intra}(k)$$

$$S_{intra}(k) = \frac{1}{(\Sigma b_{\alpha})^2} \sum_{\alpha\beta} \langle \exp(i\underset{\sim}{k}.(\underset{\sim}{r}_{ci\alpha} - \underset{\sim}{r}_{ci\beta}))\rangle \qquad \text{(IV-22)}$$

$$S_{inter}(k) = \frac{1}{N_a(\Sigma b_\alpha)^2} \sum_{i\neq j} \sum_{\alpha\beta} \langle \exp(i\underset{\sim}{k}.\underset{\sim}{R}_{ij}) \exp(i\underset{\sim}{k}.(\underset{\sim}{r}_{ci\alpha} - \underset{\sim}{r}_{cj\beta})) \rangle \quad \text{(IV-23)}$$

It can now be seen that $S_{inter}(k)$ can be rewritten in terms of the site-site distribution functions $g_{\alpha\beta}(r)$ giving

$$S_{inter}(k) = \frac{\rho}{(\Sigma b_\alpha)^2} \sum_{\alpha\beta} b_\alpha b_\beta \int d\underset{\sim}{r} \exp(i\underset{\sim}{k}.\underset{\sim}{r}) [g_{\alpha\beta}(r) - 1] \quad \text{(IV-24)}$$

This expression enables the site-site distribution function to be determined by isotope substitution experiments, provided suitable isotopes exist. The intramolecular part of the structure factor can be simplified by assuming rigid linear molecules, which is exactly the case for the molecules in the simulation, to give

$$S_{intra}(k) = \left(\frac{1}{\Sigma b_\alpha}\right)^2 \sum_{\alpha\beta} b_\alpha b_\beta \frac{\sin(k.r_{\alpha\beta})}{(k.r_{\alpha\beta})} \quad \text{(IV-25)}$$

The intermolecular term can also be rewritten in terms of the angular pair distribution function $g(r,\omega_1,\omega_2)$ giving(11)

$$S_{inter}(k) = \rho \int d\underset{\sim}{r} \exp(i\underset{\sim}{k}.\underset{\sim}{r}) \langle [g(r,\omega_1,\omega_2) - 1]$$

$$.F(k.\omega_1)F^*(k.\omega_2) \rangle_{\omega_1,\omega_2} \quad \text{(VI-26)}$$

where

$$F(k,\omega_i) = \left(\frac{1}{\Sigma b_\alpha}\right) \sum_{\alpha} b_\alpha \exp(i\underset{\sim}{k}.\underset{\sim}{r}_{ci\alpha}) \quad \text{(IV-27)}$$

$F(k,\omega_i)$ is proportional to the scattering amplitude of molecule i in orientation ω_i. However equation (IV-26) is not a simple fourier

transform as in the monatomic case. In the limit of the site-site distances becoming zero, the intramolecular contribution of equation (IV-25) tends to 1. Similarly the intermolecular terms reduce to a fourier transform of the centre of mass radial distribution, to give for the centre of mass (or monatomic) structure factor

$$S_{CM}(k) = 1 + \rho\int d\underset{\sim}{r}\, \exp(i\underset{\sim}{k}.\underset{\sim}{r})[g_{CM}(r)-1] \qquad \text{(IV-28)}$$

The structure factor $S_{CM}(k)$ can be shown to be related to the isothermal compressibility in the small wavevector limit

$$\lim_{k\to 0} S_{CM}(k) = 1 + \rho\int d\underset{\sim}{r}[g_{CM}(r)-1] = \rho kT\chi \qquad \text{(II-29)}$$

Similarly at large wavevectors the intramolecular term becomes dominant, thus in the limit

$$\lim_{k\to\infty} S(k) = S_{intra}(k) = \sum_{\alpha} b_{\alpha}^2/(\sum_{\alpha} b_{\alpha})^2 \qquad \text{(IV-30)}$$

It is also possible to rewrite the structure factor in terms of isotropic and anisotropic contributions(11)

$$S(k) = S_{fr}(k) + S_a(k) \qquad \text{(IV-31)}$$

where $S_a(k)$ is the anisotropic structure factor and $S_{fr}(k)$ is the structure factor of the molecules in the limit of free rotation. It has been shown by Gubbins et al. that $S_{fr}(k)$ is given

$$S_{fr}(k) = S_{intra}(k) + \rho\langle F(\underset{\sim}{k},\omega_i)\rangle_{\omega_i}^2 \int \exp(i\underset{\sim}{k}.\underset{\sim}{r})[g_{CM}(r)-1]dr \qquad \text{(IV-32)}$$

where the angle average of $F(\underset{\sim}{k},\omega)$ is written as

$$<F(\underset{\sim}{k},\omega)>_{\omega} = \left(\frac{1}{\sum_{\alpha} b_{\alpha}}\right) \sum_{\alpha} b_{\alpha} \frac{\sin(k,r_{ci\alpha})}{(k,r_{ci\alpha})} \qquad \text{(IV-33)}$$

It is now possible to examine anisotropic effects in the structure factor by comparison with the isotropic (free rotor) model, to obtain information on the wavevector dependence of any anisotropy.

Related properties to the neutron scattering spectra are the mean square force $<F^2>$ and the mean square torque $<\tau^2>$. In particular the mean square torque of a molecule is involved in the fourth moments of the I.R., Raman and neutron scattering spectra, as well as being a moment of the various angular autocorrelation functions discussed in Chapters VI and VII. The torque on a molecule is

$$\underset{\sim}{\tau} = -\underset{\sim}{\nabla}_{\omega} U \qquad \text{(IV-34)}$$

where U is the intermolecular potential $U(r,\omega_1,\omega_2)$ and $\underset{\sim}{\nabla}_{\omega}$ is the angular gradient operator. The hypervirial relation may now be used

$$<\tau^2> = <(\nabla_{\omega} U)^2> = kT<\nabla_{\omega}^2 U> \qquad \text{(IV-35)}$$

where ∇_{ω}^2 is the angular Laplacian. Thus the mean square torque may be written

$$<\tau^2> = \rho kT \int d\underset{\sim}{r} <g(\underset{\sim}{r},\omega_1,\omega_2)\nabla_{\omega}^2 U(r,\omega_1,\omega_2)>_{\omega_1,\omega_2} \qquad \text{(IV-36)}$$

The angular Laplacian can be expressed as a differential angular operator, which may be applied to the spherical harmonic functions(14)

$$\nabla_\omega^2 Y_{\ell m}(\Theta,\phi) = -\ell(\ell+1)Y_{\ell m}(\Theta,\phi) \qquad \text{(IV-37)}$$

enabling the mean square torque to be expressed as

$$\langle\tau^2\rangle = -4\pi\rho kT \sum_{\ell\ell' m} \ell(\ell+1) \int d\underset{\sim}{r}\, U_{\ell\ell' m}(r) g_{\ell\ell' m}(r) \qquad \text{(IV-38)}$$

The mean square force is a factor in the calculation of isotope separation effects, vapour pressures and neutron scattering forth moments. They are also important in determining the first order (in $\hbar^2$) quantum correction to the free energy of a linear molecule. The theory of this effect is fully discussed by Powles and Rickayzan(21). It is also extensively used in transport theory models, some of which are discussed in Chapters VI and VII. The treatment follows that of the mean square torque in the use of the hypervirial relation

$$\langle F^2\rangle = \langle(\nabla U)^2\rangle = kT\langle\nabla^2 U\rangle \qquad \text{(IV-39)}$$

where ∇^2 is the radial Laplacian such that

$$\nabla^2 U(r,\omega_1,\omega_2) = \left(\frac{2}{r}\right)\frac{\partial U(r,\omega_1,\omega_2)}{\partial r} + \frac{\partial^2 U(r,\omega_1,\omega_2)}{\partial r^2} \qquad \text{(IV-40)}$$

Thus the mean square force can be written as

$$\langle F^2\rangle = \rho kT \int d\underset{\sim}{r}\langle g(r,\omega_1,\omega_2)\nabla^2 U(r,\omega_1,\omega_2)\rangle_{\omega_1,\omega_2} \qquad \text{(IV-41)}$$

$$= 4\pi\rho kT \sum_{\ell\ell' m} \int g_{\ell\ell' m}(r) \frac{d}{dr}\left(r^2 \frac{d}{dr} U_{\ell\ell' m}(r)\right) dr \qquad \text{(IV-42)}$$

The mean square force and torque are related to the average curvature of the potential near its minimum. This enables average translational

and rotational Einstein frequencies to be found

$$\omega_{tr}^2 = \langle F^2 \rangle / mkT \quad : \quad \omega_{rot}^2 = \langle \tau^2 \rangle / IkT \qquad \text{(IV-43)}$$

from which the quasi-harmonic force constants $k_{tr} = m\omega_{tr}^2$ and $k_{rot} = \mu\omega_{rot}^2$ may also be deduced.

2. Special Configuration Distribution Functions.

In order to examine the orientational properties of the various distribution functions it is useful to first look at selected special configurational distribution functions to determine whether any configurations are particularly favoured. The configurations chosen for study are:

"T"	$\Theta_1 = \pi/2$:	$\Theta_2 = 0$:	ϕ_{12}-arbitary
"Parallel"	$\Theta_1 = \pi/2$:	$\Theta_2 = \pi/2$:	$\phi_{12} = 0$
"Cross"	$\Theta_1 = \pi/2$:	$\Theta_2 = \pi/2$:	$\phi_{12} = \pi/2$

Two other configurations were also considered:

"Skew"	$\Theta_1 = \pi/4$:	$\Theta_2 = \pi/4$:	$\phi_{12} = 0$
"Long"	$\Theta_1 = 0$:	$\Theta_2 = 0$:	ϕ_{12} - arbitary

but the pair correlation functions of these are not plotted as they are not strongly favoured in the first nearest neighbour peak. In all cases the special configurational pair distribution function is calculated for an angular spread of $\pm \pi/12$ about the given angles. These special distribution functions have the same properties as the normal pair correlation functions, in particular in the limit of large distances, these functions will all tend to the bulk value of 1. The configurational pair correlation functions are plotted in Figures (IV-1A)

to (VI-5A) and the corresponding potential energy curves are plotted in Figures (IV-1B) to (IV-5B) for the same systems, which are

	L*	Q*	ρ*	T*
N_2	0.328	1.159	0.700	1.61
Cl_2	0.608	0.739	0.541	1.14
Cl_2	0.608	1.321	0.546	1.21
Cl_2	0.608	2.073	0.551	1.50
CO_2	0.793	2.039	0.423	1.61

The variation of these correlation functions with temperature and density is not simple, although the points shown are at high density, low temperature and will thus show the most distinct structure. These points will be used throughout to illustrate the effects of polarity in these systems.

The relative structure of the special configuration pair correlation functions is determined by four considerations; the depth of the minimum associated with that configuration; the position of the minimum; packing constraints and the energy distribution of the molecules which is related to the temperature of the system. Variation with temperature and density will then be determined by competition between these four factors.

The distance of closest approach is allowed by the "Cross" configuration following by the "Parallel" configuration, both of which can be expected to be dominant at small distances ($r \approx \sigma$). These two configurations are also strongly favoured by the two-centre Lennard-Jones only potential. However the introduction of a quadrupole moment represented as fractional charges will increase the potential energy of these two configurations considerably, particularly for the "Parallel" configuration. By contrast the "T" configuration ($r \approx \sigma + L/2$) will become lowered in energy by the quadrupole, as will the "Skew" configuration. The "long" configuration for geometrical reasons cannot be

present at distances less than (σ + L) and is increased in potential energy by the quadrupole. This configuration does not seem to be significant either for the Lennard-Jones only case reported by Singer et al., or in the present work where its first peak heights are substantially lower.

In the case of nitrogen shown in Figure (IV-1) the potential energy contours for the different configurations are closely spread as are the relative depths of the minima, although the presence of the quadrupole ensures that the "T" configuration is the most favoured. The resultant distribution functions reflect this with the "Cross" and "Parallel" configurations occupied equally at small distances, but the "T" configuration being the most highly populated within the first nearest neighbour shell. No strong orientational preference is shown in the second nearest neighbour shell, with all three special distribution functions being approximately equal to $g_{CM}(r)$.

Chlorine, with three different quadrupole moments shows the progressive changes in structure due to the multipole. These are illustrated in Figures (IV-2) for $Q^* = 0.739$, (IV-3) for $Q^* = 1.321$ and (IV-4) for $Q^* = 2.073$. The effect of the increased bond length can be seen to spread out the positions of the minima of various configurations. The depth of the minima for the "Cross" and "T" configurations are at least an order of magnitude greater than that of the angle-averaged centre of mass potential. As the quadrupole increases in magnitude the depth of the minimum of the "Cross" configuration becomes smaller, while that of the "T" configuration becomes very much larger. The "Parallel" configuration minimum not only becomes smaller, but at $Q^* = 2.073$ actually ceases to exist. The same is true of the "long" and "skew" configuration minima. The resultant distribution functions clearly reflect these changes. At $Q^* = 0.739$, "Parallel", "Cross" and "T" configurations have almost equal weight, with a shoulder on the small r side of the first peak of $g_{CM}(r)$ probably caused by the high

population of "Parallel" and "Cross" configurations. As the quadrupole increases to $Q^* = 1.321$ the "T" configuration has a higher occupancy at the expense of the "Parallel" and "Cross" configurations. This effect is then increased at $Q^* = 2.073$ such that the "T" configuration is completely dominant and other configurations can only be present if packing constraints of the "T" configuration allow.

It is interesting that all three quadrupole cases for chlorine, show significant orientational dependence in the second nearest neighbour shell, suggesting that strong ordering in the first shell, of whatever type, must lead to some degree of ordering in the second shell.

For carbon dioxide with both a long bond length and a strong quadrupole moment, the "Parallel", "Long" and "Skew" configurations are not favoured. The "Cross" configuration while not strongly favoured energetically allows the closest approach and is thus dominant at very small distances. However again the "T" configuration is most strongly occupied and must form a great part of the orientation of the first nearest neighbour shell. These considerations do not seem to be significant in the second nearest neighbour shell.

3. Site-site Distribution Functions.

The site-site distribution functions $G_{CM}(r)$ (centre of mass), $G_{AA}(r)$ (atom-atom) and $G_{CMA}(r)$ (centre of mass-atom), calculated directly from the simulation are shown in Figures (IV-6) to (IV-10). The variation of these correlation functions with changes in temperature, although not illustrated, are as expected, namely that the height of the first peak decreases rapidly as the temperature is increased; the rest of the structure tending towards the bulk value of 1. Similar changes take place with changes in density, i.e. the first peak height decreases with decreasing density and the rest of the structure again tends towards the bulk value. However, the changes with density are

less rapid than the variation with temperature. The points shown are the same as for the special configurational functions, as these points will show the most structure being at high density and low temperature. The shape of $G_{CM}(r)$ may be expected to be determined in the same manner as for a monatomic liquid. The calculation of this, and the variation with temperature and density are fully discussed in Chapter V. Small deviations from this behaviour may occur if a particular configuration is strongly occupied at a certain distance preventing other configurations being occupied by packing considerations.

$G_{AA}(r)$ is then a function of the magnitude of $G_{CM}(r)$, the bond length of the system and the particular types of orientation preferred at a given distance. $G_{CMA}(r)$ is also determined by the same criteria.

For nitrogen with a small bond length, where only partially hindered rotation takes place, no strong orientational preferences are found except for the "T" configuration. The first peak of $G_{CM}(r)$ is situated at $\sigma + \frac{1}{2}L$ consistant with the "T" configuration. This leads to $G_{AA}(r)$ having a weakly split first peak representing atoms on either end of the "T". $G_{CMA}(r)$ is found to be almost the exact average of $G_{CM}(r)$ and $G_{AA}(r)$, with a peak at $\sigma + \frac{1}{2}L$ again consistant with the "T" configuration.

Chlorine with the three quadrupole moment values enables study of the changes in the site-site distribution functions from the case at $Q^* = 0.739$ where "Parallel", "Cross" and "T" configurations are equally preferred to the situation at $Q^* = 2.073$ where the "T" configuration is completely dominant. The effect of this transition is most clearly seen in $G_{CMA}(r)$ where a shoulder on the small r side of the first peak, probably due to the high occupation of "Parallel" and "Cross" configurations become a split first peak at $Q^* = 2.073$ with maxima at σ and $\sigma + \frac{1}{2}L$, consistant with the dominant "T" configuration. However $G_{AA}(r)$ shows very little change as the quadrupole moment increases. The splitting

of the first peak into maxima at σ and $\sigma+L$ remains the same although the magnitude of the second is slightly increased and the position of the first moved to slightly smaller r. The principal change in $G_{AA}(r)$ is probably in the second nearest neighbour shell where the maximimum on the small r side of the second peak of $G_{CM}(r)$ at $Q^* = 0.739$ is removed and becomes a maximum on the high r side at $Q^* = 2.073$. This is possibly the effect of close packing of the "T" configurations in the first shell preventing other configurations in the second shell. The effect of the quadrupole on $G_{CM}(r)$ itself is to sharpen the features, i.e. make the maxima in each shell higher and narrower. This is almost certainly due to the increase in "T" configurations to the exclusion of others in the case of the first nearest neighbour shell.

Carbon Dioxide exhibits the same features as chlorine $Q^* = 2.073$ except that the increased bond length allows $G_{CMA}(r)$ to have the smallest interaction distances, due to the "T" configuration again. The structure of $G_{AA}(r)$ in the second shell is considerably reduced probably due to atoms from one shell overlapping into the region of the next, causing cancellation of effects.

4. Orientational Spherical Harmonics.

The orientational spherical harmonics of the centre of mass pair correlation functions, which have been calculated directly from the simulation data using equations (IV-18), (IV-17) and (IV-1), are illustrated in igures (IV-11) to (IV-15) for the same systems as before. The positions of the principle maxima, minima and zeros of these functions, together with those of the site-site distribution functions and the special configurational distribution functions discussed are given in Tables (IV-1) to (IV-5).

The usefulness of the spherical harmonic expansion is expressed by equation (IV-10), which allows a four variable function to be rewritten in terms of a single variable and a series expansion. This enables the expression of integral properties of the system, such as the mean square force and torque as a summation over harmonic functions

whose properties are well known. Further, it is possible to use the harmonic series for perturbation theory expansion of anisotropic potentials where any angular symmetry can be used to simplify the series. The interpretation of individual terms in the harmonic series, in the absence of any other information can be misleading. However, as a guide to the relative values of the harmonic expansion that might be expected from the various configurations, it is possible to use equations (IV-14) and (IV-18) to calculate the expected values assuming that the function $X(r,\omega_1,\omega_2)$ is unitary within the range $\Theta_1 \pm \pi/12$, $\Theta_2 \pm \pi/12$ etc. and zero elsewhere. This is equivalent to the assumption that all the molecules are aligned in a single configuration. These values are given in Table (IV-6). It is also possible to note the correspondence between a predominant configuration at a given distance and the values of the harmonics at that distance. For the case of the Lennard-Jones only fluids discussed by Singer et al. (15) the dominant configuration at the minimum interaction distance is the "Cross" configuration which can be seen to lead to values of $g_{200}(r) \approx -g_{000}(r)$ and $g_{220}(r) \approx g_{400}(r) \approx + g_{000}(r)$. This type of behaviour is also exhibited by the "Parallel" configuration as can be seen from Table (IV-6). Where the "T" configuration is dominant (e.g. at $R^* \approx 1.31$ for Chlorine $Q^* = 2.073$). the values of the corresponding harmonics lead to $g_{220}(r) \approx -g_{000}(r)$ which is the opposite of the previous case. It is worth noting that the contributions to $g_{221}(r)$ from the configurations discussed is minimal as can be seen from Table (IV-6). Also noteworthy is the strong contribution to $g_{222}(r)$ from the "Cross" configuration and to $g_{400}(r)$ from the "Long" configuration. Further interpretation is not strictly justified by the available data as many different configurations give rise to similar values of the individual harmonics. Conversely not all configurations contribute equally to a given harmonic as is seen from Table (IV-6).

TABLE (IV-1)

Positions and Magnitudes ( ) of the maxima, minima and zeros of the distribution functions at L* = 0.328, Q* = 1.159, ρ* = 0.700 and T* = 1.61 - Nitrogen.

R*	Maxima	Minima	Zeros
$G_{CM}(r)$	1.18(3.06),2.18(1.32)	1.68(0.49)	
$G_{200}(r)$	1.30(.33),2.41	1.11(-.71),1.97(-.10)	1.20,1.71,2.15
$G_{220}(r)$	1.05(.23),1.79,2.43	1.20(-1.60),2.11	1.10,1.66,1.85,2.36
$G_{221}(r)$		1.16(-.55)	
$G_{222}(r)$		1.20(-.15)	
$G_{400}(r)$	1.05(.11)	1.50	1.26
$G_{T}(r)$	1.17(6.59),2.20(1.56)	1.56(+.24)	
$G_{11}(r)$	1.10(2.38),2.28(1.54)	1.56(0.36)	
$G_{+}(r)$	1.07(2.57),2.12(1.55)	1.56(.43)	
$G_{-}(r)$	1.23(2.88),2.36(1.41)	1.69(.46)	
$G_{--}(r)$	1.39(1.98),2.12(2.71)	1.85(.09)	

TABLE (IV-2)

Positions and Magnitudes ( ) of the maxima, minima and zeros of the distribution functions at $L^* = 0.608$, $Q^* = 0.739$, $\rho^* = 0.541$ and $T^* = 1.14$ - Chlorine.

R*	Maxima	Minima	Zeros
$G_{AA}(r)$	1.07(2.10),1.57(1.10),2.11	1.41(.98),1.78(.85)	
$G_{CM}(r)$	1.31(2.07),2.40(1.21)	1.79(.57)	
$G_{200}(r)$	1.52(.47),2.53	1.17(-.84),2.06(-.18)	1.34,1.85,2.34
$G_{220}(r)$	1.09(.66),1.62(.19),2.81	1.32(-1.35),2.32(-.16)	1.20,1.54,2.16,2.59
$G_{221}(r)$	1.56	1.25(-.44),2.07	1.45,1.88,2.36
$G_{222}(r)$		1.01(-.15)	
$G_{400}(r)$	1.07(.40),2.12	1.48(-.17)	1.39,1.81,2.34
$G_{T}(r)$	1.32(5.09),2.31(1.53)	1.72(.27)	
$G_{11}(r)$	1.11(4.48),2.10(1.70)	1.61(.23)	
$G_{+}(r)$	1.08(5.63),2.02(1.47)	1.61(.21)	
$G_{-}(r)$	1.43(2.53),2.51(1.41)	1.99(.56)	
$G_{--}(r)$	1.75(1.97),2.48(2.54)	2.08(.03)	

TABLE (IV-3)

Positions and Magnitudes ( ) of the maxima, minima and zeros of the distribution functions at L* = 0.608, Q* = 1.321, ρ^* = 0.546 and T* = 1.21 - Chlorine.

R*	Maxima	Minima	Zeros
$G_{AA}(r)$	1.05(2.10),1.58(1.14),2.12	1.37(.95),1.82(.87)	
$G_{CM}(r)$	1.30(2.46),2.37(1.25)	1.79(.56)	
$G_{200}(r)$	1.53(.32),2.50	1.16(-.67),2.06(-.14)	1.32,1.83,2.34
$G_{220}(r)$	1.11(.38),1.69	1.32(-1.81),2.23(-.18)	1.18,1.58,2.09
$G_{221}(r)$		1.26(-.59)	2.35
$G_{222}(r)$		1.26(-.16)	
$G_{400}(r)$	1.07(.18),1.30(.27),2.06	1.55	1.15,1.22,1.40,1.94
$G_{T}(r)$	1.33(6.66),2.33(1.54)	1.72(.27)	
$G_{11}(r)$	1.19(1.82),2.10(1.49)	1.51(.27)	
$G_{+}(r)$	1.02(3.01),2.04(1.53)	1.54(.29)	
$G_{-}(r)$	1.44(2.21),2.53(1.44)	1.89(.69)	
$G_{--}(r)$	1.69(3.91),2.53(2.77)	2.01(.0)	

TABLE (IV-4).

Positions and Magnitudes ( ) of the maxima, minima and zeros of the distribution functions at L* = 0.608, Q* = 2.073, ρ* = 0.551 and T* = 1.50 - Chlorine

R*	Maxima	Minima	Zeros
$G_{AA}(r)$	1.05(2.09),1.55(1.21),2.48	1.34(.91),1.83(.88)	
$G_{CM}(r)$	1.28(2.80),2.44(1.27)	1.80(.57)	
$G_{200}(r)$	1.37(.16),2.46	1.16(-.47),1.98	1.27,1.82,2.36
$G_{220}(r)$	1.08(.13),1.72,2.60	1.28(-2.48),2.25(-.24)	1.14,1.63,1.98,2.46
$G_{221}(r)$		1.24(-.71)	
$G_{222}(r)$		1.25(-.24)	
$g_{400}(r)$	1.05,1.281(.58)	1.16(-.13),1.54(-.12)	1.08,1.20,1.42,2.12
$G_{T}(r)$	1.31(8.12),2.29(1.55)	1.86(.31)	
$G_{11}(r)$	1.16(1.04),2.53(1.94)	1.60(.28)	
$G_{+}(r)$	1.10(1.14),1.92(1.15),2.50(1.57)	1.39(.45),2.15(.85)	
$G_{-}(r)$	1.39(2.10),2.50(1.45)	1.80(1.66)	
$G_{--}(r)$	1.68(1.92),2.21(2.34)	1.77(.0)	

TABLE (IV-5).

Positions and Magnitudes ( ) of the maxima, minima and zeros of the distribution functions at $L^* = 0.793$, $Q^* = 2.039$, $\rho^* = 0.423$ and $T^* = 1.61$ - Carbon Dioxide

R^*	Maxima	Minima	Zeros
$G_{AA}(r)$	1.06(1.89),1.77(1.13)	1.44(.85)	
$G_{CM}(r)$	1.35(2.03),2.54(1.11)	2.01(.77)	
$G_{200}(r)$	1.63(.15),2.73	1.18(-.43),2.24	1.37,1.95,2.54
$G_{220}(r)$	1.10(.18),1.97	1.35(-1.60),2.39(-.17)	1.18,1.75,2.13,2.65
$G_{221}(r)$		1.29(-.62)	
$G_{222}(r)$		1.31(-.18)	
$G_{400}(r)$	1.01,1.35(.35)	1.20(-.18),1.65	1.08,1.27,1.55

TABLE (IV-6).

Relative contributions to $X_{\ell\ell'm}$ from various configurations - Assuming $X(r,\Theta_1,\Theta_2,\phi_{12}) = 1$

Using $C_{200}=\sqrt{5}/2$: $C_{220}=5/4$: $C_{221}=-15/2$: $C_{222}=15/8$: $C_{400}=3/8$

	T	"Parallel"	"Cross"	"Skew"	"Long"
X_{200}	-.058	-.073	-.073	0.17	.008
X_{220}	-.123	.076	.076	.008	.016
X_{221}	0	0	0	-.059	0
X_{222}	.092	-.003	-.112	-.0002	-.012
X_{400}	.056	.071	.071	-.017	-.183

Contributions from 11 and + same except when $m\neq 0$.

The spherical harmonics may be used to find various properties of the system. In particular the energy and pressure due to a point quadrupole (see equation (II-11)) can be expressed in terms of spherical harmonics to give

$$U_{QQ} = \tfrac{1}{2}\rho Q^2 \int_0^\infty [3/2\ g_{220}(r) - g_{221}(r) + 1/4 g_{222}(r)]\ r^{-5} d\underset{\sim}{r} \qquad \text{(IV-44)}$$

$$P_{QQ} = 5/6 \rho^2 Q^2 \int_0^\infty [3/2 g_{220}(r) - g_{221}(r) + 1/4 g_{222}(r)]\ r^{-5} d\underset{\sim}{r} \qquad \text{(IV-45)}$$

From this the approximate fractional energy due to the quadrupole can be calculated as well as the quadrupolar contribution to the pressure. These quantities are given in Table (IV-7). It is apparent that the quadrupolar contribution to the pressure is always negative and also that the quadrupolar contribution to both the energy and pressure vary in a strongly non-linear manner with the magnitude of the quadrupole moment. It is also evident that the quadrupolar pressure is much slower varying with changes in temperature than the Lennard-Jones part. The fractional quadrupolar energy, within the accuracy of the integration, is approximately constant with temperature and density.

The convergence of the harmonic series has been discussed by Streett and Tildesley(8) and found to be slow for the case of hard dumbell distribution functions. For properties dependent on integration over the harmonics of the potential $u_{\ell\ell'm}(r)$, the degree of anisotropy of the potential will determine the rate of convergence of the summation. In the present work only the first six terms have been considered. In general the use of the spherical harmonic expansion of equation (IV-7) to determine the energy of the system is unsatisfactory due to the numerical course graining of the integration points at small interaction distances.

TABLE (IV-7).

T^*	ρ^*	L^*	Q^*	U_{QQ}/U_{TOT}	P^*_{QQ}
1.11	.700	.328	1.159	.1603	-.61
2.66				.1567	-.43
2.27	.626			.1485	-.35
3.60				.1838	-.26
1.14	.541	.608	.739	.0305	-.06
1.41				.0280	-.05
1.45	.485			.0264	-.04
1.74				.0274	-.03
1.21	.546	.608	1.321	.2129	-.47
1.55				.2106	-.41
1.55	.490			.2001	-.30
1.81				.1936	-.26
1.50	.551	.608	2.073	.6605	-1.84
1.85				.6885	-1.69
1.86	.494			.6817	-1.28
2.19				.7148	-1.15
1.61	.423	.793	2.038	.6471	-.82
2.14				.7441	-.71
1.83				.6938	-.59
2.39				.8756	-.50

5. Structure Factors.

To compare the present results directly with experiment it is necessary to calculate the structure factors which are defined by equations (IV-20), (IV-24) and (IV-25). For an isotropic homonuclear diatomic liquid the atom-atom structure factor becomes

$$S(k) = 1/2\left[1+\sin(k,\ell)/(k,\ell)\right] + \rho\int_0^\infty d\underset{\sim}{r}\left[g_{AA}(r)-1\right]\sin(k,r)/(k,r) \quad \text{(IV-46)}$$

whereas the centre of mass structure factor is given by equation (IV-28) and the anisotropic structure factor by a combination of equations (IV-31), (IV-32) and (IV-46). Due to errors introduced by the finite fourier transforming of the site-site distributions values of the structure factors below $k \approx 1\text{Å}^{-1}$ have no validity due to truncation effects. The resultant structure factors are illustrated in Figures (IV-16) to (IV-19) for the same systems as before.

For nitrogen, shown in Figure (IV-16) the structure factor can be compared with the neutron scattering studies of Dore and Clarke (16,17) as well as the molecular dynamics simulation of Cheung and Powles(18) also using a two-centre Lennard-Jones potential with a point quadrupole. The present calculations are in very good agreement with the results of Dore et al., both in peak height and position, although the height of the first maximum of S(k) is approximately 0.1 too high. This is due to the temperature difference; the molecular dynamics being at 66K while the neutron scattering experiment was carried out at 77K. The first peak height reported here is almost identical to that of Cheung and Powles. The second peak in S(k), in the molecular dynamics calculation has a sub-structure of a triplet which is not observed in the neutron scattering study. The origin of this effect is not clear, and is not reported by Cheung and Powles and thus may be spurious. The resultant anisotropic structure factor $S_a(k)$ is small at all values of the wavevector, and is similar in shape

to the quadrupolar contribution to $S_a(k)$ predicted by Gubbins et al.(11).

For chlorine the structure factors are illustrated in Figures (IV-17) to (IV-19) for the three values of the quadrupole moment. Tables of peak heights and positions for these systems are given in Table (IV-8) to show the effects of changing quadrupole moment. It is clear that the general shape of $S_{CM}(k)$ remains constant as the quadrupole is increased, although the heights of the peaks are increased and the structure extended to larger wavevectors. This reflects the similar changes in $G_{CM}(r)$. The atom-atom structure factor is considerably changed by the variation of the quadrupole moment. At $Q^* = 0.739$ there is a weak shoulder on the large k side of the first peak, which is absent in the $Q^* = 0.0$ calculations of Singer et al. As the quadrupole is increased to $Q^* = 1.321$ the weak shoulder becomes a significant strong feature until at $Q^* = 2.073$ the first peak splits by 0.61 Å^{-1} with the principle part moved to smaller k by 0.1 Å^{-1}. This effect is accompanied by a decrease in the height of the first peak so that the area under $k^2S(k)$ remains constant. Throughout these changes the height, shape and position of the second peak and the large wavevector structure does not change. The change in the first peak structure is likely to be correlated to the change in shape of the second nearest neighbour peak of the atom-atom distribution function, which itself is caused by packing considerations when the first nearest neighbour shell becomes strongly orientated into the "T" configuration. These results can be compared to the neutron scattering data of Clarke et al.(19) for the Bromine system which is adjacent in the periodic table differing only in mass from the chlorine system. The results for the $Q^* = 1.321$ system are in very good agreement with the experimental values for the heights of the peaks and the magnitude of the shoulder on the first peak. However, the positions of the peaks are systematically at too high wavevectors in all cases. This may well be due to the

TABLE (IV-8).

Positions and Magnitudes of maxima and minima of the structure factors for Chlorine systems - $L^* = 0.608$.

	Maxima ($\mathring{A}^{-1}$)		Minima ($\mathring{A}^{-1}$)	
	$Q^* = 0.739$	$\rho^* = 0.541$		$T^* = 1.14$
S(k)	1.85(.85),3.80(.72)		2.83(.31),4.86(.52)	
$S_{CM}(k)$	1.78(1.97),3.24(1.13)		2.35(.62),4.13(.96)	
$S_a(k)$	2.02(.30),3.80(.15)		1.46(-.27),2.91)(-.15)	
	$Q^* = 1.321$	$\rho^* = 0.546$		$T^* = 1.21$
S(k)	1.87(.81),3.82(.73)		2.84(.30),4.87(.42)	
$S_{CM}(k)$	1.79(2.13),3.25(1.22)		2.27(.55),4.06(.91)	
$S_a(k)$	2.03(.23),3.90(.17)		1.54(-.24),2.91(-.17)	
	$Q^* = 2.073$	$\rho^* = 0.551$		$T^* = 1.50$
S(k)	1.79(.76),2.40(.56),3.91(.74)		2.20(.53),2.93(.29),4.89(.42)	
$S_{CM}(k)$	1.79(2.20),3.26(1.29)		2.28(.54),4.07(.86)	
$S_a(k)$	2.36(.21),3.91(.18)		1.55(-.19),2.93(-.18)	

difference in the bond lengths (2.02 Å and 1.60 Å respectively) and the difference in atomic diameters (3.32 Å for chlorine and 3.538 Å for bromine), although their ration is approximately constant, being 0.608 and 0.630 respectively.

6. Mean Square Forces and Torques.

Values of the mean square force and torque have been calculated directly from the simulation using equations (II-40) and (II-41). The results are expressed as a function of T* for a given ρ^*, L* and Q* in Table (IV-9). The actual values of the force and torque however are not reduced, but tabulated in their correct units.

The values of the mean square torque may be compared to experimental estimates for chlorine ($p^* \approx 0$) obtained by Gill and Steele(20) by Raman spectroscopy.

T*=1.00	$\langle\tau^2\rangle \times 10^{-40} J^2$	T*=1.44	$\langle\tau^2\rangle \times 10^{-40} J^2$
Q* = 0.739	8.5		6.1
Q* = 1.321	8.8		6.1
Q* = 2.073	8.7		-
Expt.	9.4		7.1

The results shown are in reasonable agreement with experiment. The values seem roughly independent of quadrupole strength, although the effective temperature corresponding to a given T* is likely to be different due to the adjustment of the Lennard-Jones parameters.

From Table (IV-9) it can be seen that the intercept values for the mean square force and torque are approximately constant with density while the slopes are significantly reduced at lower density. From these values the average translational and rotational Einstein frequencies can be found using equation (IV-23) from which the

TABLE (IV-9).

	$\langle F^2 \rangle = A + BT^*$ $10^{-20} N^2$		$\langle \tau^2 \rangle = a + bT^*$ $10^{-40} J^2$	
ρ^*	A	B	a	b
$Q^* = 0.739$, $L^* = 0.608$				
0.541	-7.008	18.83	-3.761	12.23
0.485	-7.092	15.13	-3.664	9.81
$Q^* = 1.321$, $L^* = 0.608$				
0.546	-9.891	20.43	-4.565	13.40
0.490	-8.256	15.70	-5.010	11.11
$Q^* = 2.073$, $L^* = 0.608$				
0.551	-8.047	16.01	-4.650	13.31
$Q^* = 2.038$, $L^* = 0.793$				
0.423	-5.153	9.65	-3.718	9.87
0.381	-5.516	8.44	-3.692	8.40

quasi-harmonic force constants can also be deduced. The values of the mean square torques and forces may now be used to estimate the isotrope separation factors(14). However the principle use of the mean square torque and forces is in the determination of the moments of the dynamical correlation functions discussed in Chapters VI and VII.

7. Conclusion.

The effect of the quadrupole is seen to increase the well depth of the potential associated with various configurations, particularly the "T" configuration, while making other configurations less favourable. Configurations that give rise to small interaction distances such as the "Parallel" and "Cross" types are substantially increased in energy. The resultant distribution functions and structure factors reflect these changes in potential shape within the constraints of packing considerations at a given density and temperature. Agreement with experiment is seen to be increased by these changes in comparison with the two-centre Lennard-Jones only systems.

References.

1. C.G. Gray, in Chemical Society S.P.R., Statistical Mechanics Vol.2 (Ed. K. Singer, Chemical Society, London, 1975).
2. P.A. Egelstaff, C.G. Gray and K.E. Gubbins, MTP International Review of Science, Physical Chemistry, Series 2. (Butterworths, London, 1974).
3. A.D. Buckingham and C. Graham, Mol.Phys., 1971, 22, 335.
4. J.O. Hirschfelder, C.F. Curtiss and R.B. Bird, "Molecular Theory of Gases and Liquids" (Wiley and Sons, New York, 1954).
5. M.E. Rose, "Elementary Theory of Angular Momentum" (Wiley and Sons, New York, 1957).
6. W.A. Steele, J.Chem.Phys., 1963, 39, 3197.
7. Y.-D. Chen and W.A. Steele, J.Chem.Phys., 1969, 50, 1428.
8. W.B. Streett and D.J. Tildesley, Proc.Roy.Soc.(Lond), 1976, A348, 485.
9. M. Abramowitz and I.A. Stegun, "Handbook of Mathematical Functions" (Dover, New York, 1970).
10. W.A. Steele and R. Pecora, J.Chem.Phys., 1965, 42, 1963.
11. K.E. Gubbins, C.G. Gray, P.A. Egelstaff and M.S. Ananth, Mol.Phys., 1973, 59, 1325.
12. A.H. Narten, J.Chem.Phys., 1962, 56, 5681.
13. G. Bacon, "Neutron Diffraction", (Oxford Univ.Press, Oxford, 1975).
14. S.M. Thompson, D.J. Tildesley and W.B. Street, Mol.Phys., 1976, 32, 711.
15. K. Singer, A. Taylor and J.V.L. Singer, Mol.Phys., 1977, 33, 1757.
16. J.C. Dore, G. Walford and D.I. Page, Mol.Phys., 1975, 29, 565.
17. J.H. Clarke, J.C. Dore and R.N. Sinclair, Mol.Phys., 1975, 29, 581. Also J.H. Clarke, J.C. Dore and H. Egger, Mol.Phys., 1980, 39, 533.

18. P.S.Y. Cheung and J.G. Powles, Mol.Phys., 1976, 32, 1383.

19. J.H. Clarke, J.C. Dore, G. Walford and R.N. Sinclair, Mol.Phys., 1976, 31, 883.

20. E. Gill and D. Steele, Mol.Phys., 1977, 34, 231.

21. J.G. Powles and G. Rickayzen, Mol.Phys., 1979, 38, 1875.

FIGURES.

(IV-1A) Special Configuration g(r)'s for N_2 at ($T^* = 1.61$, $\rho^* = 0.700$, $L^* = 0.328$, $Q^* = 1.159$)

——————— $G(r)$

— — — — — — $g_{\shortparallel}(r)$ - Distances in $\mathring{A}$

— — — — — — — — $g_{\perp}(t)$

---------- $g_{+}(r)$

(IV-1B) Potential Energy curves corresponding to special configurations for N_2 at ($T^* = 1.61$, $\rho^* = 0.700$, $L^* = 0.700$, $Q^* = 1.159$)

——————— $\langle\phi(r)\rangle_{\omega_1,\omega_2}$

---------- $\phi_{+}(r)$

---------- $\phi_{\perp}(r)$ - Distances in $\mathring{A}$

— — — — — — $\phi_{\shortparallel}(r)$

— — — — — — $\phi_{--}(r)$

——————— $\phi_{-\_}(r)$

(IV-2A) Special Configuration g(r)'s - Key as for (IV-1A) for Cl_2 at ($T^* = 1.14$, $\rho^* = 0.541$, $L^* = 0.608$, $Q^* = 0739$)

(IV-2B) Potential Energy curves - Key as for (IV-1B) for Cl_2 at ($T^* = 1.14$, $\rho^* = 0.541$, $L^* = 0.608$, $Q^* = 0.739$)

(IV-3A) Special Configuration g(r)'s - Key as for (IV-1A) for Cl_2 at ($T^* = 1.21$, $\rho^* = 0.546$, $L^* = 0.608$, $Q^* = 1.321$)

(IV-3B) Potential Energy Curves - Key as for (IV-1B) for Cl_2 at ($T^* = 1.21$, $\rho^* = 0.546$, $L^* = 0.608$, $Q^* = 1.321$)

(IV-4A) Special Configuration g(r)'s - Key as for (IV-1A) for Cl_2 at ($T^* = 1.50$, $\rho^* = 0.551$, $L^* = 0.608$, $Q^* = 2.073$)

(IV-4B) Potential Energy curves - Key as for (IV-1B) for Cl_2 at ($T^* = 1.50$, $\rho^* = 0.551$, $L^* = 0.608$, $Q^* = 2.073$)

(IV-5A) Special Configuration g(r)'s - Key as for (IV-1A) for CO_2 at ($T^* = 1.61$, $\rho^* = 0.423$, $L^* = 0.793$, $Q^* = 2.039$)

(IV-5B) Potential Energy curves - Key as for (IV-1B) for CO_2 at
($T^* = 1.61$, $\rho^* = 0.423$, $L^* = 0.793$, $Q^* = 2.039$)

(VI-6) Site-Site G(r)'s for N_2 at
($T^* = 1.61$, $\rho^* = 0.700$, $L^* = 0.328$, $Q^* = 1.159$)

——————— $G_{CM}(r)$
— — — — — — — $G_{AA}(r)$ - Distances in Å
—·—·—·—·—·— $G_{CMA}(r)$

(IV-7) Site-Site G(r)'s - Key as for (IV-6) for Cl_2 at
($T^* = 1.14$, $\rho^* = 0.541$, $L^* = 0.608$, $Q^* = 0.739$)

(IV-8) Site-Site G(r)'s - Key as for (IV-6) for Cl_2 at
($T^* = 1.21$, $\rho^* = 0.546$, $L^* = 0.608$, $Q^* = 1.321$)

(IV-9) Site-Site G(r)'s - Key as for (IV-6) for Cl_2 at
($T^* = 1.50$, $\rho^* = 0.551$, $L^* = 0.608$, $Q^* = 2.073$)

(IV-10) Site-Site G(r)'s - Key as for (IV-6) for CO_2 at
($T^* = 1.61$, $\rho^* = 0.423$, $L^* = 0.793$, $Q^* = 2.039$).

(IV-11) Spherical Harmonics $G_{\ell\ell'm}(r)$ for N_2 at
($T^* = 1.61$, $\rho^* = 0.700$, $L^* = 0.328$, $Q^* = 1.159$)

——————— $G_{000}(r)$
— — — — — — — $G_{200}(r)$
——————— $G_{220}(r)$ - Distances in Å
---------- $G_{221}(r)$
——— ——— $G_{222}(r)$
— — — — — $G_{400}(r)$

(IV-12) Spherical Harmonics $G_{\ell\ell'm}(r)$ - Key as for (IV-11) for Cl_2 at
($T^* = 1.14$, $\rho^* = 0.541$, $L^* = 0.608$, $Q^* = 0.739$)

(IV-13) Spherical Harmonics $G_{\ell\ell'm}(r)$ - Key as for (IV-11) for Cl_2 at
($T^* = 1.21$, $\rho^* = 0.546$, $L^* = 0.608$, $Q^* = 1.321$)

(IV-14) Spherical Harmonics $G_{\ell\ell'm}(r)$ - Key as for (IV-11) for Cl_2 at
($T^* = 1.50$, $\rho^* = 0.551$, $L^* = 0.608$, $Q^* = 2.073$)

(IV-15) Spherical Harmonics $G_{\ell\ell'm}(r)$ - Key as for (IV-11) for CO_2 at
($T^* = 1.61$, $\rho^* = 0.423$, $L^* = 0.793$, $Q^* = 2.039$)

(IV-16) Structure Factors for N_2 at

($T^* = 1.61$, $\rho^* = .700$, $L^* = 0.328$, $Q^* = 1.159$)

——————— $S(k)$

— — — — — — — — — $S_{CM}(k)$ - Axis ($\mathring{A}^{-1}$)

---------- $S_a(k)$

(IV-17) Structure Factors - Key as for (IV-16) for Cl_2 at

($T^* = 1.14$, $\rho^* = 0.541$, $L^* = 0.608$, $Q^* = 0.739$)

(IV-18) Structure Factors - Key as for (IV-16) for Cl_2 at

($T^* = 1.21$, $\rho^* = 0.546$, $L^* = 0.608$, $Q^* = 1.321$)

(IV-19) Structure Factors - Key as for (IV-16) for Cl_2 at

($T^* = 1.50$, $\rho^* = 0.551$, $L^* = 0.608$, $Q^* = 2.073$)

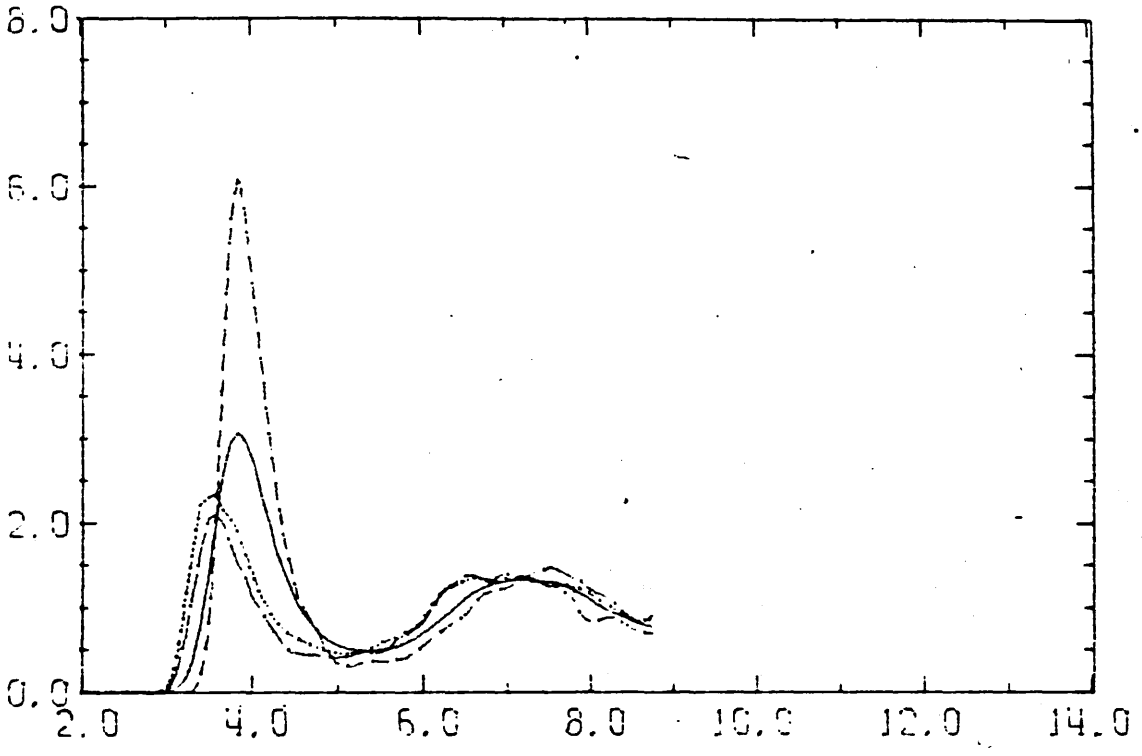

Figure (IV-1A)

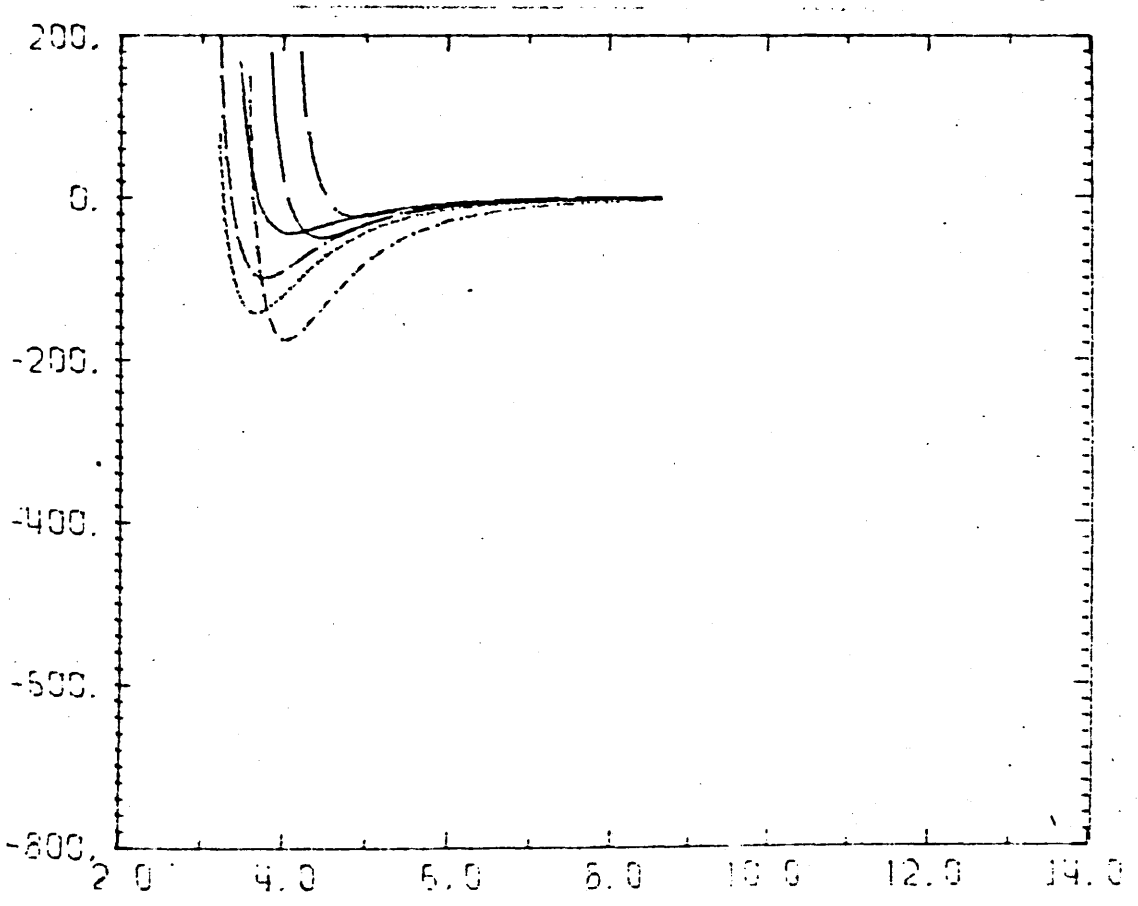

Figure (IV-1B)

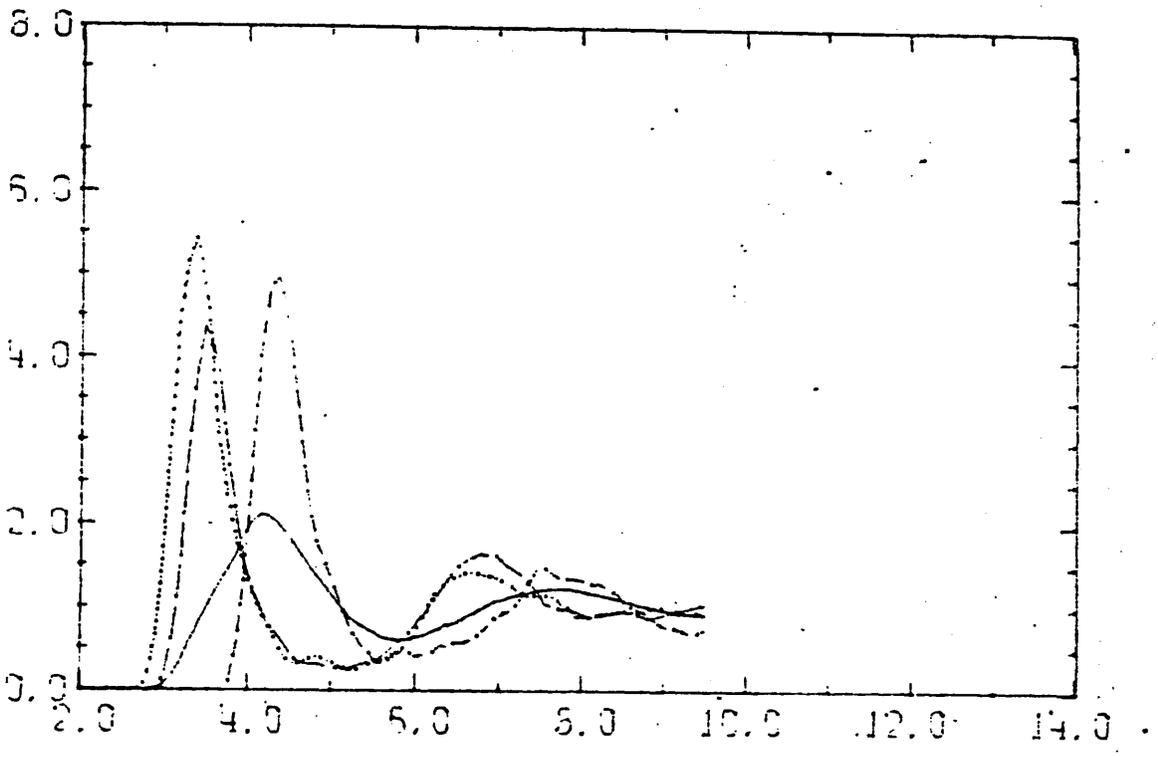

Figure (IV-2A)

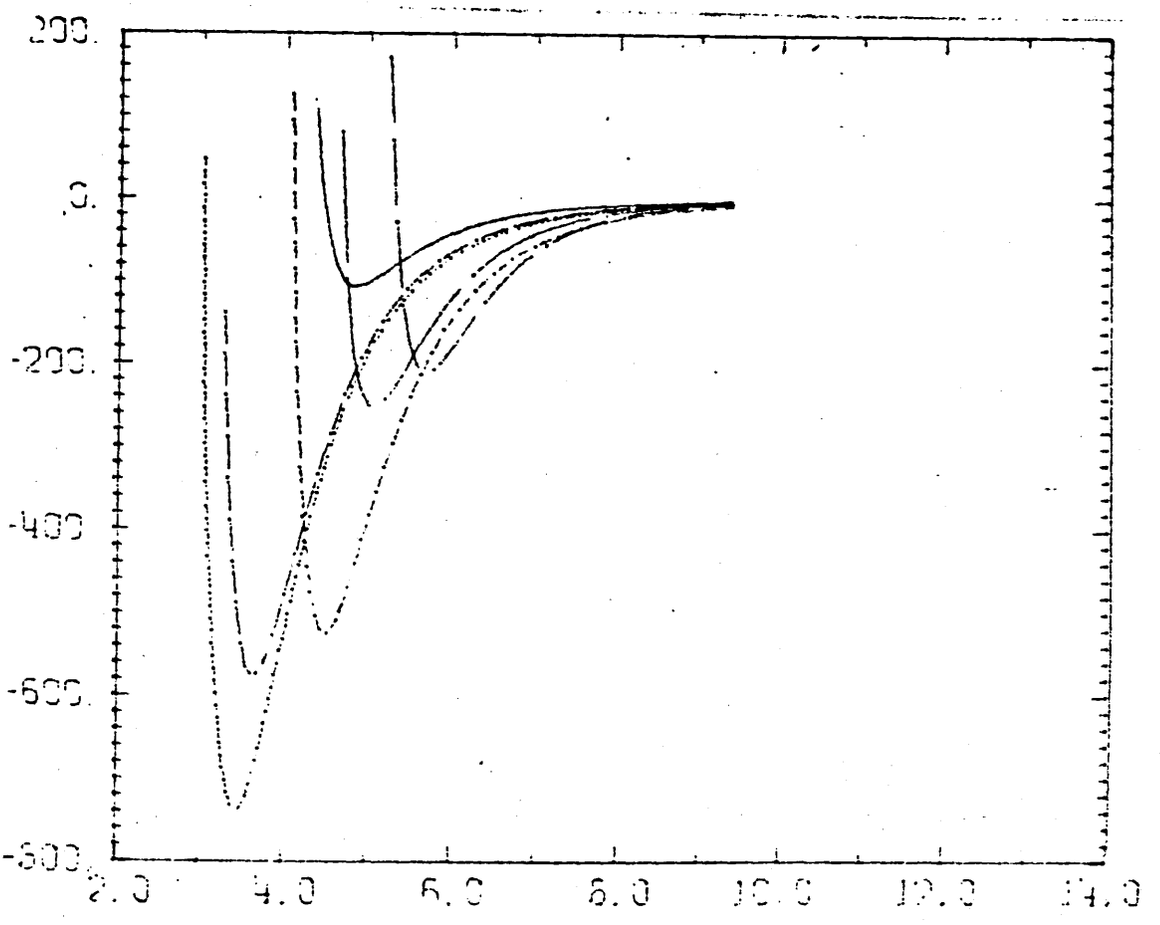

Figure (IV-2B)

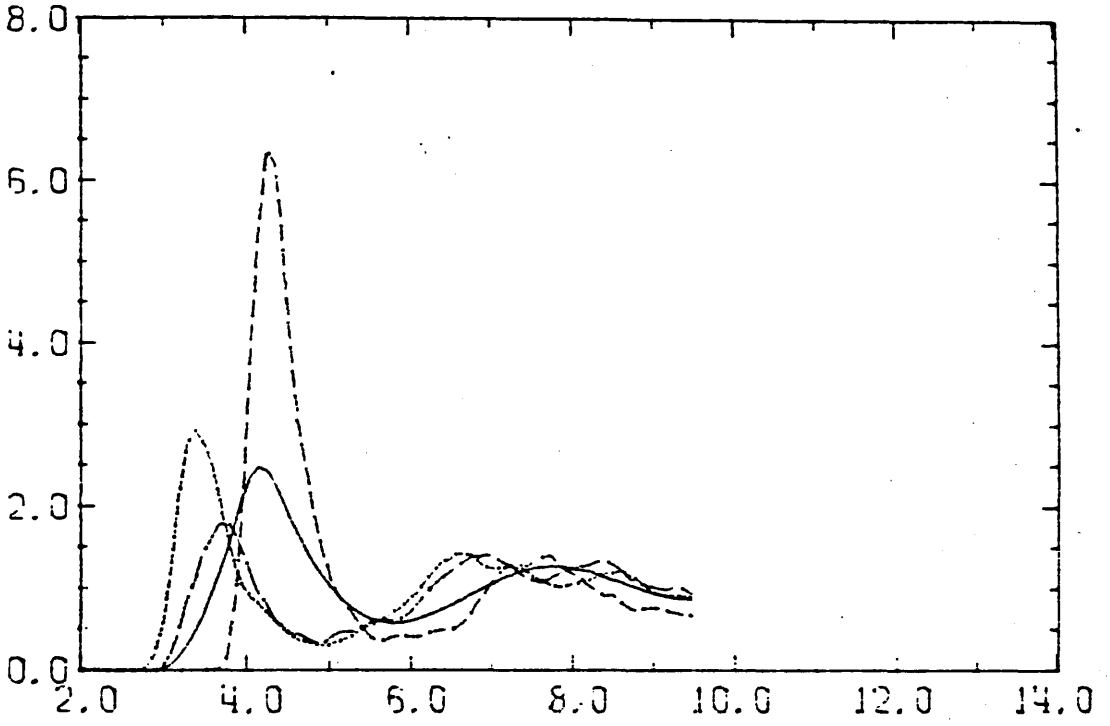

Figure (IV-3A)

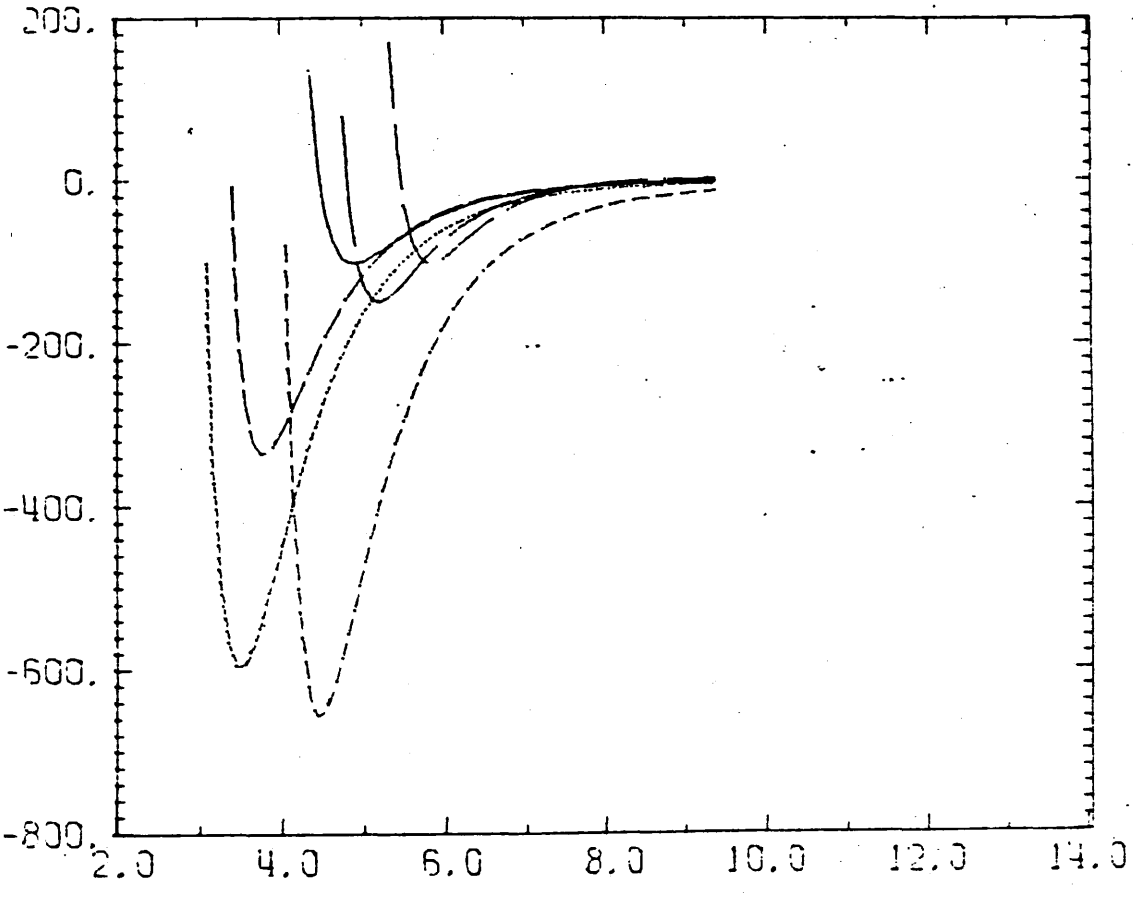

Figure (IV-3B)

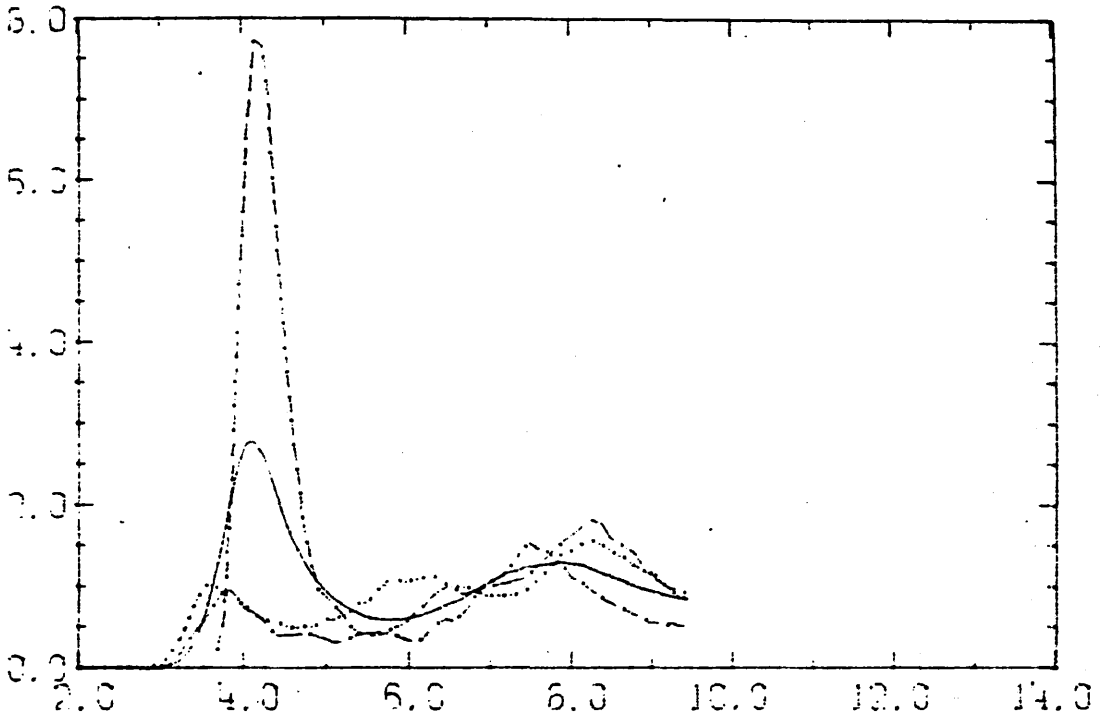

Figure (IV-4A)

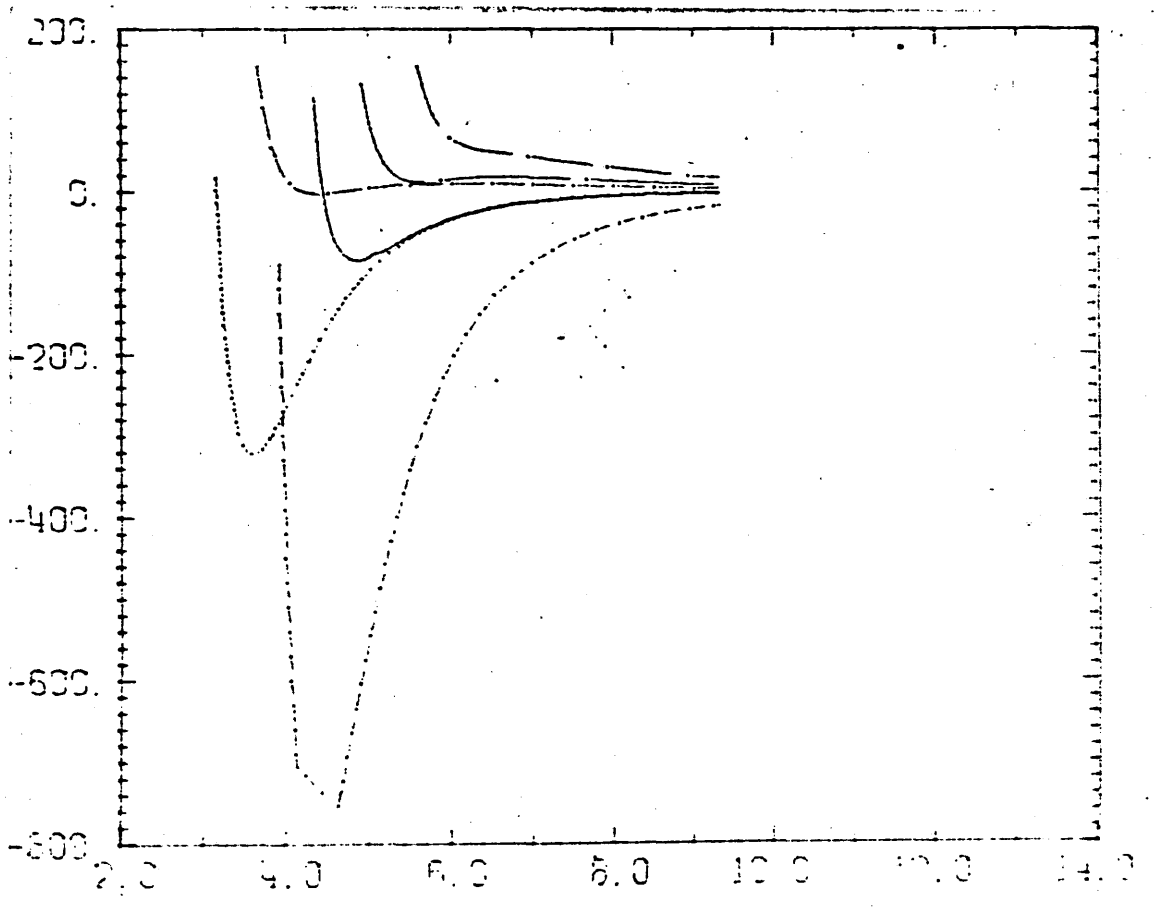

Figure (IV-4B)

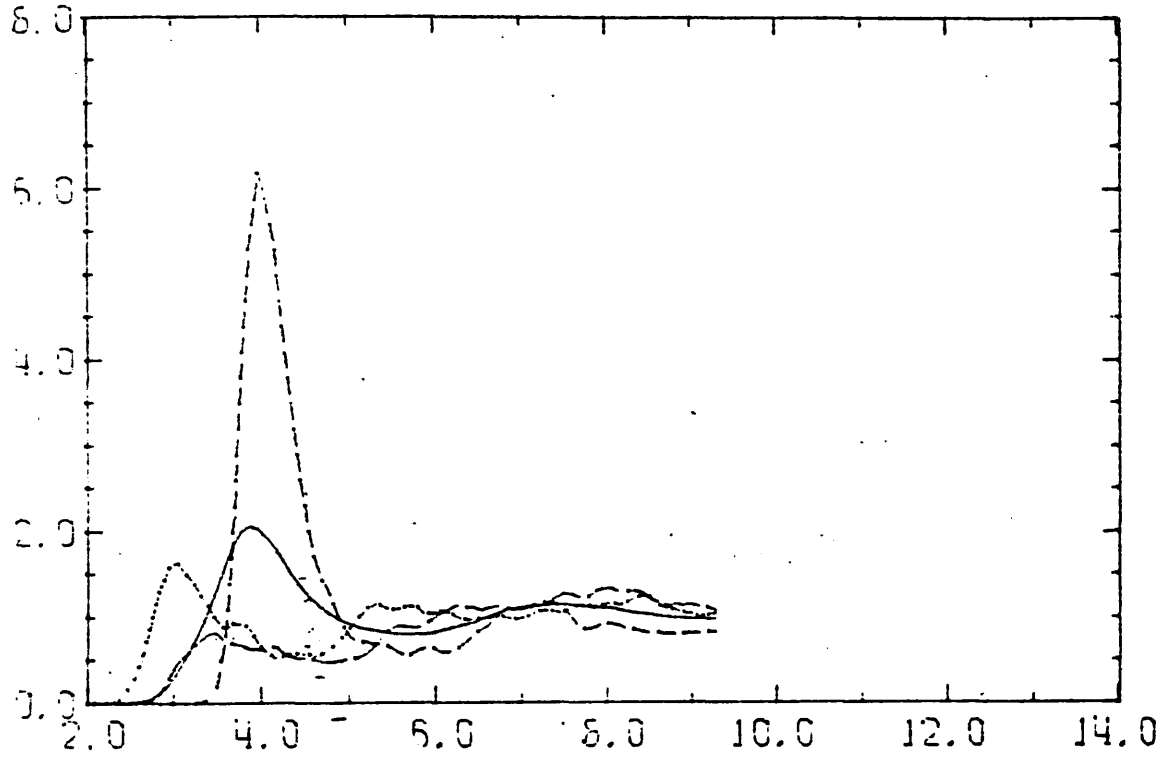

Figure (IV-5A)

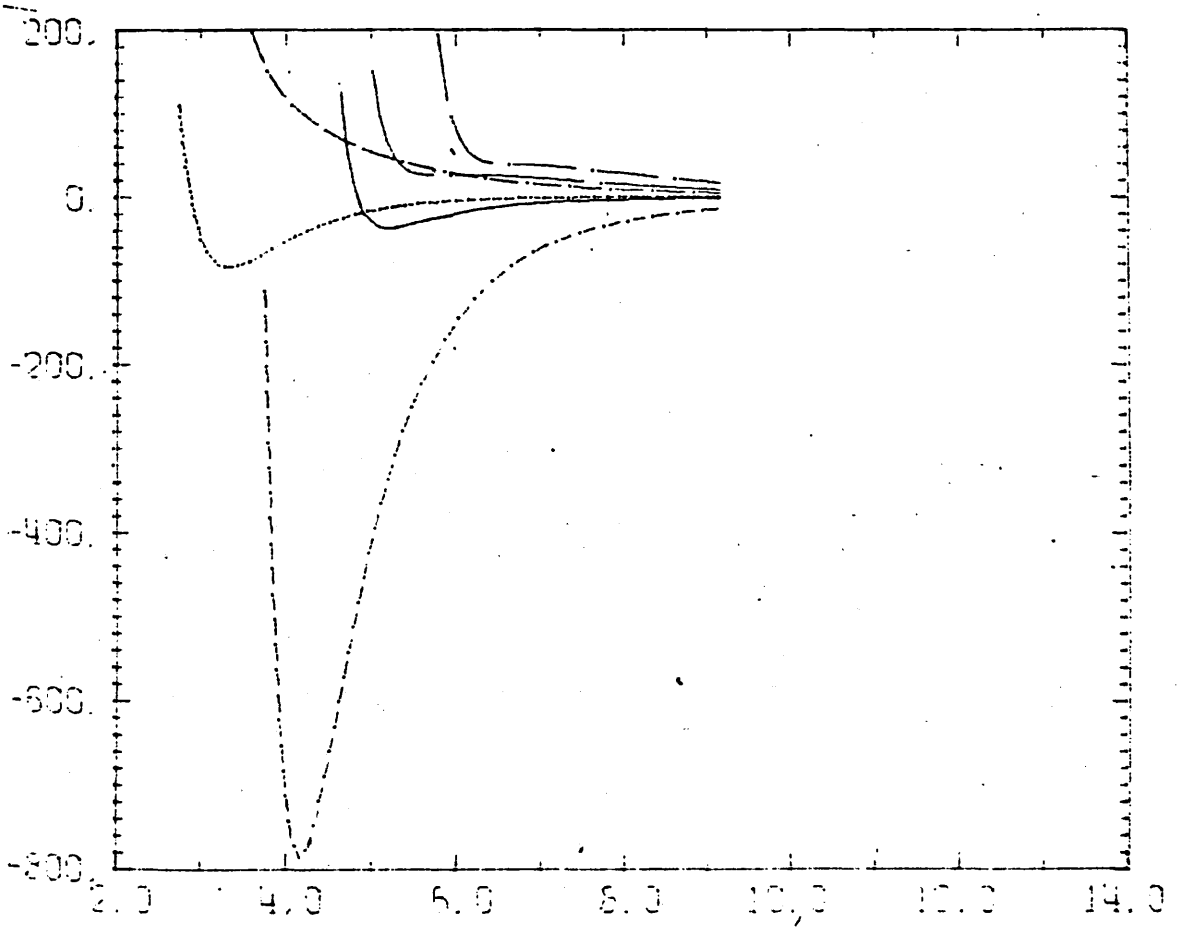

Figure (IV-5B)

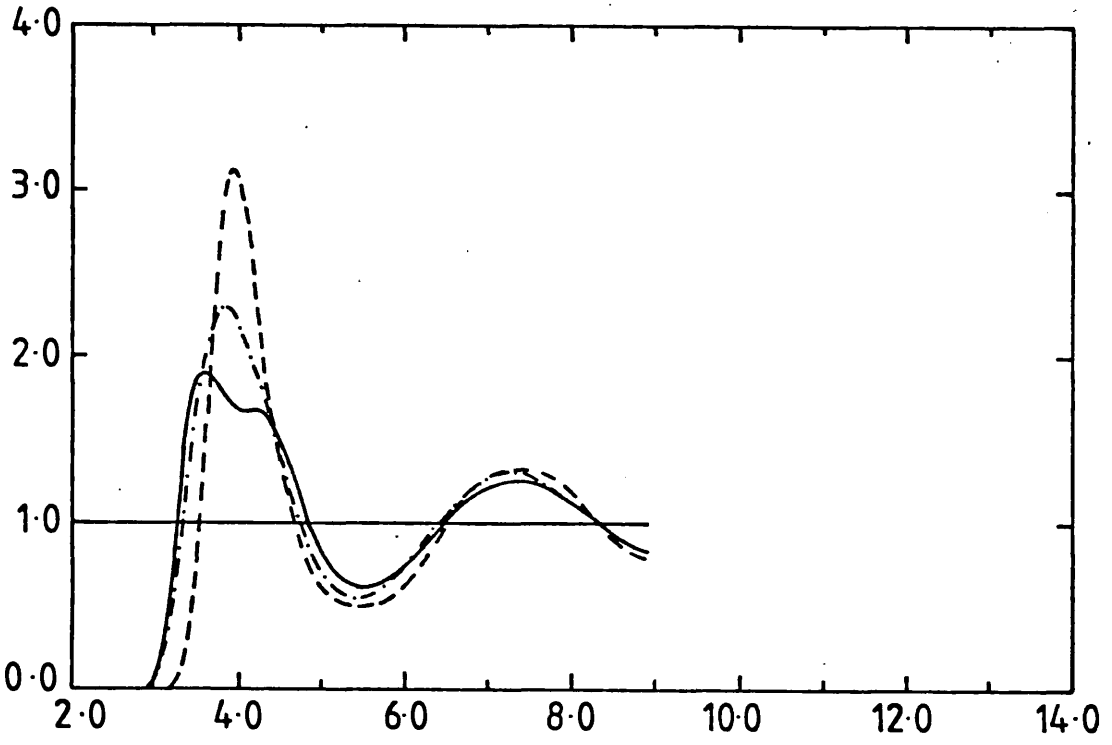

Figure (IV-6)

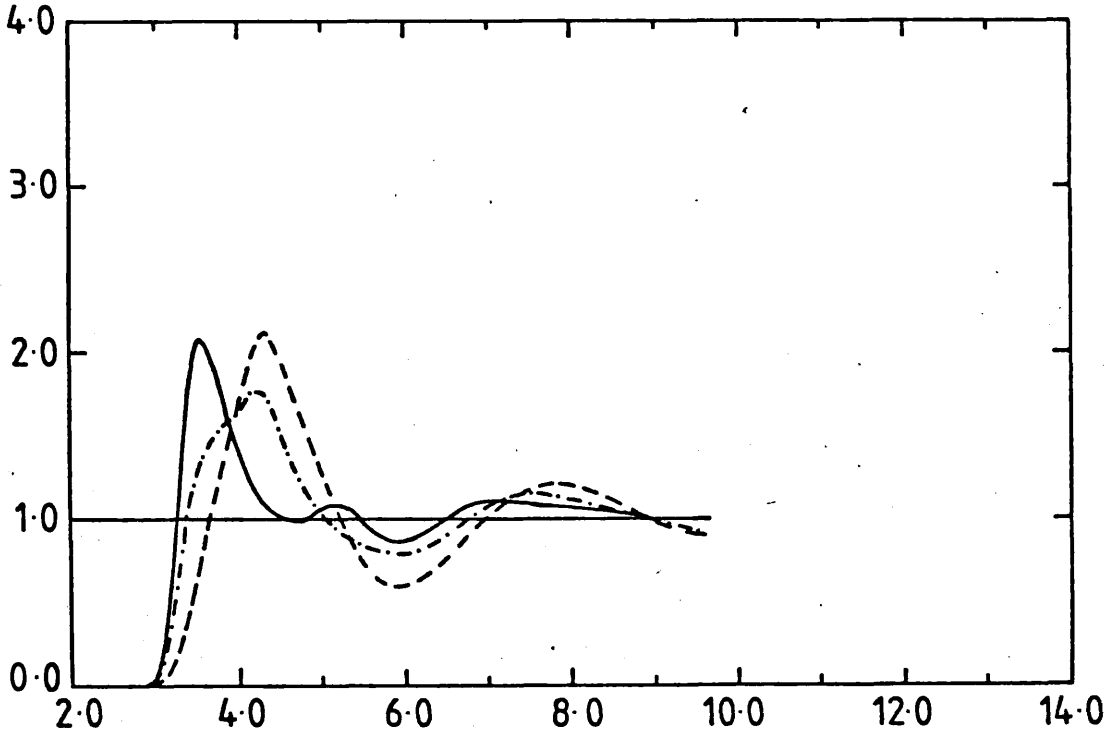

Figure (IV-7)

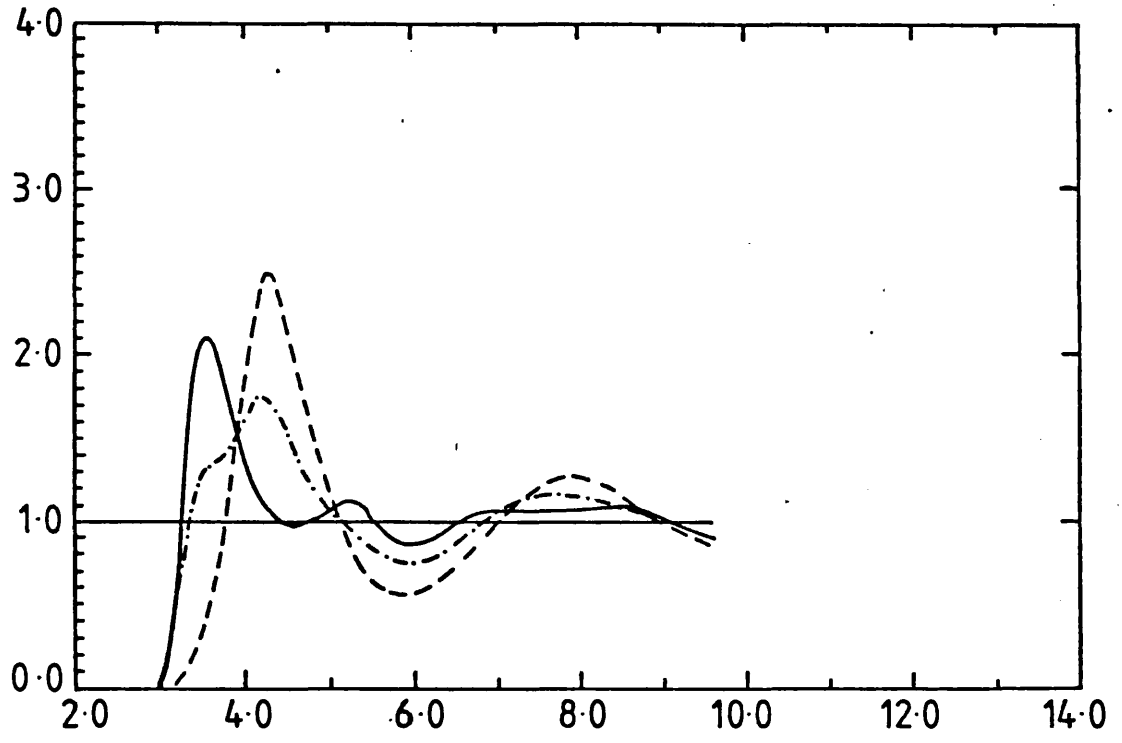

Figure (IV-8)

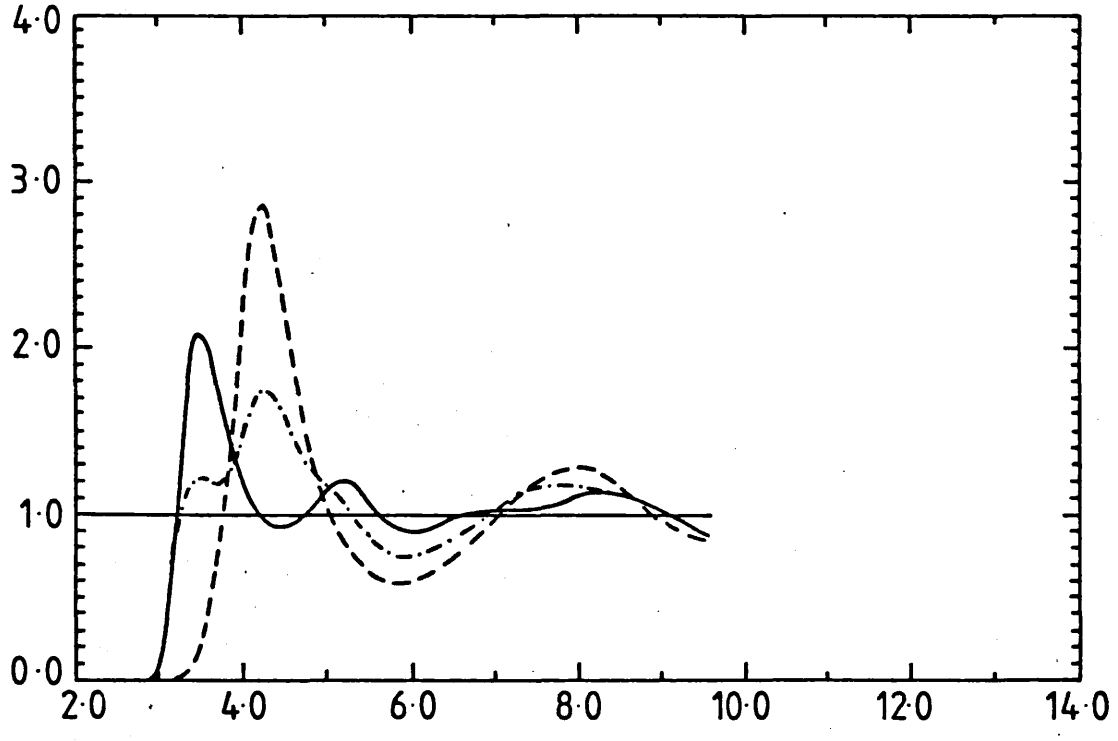

Figure (IV-9)

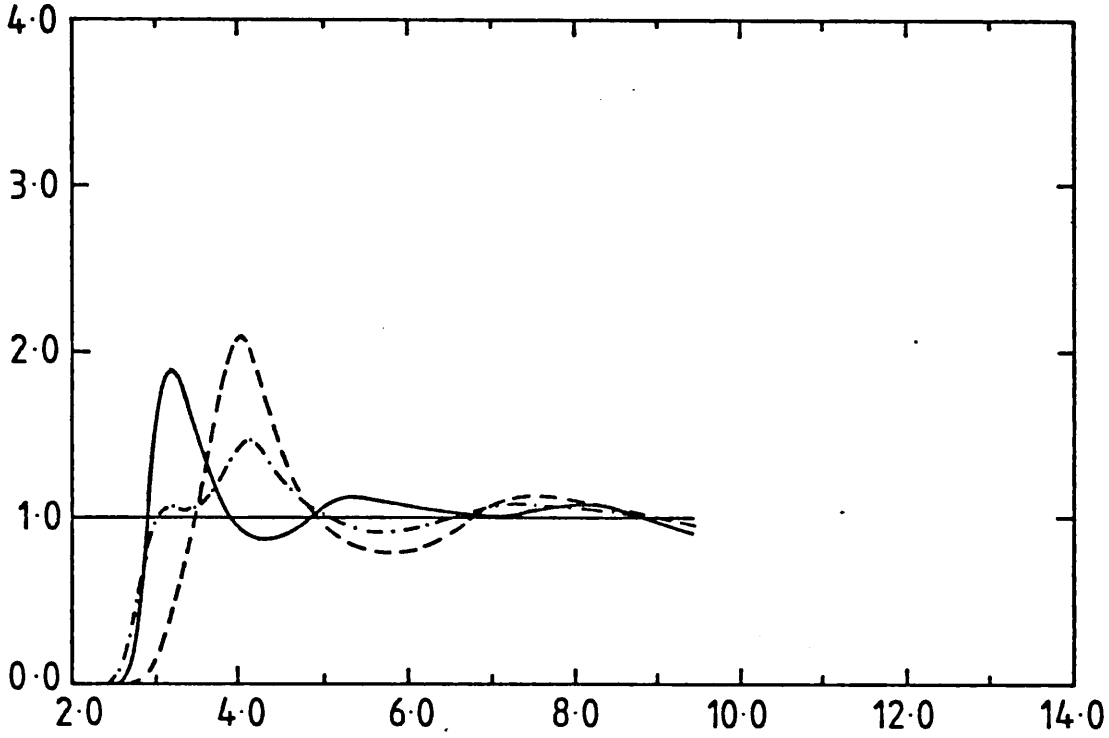

Figure (IV-10)

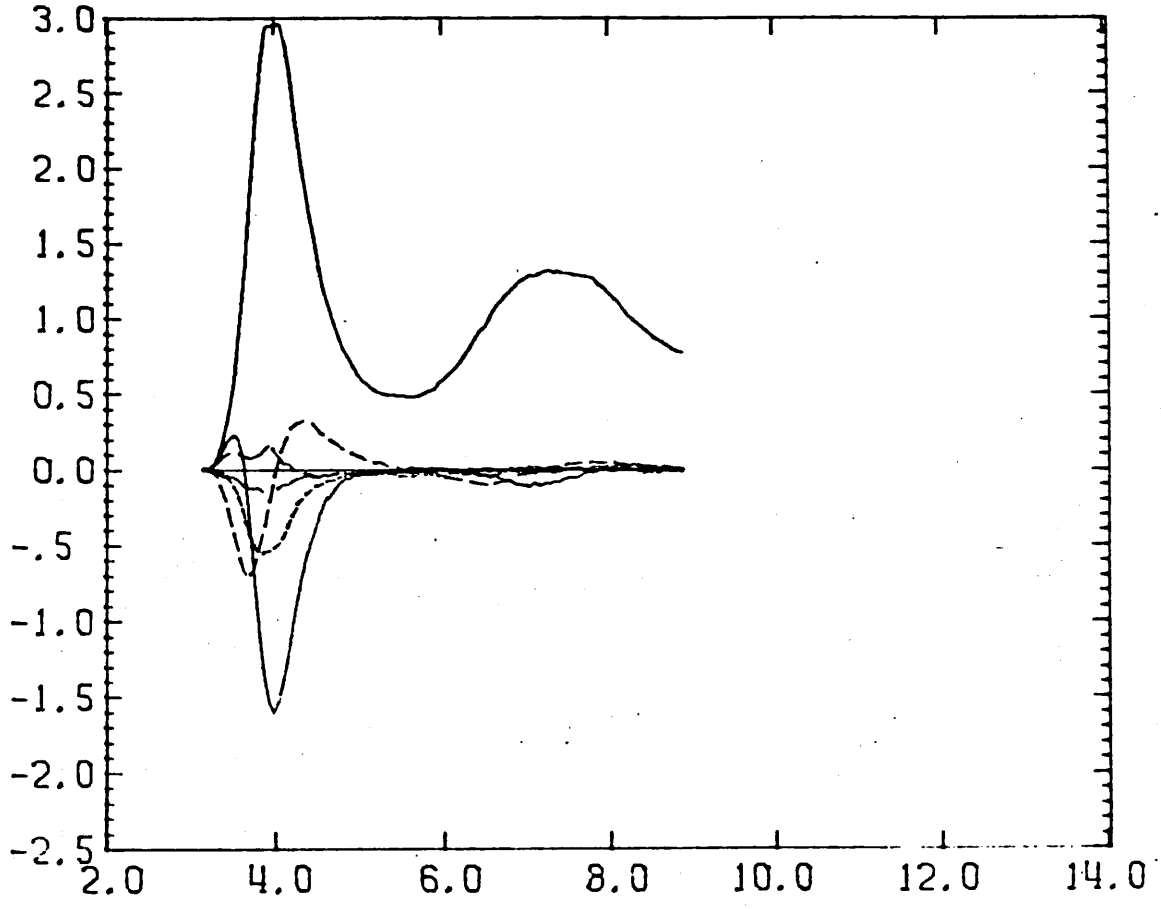

Figure (IV-11)

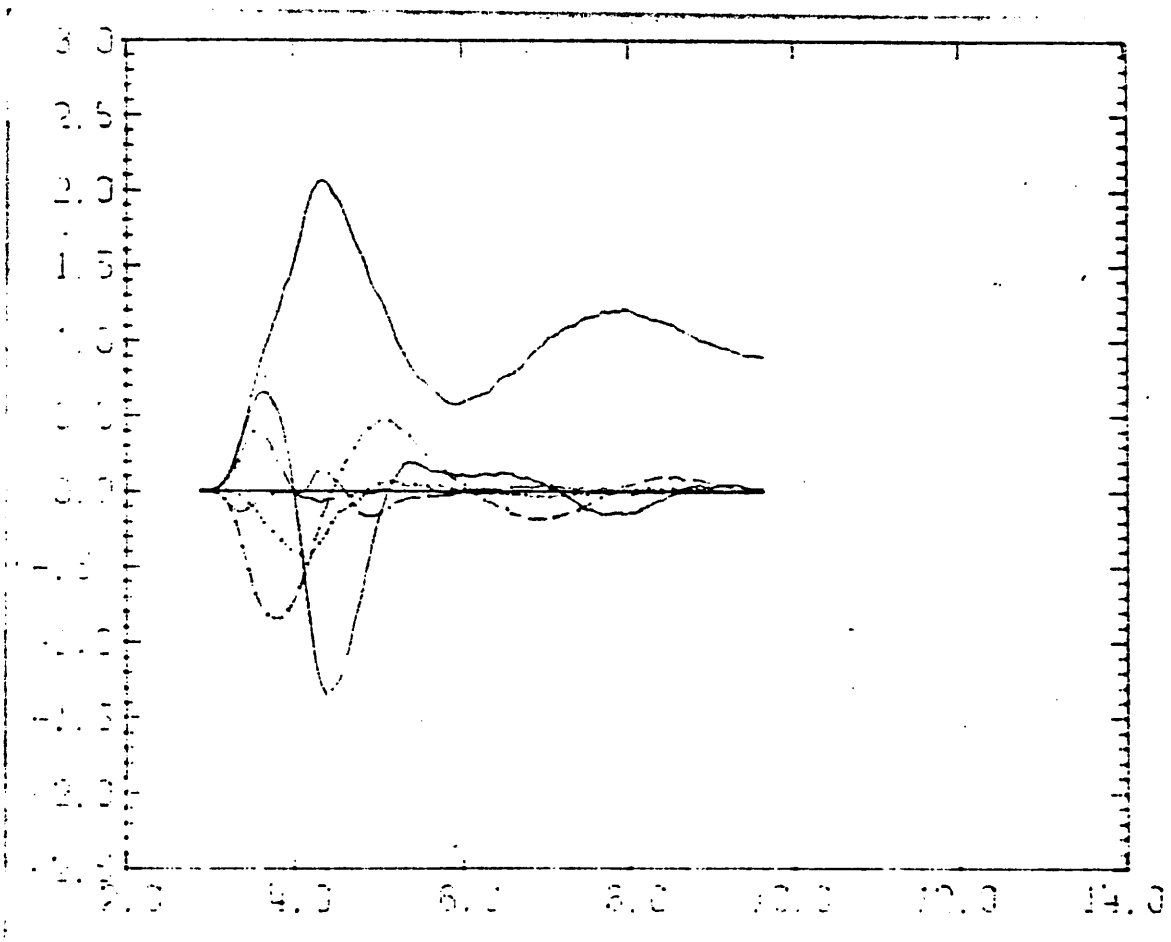

Figure (IV-12)

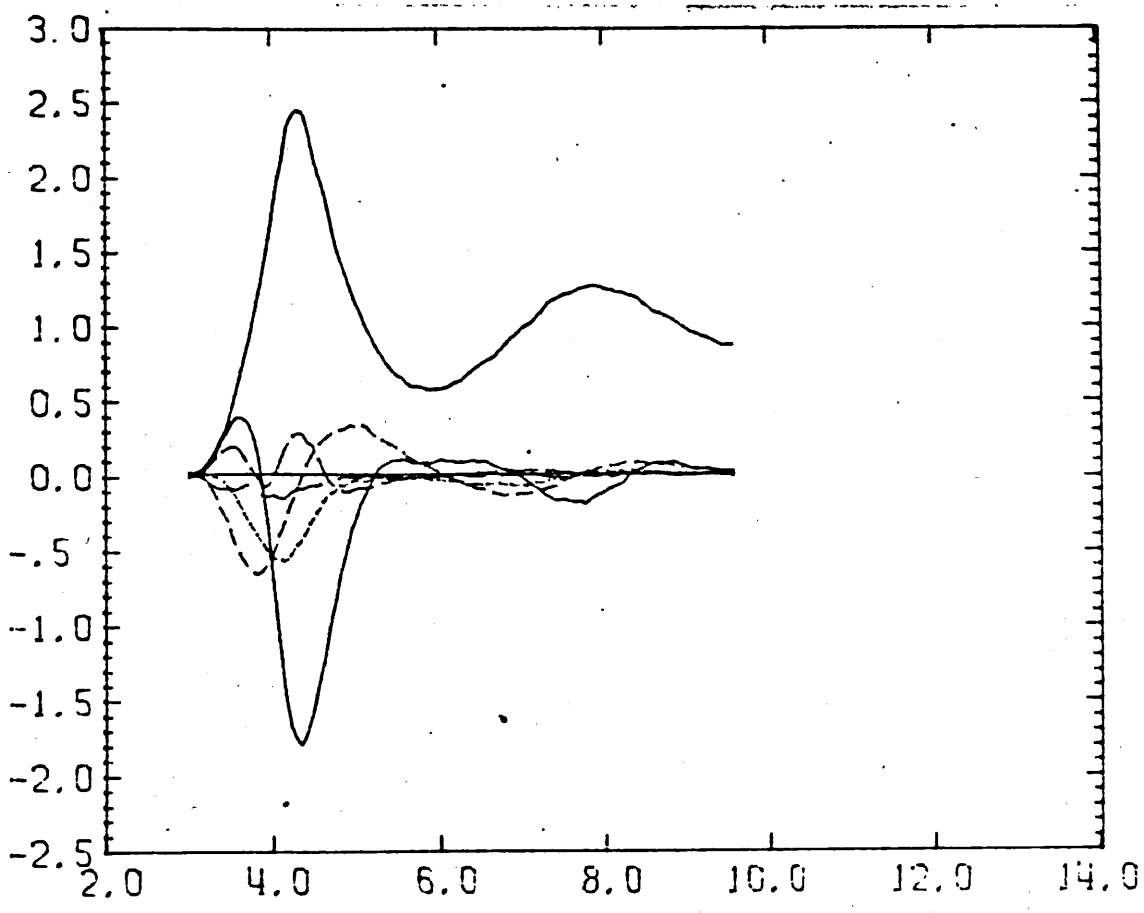

Figure (IV-13)

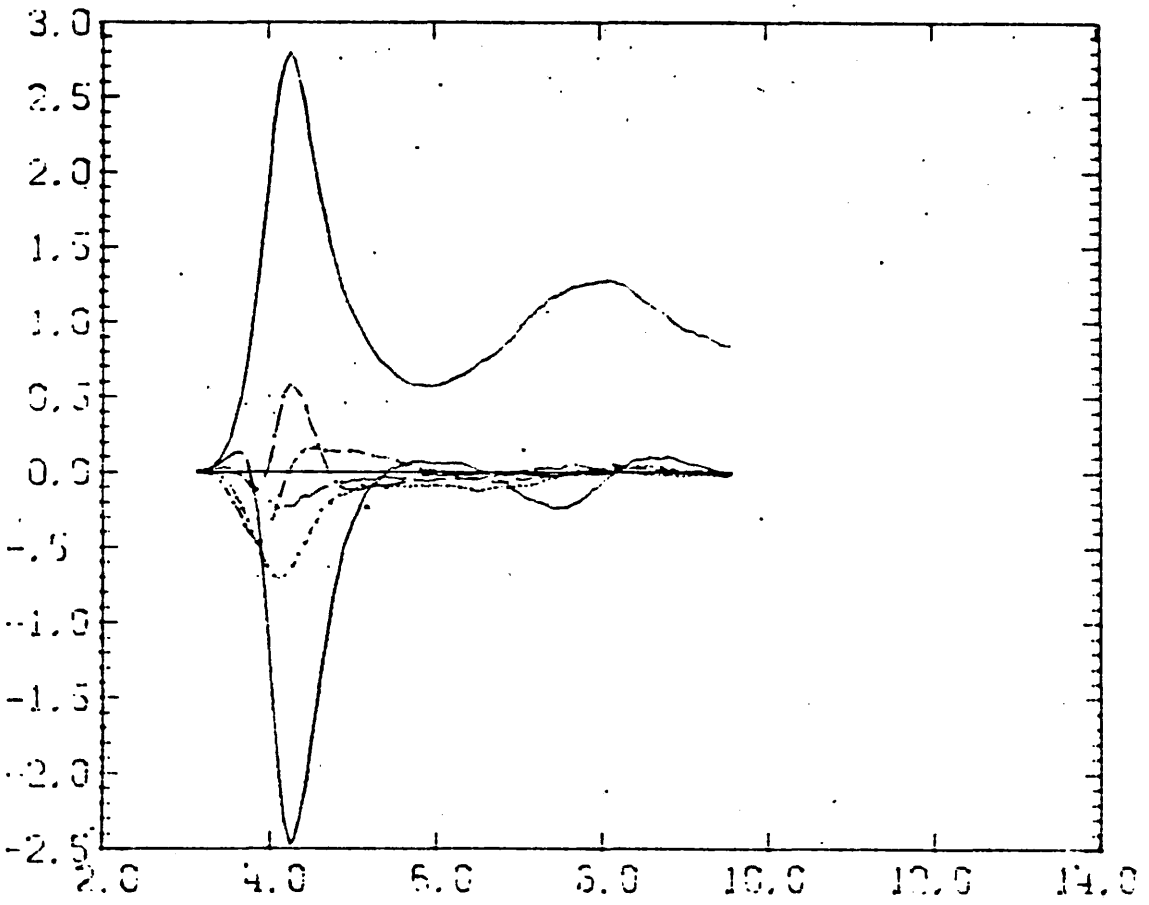

Figure (IV-14)

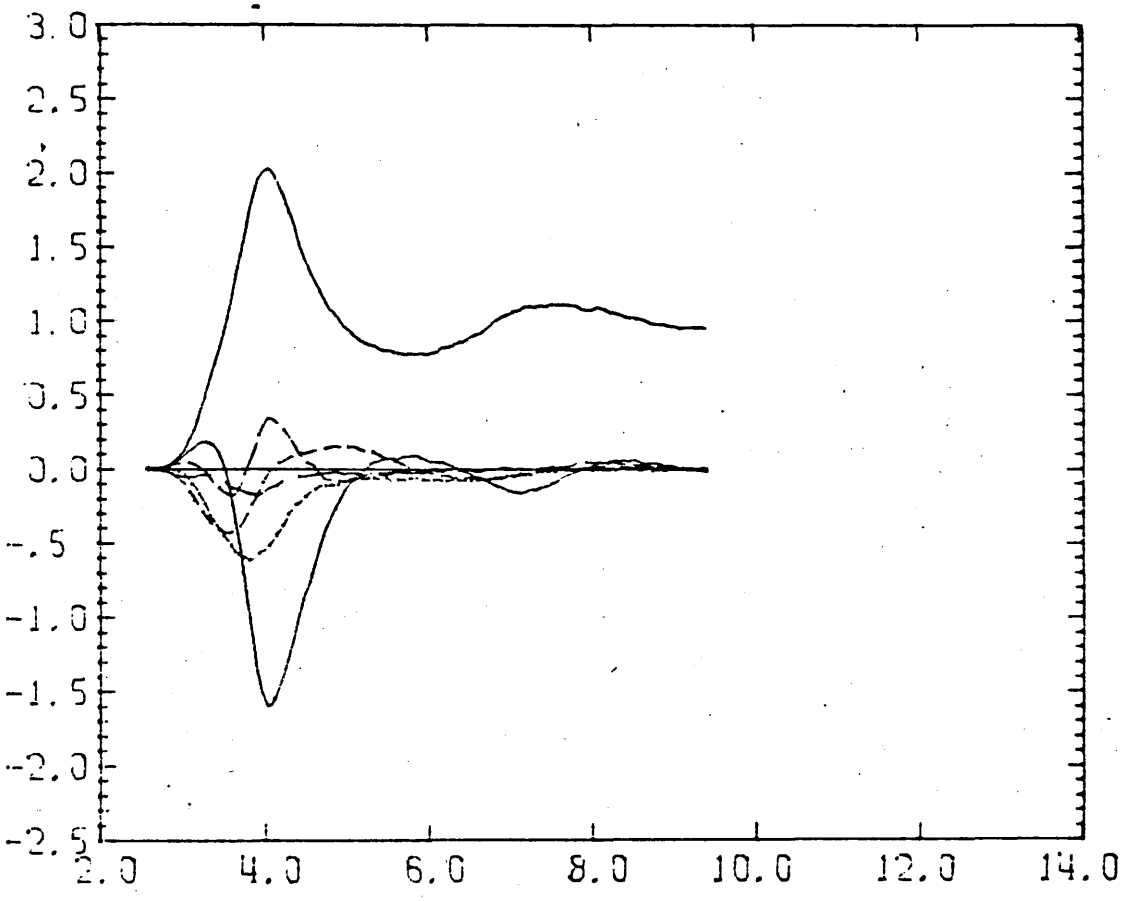

Figure (IV-15)

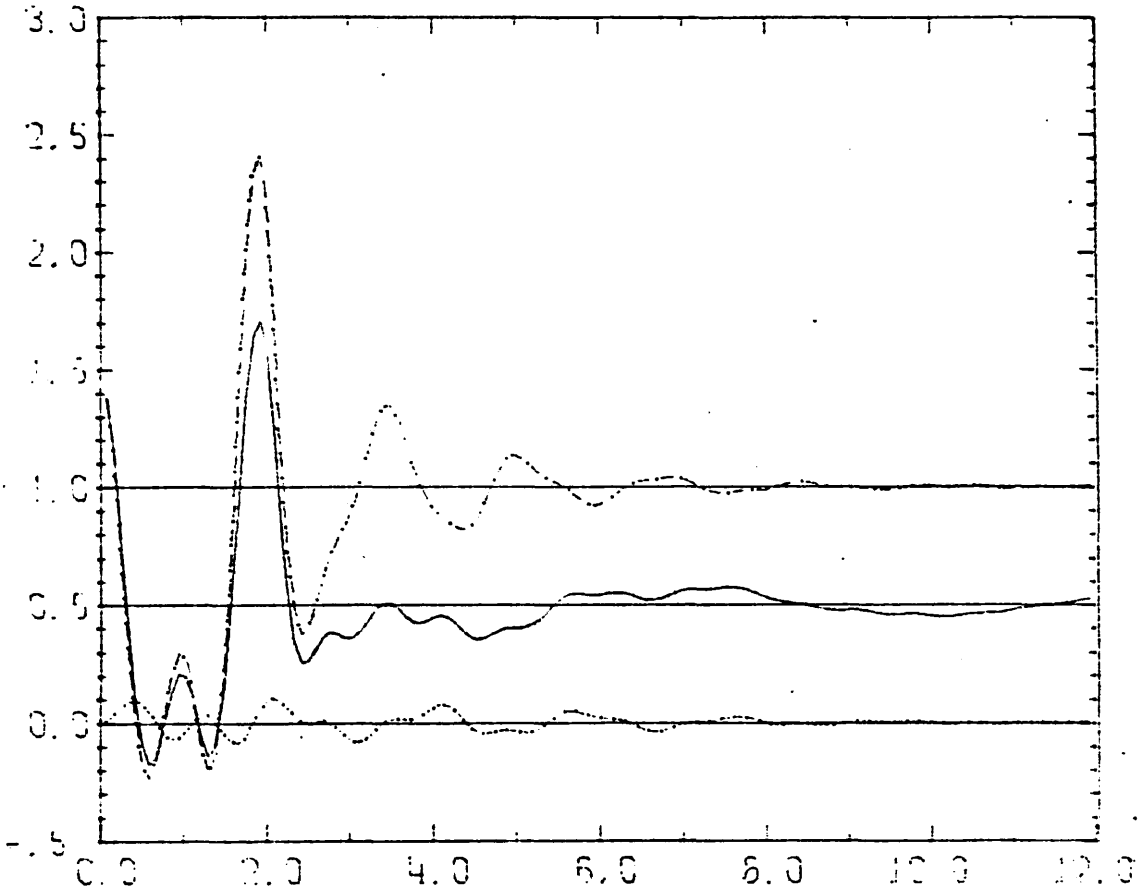

Figure (IV-16)

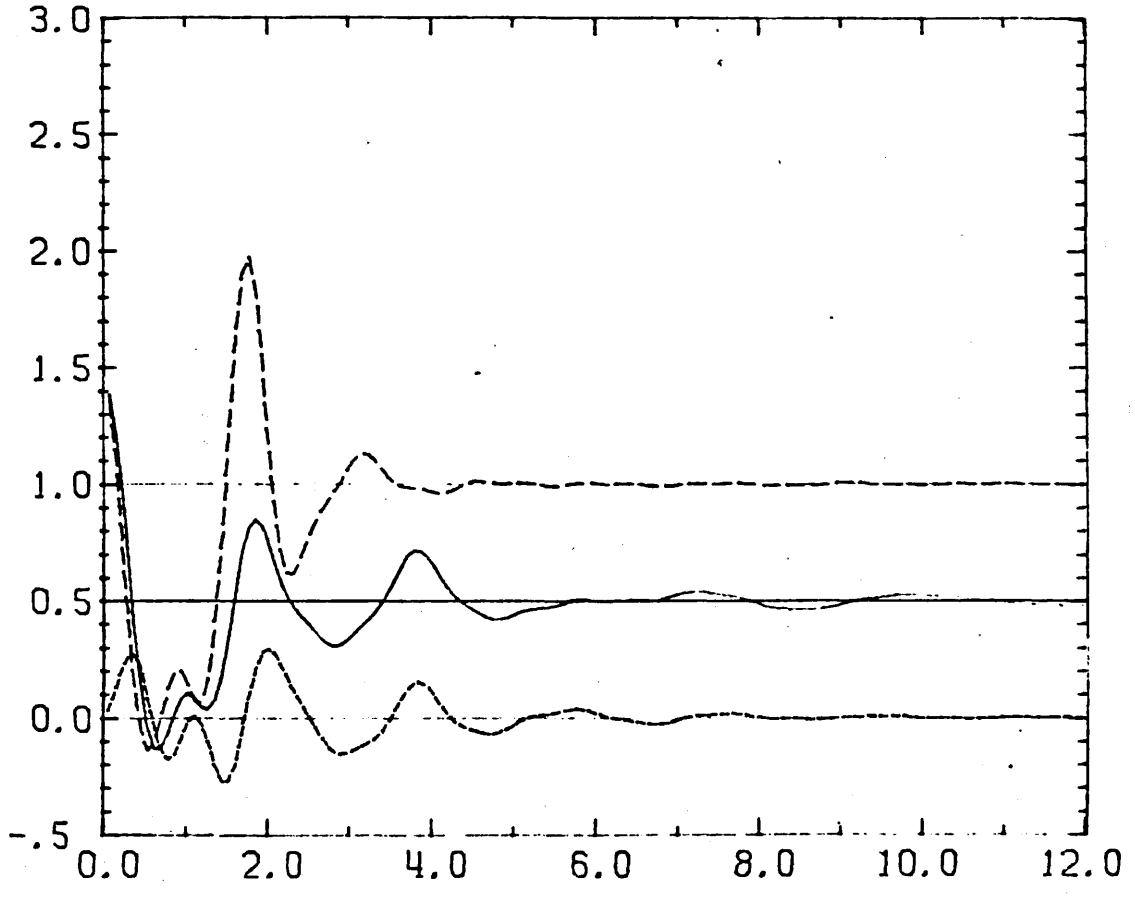

Figure (IV-17)

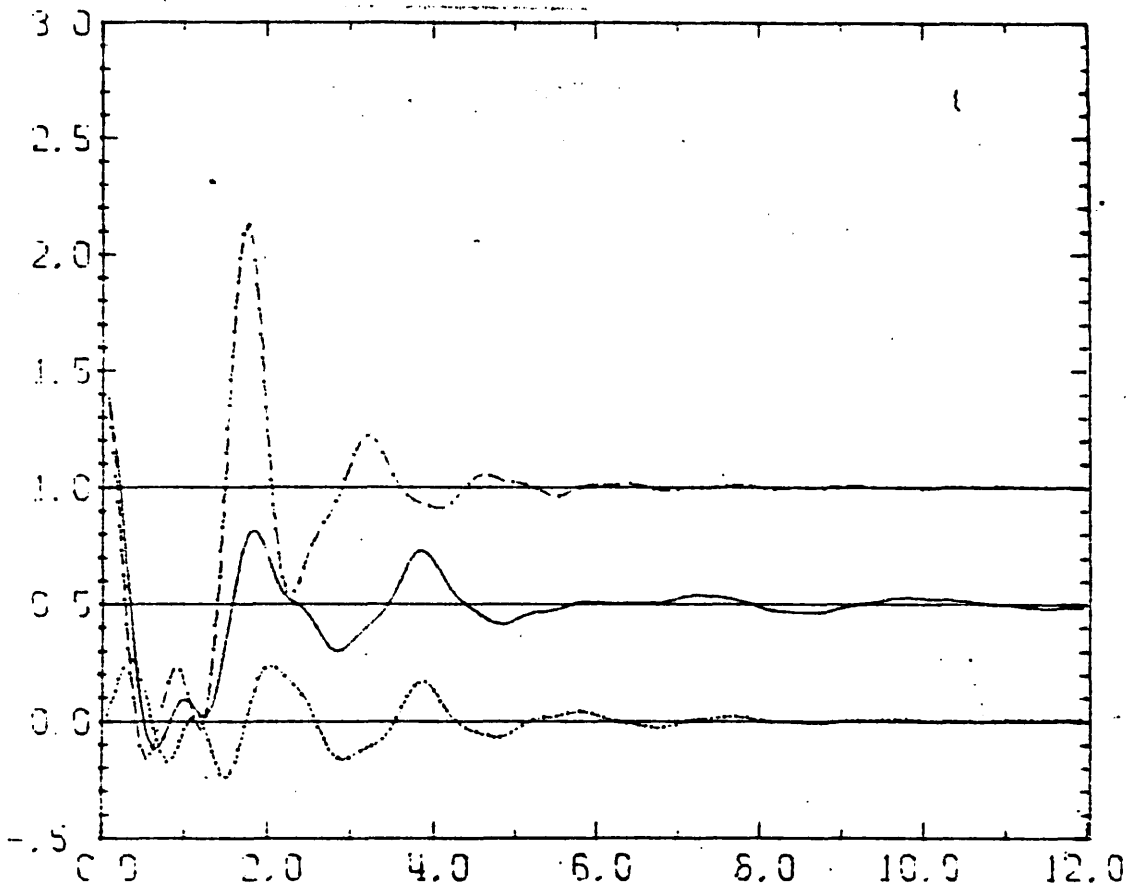

Figure (IV-18)

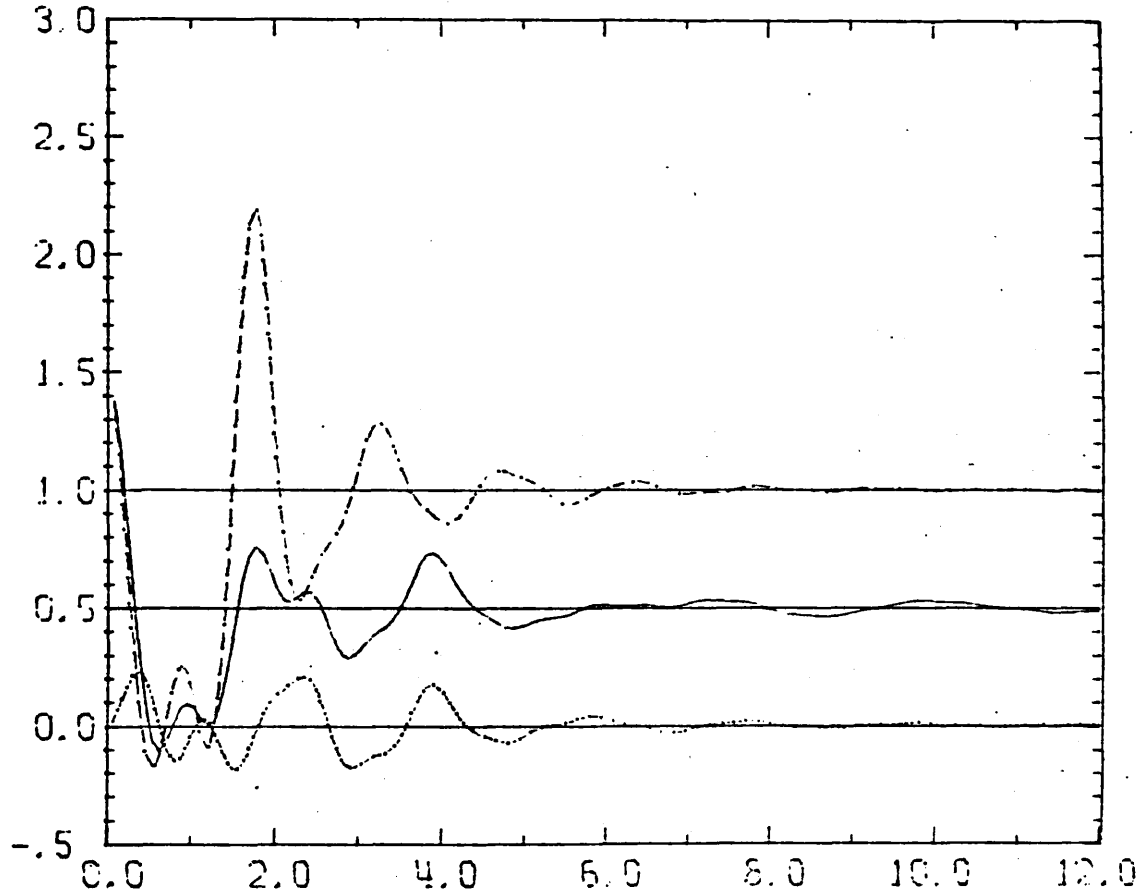

Figure (IV-19)

CHAPTER V. RISM Method.

(V-1) Introduction.

The prediction of the structural properties of liquids relies on the ability to calculate the radial distribution function g(r) for a given density. Most methods for calculating g(r) are based on the Ornstein-Zernike (OZ) equation (1)

$$h(1,2) = c(1,2) + \rho\int c(1,3)h(2,3)d3 \qquad (V\text{-}1)$$

where $h(1,2) = g(1,2)-1$ is the pair correlation function, $c(1,2)$ is the direct correlation function and ρ is the number density. This equation is derived from a fundamental property of g(r) given by

$$1 + \rho\int h(1,2)d2 = kT\left(\frac{\partial\rho}{\partial P}\right)_T \qquad (V\text{-}2)$$

This equation relates the integral of h(r) to the compressibility of the liquid. Ornstein and Zernike derived equation (V-2) from number density fluctuation in a given sub-volume of the liquid. Equation (V-2) can also be shown as the same series expansion in powers of ρ on each side. The equation does not assume pairwise additivity. Ornstein and Zernike also introduced the direct correlation function c(r), defined by equation (V-1) which when integrated over volume element d2 gives

$$[1 + \rho\int h(1,2)d2][1-\rho\int c(1,2)d2] = 1 \qquad (V\text{-}3)$$

which enables equation (V-2) to have an alternative form

$$1 - \rho\int c(1,2)d2 = \frac{1}{kT}\left(\frac{\partial P}{\partial \rho}\right)_T \qquad \text{(V-4)}$$

Another reason for the significance of g(r) is that it derives from the scattering equation

$$\chi(k) = \frac{I(k)}{I_o(k)} = 1 + \rho\int[g(r)] - 1]\, e^{-ik.r}\, dr \qquad \text{(V-5)}$$

where I(k) is the observed intensity of scattered radiation, $k = (4\pi/\lambda)\mathrm{Sin}(\Theta/2)$, λ being the wavelength and Θ the scattering angle. $I_o(k)$ is the intensity of the radiation before scattering. This equation was first given by Zernike and Prins (2). However, these equations do not relate g(r) to the intermolecular potential $\phi(r)$. Attempts to establish this relationship form the core of the theories of the structure of liquids. Integral equation methods have been reviewed by Watts (3), and perturbation theories by Smith (4). Further reviews are given by Andersen (5), Gray (6), Egelstaff, Gray and Gubbins (7), Hansen and McDonald (8), Streett and Gubbins (9) and Chandler (10). A useful review of the graph-theoretical techniques which can be used for justification of the integral equation methods is given by McDonald and O'Gorman (11).

(V-2) Integral Equation Methods.

The best known theory is that of Percus-Yevick (PY) (12) which approximates the relationship between g(r) and $\phi(r)$ by setting c(r) to

$$C_{PY}(r) = g(r)[1 - \exp[\beta\phi(r)]] \qquad \text{(V-6)}$$

where $\beta = 1/kT$, and solving by substitution into equation (V-1). The results from this approximate theory are in qualitative agreement

with those from computer simulations, but predict the first peak in g(r) to be lower than actually found. A discussion of the inadequacies of the PY results is given by Verlet and Weis (13) for hard sphere systems. For more realistic atomic potentials with attractive tails, and harsh repulsive short range interactions the PY equations are only accurate at low densities where it includes all contributions to g(r) that are Zeroth and first order in density. At higher densities the qualitative description of the effect of the attractive interactions is incorrect, failing to move the peak of g(r) towards the attractive well of the potential. The PY equations have also been solved for a system of hard-core linear molecules by Chen and Steele (14) who used spherical harmonic expansions and truncated the series of coupled equations after two terms. This yielded reasonable results for small bond lengths ($L^* = L/\sigma \leq 0.2$) and low packing fractions ($\eta = \pi\rho\sigma^3/6 \leq 0.25$). The method of Chen and Steele was extended by Morrison (15) to chlorine systems using a two-centre Lennard-Jones soft sphere potential.

A second theory is the hypernetted chain equation (HNC) which was developed from the exact cluster theory relationship between c(r) and g(r), approximating the "bridge" diagrams to zero (16,17). This led to the use of the OZ equation (V-1) together with the following approximation for c(r)

$$C_{HNC}(r) = g(r) - 1 - \ell n(g(r)) - \beta\phi(r) \qquad \text{(V-7)}$$

Although less accurate than the PY equations for high density and short range forces, for low density and short range repulsive forces, it does include all contributions to g(r) that are zero or first order in density. At low density, for long range forces, the HNC equation seems to include the Debye-Hückel screening effect for

coulombic forces. Due to its accuracy at low density for short-range repulsive and long range forces, the HNC equation has been used by Rasaiah and Friedman (18) for the calculation of g(r) in dilute ionic solutions. The more dense case of a molten salt near its triple point has also been calculated from the HNC equation by Hansen and McDonald (19), with good agreement with the corresponding molecular dynamics results.

Another theory is the Mean Spherical Approximation (MSA) which was formulated by Lebowitz and Percus (20). It is frequently applied to fluids which interact with a hard core potential and an attractive tail. This approximation uses the OZ equation (V-1) with the exact condition

$$h(r) = -1 \qquad r < d \tag{V-8}$$

where d is the diameter of the hard core particle. This is 'closed' by using the approximation

$$c(r) = -\beta\phi(r) \qquad r > d \tag{V-9}$$

This closure has the advantage that it can be solved analytically for a number of simple models. It can be demonstrated that the PY equation for a system of hard spheres is a special case of MSA, where $\phi(r) = 0$. However, equation (V-9) does not give the correct low density limit of c(r). The two most important solutions of the MSA equation have been for primitive model ionic solutions by Waisman and Lebowitz (21) and for dipolar hard spheres by Wertheim (22).

MSA does however have a number of inadequacies. These are 1) the incorrect low density limit; 2) due to its PY like approximation

at high densities for short range potentials, it predicts too low a value for the first peak of g(r); 3) it only gives results which are qualitatively correct for coulombic potentials and 4) it underestimates the effects of $\phi(r)$ at low temperatures (i.e. the lowering of the first peak at high densities and the raising of the first peak of g(r) at low densities).

(V-3) The Perturbation Theory Methods.

For perturbation methods, the pair potential is separated into two components which are

$$\phi(r) = \phi_o(r) + v(r) \qquad \text{(V-10)}$$

where $\phi_o(r)$ is the potential of the reference system (whose properties are known or can be found) and where v(r) is the perturbation. How the separation of this potential is achieved, and the magnitude of the perturbation term strongly influences the accuracy of the solution.

For systems whose structure is determined primarily by short range repulsive forces (i.e. high density, weak attractive interactions or high temperatures), the reference system is chosen to contain all short range repulsive forces, such that

$$g(r) \approx g_o(r) \qquad \text{(V-11)}$$

and implies that zeroth order perturbation theory is adequate. (The subscript o will be used to denote the functions of the reference system.) The approximation given by equation (V-11) is known as the high temperature approximat ion (HTA) proposed by Weeks, Chandler and Andersen (23,24) neglects the effects of attractive forces on the structure of liquids. The pair potential in this method is separated as

$$\phi_o(r) = \phi(r) + \varepsilon \qquad r \leq r_{min} \qquad \text{(V-12)}$$

$$= 0 \qquad r > r_{min} \qquad \text{(V-13)}$$

$$v(r) = \phi(r) - \phi_o(r) \qquad \text{(V-14)}$$

where ε is the depth of the minimum in $\phi(r)$ and r_{min} is its position.

The Blip function theory derived by Andersen, Weeks and Chandler (25) is used to find the approximate radial distribution function of a system with repulsive forces only. If $\phi_R(r)$ is a purely repulsive potential, then g(r) is approximated by

$$g(1,2) = \exp[\beta\phi_R(1,2)]Y_{HS}(1,2) \qquad \text{(V-15)}$$

and

$$Y_{HS}(1,2) = \exp[-\beta\phi_{HS}(1,2)]g_{HS}(1,2) \qquad \text{(V-16)}$$

where the subscript HS denotes the functions of a hard sphere fluid of the same density as the fluid under study, and diameter d chosen such that

$$\int d2Y_{HS}(1,2)\{\exp[-\beta\phi_R(1,2)] - \exp[-\beta\phi_{HS}(1,2)]\} = 0 \qquad \text{(V-17)}$$

where the integral is over all relative positions and orientations of the two particles. Other criteria may be used for choosing the hard sphere diameter, thus significantly changing the calculated thermodynamic properties. This estimation of the equivalent hard

sphere diameter has been more fully discussed in Chapter III. Although this method is exact in the low density limit, it is however most successful for repulsive force fluids whose potentials are not too soft or orientationally dependent. Blip function theory is usually used as a part of a perturbation theory describing both repulsive and attractive force potentials. The method, together with a modification to deal with softer potentials is fully discussed by Andersen, Chandler and Weeks (26).

HTA has been used for Lennard-Jones fluids and has been shown to give a reasonable representation down to the triple point temperature (13). HTA has also been applied to molecular fluids by Steele and Sandler (27), who examined the orientational properties of the distribution functions.

In order to account for the attractive interactions the 'random phase approximation' (RPA) has been proposed for a classical electron gas by Andersen and Chandler (28) who subsequently extended it to ionic solutions (29). This approximation is equivalent to replacing the direct correlation function c(r) by

$$c(r) = c_o(r) - \beta v(r) \qquad \text{(V-18)}$$

where v(r) is given by equation (V-14), leading to

$$g(r) = g_o(r) + C(r) \qquad \text{(V-19)}$$

$$C(r) = \frac{\beta}{(2\pi)^3} \int \hat{u}(k) \left[\chi_o(k)\right]^2 \exp(i\underset{\sim}{k}.\underset{\sim}{r})\ d\underset{\sim}{k} \qquad \text{(V-20)}$$

where

$$\chi_o(k) = 1 + \rho\hat{h}_o(k) = 1+\rho\int h_o(r)\exp(i\underset{\sim}{k}.\underset{\sim}{r})d\underset{\sim}{r} \qquad \text{(V-21)}$$

and

$$\hat{u}(k) = \frac{\hat{v}(k)}{[1 + \beta\rho\hat{v}(k)\chi_o(k)]} \qquad \text{(V-22)}$$

or

$$\chi(k) = \frac{\chi_d(k)}{[1 + \beta\rho\hat{v}(k)\chi_o(k)]} \qquad \text{(V-23)}$$

In the HTA approximation the Helmholtz free energy is given by

$$A_{HTA} = A_{do} - \tfrac{1}{2}\beta\rho^2\int g_{HTA}(r)\phi(r)d\underset{\sim}{r} \qquad \text{(V-24)}$$

where A_{do} is the reference system contribution. The RPA free energy is given by

$$A_{RPA} = A_{do} + A_{HTA} + a_{RPA} \qquad \text{(V-25)}$$

$$a_{RPA} = \frac{\frac{1}{2}}{(2\pi)^3}\int d\underset{\sim}{k}\,[\beta\rho\hat{v}(k)\chi_o(k) - \ell n[1 + \beta\rho\hat{v}(k)\chi_o(k)]] \qquad \text{(V-26)}$$

For RPA to be convergent for all wave vectors

$$\beta\rho\hat{v}(k)\chi_o(k) < 1 \qquad \text{(V-27)}$$

thus the perturbation must be weak or the density low. RPA can, inside the hard core, predict unphysical non-zero values of g(r). This is because C(r) is usually non-zero in this range.

In order to remove the non-zero effect, the optimized random phase approximation (ORPA) was proposed by Andersen and Chandler (30) in the context of ionic solution theory. ORPA was then generalised by Andersen, Chandler and Weeks (31) to the study of simple liquids, including Lennard-Jones fluids. The method demands that g(r), and thus C(r) be zero within the hard core. This is accomplished by changing v(r) for r < d, which alters $\hat{v}(k)$ and $\hat{u}(k)$ for all wavevectors, giving an optimized value of a_{RPA}. v(r) for r < d is chosen such that

$$g_{RPA}(r) = - (2/\rho^2)\left[(\delta A_{RPA})/\delta\beta v(r)\right] = 0 : \quad r < d \qquad \text{(V-28)}$$

This is equivalent to demanding that

$$\left[\delta a_{RPA}/\delta v(r)\right] = 0 \quad : \quad r < d \qquad \text{(V-29)}$$

where a_{RPA} is given by equation (V-26). Thus ORPA is any one of equations (V-23,18,19) or equation (V-25) together with equation (V-29). ORPA can be shown to reduce to MSA when the exact g(r) (hard sphere) is replaced by its PY counterpart. ORPA has been applied to the calculation of the structural and thermodynamic properties of primitive model ionic solutions (32) and Lennard-Jones fluids (31,32) by Andersen, Chandler and Weeks who show that ORPA is accurate at high and moderate densities, but not at low densities. ORPA underestimates the effect of the perturbation potential at high densities and although it predicts changes in the right direction, they are not large enough. At low densities it can easily predict negative correlation functions for repulsive interactions, but again underestimates the effects of attractive interactions.

In a further study of optimized cluster theory by Andersen and Chandler (33), a formal cluster expansion for the structure of a fluid, and ideas about the truncation of the infinite cluster series were presented, which reduce to practicable approximate expressions. They suggested for the pair correlation function the exponential approximation (EXP) which is given by

$$g_{EXP}(r) = g_o(r)\exp[C(r)] \qquad \text{(V-30)}$$

where C(r) is given by equation (V-20). For the free energy the ORPA+B_2 approximation was suggested, and is given by

$$A \approx A_d + A_{HTA} + A_{ORPA} + B_2 \qquad \text{(V-31)}$$

where A_{ORPA} is equivalent to a_{RPA} given in equation (V-26) with $\hat{v}(k)$ determined by the optimization condition equation (V-29). The B_2 term is given by

$$B_2 = \tfrac{1}{2}\rho^2\int h_o(r).\tfrac{1}{2}[C(r)]^2 d\underset{\sim}{r} + \tfrac{1}{2}\rho^2\int g_o(r) \sum_{n=3}^{\infty} \frac{1}{n!}[C(r)]^n \, d\underset{\sim}{r} \qquad \text{(V-32)}$$

The accuracy of these approximations was investigated (32) and found to be in very good agreement with computer simulation results, both for Lennard-Jones fluids and ionic solutions. The approximation is found to be accurate at all densities for short and long ranged perturbations, provided that the attractive tail of the pair potential is small in majnitude (i.e. $\beta\phi(r) < 1.5$ for $r > d$). In each of the following three limits; low density, high density and high temperature, both ORPA+B_2 and EXP approximations are asymptotically correct. For

low density and coulombic tails, the EXP approximation gives Debye-Hückel screening. While for Lennard-Jones fluids at high density, EXP predicts only small corrections of the correct sign to HTA. These optimized cluster approximations are reviewed in detail by Andersen, Chandler and Weeks (26).

(V-4) RISM THEORY.

Introduction.

The extension of optimized cluster theory (33) to molecular fluids by Chandler and Andersen (34) gave rise to the reference interaction site model approximation (RISM). In this model the molecule is composed of m rigidly connected hard spheres. The αth sphere has a diameter of d_α and is located at the αth site whose position on the jth molecule is given by

$$\underset{\sim}{r}_j^\alpha = \underset{\sim}{R}_j + \underset{\sim}{\ell}_j^\alpha \qquad \text{(V-33)}$$

where $\underset{\sim}{R}_j$ is the position of the origin of the jth molecule (orientation $\underset{\sim}{\Omega}_j$), whose bond vector from the origin to the αth site is $\underset{\sim}{\ell}_j^\alpha$. (See Figure (V-1)). The pair potential is then given by

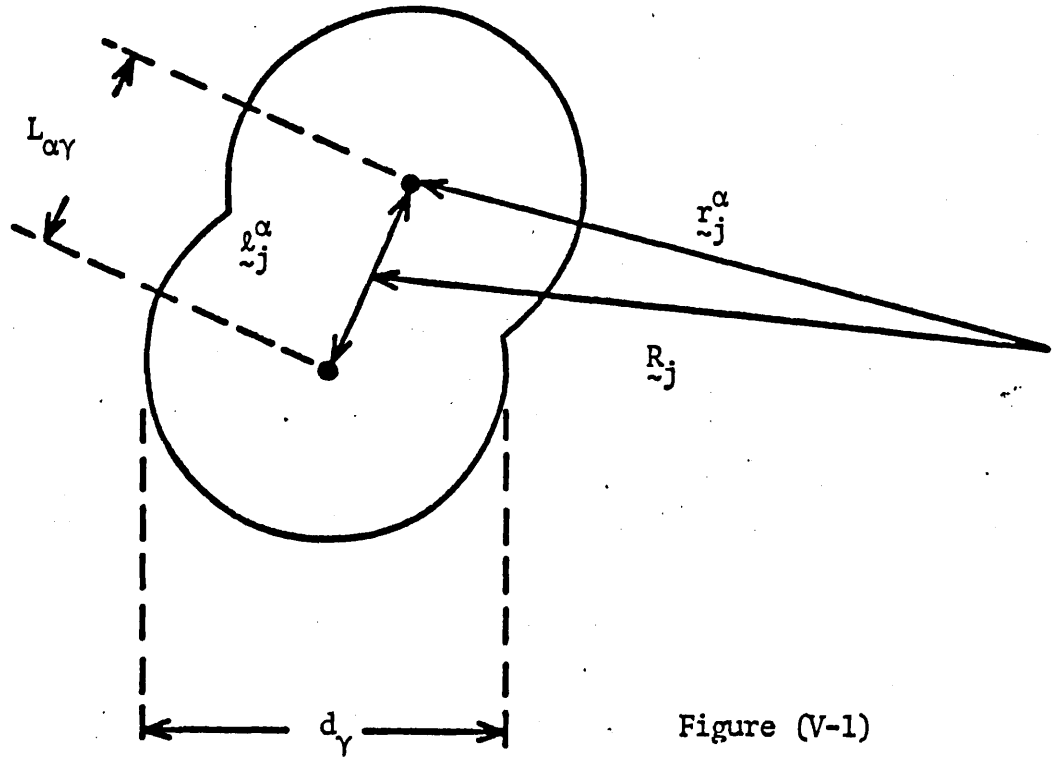

Figure (V-1)

$$w_{IS}(i,j) = \sum_{\alpha=1}^{m} \sum_{\gamma=1}^{m} w_{\alpha\gamma}(|\underset{\sim}{r}_i^{\alpha} - \underset{\sim}{r}_j^{\gamma}|) \qquad \text{(V-34)}$$

where

$$w_{\alpha\gamma}(r) = u_{d\alpha\gamma}(r) + u_{\alpha\gamma}(r) \qquad \text{(V-35)}$$

$u_{d\alpha\gamma}(r)$ being a hard sphere potential of diameter $d_{\alpha\gamma}$ and $u_{\alpha\gamma}(r)$ is the perturbation potential. The restriction that the hard sphere diameters should be additive (i.e. $d_{\alpha\gamma} = (d_{\alpha}+d_{\gamma})/2$) need not hold.

The Helmholtz free energy for molecular systems can be obtained from the canonical ensemble partition function Q by

$$A = -\Delta a/kTV = \ell nQ/V \qquad \text{(V.36)}$$

where

$$Q = \frac{1}{(V\Omega)^N} \int d\underset{\sim}{R}^N d\underset{\sim}{\Omega}^N \exp\left[-\sum_{i<j=1}^{N} w(r_{ij})/kT\right] \qquad \text{(V-37)}$$

where

$$\int d\underset{\sim}{\Omega}_i = \underset{\sim}{\Omega} = \begin{cases} 4\pi \text{ - linear molecule} \\ 8\pi^2 \text{ - non-linear molecule} \end{cases} \qquad \text{(V-38)}$$

The full two-particle distrib ution function $g(\underset{\sim}{R},\underset{\sim}{\Omega},\underset{\sim}{\Omega}')$ for molecular systems is defined by

$$\frac{\rho^2}{\Omega^2} g(\underset{\sim}{R},\underset{\sim}{\Omega},\underset{\sim}{\Omega}') = \left\langle \sum_{\substack{i=1 \\ (i\neq j)}}^{N} \sum_{j=1}^{N} \delta(\underset{\sim}{R}_i)\delta(\underset{\sim}{R}_j - \underset{\sim}{R})\delta(\underset{\sim}{\Omega}_i - \underset{\sim}{\Omega})\delta(\underset{\sim}{\Omega}_j - \underset{\sim}{\Omega}') \right\rangle \qquad \text{(V-39)}$$

The site-site radial distribution function $g_{\alpha\gamma}(r)$ is defined by

$$g_{\alpha\gamma}(r) = \Big\langle \sum_{\substack{i=1 \\ (i\neq j)}}^{N} \sum_{j=1}^{N} \delta(\underset{\sim}{r}_i^{\alpha})\delta(\underset{\sim}{r}_j^{\alpha}-\underset{\sim}{r}) \Big\rangle \tag{V-40}$$

$$= \frac{\rho^2}{\Omega^2} \int d\underset{\sim}{R}\, d\underset{\sim}{R}'\, d\underset{\sim}{\Omega} d\underset{\sim}{\Omega}' g(\underset{\sim}{R}-\underset{\sim}{R}', \underset{\sim}{\Omega}, \underset{\sim}{\Omega}')$$

$$\times \delta(\underset{\sim}{R}+\underset{\sim}{\ell}^{\alpha}(\underset{\sim}{\Omega}))\, \delta(\underset{\sim}{R}'+\underset{\sim}{\ell}^{\gamma}(\underset{\sim}{\Omega}')-\underset{\sim}{r}) \tag{V-41}$$

The radial distribution functions are then related to the free energy by the following functional derivative relationships

$$g(\underset{\sim}{R}, \underset{\sim}{\Omega}, \underset{\sim}{\Omega}') = \frac{-2kT\Omega^2}{\rho^2} \left[\frac{\delta A}{\delta \omega(\underset{\sim}{R}, \underset{\sim}{\Omega}, \underset{\sim}{\Omega}')} \right] \tag{V-42}$$

$$g_{\alpha\gamma}(r) = \frac{-2kT}{\rho^2} \left[\frac{\delta A}{\delta u_{\alpha\gamma}(r)} \right] \tag{V-43}$$

The cluster expansions of Andersen and Chandler (33) used for simple fluids are extended to molecular fluids by substituting for the integration over a particle by an integration over position and orientation. Thus

$$\rho \int d\underset{\sim}{r}_i \rightarrow (\rho/\Omega) \int d\underset{\sim}{R}_i d\underset{\sim}{\Omega}_i \equiv (\rho/\Omega) \int di \tag{V-44}$$

(V-5) Theory of Reference System.

To determine the properties of the reference system, in which the pair interactions are given by

$$U_{Ref}(r) = \sum_{\alpha,\gamma=1}^{m} U_{d\alpha\gamma}(|\underset{\sim}{r}_1^{\alpha}-\underset{\sim}{r}_2^{\gamma}|) \tag{V-45}$$

and a method similar to the PY equation for hard spheres was used. The direct correlation function c(r) is defined by the OZ equation (V-1) where h(r) is given by

$$h(r) = g(\underset{\sim}{R}_{12},\underset{\sim}{\Omega}_1,\underset{\sim}{\Omega}_2)-1 \qquad \text{(V-46)}$$

The pair potential is infinite if any pair of spheres of molecules 1 and 2 overlap and is otherwise zero. The PY closure for such a fluid of hard sphere molecules is

$$\begin{aligned} C_{PY}(1,2) &= 0 \quad : \quad \text{No Overlap (approximate)} \\ h_{PY}(1,2) &= -1 \quad : \quad \text{Overlap (exact)} \end{aligned} \qquad \text{(V-47)}$$

The solution of the OZ equation with PY closure for molecular fluids involves angular expansions which rapidly becomes intractable. However, the RISM method consists of a generalization of the PY relationship to molecular fluids, in which the direct correlation function is the sum of the site-site functions. This can be treated analytically. This can be written

$$C_{ref}(r) = C_o(r) + \Delta_c(r) \qquad \text{(V-48)}$$

where

$$C_o(r) = \sum_{\alpha,\gamma} c_{\alpha\gamma}(|\underset{\sim}{r}_1^{\alpha}-\underset{\sim}{r}_2^{\gamma}|) \qquad \text{(V-49)}$$

and

$$C_{\alpha\gamma}(r) = 0 \qquad \text{for} \qquad r > d_{\alpha\gamma} \qquad \text{(V-50)}$$

Equation (V-50) is implied by the PY approximation. However, from the expansion of c(r) it can be seen that $\Delta c(r)$ is not zero. The

"best" choice for $c_{\alpha\gamma}(r)$ functions is one for which $C_{ref}(r) \approx C_o(r)$. The solution of the OZ equation when $\Delta c(r) = 0$ is denoted by $h_o(r)$. Thus

$$h_o(1,2) = C_o(1,2) + (\rho/\Omega)\int d3\ C_o(1,3)\ h_o(2,3) \qquad \text{(V-51)}$$

then

$$h_{ref}(1,2) = h_o(1,2) + O(\Delta_c) \qquad \text{(V-52)}$$

Neglecting the Δc term in equation (V-52) is a poor approximation as it becomes impossible to ensure the closure $h_{ref}(r) = -1$ when molecules 1 and 2 overlap. This leads to the study of the site-site correlation functions defined by

$$h^{\alpha\gamma}_{ref}(r) = \Omega^{-1}\int d1d2\,\delta(\underset{\sim}{R}_1+\underset{\sim}{\ell}^{\alpha}_1)\,\delta(\underset{\sim}{R}_2-\underset{\sim}{\ell}^{\gamma}_2-\underset{\sim}{r})\ h_{ref}(1,2) \qquad \text{(V-53)}$$

where

$$h_{ref}(1,2) = c_o(1,2) + \sum_{n=1}^{\infty} \rho^n \int d3....d(n+2)$$

$$x C_o(1,3).C_o(3,4)....C_o((n+2),2) \qquad \text{(V-54)}$$

with $c_o(\underset{\sim}{R}_{12},\underset{\sim}{\Omega}_1,\underset{\sim}{\Omega}_2)$ given by equation (V-49). Equation (V-53) can be shown to give the following Ornstein-Zernike like equation (34,35) in terms of the site-site functions.

$$h_{ref}(r) = \omega^* c^* \omega(r) + \rho\omega^* c^* h_{ref}(r) \qquad \text{(V-55)}$$

where * denotes a convolution and $h(r)$, $\omega(r)$ and $c(r)$ are matrices having elements $h^{ref}_{\alpha\gamma}(r)$, $\omega_{\alpha\gamma}(r)$ and $c_{\alpha\gamma}(r)$. It is useful to note that equation (V-1) for spherical molecules becomes

$$h(r) = c(r) + \rho c*h(r) \tag{V-56}$$

and

$$c*h(r) = \int d\underset{\sim}{r}' c(|\underset{\sim}{r}-\underset{\sim}{r}'|)h(\underset{\sim}{r}')$$

The Fourier transform of equation (V-55) gives

$$\hat{h}_{ref}(k) = \hat{\omega}(k)\hat{c}(k)\left[\underset{\sim}{1}-\rho\hat{\omega}(k)\hat{c}(k)\right]^{-1}\hat{\omega}(k) + O(\Delta c(k)) \tag{V-57}$$

where M^{-1} denotes the matrix inverse and $\underset{\sim}{1}$ the unit matrix. The $\omega_{\alpha\gamma}(k)$ function is the internal structure factor defined by

$$\hat{\omega}_{\alpha\gamma}(k) = \Omega^{-1}\int d\underset{\sim}{\Omega}_1 \exp\left[i\underset{\sim}{k}.(\underset{\sim}{\ell}^{\alpha}_1-\underset{\sim}{\ell}^{\gamma}_2)\right] \tag{V-58}$$

$$= S_{\sim}(k|\underset{\sim}{\ell}^{\alpha}_1-\underset{\sim}{\ell}^{\gamma}_2|)/k(|\underset{\sim}{\ell}^{\alpha}_1-\underset{\sim}{\ell}^{\gamma}_2|) \tag{V-59}$$

It is now possible to neglect Δ_c terms without producing unphysical effects, and so obtain

$$\left[h^{\alpha\gamma}_{ref}(r)\right]_{RISM} = (2\pi)^{-3}\int d\underset{\sim}{k}\left[\hat{\omega}(k)\hat{c}(k)\left[\underset{\sim}{1}-\rho\hat{\omega}(k)\hat{c}(k)\right]^{-1}\hat{\omega}(k)\right]$$

$$x \exp(i\underset{\sim}{k}.\underset{\sim}{r}) \tag{V-60}$$

The 'best choice' for $c_{\alpha\gamma}(r)$ function is such that

$$h^{\alpha\gamma}_{ref}(r) = -1 \qquad \text{for} \qquad r \leq d \tag{V-61}$$

Thus the RISM theory consists of equations (V-50,60,61). These equations have been shown by Ladanyi and Chandler (36) to have the following limiting properties -

1) That the solutions of the RISM equations give cusps and discontinuities at precisely the same positions as those of the exact $h_{\alpha\gamma}(r)$.

2) As the site-site intramolecular distances $h_{\alpha\gamma} \to \infty$ the site-site correlation functions can be calculated as if the molecular fluid were a mixture, where the interaction sites are treated as independent particles. The solution in this case is the same as the PY solution for mixtures.

3) If for any reason there is only one effective interaction site in a molecule then the RISM equations reduce to the PY equation.

In passing, it is useful to note that the contribution to $h^{\alpha\gamma}_{ref}(r)$ from the first term on the right hand side of equation (V-55) is

$$c_{\alpha\gamma}(r) + \sum_{\eta=1}^{m} \int d\underset{\sim}{r}' \{ s^{(2/m)}_{\alpha\eta}(|\underset{\sim}{r}-\underset{\sim}{r}'|) c_{\eta\gamma}(r') + c_{\alpha\eta}(|\underset{\sim}{r}-\underset{\sim}{r}'|) s^{(2/m)}_{\eta\gamma}(r')$$

$$+ \sum_{\nu=1}^{m} \int d\underset{\sim}{r}'' s^{(2/m)}_{\alpha\eta}(|\underset{\sim}{r}-\underset{\sim}{r}'|) c_{\eta\nu}(|\underset{\sim}{r}'-\underset{\sim}{r}''|) s^{(2/m)}_{\nu\gamma}(r'') \} \tag{V-62}$$

and

$$w_{\alpha\gamma}(r) = \delta_{\alpha\gamma}\delta(\underset{\sim}{r}) + s^{(2/m)}_{\alpha\gamma}(r) \tag{V-63}$$

where

$$s_{\alpha\gamma}^{(2/m)}(|r-r'|) = \int d\underset{\sim}{R}_2 d\underset{\sim}{\Omega}_2 \delta(r_2^{\alpha}-r)\delta(r_2^{\gamma}-r') \tag{V-64}$$

$$= \frac{(1-\delta_{\alpha\gamma})\delta(|r-r'|-L_{\alpha\gamma})}{4\pi L_{\alpha\gamma}^2} \tag{V-65}$$

where

$$L_{\alpha\gamma} = |\underset{\sim}{\ell}_1^{\alpha}-\underset{\sim}{\ell}_1^{\gamma}|$$

(V-6) Theory of Perturbations.

Having found $g_{ref}^{\alpha\gamma}(r)$, it is now possible to calculate the effect of the perturbation potential $v_{\alpha\gamma}(r)$ by means of

$$v_{\alpha\gamma}(r) = w_{\alpha\gamma}(r) - ud_{\alpha\gamma}(r) \tag{V-66}$$

perturbation theory. Applying HTA, the simplest approximation gives

$$A_{HTA} = A_{ref} + (\rho^2/2) \sum_{\alpha,\gamma} \int g_{ref}^{\alpha\gamma}(r)\phi_{\alpha\gamma}(r)\, d\underset{\sim}{r} \tag{V-67}$$

where

$$\phi_{\alpha\gamma}(r) = -v(|\underset{\sim}{r}_1^{\alpha}-\underset{\sim}{r}_2^{\gamma}|)/kT \tag{V-68}$$

Corrections to this approximation must account for the effects of perturbations on the structure. The corrections are given by the ring diagram sum, which contain perturbation and h_{ref} bonds and are discussed by Andersen and Chandler (33). All ring diagrams involving n perturbation bonds are then written as one generalized ring defined by

$$F_{ref}(1,2) = (\rho/\Omega)\delta(\underset{\sim}{R}_1-\underset{\sim}{R}_2)\delta(\underset{\sim}{\Omega}_1-\underset{\sim}{\Omega}_2) + (\rho/\Omega)^2 h_{ref}(1,2) \qquad \text{(V-69)}$$

This function is a generalization of the hypervex function $F_{ref}(r) = \rho\delta(\underset{\sim}{r}) + \rho^2 h_{ref}(\underset{\sim}{r})$. The generalized ring involving n perturbation bonds is

$$R^{(n)} = (2nV)^{-1}\int d1d2....d(2n)$$

$$x \sum_{\alpha,\gamma}\sum_{\lambda,\xi} .... \sum_{\eta,\nu} \phi_{\alpha\gamma}(1,2)F_{ref}(2,3)$$

$$x\, \phi_{\lambda\xi}(3,4)....\phi_{\eta\nu}(2n-1,2n)F_{ref}(2n,1) \qquad \text{(V-70)}$$

and is the general ring diagram contributing to ORPA. Provided Fourier transforms of $\phi_{\alpha\gamma}(1,2)$ exist, then for example n=3

$$R^{(3)} = (6V)^{-1}(2\pi)^{-9}\int d1....d6\int d\underset{\sim}{k}_1 d\underset{\sim}{k}_2 d\underset{\sim}{k}_3$$

$$x \sum_{\alpha,\gamma}\sum_{\lambda,\xi}\sum_{\eta,\nu} \hat{\phi}_{\alpha\gamma}(k_1)\hat{\phi}_{\lambda\xi}(k_2)\hat{\phi}_{\eta,\nu}(k_3)$$

$$x\, F_{ref}(2,3)F_{ref}(4,5)F_{ref}(6,1)$$

$$x \exp[i\underset{\sim}{k}_1(\underset{\sim}{r}_1^{\alpha}-\underset{\sim}{r}_2^{\gamma}) + i\underset{\sim}{k}_2(\underset{\sim}{r}_3^{\lambda}-\underset{\sim}{r}_4^{\xi}) + i\underset{\sim}{k}_3(\underset{\sim}{r}_5^{\eta}-\underset{\sim}{r}_6^{\nu})] \qquad \text{(V-71)}$$

These integrals over configurations are performed by noting that $\underset{\sim}{r}_i^{\alpha} = \underset{\sim}{R}_i + \underset{\sim}{\ell}_i^{\alpha}$, thus

$$(2\pi)^{-3}\int dm\,dj F_{ref}(m,j)\exp\left[-i(\underset{\sim}{k}.\underset{\sim}{r}^{\alpha}_{m} + \underset{\sim}{k}'.\underset{\sim}{r}^{\gamma}_{j})\right]$$

$$= \delta(k+k')\left[\rho\omega_{\alpha\gamma}(k) + \rho^{2}\hat{h}_{ref}(k)\right]$$

$$\equiv \delta(k+k')\Gamma_{\alpha\gamma}(k) \qquad \text{(V-72)}$$

Using equation (V-72) one obtains for $R^{(3)}$

$$R^{(3)} = \left[6(2\pi)^{3}\right]^{-1}\int d\underset{\sim}{k} \sum_{\alpha,\gamma}\sum_{\lambda,\xi}\sum_{\eta,\nu} \hat{\phi}_{\alpha\gamma}(k)\hat{\phi}_{\lambda\xi}(k)\hat{\phi}_{\eta,\nu}(k)$$

$$x\ \Gamma_{\gamma\lambda}(k)\Gamma_{\xi\eta}(k)\Gamma_{\nu\alpha}(k)$$

$$= \left[6(2\pi)^{3}\right]^{-1}\int d\underset{\sim}{k}\ Tr\left[\hat{\phi}(k)\Gamma(k)\right]^{3} \qquad \text{(V-73)}$$

where Tr denotes the trace of the resultant matrix. The summation of all the generalized rings ($n \geq 2$) now gives

$$a_{RING} = \sum_{n=2}^{\infty} R^{(n)}$$

$$= -\left[2(2\pi)^{3}\right]^{-1}\int d\underset{\sim}{k}\{Tr\left[\Gamma(k)\hat{\phi}(k)\right] + \ell nDet\left[\underset{\sim}{1}-\Gamma(k)\hat{\phi}(k)\right]\} \qquad \text{(V-74)}$$

where Det denotes the determinant of the matrix. (N.B. For a diagonalizable matrix A, $Tr\ell nA = \ell nDetA$)

Now the ORPA free energy is given by

$$A_{ORPA} = A_{HTA} + a_{RING} \qquad \text{(V-75)}$$

Thus from the functional derivative relationship given in equation (V-43), the correlation functions are obtained

$$g^{\alpha\gamma}_{ORPA}(r) = g^{\alpha\gamma}_{ref}(r) + \rho^{-2}(2\pi)^{-3}\int d\underset{\sim}{k}\, \exp[-i\underset{\sim}{k}.\underset{\sim}{r}]$$

$$x\ \{\Gamma(k)\hat{\phi}(k)\,[\underset{\sim}{1}-\Gamma(k)\hat{\phi}(k)]^{-1}\Gamma(k)\}_{\alpha\gamma} \qquad \text{(V-76)}$$

The optimized perturbation used in equations (V-75,76) is the solution to the variational equation

$$[\delta a_{RING}/\delta v_{\alpha\gamma}(r)] = 0 \qquad \text{for} \qquad r < d_{\alpha\gamma} \qquad \text{(V-77)}$$

which is equivalent to applying the exact restriction

$$h_{\alpha\gamma}(r) = -1 \qquad \text{for} \qquad r < d_{\alpha\gamma} \qquad \text{(V-78)}$$

This perturbation method for molecular fluids, solved on a site-site basis may be applied to Monte Carlo and molecular dynamics generated reference site-site distribution functions. In the special case that the RISM equations are used to give $g^{\alpha\gamma}_{ref}(r)$, then equations (V-76,77) can be shown to yield

$$h_{\alpha\gamma}(r) = (2\pi)^{-3}\int d\underset{\sim}{k}\, \exp(i\underset{\sim}{k}.\underset{\sim}{r})\{\omega(k)\hat{c}(k)\,[\underset{\sim}{1}-\rho\omega(k)\hat{c}(k)]^{-1}\omega(k)\}_{\alpha\gamma} \qquad \text{(V-79)}$$

where the matrix elements of the $c_{\alpha\gamma}(r)$ matrix are defined by

$$C_{\alpha\gamma}(r) = -\, v_{\alpha\gamma}(r)/kT \qquad \text{for} \qquad r \geq d_{\alpha\gamma} \qquad \text{(V-80)}$$

and determined for $r < d_{\alpha\gamma}$ by equation (V-78). Thus equations (V-78,79,80) form the solution for $g_{\alpha\gamma}(r)$, and when all the interaction sites on a molecule are at the same point these equations reduce to the MSA equations.

(V-7) Treatment of Soft Cores.

The molecular correlation function is a function of the Mayer cluster function, given by

$$f(1,2) = -1 + \exp[-w(1,2)/kT] \qquad \text{(V-81)}$$

and for hard core RISM systems by

$$[f_{\alpha\gamma}(r)]_{RISM} = fd\alpha\gamma(r) = -1 \quad \text{for} \quad r < d \qquad \text{(V-82)}$$

$$= 0 \quad \text{for} \quad r \geq d$$

where $y_{\alpha\gamma}(r)$, the indirect correlation function may be defined by

$$y_{\alpha\gamma}(r) = \exp[-w_{\alpha\gamma}(r)/kT].g_{\alpha\gamma}(r) \qquad \text{(V-83)}$$

which gives

$$h_{\alpha\gamma}(r) = f_{\alpha\gamma}(r) + [1 + f_{\alpha\gamma}(r)].[y_{\alpha\gamma}(r)-1] \qquad \text{(V-84)}$$

It can also be shown that

$$C_{\alpha\gamma}(r) = f_{\alpha\gamma}(r).y_{\alpha\gamma}(r) \qquad \text{(V-85)}$$

Thus for hard core systems

$$y_{\alpha\gamma}(r) = - C_{\alpha\gamma}(r) \quad \text{for} \quad r < d \qquad \text{(V-86)}$$

$$= g_{\alpha\gamma}(r) \quad \text{for} \quad r \geq d$$

It can also be shown that $y_{\alpha\gamma}(r)$ is a continuous function (36). Then from equations (V-82) and (V-84) for a RISM fluid

$$h_{\alpha\gamma}(r) = -1 \qquad \text{for} \quad r < d \tag{V-87}$$

$$= -1 + y_{\alpha\gamma}(r) \qquad \text{for} \quad r \geq d$$

$h_{\alpha\gamma}(r)$ is discontinuous at $r = d_{\alpha\gamma}$. The magnitude of the discontinuity is $y_{\alpha\gamma}(d_{\alpha\gamma})$. As $y_{\alpha\gamma}(r)$ is continuous, there are no other discontinuities.

While $y_{\alpha\gamma}(r)$ is a continuous function, its derivatives are not. This can be demonstrated by differentiating the integrals which arise from the cluster series expansion of $y_{\alpha\gamma}(r)$. If the function is discontinuous at $r = d_{\alpha\gamma}$ then the derivative will be discontinuous at

$$r = |d_{\alpha\eta} \pm L_{\eta\gamma}| \qquad 1 \leq \eta \leq m \text{ but } \eta \neq \gamma \tag{V-88}$$

$$= |d_{\gamma\eta} \pm L_{\eta\alpha}| \qquad 1 \leq \eta \leq m \text{ but } \eta \neq \alpha$$

In certain special cases it is possible for $y_{\alpha\gamma}(r)$ to have cusps located at other positions too.

The smoothing of these discontinuities and cusps is carried out by a method similar to the blip-function expansion (36). Let the subscript d denote the functions of the RISM fluid, which has the same $L_{\alpha\gamma}$'s and density as the system of interest for which $w_{\alpha\gamma}(r)$ is a continuous repulsive potential. The Mayer functions of the RISM fluid are then given by equation (V-82) where the site-site diameters are chosen such that

$$0 = \int_0^\infty dr \Delta f_{\alpha\gamma}(r) \tag{V-89}$$

or equivalently

$$d_{\alpha\gamma} = - \int_0^\infty dr\, f_{\alpha\gamma}(r) \tag{V-90}$$

where

$$\Delta f_{\alpha\gamma}(r) = (-1 + \exp[-w(r)/kT]) - fd\alpha\gamma(r)$$

$$= f_{\alpha\gamma}(r) - fd\alpha\gamma(r) \tag{V-91}$$

A fuller discussion on the criteria for choosing hard sphere diameters is given in Chapter III. A 'softness' parameter ξ giving a measure of the width of the blip function $\Delta f_{\alpha\gamma}(r)$ is roughly $d_{\alpha\gamma}^{-1}$ times the range of values over which $\Delta f_{\alpha\gamma}(r)$ is non-zero, and may be estimated by

$$\xi = d_{\alpha\gamma}^{-1} \int_0^\infty dr |\Delta f_{\alpha\gamma}(r)| \tag{V-92}$$

Due to equation (V-89), this implies that for any function F(r)

$$\int_0^\infty dr\, \Delta f_{\alpha\gamma}(r) F(r) \approx O(\xi^2) \tag{V-93}$$

To study the effect of changing from $fd\alpha\gamma(r)$ to $fd\alpha\gamma(r) + \Delta f_{\alpha\gamma}(r)$, it is useful to separate $y_{\alpha\gamma}(r)$ into two parts; first a smooth function and second a function that contains the cusps present in $yd\alpha\gamma(r)$, on assuming that they occur in the positions given by

equation (V-88)

$$y_{\alpha\gamma}(r) = y^{(s)}_{\alpha\gamma}(r) + y^{(c)}_{\alpha\gamma}(r) \tag{V-94}$$

where $y^{(c)}_{\alpha\gamma}(r)$ is defined by

$$y^{(c)}_{\alpha\gamma}(r) = \rho \sum_{\eta=1}^{m} \int d\underset{\sim}{r}' \{A_{\alpha\eta\gamma} s^{(2/m)}_{\alpha\eta}(r') f_{\eta\gamma}(|\underset{\sim}{r}-\underset{\sim}{r}'|)$$

$$+ A_{\gamma\eta\alpha} f_{\alpha\eta}(r') S^{(2/m)}_{\eta\gamma}(|\underset{\sim}{r}-\underset{\sim}{r}'|)\} \tag{V-95}$$

the S functions are given by equation (V-65) and the constants $A_{\alpha\eta\gamma}$ defined by

$$A_{\alpha\eta\gamma} = \frac{[2L_{\alpha\eta}(L_{\alpha\eta}+d_{\eta\gamma})]}{d_{\eta\gamma}} \{\lim_{\varepsilon\to 0+} [\dot{y}_{d\alpha\gamma}(L_{\alpha\eta}+d_{\eta\gamma}-\varepsilon) - \dot{y}_{d\alpha\gamma}(L_{\alpha\eta}+d_{\eta\gamma}+\varepsilon)]\} \tag{V-96}$$

where

$$\dot{y}_{d\alpha\gamma}(r) = \frac{dy_{\alpha\gamma}(r)}{dr}$$

Now examining the properties of the smooth part $y^{(s)}_{\alpha\gamma}(r)$, let $K_{\alpha\gamma\eta\nu}(\underset{\sim}{r},\underset{\sim}{r}')$ be the functional derivative of $y^{(s)}_{\alpha\gamma}(r)$ with respect to $f_{\eta\nu}(r')$

$$K_{\alpha\gamma\eta\nu}(\underset{\sim}{r},\underset{\sim}{r}') = \left[\frac{\delta y^{(s)}_{\alpha\gamma}(\underset{\sim}{r})}{\delta f_{\eta\nu}(\underset{\sim}{r}')}\right] \tag{V-97}$$

Using equation (V-91) and integrating equation (V-97) one obtains

$$y^{(s)}_{\alpha\gamma}(r) = y^{(s)}_{d\alpha\gamma}(r) + \sum_{\eta,\nu=1}^{m} \int d\underset{\sim}{r}' K_{\alpha\gamma\eta\nu}(r,r') \Delta f_{\eta\nu}(r') \tag{V-98}$$

where $K_{\alpha\gamma\eta\nu}(r,r')$ is a continuous function. Then from equation (V-93)

$$y^{(s)}_{\alpha\gamma}(r) = y^{(s)}_{d\alpha\gamma}(r) + O(\xi^2) \tag{V-99}$$

and

$$y_{\alpha\gamma}(r) = y^{(s)}_{d\alpha\gamma}(r) + y^{(c)}_{\alpha\gamma}(r) + O(\xi^2) \tag{V-100}$$

with the result that

$$g_{\alpha\gamma}(r) = [1+f_{\alpha\gamma}(r)][y^{(s)}_{d\alpha\gamma}(r) + y^{(c)}_{\alpha\gamma}(r)] + O(\xi^2) \tag{V-101}$$

Thus the pair correlation functions of fluids with smooth repulsive forces can be calculated to ξ^2 order.

(V-8) Method of Solution.

The RISM equations are solved by application of the variational method originally presented by Chandler and Andersen (34). The functional derivative I_{RISM} is defined such that it satisfies the relation

$$\rho^{-2}\left[\frac{\delta I_{RISM}}{\delta C_{\alpha\gamma}(r)}\right] = [g_{\alpha\gamma}(r)]_{RISM} \tag{V-102}$$

differentiating equation (V-79) yields

$$I_{RISM} = \rho^2 \sum_{\alpha,\gamma} \hat{c}_{\alpha\gamma}(0) - (2\pi)^{-3} \int d\underset{\sim}{k}$$

$$x \{Tr[\rho\omega(k)\hat{c}(K)] + \ell nDet[\underset{\sim}{1}-\rho\omega(k)\hat{c}(k)]\} \tag{V-103}$$

The closure $h_{\alpha\gamma}(r) = -1$ for $r < d_{\alpha\gamma}$ can be expressed as

$$\left[\frac{\delta I_{RISM}}{\delta c_{\alpha\gamma}(r)}\right] = 0 \qquad \text{for } r < d \tag{V-104}$$

with equations (V-103,104) forming a variational method for solving the RISM equations. In particular, a power series approximation is used for the $c_{\alpha\gamma}(r)$ functions inside the hard core

$$c_{\alpha\gamma}(r) = \eta(d_{\alpha\gamma}-r) \sum_{i=1}^{n} a_i^{\alpha\gamma} \left[(r/d_{\alpha\gamma}) - 1\right]^{(i-1)} \tag{V-105}$$

and $\eta(x)$ is a step function given by

$$\eta(x) = 0 \qquad \text{for} \qquad x < 0 \tag{V-106}$$

$$= 1 \qquad \text{for} \qquad x \geq 0$$

I_{RISM} is now a function of the power series coefficients $a_i^{\alpha\gamma}$ and thus equation (V-104) becomes

$$\left[\frac{\delta I_{RISM}}{\delta a_i^{\alpha\gamma}}\right] = 0 \qquad \text{for} \qquad r \leq d_{\alpha\gamma} \tag{V-107}$$

which gives a system of $n\left[\frac{1}{2}m(m+1)\right]$ coupled algebraic equations. These are solved using a multidimensional Newton-Raphson technique. Following Lowden and Chandler (37) the expression for I_{RISM} was replaced by

$$I_{RISM} = \rho^2 \sum_{\alpha,\gamma=1}^{m} \int_0^\infty d\underset{\sim}{r}\left[C_{\alpha\gamma}(r) + \tfrac{1}{2} C^2_{\alpha\gamma}(r)\right]$$

$$- \frac{1}{(2\pi)^3} \int_0^\infty d\underset{\sim}{k} \{Tr\left[\rho\omega(k)\hat{c}(k) + \tfrac{1}{2}\rho^2\hat{c}^2(k)\right]$$

$$+ \ell nDet\left[\underset{\sim}{1}-\rho\omega(k)\hat{c}(k)\right]\} \qquad \text{(V-108)}$$

This was found to be numerically more stable at large wavevectors. The fourier transform of a function f(r) in three- dimensions is simply

$$\hat{f}(k) = (2\pi)^{-3} \int f(r)\exp\left[i\underset{\sim}{k}.\underset{\sim}{r}\right] d\underset{\sim}{r} \qquad \text{(V-109)}$$

which can be shown (38) to be equivalent to

$$\hat{f}(k) = 4\pi.(2\pi)^{-3} \int_0^\infty f(r) \frac{Sin(k.r)}{(k.r)} r^2 dr \qquad \text{(V-110)}$$

$$= \frac{1}{2\pi^2 k} \int_0^\infty [r.f(r)]Sin(k.r)\, dr \qquad \text{(V-111)}$$

The preservation of area across the transform, i.e. Parseval's Identity, must be maintained

$$\int[f(r)]^2 d\underset{\sim}{r} = (2\pi)^{-3} \int [\hat{f}(k)]^2 d\underset{\sim}{k} \qquad \text{(V-112)}$$

thus implying that trapezoid rule is the most accurate for preservation of area, as it does not attempt to interpolate the function.

The solution is obtained by requiring the derivatives of equation (V-107) to be less than a given tolerance.

The molecular structure factor S(k), which is directly related to the scattering function $\chi(k)$ of equation (V-5) is defined by

$$S(k) = \left(\sum_{\alpha=1}^{m} b_\alpha^2\right)^{-1} \sum_{\alpha,\gamma=1}^{m} b_\alpha b_\gamma \left\langle \frac{1}{N} \sum_{mi,j=1}^{N} \exp\left[i\underset{\sim}{k}.(\underset{\sim m}{r}^\alpha - \underset{\sim j}{r}^\gamma)\right] \right\rangle \qquad \text{(V-113)}$$

may be expressed in terms of the site-site correlation functions by

$$S(k) = \left(\sum_{\alpha=1}^{m} b_\alpha^2\right)^{-1} \sum_{\alpha,\gamma=1}^{m} b_\alpha b_\gamma \left[\omega_{\alpha\gamma}(k) + \rho \hat{h}_{\alpha\gamma}(k)\right] \qquad \text{(V-114)}$$

where b_α is the coherent neutron scattering amplitude for type α nuclei, and tables of b_α are given by the Neutron Diffraction Commission (39). In the ideal gas limit (i.e. completely random structure) equation (V-114) reduces to

$$S_{ideal}(k) = \left(\sum_{\alpha=1}^{m} b_\alpha^2\right)^{-1} \sum_{\alpha,\gamma=1}^{m} b_\alpha b_\gamma \, \omega_{\alpha\gamma}(k) \qquad \text{(V-115)}$$

Finally by applying the method of Hsu, Chandler and Lowden (40) the spherical harmonics of the pair correlation function were calculated. For these the site-site distances were expressed in terms of the orientational angles Θ_1, Θ_2, ϕ_{12} and the distance R between the centres of mass as illustrated in Figure (II-1). The site-site distances are then

$$|\underset{\sim 1}{r}^\alpha - \underset{\sim 2}{r}^\gamma| = r_{12}^{\alpha\gamma} = f(R,\Theta_1,\Theta_{21},\phi_{12}) \qquad \text{(V-116)}$$

The probability of a pair of molecules at a distance R being in a particular configuration specified by $\Theta_1,\Theta_2,\phi_{12}$ is estimated as the product of the site-site probability functions

$$P(R,\Theta_1,\Theta_{21},\phi_{12}) = \prod_{\alpha\gamma} g_{\alpha\gamma}(|\underset{\sim}{r}_1^{\alpha}-\underset{\sim}{r}_2^{\gamma}|) \qquad \text{(V-117)}$$

This must be normalized by integrating over all angles to form a weighting function $W(R,\Theta_1,\Theta_2,\phi_{12})$

$$W(R,\Theta_1,\Theta_2,\phi_{12}) = \frac{P(R,\Theta_1,\Theta_2,\phi_{12})}{(16\pi^2)^{-1}\int_0^{2\pi}\int_0^{\pi}\int_0^{\pi} P(R,\Theta_1,\Theta_2,\phi_{12})\,d\Theta_1 d\Theta_2 d\phi_{12}} \qquad \text{(V-118)}$$

The angular radial distribution function is then

$$G(R,\Theta_1,\Theta_{21},\phi_{12}) = g_{cc}(R)W(R,\Theta_1,\Theta_{21},\phi_{12}) \qquad \text{(V-119)}$$

where $g_{cc}(r)$ is the centre of mass site radial distribution function, i.e. the probability of finding a pair of molecules separated by a distance R. The spherical harmonics are then simply obtained by integrating $G(R,\Theta_1,\Theta_2,\phi_{12})$ with the appropriate $Y_{\ell\ell'm}$ harmonic function over all angles as discussed in Chapter IV giving

$$G_{\ell\ell'm}(R) = (16\pi^2)^{-1}\int_0^{2\pi}\int_0^{\pi}\int_0^{\pi} Y_{\ell\ell'm}(\Theta_1,\Theta_2,\phi_{12})G(R,\Theta_1,\Theta_2,\phi_{12})\,d\Theta_1 d\Theta_2 d\phi_{12}$$

(V-120)

where $G_{\ell\ell'm}(R)$ is the spherical harmonics of molecular orientation of the centre-of-mass radial distribution function.

RESULTS AND DISCUSSION.

(V-9) Hard Core Molecules.

The first solutions to the RISM equations were found by Lowden and Chandler (41) for diatomic molecules modeled by two hard core interaction sites. Their method was then extended to multi-site molecular liquids including three-sited carbon disulphide, five-sited carbon tetrachloride and benzene with six sites (42,43).

In order to test the accuracy of the solution method, it was decided to reproduce the results of Lowden and Chandler for the three-sited models of carbon disulphide and carbon diselenide. The coefficients of the order 4 polynomial representation of $c_{\alpha\gamma}(r)$ given in equation (V-105) at the solution were compared with the values given by Lowden (43) for carbon disulphide at high and low density and carbon diselenide. (The parameters used were strictly those of Lowden for proper comparison.) The calculated coefficients and the solution curves themselves were found to be in agreement.

Having verified the solution method for the RISM equations it was decided to investigate

1) The changes in the pair distribution functions with variations in density and bond length for hard core systems;

2) Angular properties of the RISM solutions in comparison with other theories such as PY and blip-function theories in their angular expansions;

3) The solution for realistic soft-core potentials;

4) The solution for realistic soft-core potentials with attractive tails.

It was found from the calculations that the solutions to the RISM equations were unstable at high densities ($\rho^*=\rho d^3 \geq 0.7$). The method often produced negative structure factors at very small wave-vectors for high densities, which prevented any further convergence

towards a solution. It seems likely that these negative structure factors are produced by the matrix inverse $|\underline{1}-\rho\omega(k)\hat{c}(k)|^{-1}$ in equation (V-60) becoming badly behaved due to domination by the second term in the inverse. The method of solution is also limited to bond lengths considerably greater than the smallest distance Δr between integration points. This being due to the oscillations in the $\omega_{\alpha\gamma}(k)$ function becoming very rapid for very small bond lengths, and resulting in the integrals over the products of the $\omega_{\alpha\gamma}(k)$ functions becoming unstable. This instability makes it impossible to find a solution of the RISM equations within a given tolerance, as the values of I_{RISM} fluctuate greatly with small changes in the $a_i^{\alpha\gamma}$ polynomial coefficients.

The density and bond length dependence was investigated by solving the equations for $L^*=0.2$, 0.4 and 0.6, where $L^*=L/\sigma$ and σ is the diameter of the atom site of the diatomic molecule, at a density of $0.5\rho^*(\rho^*=\rho\sigma^3)$ and for $L^*=0.6$ at $\rho^*=0.2664$. This choice of density and bond length allows comparison with the truncated PY-equation method of Chen and Steele (14), and also with the blip-function expansion of Steele and Sandler (27). Computer simulations of these systems have been carried out by Streett and Tildesley (44), by Monte Carlo methods. For comparison with the RISM results the computer simulation results, either from Monte Carlo or molecular dynamics methods will be taken as exact results. In each case the RISM equations were solved for a three-site model, the outer two sites being at the atomic nuclei, and the third site at the centre of mass.

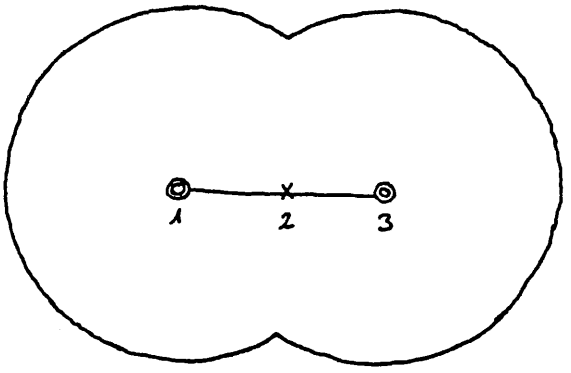

The minimum site-site interaction distances are then given by

$$d_{22} = (d_{11}^2 - (L/2)^2)^{\frac{1}{2}}$$

$$d_{12} = \tfrac{1}{2}(d_{11} + d_{22}) \qquad \text{(V-121)}$$

A comparison of the atom-atom site distribution function for a symmetric diatomic, solved with and without an auxiliary site at the centre of mass is given by Chandler, Hsu and Streett (45). In general the auxiliary site is shown to improve agreement with computer simulation results and is particularly applicable for the hard core contact ($r=d_{\alpha\gamma}$) results.

Considering first the case of $L^*=0.4$, $\rho^*=0.5$, the RISM solutions are given in Figure (V-2,3,4) which illustrate the site-site distribution functions, the structure factor and the spherical harmonics respectively. Comparison of the centre-of-mass distribution function with the computer simulation results of Streett and Tildesley (44) show qualitative agreement. For the calculation of the structure factor the values of the coherent neutron scattering amplitude for each atom was taken to be 0.5×10^{-4}, so that the value

of $\delta_{ideal}(0)$ was equal to the number of nuclei in the molecule,, as a form of normalization of the function. The spherical harmonics for these hard core systems show spurious rapid oscillations particularly for the 221, 222 and 400 harmonics at distances less than half a bond length above the hard core diameter. This discrepancy is due to the inaccuracy of 20-point Gauss-Legendre quadrature for functions which are discontinuous within the range of integration. The discontinuity is introduced by the presence of the hard core which makes $G(R,\Theta_1,\Theta_2,\phi_{12})$ discontinuous, being a function of a product involving the atom-atom distribution function. These rapid oscillations, thus arise from inaccurate angular integration, and are smaller in magnitude than the spherical harmonics and thus should be disregarded.

The main features of the site-site distribution functions calculated from the RISM equations, are correct, yielding cusp-like features in the positions predicted by equations (V-87,88). The Fourier transform of these produces a structure factor with a strong peak at 1.72Å^{-1}, rapidly decaying to ideal gas behaviour at large wavevectors (see Figure (V-3)). The spherical harmonics (Figure (V-4)) show some degree of agreement with those calculated by Streett and Tildesley. However, the minimum approach distances used by Streett and Tildesley do not agree with those used in this work, although how this would affect the spherical harmonics is not known. Despite this discrepancy there is qualitative if not quantitative agreement for g000, in the height of the first peak and position of the first minimum.

There is however only qualitative agreement for g200 caused by a noticeable inflection in the RISM curve at $(\sigma+L)$, although the rest of the curve is in very good agreement with that of Streett and Tildesley. This effect is related to a difference in the relative probabilities of $\top$ configurations ($\Theta_1 = \pi/2$, $\Theta_2 = 0$). The strong

negative lobe of g200 for small separations arises when there is a strong probability of θ_1 and θ_2 being approximately $\pi/2$, as in the parallel (||) ($\theta_1 = \pi/2$, $\theta_2 = \pi/2$, $\phi_{12} = 0$) or crossed (+) ($\theta_1 = \pi/2$, $\theta_2 = \pi/2$, $\phi_{12} = \pi/2$) configurations. g200 will be zero when positive and negative contributions cancel, this occurring when $\langle \cos^2\theta \rangle = 1/3$. For the T configuration the average over all molecules would give g200 = $\frac{1}{2}$g000. Unlike g200 curves from simulation data, the g200 function predicted by the RISM equations exhibits damped oscillations, and thus orientation in the second nearest neighbour sphere and beyond.

For the g220 harmonic there is very poor agreement caused by the lack of any negative lobe beginning at approximately 1.25R* where $R^* = R/\sigma$ ($1.25R^* \approx (\sigma + L/2)$). This effect is characteristic of all solutions to the RISM equations. The strong initial positive lobe of g220 indicates $\theta_1 \approx \theta_2 \approx \pi/2$ implying || and + configurations dominate at small distances. For the T configuration the g220 function values are at their lowest. The RISM equations fail to predict a strong negative lobe for g220, being caused by an inability to give a sufficiently high probability to the T configuration within the first nearest neighbour shell.

The solution at 0.6L*, 0.5ρ* exhibits the same general features. The increase in bond length causes a shift in the cusp-like features of the site-site distribution functions in Figure (V-5). The contact value of the atom-atom distribution function is increased by a factor of about 40%, with shoulders appearing at (d_{11}+L) and (d_{11}+1.7L) at approximately 0.5L before the maximum of the peak of the centre-centre distribution function. A weak cusp-like feature also begins to become apparent at (d_{11}+0.5L). This results in the

structure factor in Figure (V-6) having a much less pronounced first peak at $1.78\mathring{A}^{-1}$ although a second peak at $3.87\mathring{A}^{-1}$ has emerged. There also appears to be a larger deviation from the ideal gas case for large wavevectors.

The spherical harmonics at 0.6L*, 0.5ρ* in Figures (V-7) show stronger orientational dependence than for 0.4L*, the harmonics being more structured particularly at longer ranges. However, at this longer bond length the solutions for the RISM equations begin to be qualitatively different to the computer simulation results of Streett and Tildesley.

For g000 the Monte Carlo calculations exhibit a strong shoulder on the small r side of the first nearest neighbour peak being substantially smeared out on the large r side. These are features which are not reproduced either in the RISM calculations nor the zero-order blip function theory results of Steele and Sandler (27). Both of these are in substantial qualitative agreement although the RISM method predicts a significantly lower first peak.

A possible explanation of the difference between the RISM and Monte Carlo results could be in the minimum approach distances given by Streett and Tildesley as 0.989σ, 0.959σ and 0.905σ for L*=0.2,0.4 and 0.6 respectively and shown as such in the graphs of their paper (44). However, these minimum approach distances in fact correspond to elongations of L* = 0.2958, 0.5668 and 0.8508 respectively, which may well alter the packing of the molecules and thus the radial distribution functions.

The g200 harmonic at 0.6L*, 0.5ρ* has the same negative lobe at small distances as in the 0.4L*, 0.5ρ* case, but the inflection in the curve at (σ+L) has become a positive lobe which slowly decays in

oscillations through the second nearest neighbour shell. It can be seen that these inflections and positive lobes appearing at (σ+L) seem to be a general feature of the RISM calculations, and are not reproduced by the Monte Carlo results.

The slight negative lobe for g220 at 0.4L*, 0.5ρ* has become stronger at 0.6L*, with the positive lobe at (σ+L) being stronger, before oscillating to zero. The same characteristics hold for g400, although the positive lobe at (σ+L) is much weaker for the 0.6L* case. The g221 harmonic is unchanged in shape, but is slightly stronger, while the g222 function again rapidly oscillates spuriously about just below zero. This variation of the RISM harmonic functions with increasing bond length shows increasing orientational dependence at the larger bond length, which would be expected.

The calculation of the spherical harmonics at ρ*=0.2664, L*=0.6 enables a full comparison to be made with the Monte Carlo method of Streett and Tildesley (44), the truncated PY approximation of Chen and Steele (14) and the blip function (HTA) calculations of Steele Sandler (27). The RISM calculated spherical harmonics are shown in Figure (V-8), whilst the corresponding site-site distribution functions and the structure factor are shown in Figures (V-9,10) respectively. The relative magnitudes of the peak value for various harmonics are given in Table (V-1), which shows that the four methods give similar results.

TABLE (V-1).

Heights of 1st peaks.

	RISM	MC(44)	PY(14)	blip-function(27)
g000	1.35	1.40	1.40	1.45
g200	-0.65	-0.55	-0.55	-0.60
g220	+0.45	+0.40	+0.40	+0.40
g221	-0.10	-0.175	-0.175	-0.15
g222	-	-	-	-0.05
g400	+0.35	-	-	+0.25

Despite the similar results achieved by these methods for small separations, at larger distances discrepancies between RISM and the other three methods, which are qualitative in nature, appear, these discrepancies being -

1) The g200, g220 and g400 harmonics all have an inflection at $(\sigma+L)$.

2) The inflection causes shifts to slightly larger separations and diminution of the positive lobe of g200.

3) The negative lobe of g220 does not exist, although there is a minima of zero between two positive lobes.

These results mean that all methods are in almost quantitative agreement for the orientational properties at small distances. However, at larger separations the RISM equations predict substantially different orientational dependence. It would be instructive to analyse the results of the different methods in terms of special configurations, as the inability to predict a negative lobe for g220 may be due to the absence of a particular configuration. It is likely that this is related to the $\top$ configuration, which has the correct angular properties to produce such a difference in the harmonics. This would mean that the RISM method always seriously underestimates the probability of $\top$ configurations occuring.

(V-10) Lennard-Jones Repulsive Systems.

Having discussed the static properties of hard sphere liquids, the RISM equations were then used to look at soft-sphere liquids, by comparison with the computer simulation results of Singer, Taylor and Singer (46) which will be regarded as exact. The system chosen initially was that of chlorine, using the methods for calculating the solution already discussed. The parameters used were $T^*=1.0998$, $\rho^*=0.54067$, $d\overset{*}{a}_{13}=1.0121$ (reduced atom-atom hard sphere diameter) and $L^*=0.60241$.

The potential separation was carried out by the Weeks, Chandler and Andersen method (23,24) discussed earlier (see equations (V-12,13,14)) but on a site-site basis. Thus the HTA repulsive potential is given by

$$\phi^{o}_{\alpha\gamma}(r) = 4\varepsilon\left[\left(\frac{\sigma}{r}\right)^{12} - \left(\frac{\sigma}{r}\right)^{6}\right] + \varepsilon \qquad \text{for } r \leq r_{min}$$

$$= 0 \qquad \text{for } r > r_{min} \qquad \text{(V-122)}$$

where $r_{min} = 2^{1/6}\sigma$. The site-site diameters were then chosen according to equations (V-89,90,91) with $w(r) = \phi^{o}_{\alpha\gamma}(r)$, i.e.

$$d_{11} = -\int_{o}^{\infty} dr\left(-1+\exp\left[-\phi^{o}_{\alpha\gamma}(r)/kT\right]\right) \qquad \text{(V-123)}$$

When calculating the effect of the softening of the interactions changes to the minimum interaction distances of the non-potential interactions (i.e. atom/centre and centre/centre) must be made so that no hard-core interactions are allowed to be present. This is accomplished by decreasing the centre/centre and atom/centre minimum interactions distances respectively, geometrically

$$d_{22} = (d_{11}^2 - (L/2)^2)^{\frac{1}{2}} - 0.1\text{Å} \qquad \text{(V-124)}$$

$$d_{12} = d_{22} - 0.1\text{Å}$$

Non-additivity of diameters is allowed as the RISM method does not require the site-site hard sphere diameters to be the same or even consistent, compared with hard sphere calculation. Use of this was made by Hsu, Chandler and Lowden (40), who enlarged the centre/centre diameter in diatomic to simulate repulsive quadrupole interactions.

TABLE (V-2).

Positions of the maxima, minima and zeros of distribution functions as $T^*=1.0998$, $\rho^*=0.54067$, $L^*=0.60241$ without attractive perturbation.

	Maxima at	Minima at	Zeros at
gAA(r)	1.04,1.525,2.07	1.42,1.745	-
g000(r)	1.29,2.29	1.76,2.81	-
g200(r)	1.52,2.69	1.17,2.18	1.40,1.97,2.45
g220(r)	1.085,1.54,2.05	1.33,1.76	1.24,1.46,1.67 1.90,2.26
g221(r)	-	1.17	1.41
g222(r)	-	1.00	1.26
g400(r)	1.06,1.26,1.60	1.23,1.42	1.33,1.535,1.86

All distances expressed in reduced units ($R^*=R/\sigma$)

The resultant site-site distribution functions are shown in Figure (V-11). These are in qualitative agreement with the calculations of Singer et al., correctly estimating the heights of the first peaks of the atom/atom and centre of mass radial distribution

functions (gAA(r) and $g_{COM}(r)$). However, the RISM gAA(r) does not quantitatively reproduce the small maxima at (σ+L), which is thought to correspond to the distance between the outer two, of three collinear atoms in adjacent molecules (44). Similarly the simulation data shows a shoulder on the small r side of the first peak of $g_{COM}(r)$ which is not present in the RISM counterpart, although there is a slight change in the curvature at approximately the same distance. Comparing the spherical harmonics calculated from the site-site distribution functions of chlorine like systems of hard spheres at 0.6L*, 0.5ρ* with soft-spheres at 0.60241L*, 0.54067ρ* (see Figure (V-12)) show close similarity. Despite this there are significant differences between the hard and soft sphere systems which are that

a) The magnitude of the negative lobe of g220 at (σ+0.7L) is deeper for the soft sphere system. The magnitude of the positive lobe of g220 at (σ+L) and (σ+2L) are also increased.

b) The magnitude of the positive lobe of g200 at (σ+L) is increased as is the negative lobe at (σ+2L) for the soft spheres. All other harmonics remain unchanged. This indicates an increase in orientational dependence in the second nearest neighbour shell for soft-spheres, although from this limited information of the harmonics it is difficult to postulate a reason for the increase in magnitude of the positive lobes of g200 and g220 at (σ+L). The positions of the maxima, minima and zeros of the soft-spheres distribution functions at 0.60241L*, 0.54067ρ* are given in Table (V-2).

Compared to the molecular dynamics calculations, the RISM equations again give a degree of qualitative agreement, but they do not, however, give quantitative agreement to the computer simulation spherical harmonics.

The principle differences are

1) RISM does not predict a shoulder on the left-hand side of g000, found by Singer et al. (46) and thought to be caused by an increase

in ⊤ configurations, which are favoured at small distances for high densities.

2) g200 has a shoulder inflection feature between the maxima at (σ+L) and the minima at (σ+2L).

3) The g220 harmonic is very poorly represented; the maxima at 1.085R* is too low by approximately 10%, the minima at (σ+L/2) is too small by a factor of 2. The maxima at (σ+L) is well represented, however, the shoulder feature at approximately 2.0R*, becomes a minima at 1.90R* followed by a maximum at 2.0R*, from which the RISM function goes to zero, without reproducing the simulation minima at 2.40R*.

4) The maxima of g221 at 1.51R* is not reproduced, as is the maxima of g222 at 1.17R*.

5) The first peak height of g400 is too low by 20%.

This shows that the RISM equations have two principle failings in the calculation of the angular properties of radial distribution functions these being firstly that the ⊤ configuration is given too low probability within the left-hand side of the first peak of g000, which is shown by the g000 and g200 harmonics. Secondly, the ⊤ configuration also has too low a probability in the middle of the first peak of g000, which is shown by the weak negative lobe of g220.

These findings are reinforced by repeating the RISM calculations for chlorine at a higher temperature and lower density, i.e. T*=1.6789, ρ*=0,48477, $d^*_{a_{13}}$ = 0.99557 and L*=0.60241. The site-site correlation functions are shown in Figure (V-13) with the corresponding spherical harmonics in Figure (V-14). A table of the distribution function maxima, minima and zeros is also given in Table (V-3).

TABLE (V-3).

Positions of maxima, minima and zeros of distribution functions at $T^*=1.6789$, $\rho^*=048477$, $L^*=0.60241$ without attractive perturbation.

	Maxima at	Minima at	Zeros at
gAA	1.06,2.41	1.82,2.89	-
g000	1.33,2.40	1.85,2.98	-
g200	1.56,2.89	1.21,2.27	1.45,2.08,2.63
g220	1.12,1.56,2.09	1.37,1.78	1.28,1.48,1.68, 1.93,2.61
g221	-	1.19	1.77
g222	-	1.00	1.31
g400	1.07,1.62	1.45	1.34,1.56,1.89

The principle effects from an increase in temperature and decrease in density are as expected

1) a decrease in the magnitude of the first peaks of the distribution functions;

2) a loss of structure for distances greater than $1.5R^*$ which result in the size of the maxima and minima being greatly reduced;

3) the distribution functions decay to zero within a shorter distance;

4) the positions of the maxima and minima are shifted to slightly larger distances (see Table (V-3)).

However the difficulties encountered with the RISM solution at lower density still persist. This does imply that the inaccuracies of the RISM solution are density and temperature independent, and are a consequence of the RISM equations themselves. For comparison the zero-density spherical harmonics are shown in Fig. (V-15). These do not

predict any angular structure beyond 1.5R*, but have the same structure as the RISM solutions for smaller distances, with approximately a third greater magnitude. This shows that the RISM equations are a first order approximation to the anisotropic structure of the liquid.

(V-11) Perturbations - Full Lennard-Jones systems.

The effects of the Lennard-Jones attractive potential perturbation was studied by the methods discussed in section (V-6) and the RISM method was solved using equations (V-78,79,80). The perturbation potential, in accordance with the Weeks, Chandler and Andersen potential separation, discussed in the previous section is then given by

$$\begin{aligned} v_{\alpha\gamma}(r) &= -\varepsilon && r \leq r_{min} \\ &= 4\varepsilon \left\{ \left(\frac{\sigma}{r}\right)^{12} - \left(\frac{\sigma}{r}\right)^{6} \right\} && r > r_{min} \end{aligned} \qquad \text{(V-125)}$$

which is then used to specify C(r) outside the hard core by equation (V-79).

To compare the RISM solution for the repulsive only forces and the solution with the attractive perturbation, the RISM equations were resolved for the chlorine-like system at T*=1.0998, ρ^*=0.54067, da^*_{13}=1.0121, and L*=0.60241. The differences between the two solutions are very slight being characterized by small changes in the magnitudes of the principle maxima and minima of the distribution functions, shown in Table (V-4).

TABLE (V-4).

Positions and Magnitude of principle features of distribution functions, at $T^*=1.0998$, $\rho^*=0.54067$, $da^*_{13}=1.0121$ and $L^*=0.60241$.

Position (Magnitude) R*	Soft-Sphere with Attractive Perturbation	Soft-Sphere only
gaa	1.04(2.161),1.525(1.004)	1.04(2.203),1.525(1.027)
g_{COMA}	1.23(1.747),1.70(0.782)	1.23(1.735),1.73(0.796)
g000	1.29(1.915),1.74(0.602)	1.29(1.897),1.76(0.618)
g200	1.17(-1.032),1.52(0.548)	1.17(-1.004),1.52(0.539)
g220	1.085(0.809),1.33(-0.538)	1.085(0.782),,1.33(-0.503)
g221	1.19(-0.222)	1.17(-0.215)
g222	1.00(-0.217)	1.00(-0.209)
g400	1.06(0.549),1.26(0.154) 1.44(-0.251)	1.06(0.528),1.26(0.161) 1.42(-0.266)

It can be seen from this table that the magnitude of the spherical harmonics is increased slightly although the positions of the features remain unchanged. The same is true of g000 and g_{COMA}, whilst the first peak of gAA is slightly reduced. The full calculation was also carried out at the lower density and higher temperature, i.e. $T^*=1.6789$, $\rho^*=0.48477$, and the differences for two solutions in this case are given in Table (V-5). These can be seen to be qualitatively the same as before. The energy of the system can be calculated from the site-site distribution functions,

$$E = \frac{1}{2}\rho N_A \sum_{\alpha\gamma} \int_0^\infty g_{\alpha\gamma}(r).u_{\alpha\gamma}(r)\ d\underset{\sim}{r} \qquad \text{(V-126)}$$

TABLE (V-5).

Position and Magnitude of principle features of distribution functions at $T^*=1.6789$, $\rho^*=0.48477$, $da^*_{13}=0.99557$ and $L^*=0.60241$.

Position (Magnitude) R*	Soft-Sphere with Attractive Perturbation	Soft-Sphere only
gaa	1.06(1.688),1.81(0.866)	1.06(1.692),1.82(0.872)
g_{coma}	1.27(1.598),1.85(0.839)	1.27(1.576),1.86(0.846)
g000	1.33(1.752),1.83(0.717)	1.33(1.731),1.85(0.734)
g200	1.21(-0.943),1.56(0.320)	1.21(-0.910),1.56(0.290)
g220	1.12(0.685),1.37(-0.277)	1.12(0.654),1.37(-0.246)
g221	1.21(-0.163)	1.19(-0.154)
g222	1.00(-0.147)	1.00(-0.140)
g400	1.07(0.449),1.45(-0.171)	1.07(0.426),1.45(-0.176)

the resultant values being given in Table (V-6).

TABLE (V-6).

System T*	ρ^*	L*	RISM(HTA) Soft-Sphere Only	RISM(ORPA) Soft-Sphere with Perturbation -E/kJmol^{-1}	MD
1.0998	0.54067	0.60241($C\ell_2$)	19.02	19.18	19.32[≠]
1.6789	0.48477	0.60241($C\ell_2$)	12.62	12.83	13.31[≠]
1.06	0.608	0.51327(F_2)	-	5.90	5.93[≠]
1.3447	0.42320	0.78622(CO_2)	-	9.55	9.80[≠]
1.5246	0.70041	0.32924(N_2)	-	5.37	5.52[†]

[≠] Singer et al. (46) [†] Barojas et al. (47)

The agreement with the molecular dynamics values at the selected points is very good for the RISM(HTA) calculations. The agreement is improved by the RISM(ORPA) values for which the maximum error is only 3.6% as compared with 5.2% for the RISM(HTA) values. Another simple test of the method is the calculation of the isothermal compressibilities χ_T from

$$\hat{S}(0) = (1 + \rho\hat{h}_{11}(0)) = \rho kT\chi_T \qquad \text{(V-127)}$$

where $\hat{h}_{11}(0)$ is the zero wavevector value of the Fourier transform for the atom-atom pair correlation function. Values for the isothermal compressibility for the associated hard sphere RISM fluids are given in Table (V-7). Also included in the table are values of the isothermal compressibility calculated from the centre of mass pair correlation function χ_T^{COM}, which corresponds to the assumption of an isotropic system. The values for the hard sphere associated fluids are found to be in only fair agreement with the molecular dynamics restuls. The values of χ_T^{COM} also seem to be a fair agreement

TABLE (V-7).

System T*	ρ*	L*	RISM (HTA) χ_T^{COM}/bar$^{-4}\times10^{-5}$	RISM (ORPA) χ_T^{COM}/bar$^{-4}\times10^{-5}$	RISM (HTA) χ_T/bar$^{-1}\times10^{-5}$	RISM (ORPA) χ_T/bar$^{-1}\times10^{-5}$	MD
1.0998	0.54067	0.60241($C\ell_2$)	2.9	4.9	2.7	5.7	4.9[≠]
1.6789	0.48477	0.60241($C\ell_2$)	4.6	8.4	3.9	7.8	13.2[≠]
1.06	0.608	0.51327(F_2)	-	26.5	-	8.1	8.5[≠]
1.5246	0.70041	0.32924(N_2)	-	118.8	-	14.3	16.3[†]

[≠] Singer et al. (46) [†] Barojas et al. (47)

for chlorine-like systems, however for more isotropic systems with shorter bond lengths the agreement becomes very poor. The agreement for the configurational energy suggests that the RISM equations predict the correct structure of gAA at small and medium distances (i.e. within the range of the attractive part of the potential) while the isothermal compressibility results indicate that the long-range structure (i.e. zero-wavevector) is only a fair representation of that calculated from molecular dynamics. For both the energy and particularly the isothermal compressibility the ORPA solutions can be seen to be in considerably better agreement with the molecular dynamics values than the HTA solutions throughout the temperature density range. This shows that the effects of the attractive perturbation can only be neglected at high density and temperature. However, with the addition of an attractive perturbation there is little improvement in the representation of the angular properties of the fluids, in terms of the values of the spherical harmonics. An indication of the discrepancy within the RISM(ORPA) solution has been from the calculation of the mean square torque, discussed by Thompson et al. (48). This is given by

$$\langle\tau^2\rangle = -4\pi\rho \sum_{\ell\ell'm} \ell(\ell+1) \int_0^\infty u_{\ell\ell'm}(r) g_{\ell\ell'm}(r)\, r^2\, dr \ldots. \qquad \text{(V-128)}$$

using a Barker-Henderson type diameter defined by equation (V-129) to give a minimum effective interaction distance approximation for evaluating the integral equation (V-128). This is achieved by setting $u_{\ell\ell'm}(r)$ to zero for $r < \langle d_{BH}\rangle$ which is given by

$$\langle d_{BH}\rangle = \int_0^\infty \frac{1}{16\pi^2} \int_0^{2\pi}\int_0^{\pi}\int_0^{\pi} [1-\exp(-\beta\phi_o^{\alpha\gamma}(r))]\, d\theta_1 d\theta_2 d\phi_{12} dr \qquad \text{(V-129)}$$

where $\phi_o^{\alpha\gamma}(r)$ is given by equation (V-12). For full discussion on this approximation to the integral see Chapter III. The resultant values for the mean square torques are given in Table (V-8). As pointed out in Chapter III these values become very unreliable for long bond lengths, and give generally values which are too low for shorter bond lengths. Bearing this in mind, the values for the chlorine and fluorine systems seem reasonable, however the results for nitrogen must be regarded as disappointing.

TABLE (V-8).

System T*	ρ*	L*	RISM(ORPA) $\langle\tau^2\rangle\times10^{-40}J^2$	MD $\langle\tau^2\rangle\times10^{-40}J^2$
1.0341	0.54067	0.60241(Cl_2)	4.5	7.15≠
1.6789	0.48477	0.60241(Cl_2)	6.3	9.4≠
2.31	0.522	0.54217(Cl_2)	6.5	-
1.06	0.608	0.51327(F_2)	0.16	0.48≠
1.3447	0.4230	0.78622(CO_2)	155.3	10.5≠
1.5246	0.70041	0.32924(N_2)	0.05	1.7†

≠ Singer et al. (46) † Thompson et al. (48)

Solutions to the RISM equations were also carried out for nitrogen, fluorine and carbon dioxide systems as before, using soft-spheres with attractive potential perturbation. The site-site distribution functions of nitrogen at T*=1.5246, ρ*=0.70041, da^*_{13}=0.99947 and L*=0.32924, are shown in Figure (V-16) with the associated spherical harmonics in Figure (V-17). The RISM solutions are a poor representation of the spherical harmonics, when compared to the results of Cheung and Powles (49,50) and those of Streett and

Tildesley (51). In particular the first minimum of g200 is overestimated by a factor of almost two, whereas the g220 and g400 harmonics have no negative regions at all, and the oscillations of g200 appear to have very little damping towards large distances. This poor representation of nitrogen by the RISM method is probably due to two causes -

1) the bond length of nitrogen is too small for very accurate solution of the RISM equations within the limitations of memory store of the computer program used for the calculation;

2) the density of $\rho^*=0.7$ is also towards the upper limits for which there exists a solution to the RISM equations. The accuracy of the equations is also reduced at very high densities. It is interesting however that despite these defects the method still yields very reasonable values for the configurational energy and isothermal compressibility. The positions of the maxima, minima and zeros of the distribution functions for this system are given in Table (V-9).

The corresponding solutions for fluorine at $T^*=1.06$, $\rho^*=0.608$, $da^*_{13}=1.01346$ and $L^*=0.51327$ are shown in Figures (V-18,19). The positions of the various maxima, minima and zeros are also given in Table (V-10). The atom-atom structure factor is in close agreement with that calculated from molecular dynamics (46) except that the main peak is shifted to a slightly larger wavevector. However, whilst the agreement is good for g_{COMA}, the RISM atom-atom distribution lacks a secondary peak at $(\sigma+L)$, but has a shoulder feature instead. The spherical harmonics show the same deficiencies discussed earlier, but are however in almost quantitative agreement except for the magnitude of the negative lobe of g220 at $(\sigma+L/2)$ which is underestimated by a factor of almost three. This feature and the deficiency of the secondary peak of gAA at $(\sigma+L)$ is again due to the inability of the

TABLE (V-9).

Positions of maxima, minima and zeros of distribution functions at $T^*=1.5246$, $\rho^*=0.70041$, $L^*=0.32924$ with attractive perturbation.

	Maxima at	Minima at	Zeros at
gAA	1.14,2.19	1.63,2.64	-
g000	1.18,2.20	1.59,2.64	-
g200	1.56,2.58	1.13,2.13	1.39,1.84,2.39,2.84
g220	1.11,1.59	1.43,2.46	1.40,1.46,2.39,2.57
g221	-	1.11	1.56
g222	-	1.05	1.36
g400	1.06,1.62,2.09	1.39,1.92	2.39

TABLE (V-10).

Positions of maxima, minima and zeros of distribution functions at $T^*=1.06$, $\rho^*=0.608$, $L^*=0.51327$ with attractive perturbation.

	Maxima at	Minima at	Zeros at
gAA	1.05,2.08,3.13	1.69,2.66	-
g000	1.24,2.21,3.19	1.66,2.69	-
g200	1.46,2.61	1.17,2.11,3.11	1.36,1.91,2.39,2.88,3.38
g220	1.10,1.48,2.04, 2.47,3.03	1.30,1.73,2.33 2.66	1.23,1.40,1.63,1.84,2.26, 2.26,2.81,3.33
g221	1.87	1.17,2.18	1.66,2.04,2.63
g222	-	1.01	1.23
g400	1.06,1.51,2.05	1.37,2.37	1.29,1.46,1.85,2.29,2.52

RISM method to predict T configurations with sufficiently high probability in this region.

Finally the RISM equations were solved for carbon dioxide at $T^*=1.3447$, $\rho^*=0.42320$, $d\overset{*}{a}_{13}=1.00441$ and $L^*=0.78622$. The pair distribution functions are shown in Figure (V-20) with the spherical harmonics in Figure (V-21). The maxima, minima and zeros of the distribution functions are also tabulated in Table (V-11).

TABLE (V-11).

Positions of the maxima, minima and zeros of the distribution functions at $T^*=1.3447$, $\rho^*=0.42320$, $L^*=0.78622$ with attractive perturbation.

	Maxima at	Minima at	Zeros at
gAA	1.06,1.75,2.06	1.50,1.88,2.44	-
g000	1.38,2.44	1.92,2.97	-
g200	1.69,2.67	1.21,2.16	1.50,1.95,2.49,2.93
g220	1.08,1.74,2.75	1.43,2.42	1.29,1.64,2.21,2.64,3.03
g221	1.64	1.21	1.51,2.00
g222	-	0.97	1.31
g400	1.05,1.34,1.79	1.28,1.58,2.57	1.44,1.71,2.42,2.75

This solution is in good, almost quantitative agreement with the computer simulation results of Singer et al., however, again there are two significant features that the RISM method fails to reproduce -

1) a shoulder on the small r side of the first peak of g_{COM};

2) the magnitude of the negative lobe of g220, which is underestimated by a factor of two.

The agreement with the atom-atom distribution function is however very good, the value for the configurational energy being in good agreement with the value from the molecular dynamics simulation. However it is significant that the shoulder on the small r side of the first peak of

g_{COM}, is also shown by the zero-density spherical harmonics (see Figure (V-22)). The feature is not so pronounced as in the simulation results, but shows this shoulder to be an artifact of the potential itself, which the RISM method should reproduce.

(V-12) Conclusion.

The RISM method is found to be a good representation, to first order, of the equilibrium properties of molecular liquids, giving very reasonable values for the configurational energy and isothermal compressibility. However the RISM equations can be seen to have two principle deficiencies for the angular properties. These are:

1) a failure to predict the T-configuration within the first nearest neighbour shell with sufficiently high probability;

2) sizeable oscillations occuring in g200 at large distances.

This would indicate that firstly, the orientational correlation is being maintained, and thus the RISM equations are not sufficiently angle averaged at large distances. Secondly the RISM equations are only a first order approximation to the angular properties of molecular liquids. It is also significant that these angular deficiencies appear to be density and temperature independent, suggesting that they are implicit in the RISM equations themselves. This may well arise from a failure of the site-site formalism to take account of excluded volume effects. However the inclusion of these effects with the RISM equations is likely to be long and complicated, and would reduce the simplicity of the approach.

The RISM(HTA) solutions are seen to be in good agreement with the corresponding computer simulation results, particularly at high temperature and density. They do not, however, predict values for the isothermal compressibility, close to the simulation values. This is

probably due to the failure of the model to account for long range attractions.

The RISM(ORPA) improve the results of RISM(HTA) by accounting for the attractive interactions in the fluid in a simple manner. This results in improved values for the isothermal compressibility, and gives values for the configurational energy close to the simulation results. However, the RISM(ORPA) solutions seem to retain the difficulties associated with the ORPA method which was applied to atomic fluids discussed earlier. RISM(ORPA) underestimates the effects of the attractive perturbation throughout all densities, while predicting changes in the correct direction. Attempts were made to use this method to include the site-site coulombic interactions associated with dipole and quadrupole moments in the discrete charge model discussed in Chapter II. However, the size of the perturbation associated with the smallest quadrupole moment was found to be an order of magnitude larger than the equations were able to give solutions for, without predicting completely unphysical effects such as negative correlation functions. This failure is particularly disappointing in view of the lack of other simple methods for including the effects of this type of interaction. The methods based on spherical harmonic formalisms being unsatisfactory in the study of large multicentre molecules.

It should also be noted that the application of the soft-spheres treatment only gives correlation functions accurate to first order in the 'softness' parameter ξ. Thus values for the isothermal compressibility calculated after the application of the soft-core treatment were in very poor agreement with the simulation results.

A useful extension of these studies would be to calculate the improvement in the solutions using the EXP approximation, discussed earlier, applied to the RISM method. This would probably improve the solutions for Lennard-Jones fluids, although the magnitude of the

perturbation for dipolar and quadrupolar fluids is still too large to allow physical solutions.

CHAPTER V. REFERENCES.

1) L.S. Ornstein and F. Zernike - Proc.Akad.Sci. (Amsterdam) 1914, 17, 793.

2) F. Zernike and J.A. Prins - Z.Physik. 1927, 41, 184.

3) R.O. Watts - Statistical Mechanics (ed: K.Singer) 1973, 1, 1 (London : Chem.Soc.)

4) W.R. Smith - Statistical Mechanics (ed: K.Singer) 1973, 1, 73 (London : Chem.Soc.)

5) H.C. Andersen - Ann.Rev.Phys.Chem. 1975, 26, 145.

6) C.G. Gray - Statistical Mechanics (ed: K.Singer) 1975, 2, 300 (London : Chem.Soc.)

7) P.A. Egelstaff, C.G. Gray and K.E. Gubbins - In Molecular Structure and Properties, International Review of Science, Physical Chemistry (ed: A.D. Buckingham) 1975, 2, 316 (London : Butterworth)

8) J.P. Hansen and I.R. McDonald - Theory of Simple Liquids, (Academic Press, London, 1976)

9) W.B. Streett and K.E. Gubbins - Ann.Rev.Phys.Chem. 1977, 28, 373.

10) D. Chandler - Ann.Rev.Phys.Chem. 1978, 29, 441.

11) I.R. McDonald and S.P. O'Gorman - Phys.Chem.Liq. 1978, 8, 57.

12) J.K. Percus and G.J. Yevick - Phys.Rev. 1958, 110, 1.

13) L. Verlet and J-J. Weis - Phys.Rev. 1972, A5, 939.

14) Y-D. Chen and W.A. Steele - J.Chem.Phys. 1971, 54, 703.

15) P.F. Morrison - Ph.D. Thesis, California Institute of Technology, 1972

16) J.M.J. van Leeuwen, J. Groneveld and J. de Boer - Physics 1959, 25, 792.

17) E. Meeron - J. Math.Phys. 1960, 1, 192.

18) J.C. Rasaiah and H.L. Friedman - J.Chem.Phys. 1968, 48, 2742.

19) J.P. Hansen and I.R. McDonald - Phys.Rev. 1975, A11, 2111.

20) J.L. Lebowitz and J. Percus - Phys.Rev. 1966, 144, 251.

21) E. Waisman and J.L. Lebowitz - J.Chem.Phys. 1970, 52, 4307.

22) M.S. Wertheim - J.Chem.Phys. 1971, 55, 4291.

23) D. Chandler and J.D. Weeks - Phys.Rev.Lett. 1970, 25, 149.

24) J.D. Weeks, D. Chandler and H.C. Andersen - J.Chem.Phys. 1971, 54, 5237.

25) H.C. Andersen, J.D. Weeks and D. Chandler - Phys.Rev. 1971, A4, 1597.

26) H.C. Andersen, D. Chandler and J.D. Weeks - Adv.Chem.Phys. 1976, 34, 105.

27) W.A. Steele and S.I. Sandler - J.Chem.Phys. 1974, 61, 1315.

28) H.C. Andersen and D. Chandler - J.Chem.Phys. 1970, 53, 547.

29) D. Chandler and H.C. Andersen - J.Chem.Phys. 1971, 54, 26.

30) H.C. Andersen and D. Chandler - J.Chem.Phys. 1971, 55, 1497.

31) H.C. Andersen, D. Chandler and J.D. Weeks - J.Chem.Phys. 1972, 56, 3812.

32) H.C. Andersen, D. Chandler and J.D. Weeks - J.Chem.Phys. 1972, 57, 2626.

33) H.C. Andersen and D. Chandler - J.Chem.Phys. 1972, 57, 1918.

34) D. Chandler and H.C. Andersen - J.Chem.Phys. 1972, 57, 1930.

35) D. Chandler - J.Chem.Phys. 1973, 59, 2742.

36) B.M. Ladanyi and D. Chandler - J.Chem.Phys. 1975, 62, 4308.

37) L.J. Lowden and D. Chandler - J.Chem.Phys. 1974, 61, 5228.

38) H.J. Friedman - Ionic Solution Theory (Interscience, New York, 1962).

39) Neutron Diffraction Commission (G.E. Bacon - Chairman) - Acta Cryst. 1969, A25, 391.

40) C.S.Hsu, D. Chandler and L.J. Lowden - Chem.Phys. 1976, 14, 213.

41) L.J. Lowden and D. Chandler - J.Chem.Phys. 1973, 59, 6587.

42) L.J. Lowden and D. Chandler - J.Chem.Phys. 1974, 61, 5228.

43) L.J. Lowden - Ph.D. Thesis (Univ. Illinois 1975).

44) W.B. Streett and D.J. Tildesley - Proc.R.Soc.Lond. 1976, A348, 485.

45) D. Chandler, C.S. Hsu and W.B. Streett - J.Chem.Phys. 1977, 66, 5231.

46) K. Singer, A. Taylor and J.V.L. Singer - Mol.Phys. 1977, 33, 1757.

47) J. Barojas, D. Levesque and B. Quentrec - Phys.Rev. 1973, A7, 1092.

48) S.M. Thompson, D.J. Tildesley and W.B. Streett - Mol.Phys. 1976, 32, 711.

49) P.S.Y. Cheung and J.G. Powles - Mol.Phys. 1975, 30, 921.

50) P.S.Y. Cheung and J.G. Powles - Mol.Phys. 1976, 32, 1383.

51) W.B. Streett and D.J. Tildesley - Proc.R.Soc.Lond. 1977, A355, 239.

FIGURES.

(V-1) Diagram of RISM molecule - See Text.

(V-2) Site-site G(r)'s -

Hard Core RISM molecule at ($L^* = 0.4$, $\rho^* = 0.5$)

——————— $G_{CM}(r)$

– – – – – – – $G_{AA}(r)$ - Distances in Å

—·—·—·— $G_{CMA}(r)$

(V-3) Structure Factors

Hard Core RISM molecule at ($L^* = 0.4$, $\rho^* = 0.5$)

——————— $S(k)$

- - - - - - - - - - - $S_{ideal}(k)$ - Axis ($Å^{-1}$)

(V-4) Spherical Harmonics $G_{\ell\ell'm}(r)$

Hard Core RISM molecule at ($L^* = 0.4$, $\rho^* = 0.5$)

——————— $G_{000}(r)$

- - - - - - - - - - - $G_{200}(r)$

———·——— $G_{220}(r)$ - Distances in Å

····· $G_{221}(r)$

——·———·—— $G_{222}(r)$

——·——·——·—— $G_{400}(r)$

(V-5) Site-site G(r)'s - Key as for (V-2)

Hard Core RISM molecule at ($L^* = 0.6$, $\rho^* = 0.5$)

(V-6) Structure Factors - Key as for (V-3)

Hard Core RISM molecule at ($L^* = 0.6$, $\rho^* = 0.5$)

(V-7) Spherical Harmonics $G_{\ell\ell'm}(r)$ - Key as for (V-4)

Hard Core RISM molecule at ($L^* = 0.6$, $\rho^* = 0.5$)

(V-8) Spherical Harmonics $G_{\ell\ell'm}(r)$- Key as for (V-4)

Hard Core RISM molecule at ($L^* = 0.6$, $\rho^* = 0.2664$)

(V-9) Site-site G(r)'s - Keys as for (V-2)

Hard Core RISM molecule at ($L^* = 0.6$, $\rho^* = 0.2664$)

(V-10) Structure Factors - Key as for (V-3)

Hard Core RISM molecule at ($L^* = 0.6$, $\rho^* = 0.2664$)

(V-11) Site-site G(r)'s - Key as for (V-2)

Soft Core RISM molecule - No attractive perturbation at

($T^* = 1.10$, $\rho^* = 0.541$, $L^* = 0.602$) - Chlorine

(V-12) Spherical Harmonics $G_{\ell\ell'm}(r)$ - Key as for (V-4)

Soft Core RISM molecule - No attractive perturbation at

($T^* = 1.10$, $\rho^* = 0.541$, $L^* = 0.602$) - Chlorine

(V-13) Site-site G(r)'s - Key as for (V-2)

Soft-Core RISM molecule - No attractive perturbation at

($T^* = 1.68$, $\rho^* = 0.485$, $L^* = 0.602$) - Chlorine

(V-14) Spherical Harmonics $G_{\ell\ell'm}(r)$ - Key as for (V-4)

Soft Core RISM molecule - No attractive perturbation at

($T^* = 1.68$, $\rho^* = 0.485$, $L^* = 0.602$) - Chlorine

(V-15) Zero-Density Spherical Harmonics $G_{\ell\ell'm}(r)$ - Key as for (V-4) at

($T^* = 1.68$, $L^* = 0.602$) - Chlorine

(V-16) Site-site G(r)'s - Key as for (V-2)

Soft-Core RISM molecule - with attractive perturbation at

($T^* = 1.52$, $\rho^* = 0.700$, $L^* = 0.329$) - Nitrogen

(V-17) Spherical Harmonics $G_{\ell\ell'm}(r)$ - Key as for (V-4)

Soft Core RISM molecule - with attractive perturbation at

($T^* = 1.52$, $\rho^* = 0.700$, $L^* = 0.329$) - Nitrogen

(V-18) Site-site G(r)'s - Key as for (V-2)

Soft Core RISM molecule - with attractive perturbation at

($T^* = 1.06$, $\rho^* = 0.608$, $L^* = 0.513$) - Fluorine

(V-19) Spherical Harmonics $G_{\ell\ell'm}(r)$ - Key as for (V-4)

Soft Core RISM molecule - with attractive perturbation at

($T^* = 1.06$, $\rho^* = 0.608$, $L^* = 0.513$) - Fluorine

(V-20) Site-site G(r)'s - Key as for (V-2)

Soft Core RISM molecule - with attractive perturbation at

($T^* = 1.34$, $\rho^* = 0.423$, $L^* = 0.786$) - Carbon Dioxide

(V-21) Spherical Harmonics $G_{\ell\ell'm}(r)$ - Key as for (V-4)

Soft Core RISM molecule - with attractive perturbation at

($T^* = 1.34$, $\rho^* = 0.423$, $L^* = 0.786$) - Carbon Dioxide

(V-22) Zero-Density Spherical Harmonics $G_{\ell\ell'm}(r)$ - Key as for (V-4) at

($T^* = 1.34$, $L^* = 0.786$) - Carbon Dioxide

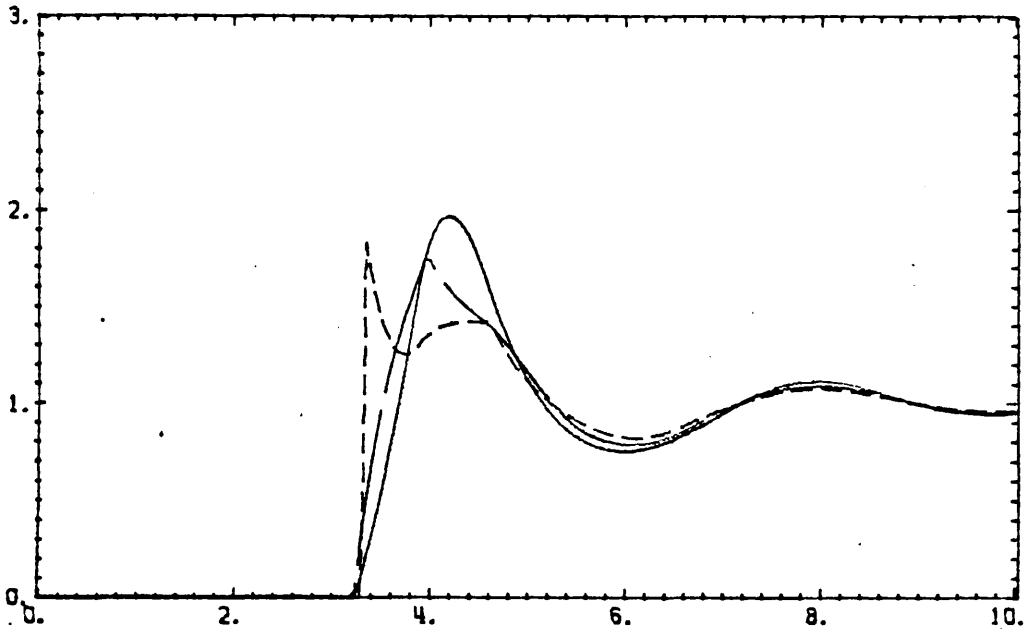

Fig. (V-2)

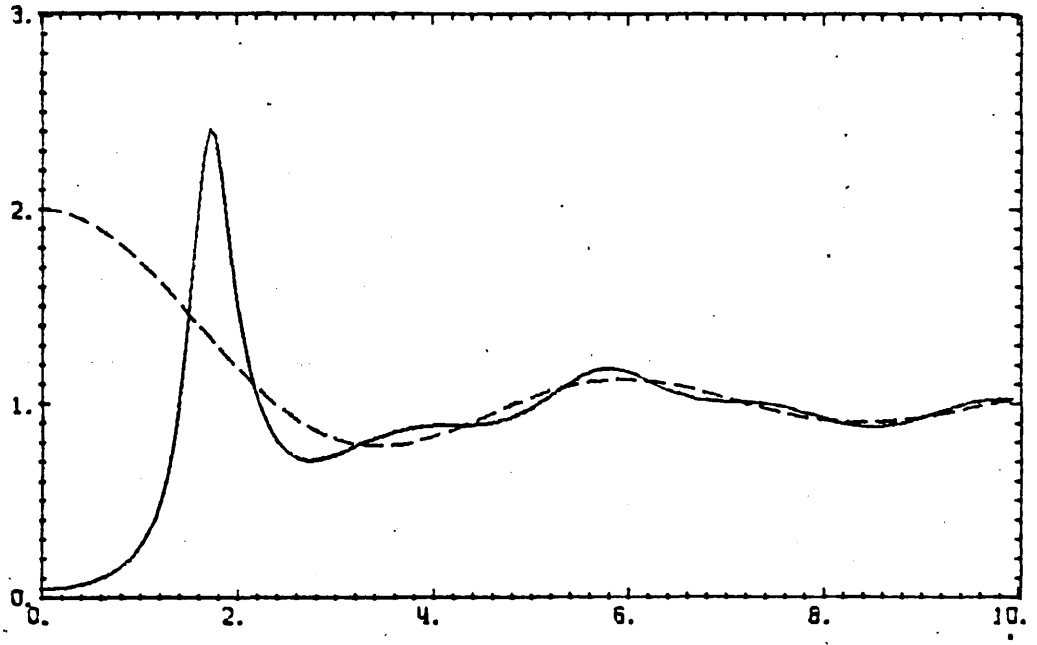

Fig. (V-3)

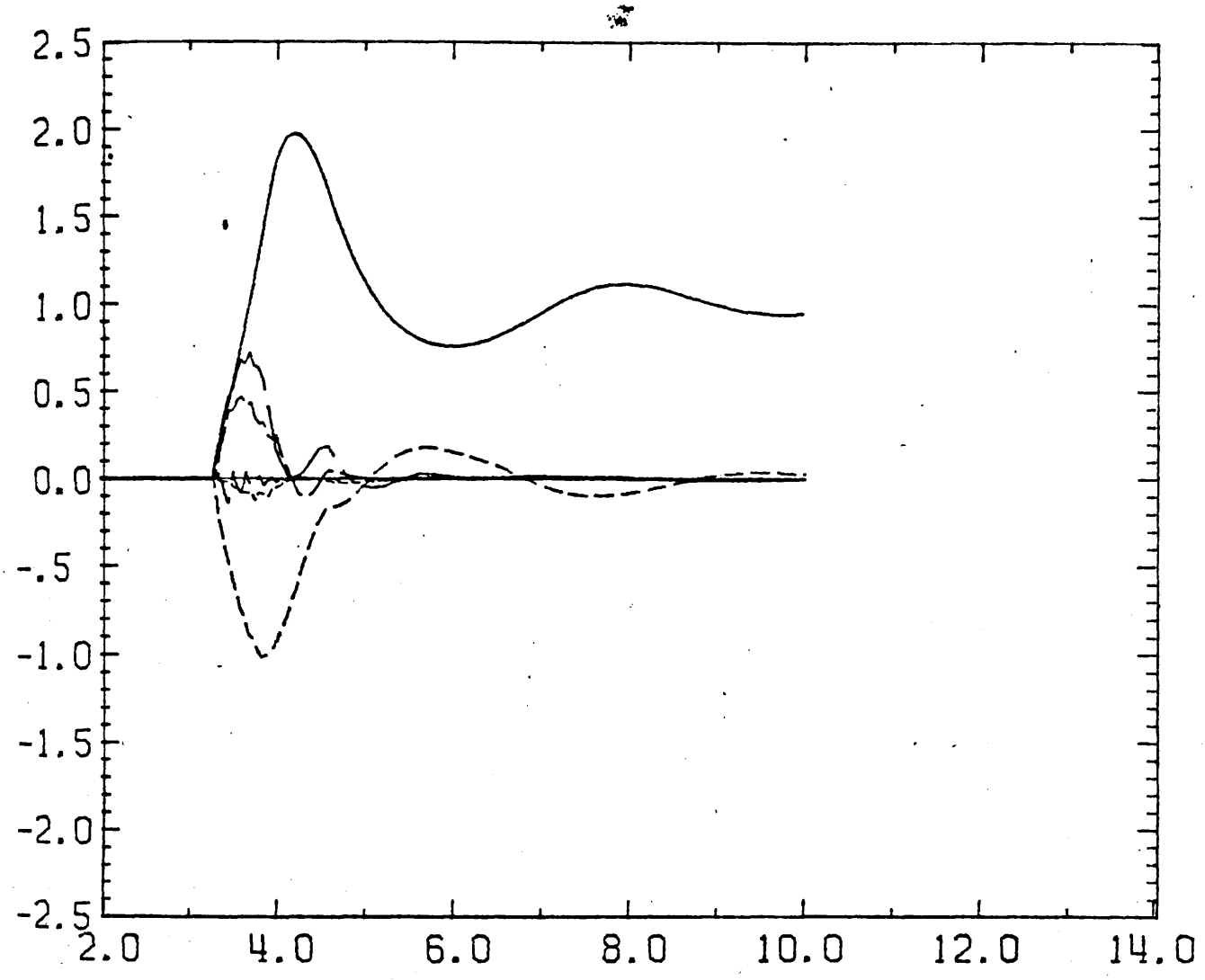

Fig. (V-4)

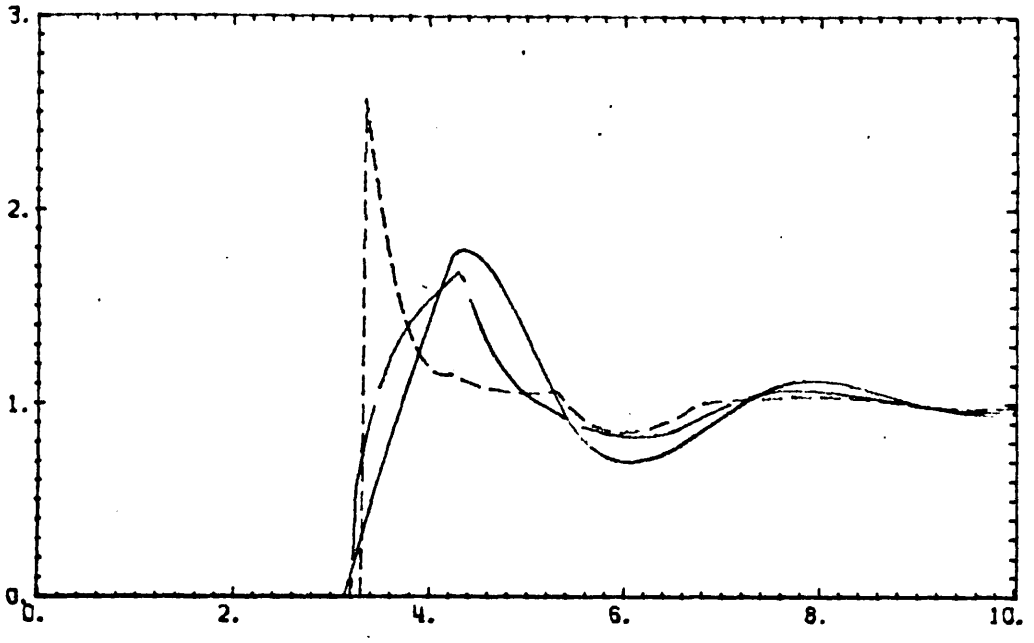

Fig. (V-5)

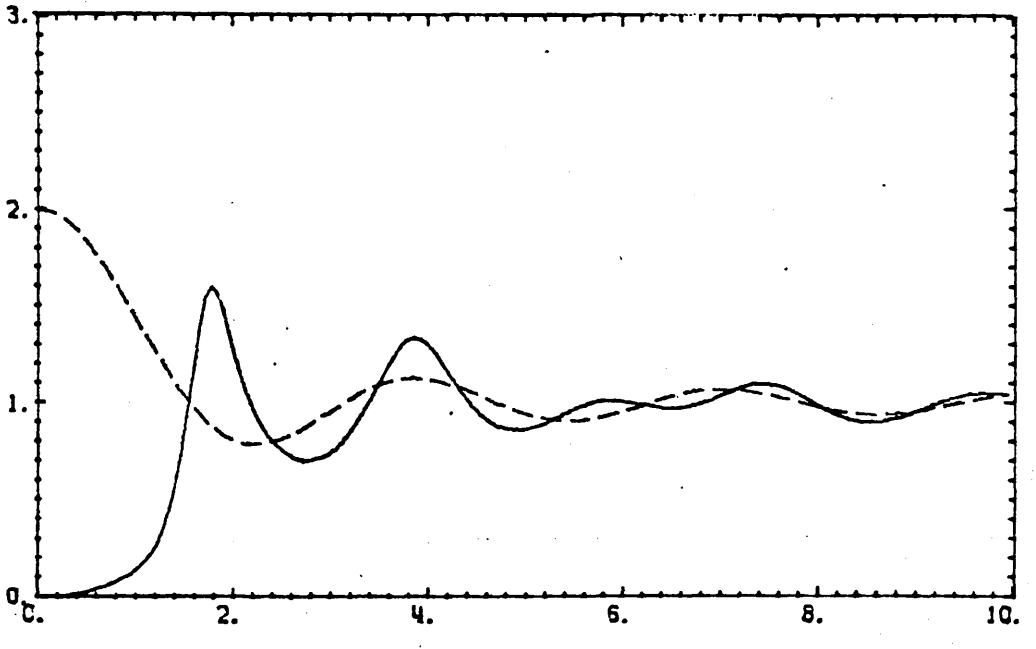

Fig. (V-6)

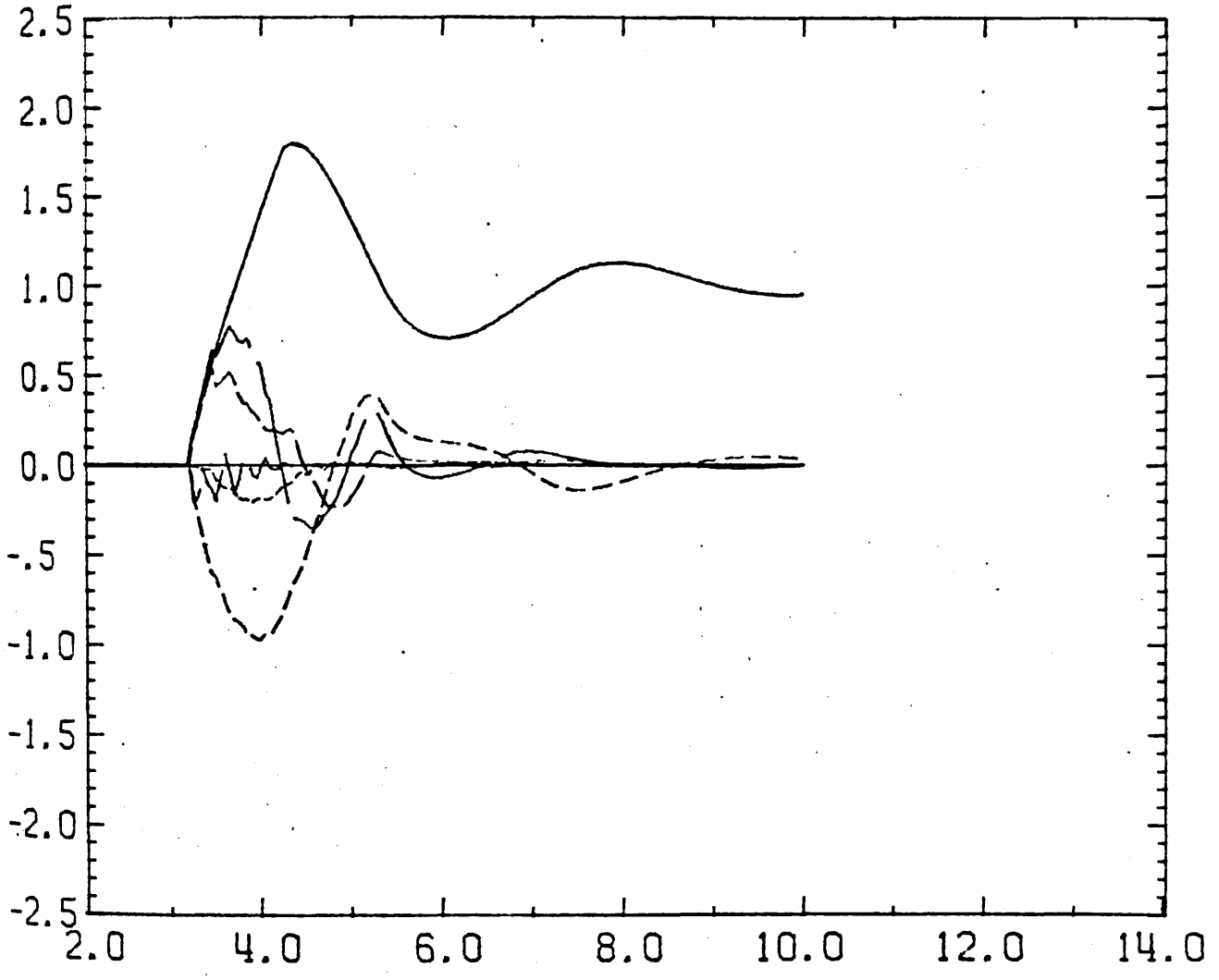

Fig. (V-7)

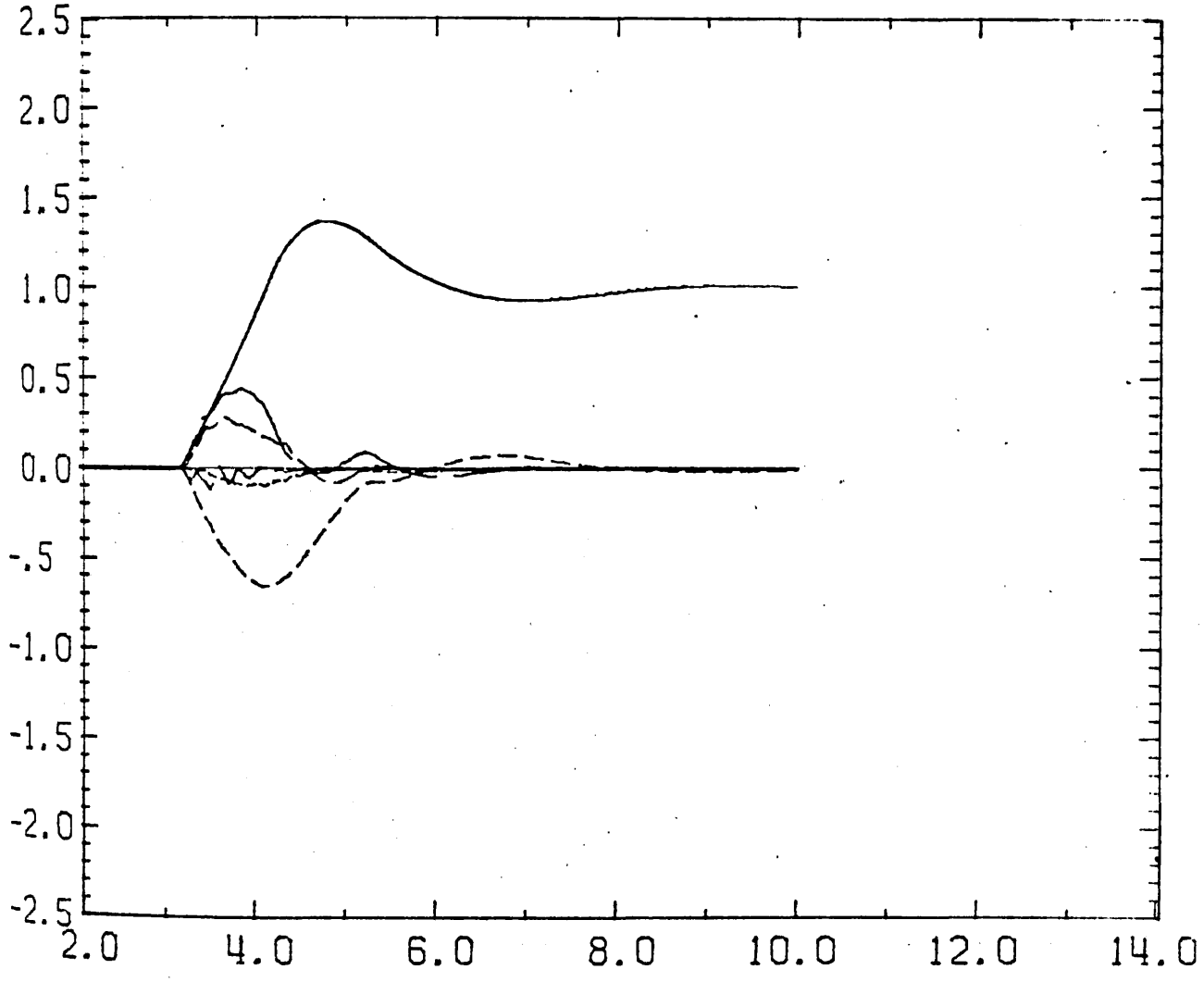

Fig. (V-8)

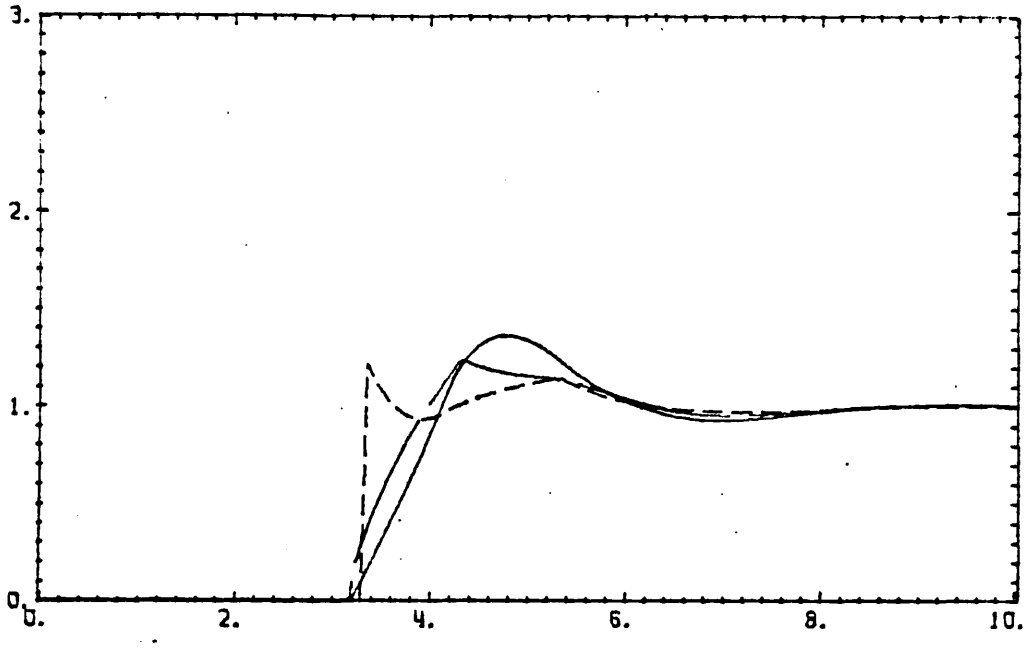

Fig. (V-9)

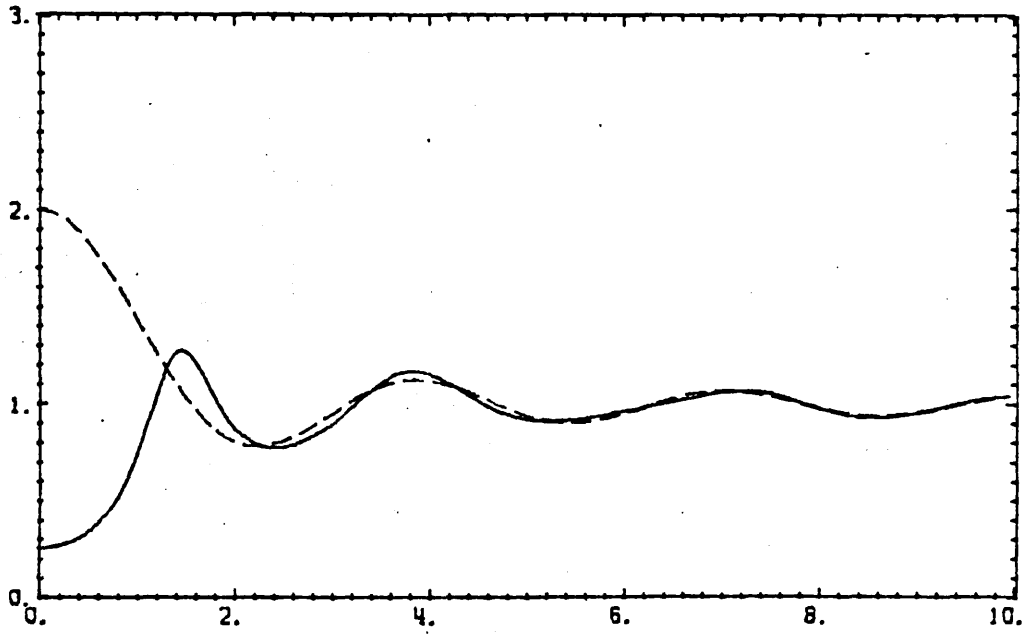

Fig. (V-10)

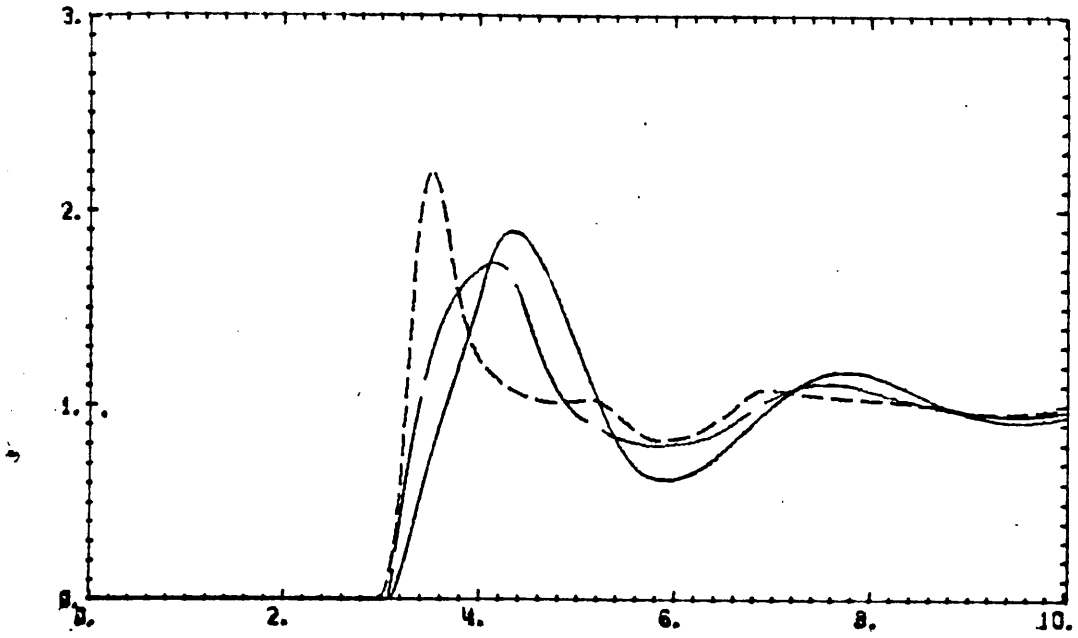

Fig. (V-11)

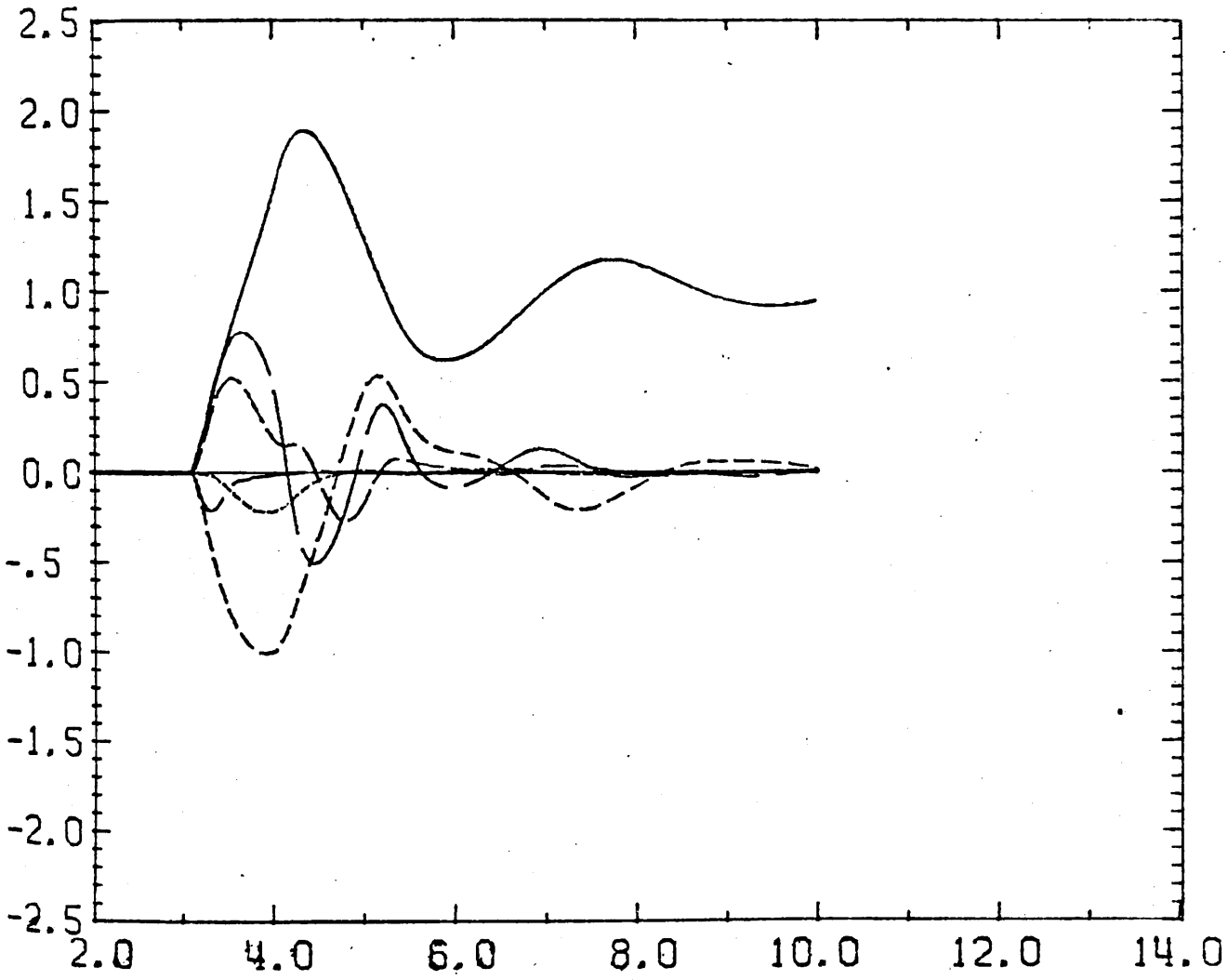

Fig. (V-12)

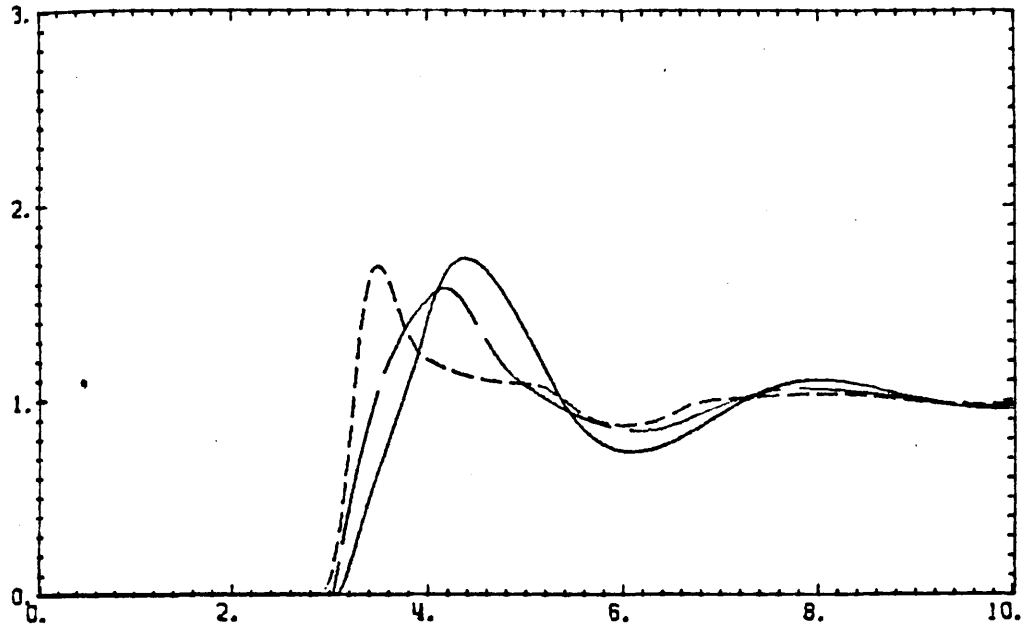

Fig. (V-13)

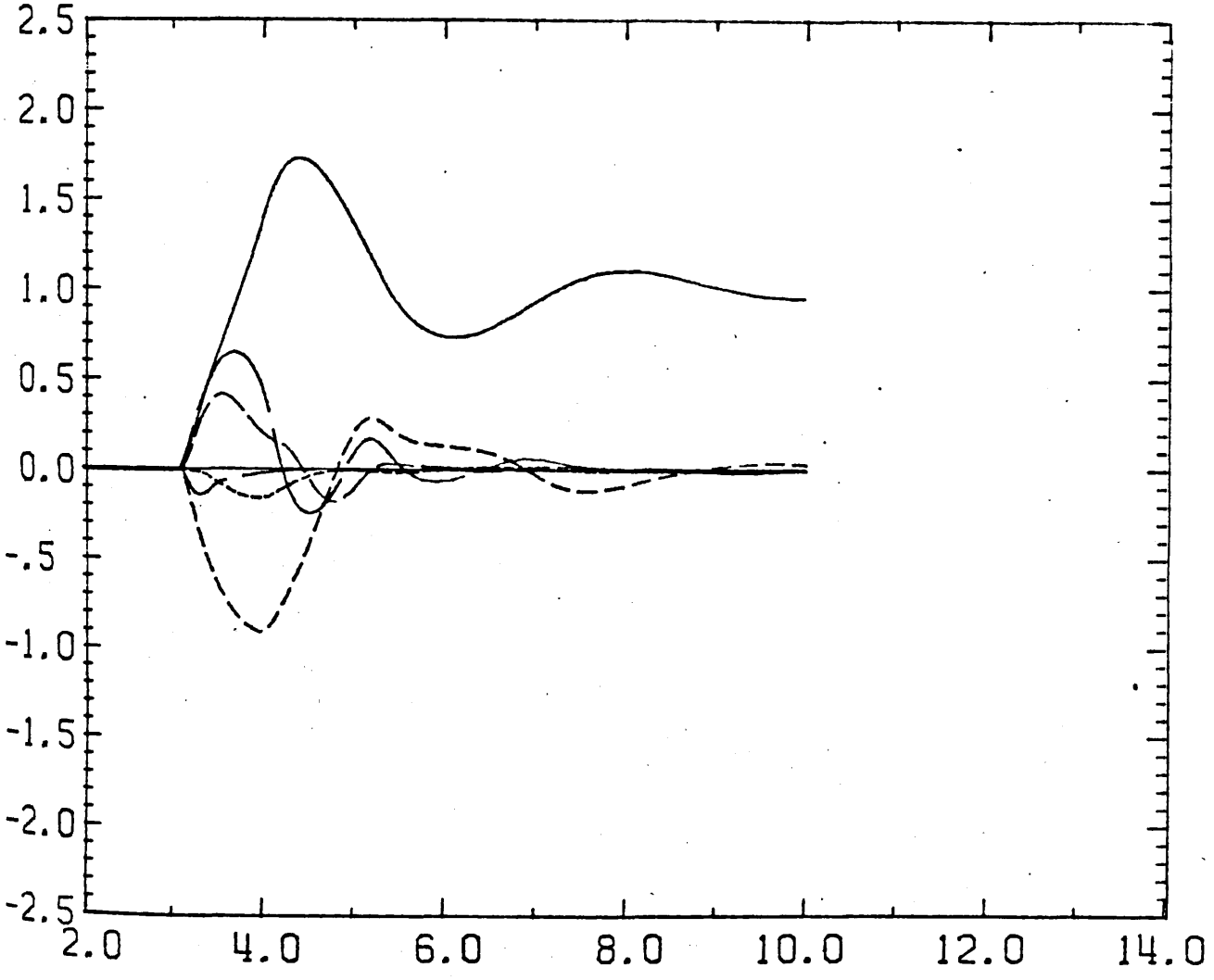

Fig. (V-14)

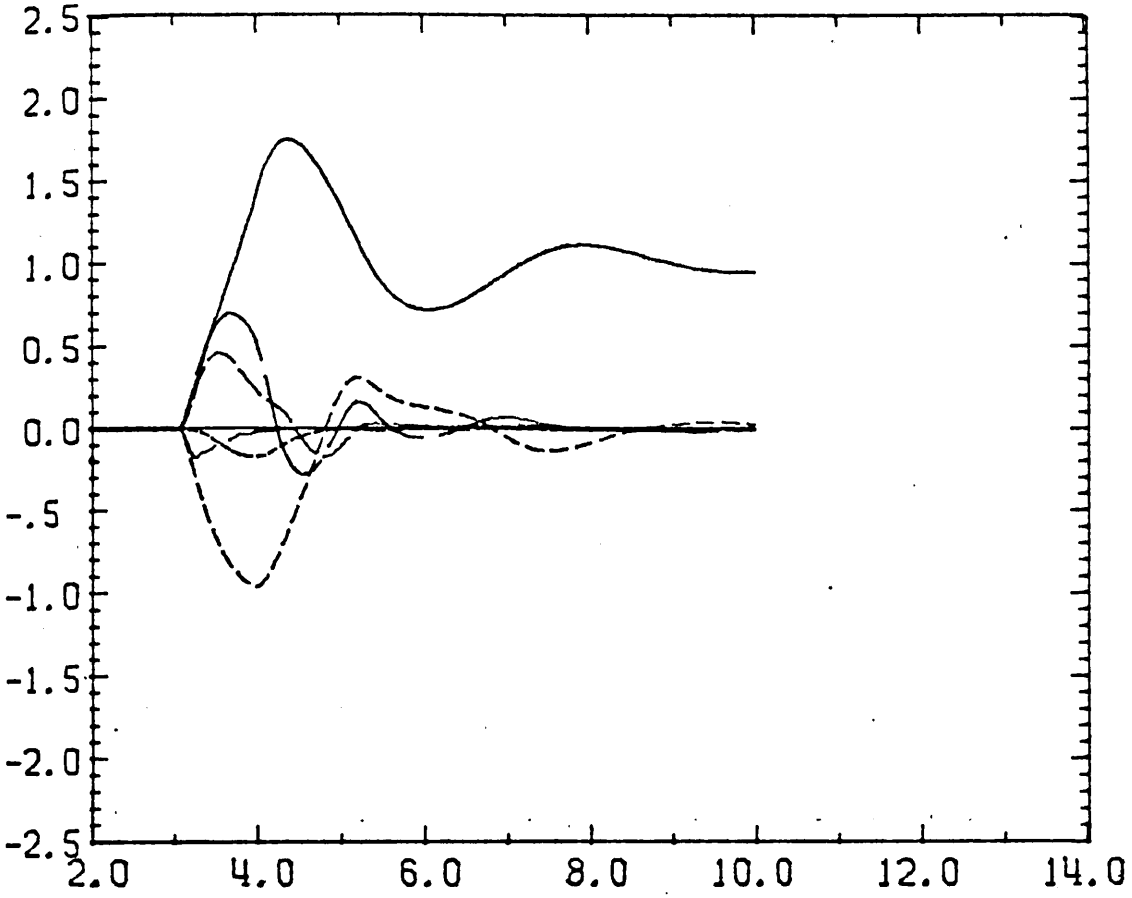

Fig. (V-14)

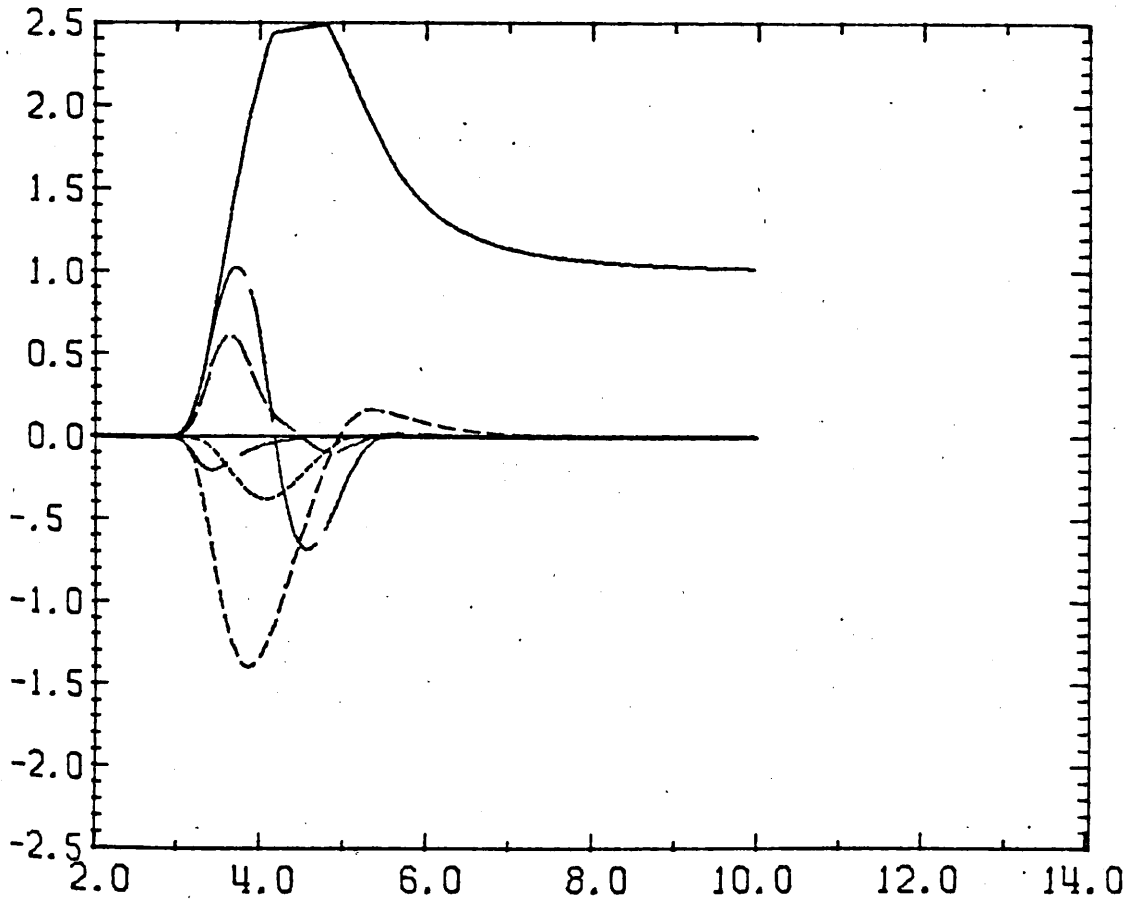

Fig. (V-15)

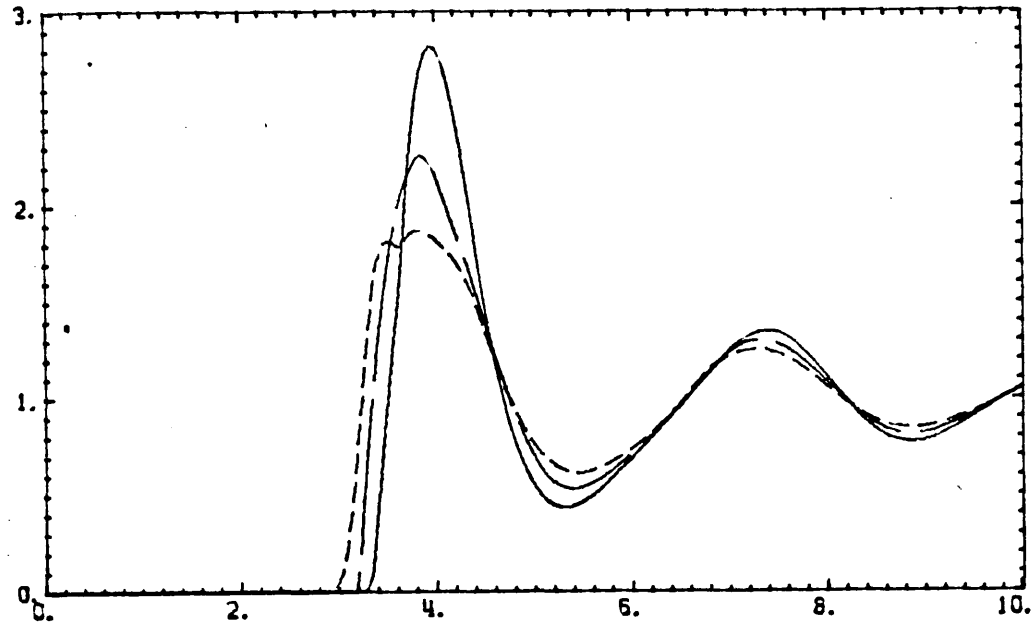

Fig. (V-16)

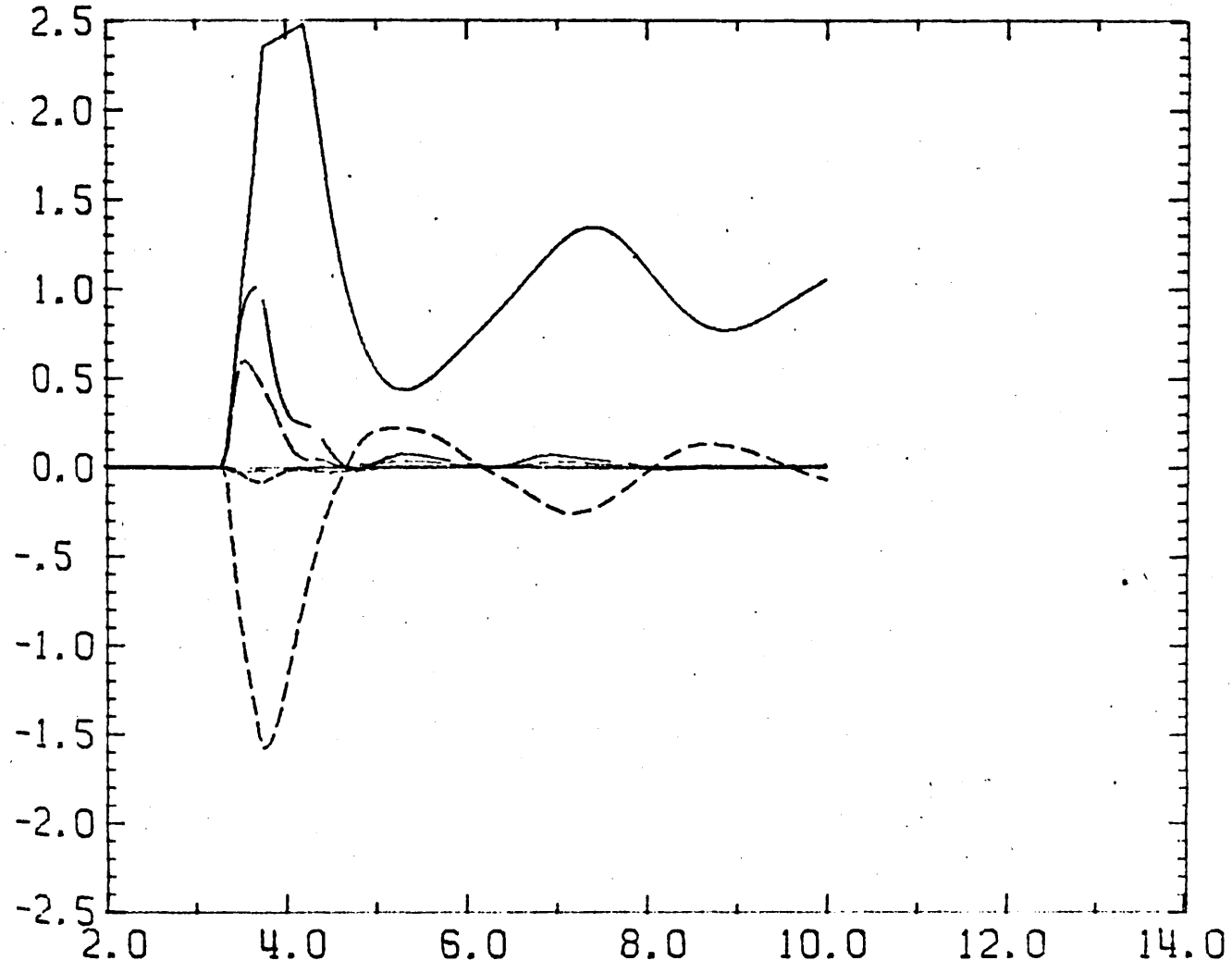

Fig. (V-17)

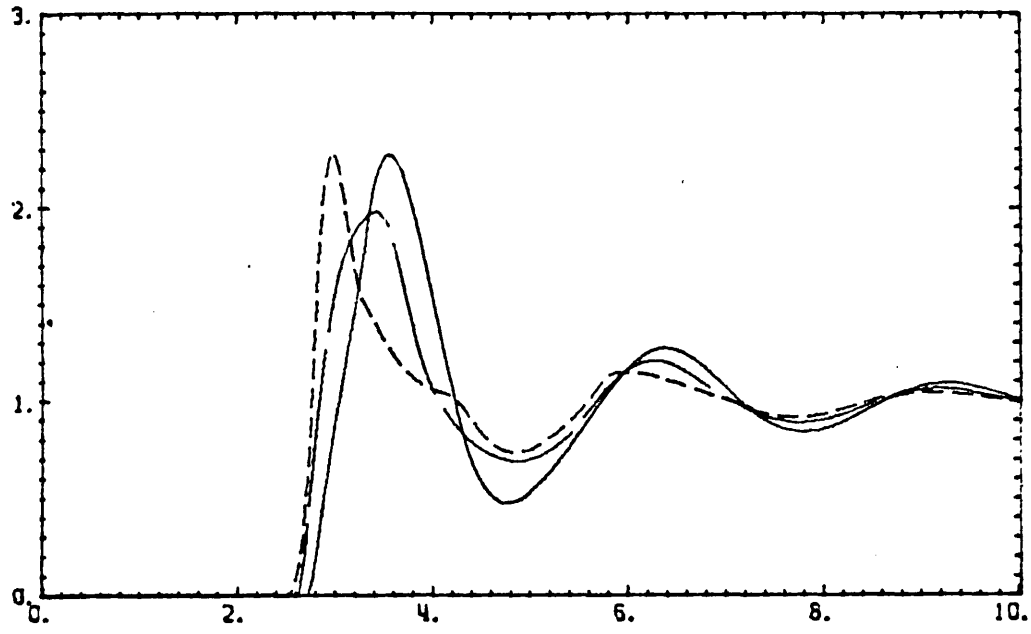

Fig. (V-18)

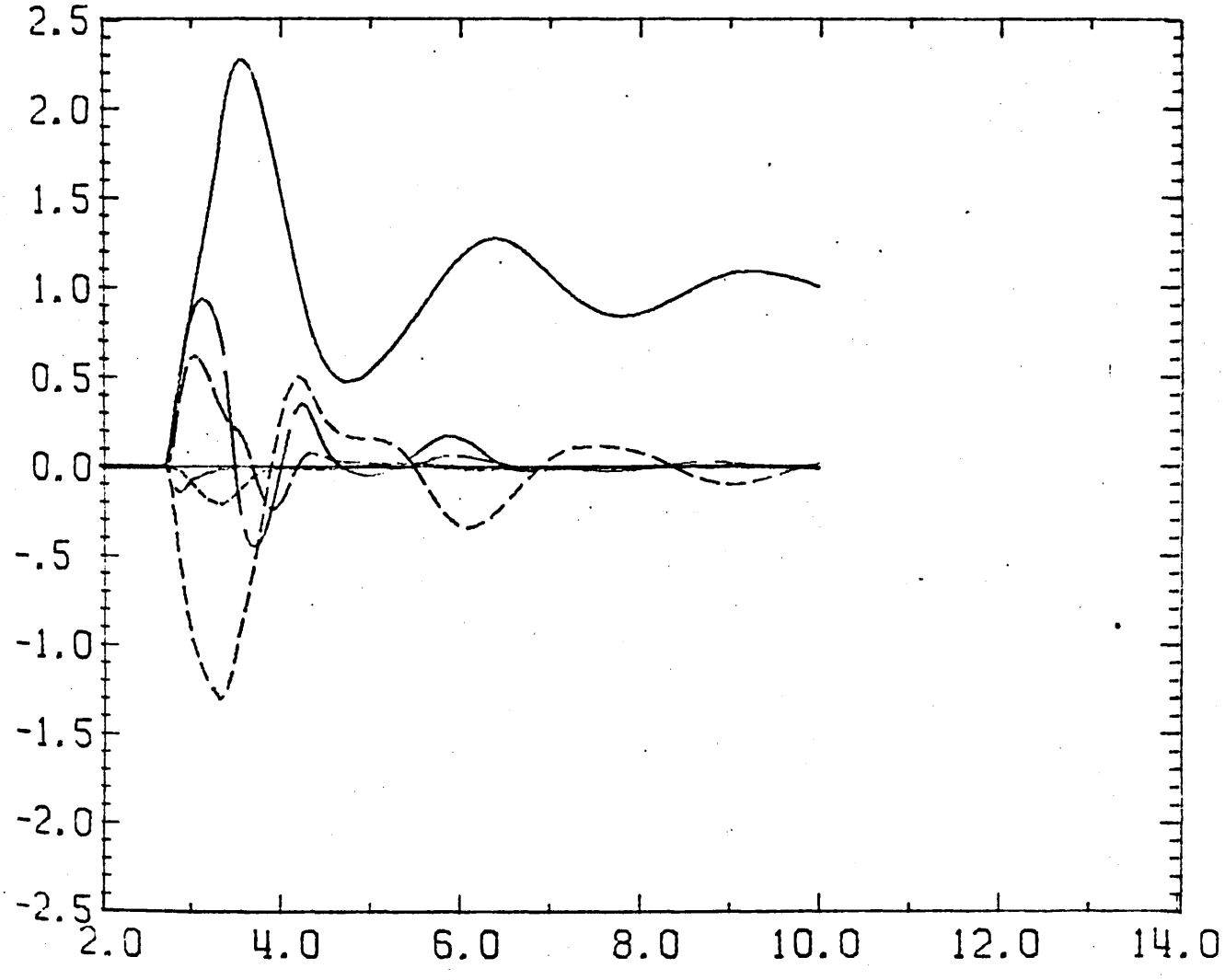

Fig. (V-19)

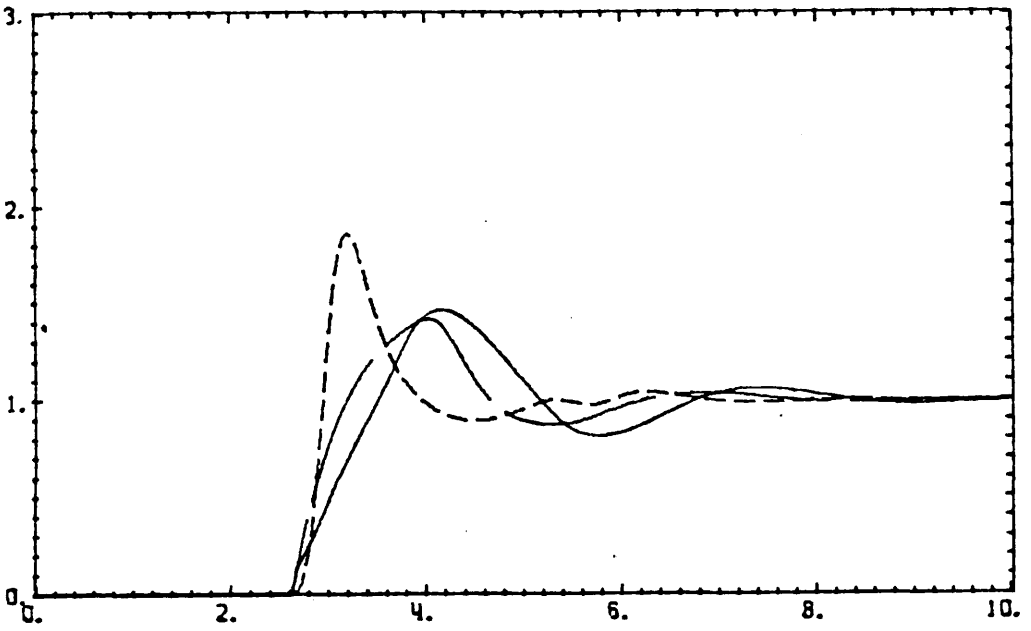

Fig. (V-20)

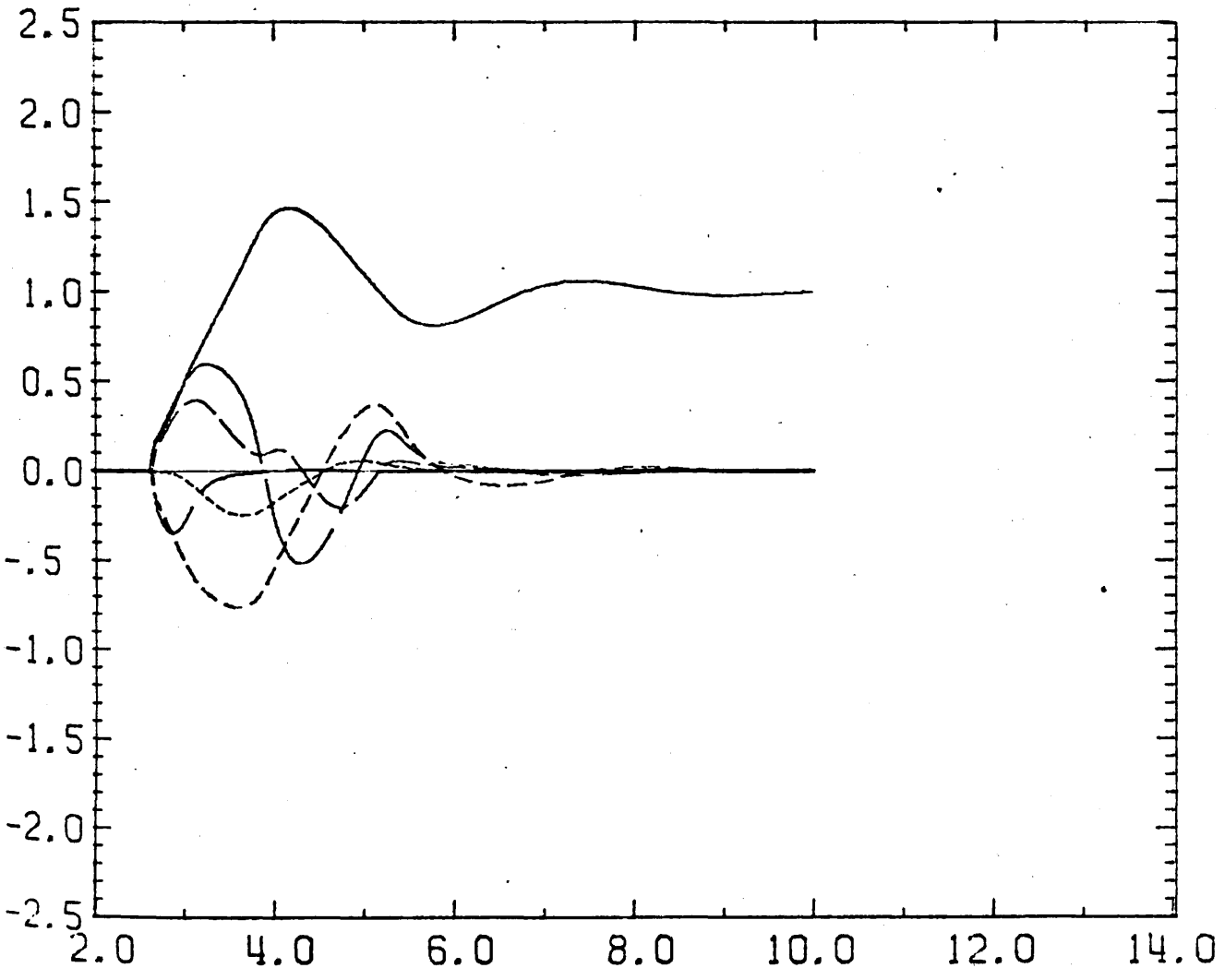

Fig. (V-21)

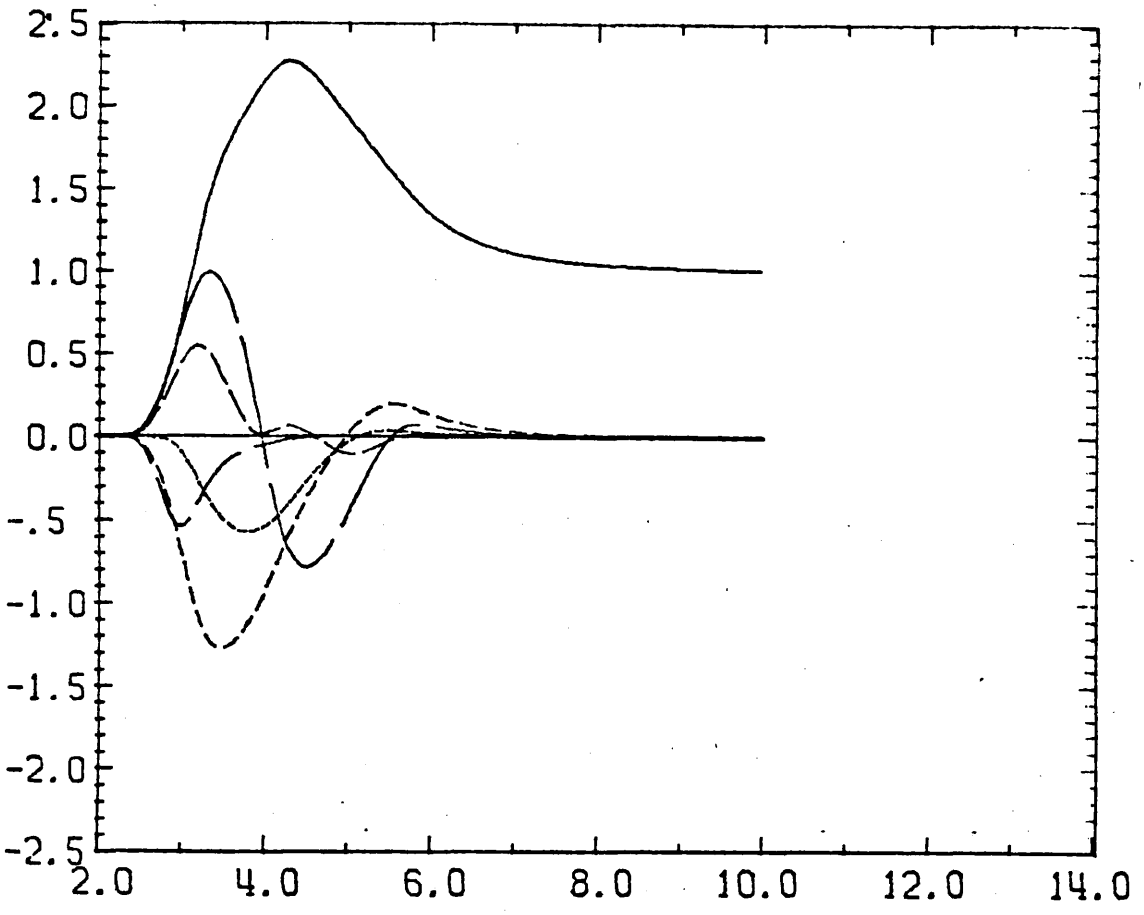

Fig. (V-22)

CHAPTER VI. DYNAMICS.

(VI-1) Introduction.

Correlation functions of dynamical variables have been extensively investigated due to their direct relationship to many experimentally observable properties of liquids, e.g. light scattering, which is determined by relaxation of density or polarizability fluctuations; spectral broadening which is due to the relaxation of excited states and transport processes such as diffusion, bulk viscosity, thermal conductivity and also electrical conductivity. Both theoretical and experimental work has been discussed by Temperley, Rowlinson and Rushbrooke(1) and Egelstaff(2). The relationship between the experimental quantities and theoretical correlation functions has been shown by Berne and Harp(3), Berne and Pecora(4) and reviewed by Williams(5). In addition an extensive review of time-dependent properties of liquids has also been given by Berne(6), who with Harp were the first to investigate the dynamical properties of linear molecules by molecular dynamics simulation(7).

Reviews of the theory of time correlation functions have been given by Zwanzig(8) and later by Gubbins(9) and Schofield(10). Another useful discussion, with particular emphasis on transport coefficients is given by Rice and Gray(11). A further introduction to the theory of time correlation functions and transport coefficients is given by Hansen and McDonald(12). Additional treatments of correlation functions are given by Steele(13), who also discusses the subject in the context of molecular rotation(14). Correlation functions and fluctuation-dissipation theorem are reviewed by Kubo(15) and an introductory article on the statistical theory of irrevsible processes is given by Weiss(16).

Other recent reviews of dynamical properties are given by Copley and Lovesey(17) on the experimental and theoretical properties of monatomic fluids and by Haile, Gubbins and Streett(18) concerned with the computer simulation aspects. The whole subject of rotational motion was also discussed at the Faraday Symposium(19).

(VI-2) Definition and Elementary Properties.

Assuming the classical Hamiltonian to have the form

$$H_N = 1/2 \sum_{i=1}^{N} \underset{\sim}{P}^2_i/M_i + \phi_N(\{\underset{\sim}{r}_i\}) \qquad \text{(VI-1)}$$

where M_i is the mass of particle i and $\phi_N(\{\underset{\sim}{r}_i\})$ is the translational invariant potential energy function. The time dependence of any dynamical quantity $A(t) = A(\underset{\sim}{r}^N(t), \underset{\sim}{p}^N(t))$ which is a function of the positions and momenta of the ensemble only, is given by the Poisson bracket expression(20), written as

$$\frac{dA(t)}{dt} = - i\mathcal{L}A(t) \qquad \text{(VI-2)}$$

where $\mathcal{L}$ is the Liouville operator

$$\mathcal{L} = i \sum_{k=1}^{N} \left(\frac{\partial H_N}{\partial \underset{\sim}{p}_k} \cdot \frac{\partial}{\partial \underset{\sim}{r}_k} - \frac{\partial H_N}{\partial \underset{\sim}{r}_k} \cdot \frac{\partial}{\partial \underset{\sim}{p}_k} \right) \qquad \text{(VI-3)}$$

now equation (VI-2) can be integrated formally to give

$$A(\underset{\sim}{r}^N(t), \underset{\sim}{p}^N(t)) = \exp[-it\mathcal{L}(\underset{\sim}{r}^N(0), \underset{\sim}{p}^N(0))] . A(\underset{\sim}{r}^N(0), \underset{\sim}{p}^N(0)) \qquad \text{(VI-4)}$$

It should be noted that equation (VI-4) is an operator expression and has meaning only if the exponential is expanded in powers of $i\mathcal{L}t$. Now the N-particle distribution function for an equilibrium ensemble is

$$D_N^0 = C\, e^{-H_0/kT} \qquad \text{(VI-5)}$$

where D_N^0 is time independent and C is a constant. Now if a small perturbation H_{ext} is added to the Hamiltonian H_0 of the equilibrium ensemble to give

$$H = H_0 + H_{ext} \qquad \text{(VI-6)}$$

then the distribution function D_N will be perturbed by an amount ΔD_N

$$D_N = D_N^0 + \Delta D_N \qquad \text{(VI-7)}$$

The response at time t to a perturbation applied at $t = -\infty$ is given by

$$\Delta D_N(t) = \int_{-\infty}^{t} \left(\frac{d\Delta D_N}{dt}\right)_{t=t'} dt' \qquad \text{(VI-8)}$$

The time derivative of ΔD_N is obtained by separating the Liouville equation operator into two parts

$$\mathcal{L} = \mathcal{L}_0 + \Delta\mathcal{L} \qquad \text{(VI-9)}$$

where $\mathcal{L}_0$ is the operator defined by equation (VI-3) with the Hamiltonian given by H_0 and similarly for $\Delta\mathcal{L}$ with $H = H_{ext}$. However, equation (VI-8) remains true whether this is done or not. Now since D_N^0 is independent of time we obtain

$$d/dt[\Delta D_N] = d/dt[D_N] \qquad \text{(VI-10)}$$

Now using equations (VI-7) and (VI-9) we obtain

$$d/dt[\Delta D_N] = i(\mathcal{L}_o D_N^o + \mathcal{L}_o \Delta D_N + \Delta\mathcal{L} D_N^o + \Delta\mathcal{L}\Delta D_N) \qquad \text{(VI-11)}$$

Assuming that the $\Delta\mathcal{L}\Delta D_N$ term is negligable, which is justified only if $\Delta\mathcal{L}$ is so small that a linear approximation is valid, and noting that D_N^o is time-independent gives

$$d/dt[\Delta D_N] = i(\mathcal{L}_o \Delta D_N + \Delta\mathcal{L} D_N^o) \qquad \text{(VI-12)}$$

Using equations (VI-3) and (VI-5) an expression can be obtained for $i\Delta\mathcal{L}D_N^o$ which is

$$i\Delta\mathcal{L}D_N^o = (D_N^o/kT)\, i\mathcal{L}_o \text{Hext} \qquad \text{(VI-13)}$$

In most cases the perturbation Hext may be expressed as

$$\text{Hext} = -F(t)A(\underset{\sim}{r}^N(t), \underset{\sim}{p}^N(t)) \qquad \text{(VI-14)}$$

where F(t) contains the time dependence, if any, of the perturbation, and thus equation (VI-13) becomes

$$i\Delta\mathcal{L}D_N^o = [D_N^o F(t)/kT]\dot{A}_o \qquad \text{(VI-15)}$$

where $\dot{A}_o$ is the time derivative of A in the equilibrium ensemble, in the absence of the perturbing Hamiltonian. Now equation (VI-12) can be integrated to give

$$\Delta D_N(t) = i\int_{-\infty}^{t} \exp[-i(t'-t)\mathcal{L}_o]\Delta\mathcal{L}D_N^o \, dt' \qquad \text{(VI-16)}$$

where the functions of $\underset{\sim}{r}$ and $\underset{\sim}{p}$ must be evaluated for the equilibrium ensemble. Using equation (VI-15) this can be rewritten as

$$\Delta D_N(t) = (D_N^o/kT)\int_{-\infty}^{t} F(t')\exp[-i(t'-t)\mathcal{L}_o]\dot{A}_o dt' \qquad \text{(VI-17)}$$

The operator in equation (VI-17) causes a time shift in the variable of $\dot{A}_o$, starting in equilibrium ensemble following its evolution for an interval (t'-t) giving

$$\Delta D_N(t) = (D_N^o/kT)\int_{-\infty}^{t} F(t')\dot{A}_o(t'-t)dt'$$

$$= (D_N^o/kT)\int_{-\infty}^{0} F(t+\tau)\dot{A}_o(\tau)d\tau \qquad \text{(VI-18)}$$

Now the change in a function $B(\underset{\sim}{r}^N(t),\underset{\sim}{p}^N(t))$ at time t due to the perturbation is

$$\langle\Delta B(t)\rangle = \int\Delta D_N(t)B d\Gamma \qquad \text{(VI-19)}$$

where $d\Gamma$ denotes a volume element of phase space. Substituting this into equation (VI-18) gives

$$\langle\Delta B(t)\rangle = \int_{-\infty}^{0} F(t+\tau)G_{\dot{A}B}(\tau)d\tau \qquad \text{(VI-20)}$$

and the correlation function $G_{\dot{A}B}(\tau)$ is

$$G_{\dot{A}B}(\tau) = 1/kT\int D_N^o\, B(0)\dot{A}(\tau)d\Gamma \qquad \text{(VI-21)}$$

where $\dot{A}(\underset{\sim}{r}^N(\tau),\underset{\sim}{p}^N(\tau))$ is calculated after an interval τ from the

evaluation of $B(\underset{\sim}{r}^N(0),\underset{\sim}{p}^N(0))$. The probability distribution of $\underset{\sim}{r}^N$ and $\underset{\sim}{p}^N$ is given by D_N^o, which thus governs the values of B and the initial values of A in the equilibrium ensemble. This approach follows very closely that given by Steele[13].

Alternatively the correlation function may be regarded as a time-average

$$\langle B(t+s)A(t)\rangle = \lim_{\tau\to\infty} 1/\tau \int_0^\tau B(t+s+t')A(t+t')dt' \qquad \text{(VI-22)}$$

where the average is carried out over all possible states of the system at time t.

The properties of time correlation functions are directly related to the Hamiltonian governing the equation of motion of the system. The canonical ensemble correlation of variables A and B $\langle A.B\rangle$ for which the Hamiltonian of the system is classical, and thus symmetric with respect to time, yields the following properties of correlation functions.

1) They are stationary.

$$\langle A(0).B(t)\rangle = \langle A(t_o).B(t_o+t)\rangle \qquad \text{(VI-23)}$$

2) They are symmetric (even) with respect to time and thus all odd time derivatives at t=0 are zero

$$\left(\frac{d^{(2n+1)}}{dt^{(2n+1)}}\langle A(0).B(t)\rangle\right)_{t=0} = 0 \qquad \text{for } n=0,1,2..... \qquad \text{(VI-24)}$$

3) If A and B are real or Hermitean variables, then it follows that the correlation function is real and

$$|\langle A(0).B(t)\rangle| \leq \langle A(0).B(0)\rangle \geq 0 \qquad \text{(VI-25)}$$

4) If the Hamiltonian is differentiable then the correlation functions will have Taylor series expansions about t=0

$$\langle A(0).B(t)\rangle = \sum_{S=0}^{\infty} a_s t^s/S! \qquad \text{(VI-26)}$$

where

$$a_s = \langle A(0).\mathcal{L}^S B(0)\rangle \qquad \text{(VI-27)}$$

5) Applying the stationary condition equation (VI-23) gives

$$\frac{\langle A(0).B(t)\rangle}{\langle A(0).B(0)\rangle} = \sum_{S=0}^{\infty} \frac{(-1)^s}{(2s)!} A_s t^{2s} \qquad \text{(VI-28)}$$

where

$$A_s = \frac{\langle A^{(s)}(0).B^{(s)}(0)\rangle}{\langle A(0).B(0)\rangle}$$

$A^{(s)}(0)$ denoting the Sth time derivative of A(t) at t=0. From this can be obtained[10].

$$A_{S+1}/A_s \leq A_{s+2}/A_{s+1} \qquad \text{(VI-29)}$$

and thus the radius of convergence of the Taylor series expansion is given by a time τ_c

$$\tau_c = \lim_{S\to\infty} 2s(2s-1)\ A_s/A_{s+1} \qquad \text{(VI-30)}$$

6) Finally, in general

$$\langle A(0).B(t)\rangle = \langle B(0).A(t)\rangle \qquad \text{(VI-31)}$$

from which is obtained

$$\langle A(0).B(t)\rangle = \langle B(t).A(0)\rangle = \langle B(0).A(-t)\rangle \qquad \text{(VI-32)}$$

A consequence of this is that we can write

$$d/dt\langle A(t.)B(t_o+t)\rangle = \langle A(t_o)\dot{B}(t_o+t)\rangle + \langle \dot{A}(t_o)B(t_o+t)\rangle \qquad \text{(VI-33)}$$

and thus

$$\langle A.\dot{B}(t)\rangle = -\langle \dot{A}.B(t)\rangle \qquad \text{(VI-34)}$$

However, in the case of quantum dynamics, the Hamiltonian becomes unsymmetric with respect to time reversal, and thus the limiting properties of the correlation functions in this case are substantially altered.

The correlation functions used throughout are normalized and defined by

$$C_A(t) = \langle A(0).A(t)\rangle / \langle A(0)^2\rangle \qquad \text{(VI-35)}$$

which is computationally evaluated by a method due to Gosling(22). High accuracy and continuity of the first two derivatives of the correlation functions are assured if they are evaluated for every time step in such a way that each time step has exactly the same statistical weighting in the time average.

(VI-3) Translational Motion.

In order to study the translational motion, the centre of mass (COM) velocity autocorrelation function (acf) $C_v(t)$ was evaluated

$$C_v(t) = \langle \dot{\underset{\sim}{R}}_i(0) . \dot{\underset{\sim}{R}}_i(t) \rangle / \langle \dot{\underset{\sim}{R}}(0) . \dot{\underset{\sim}{R}}(0) \rangle$$

$$= (3kT/M) \langle \dot{\underset{\sim}{R}}_i(0) . \dot{\underset{\sim}{R}}_i(t) \rangle \qquad \text{(VI-36)}$$

The COM force acf is given by the second derivative of $C_v(t)$, and was not computed directly.

$$C_F(t) = -d^2/dt^2 C_v(t) = \langle \ddot{\underset{\sim}{R}}_i(0) . \ddot{\underset{\sim}{R}}_i(t) \rangle / \langle \ddot{\underset{\sim}{R}}_i(0) . \ddot{\underset{\sim}{R}}_i(0) \rangle \qquad \text{(VI-37)}$$

Unfortunately strict comparison with the basic 2-centre Lennard-Jones systems (2LJC) results of Singer et al.(21).is not possible for the reasons discussed in Chapter III. However, as a guide of comparability the reduced units $T^* = kT/\varepsilon$, $\rho^* = \rho\sigma^3$, $L^* = L/\sigma$ and $Q^* = Q/(\varepsilon\sigma^5)^{\frac{1}{2}}$ have been used together with the additional units $D^* = D(M/\varepsilon)^{\frac{1}{2}}\sigma^{-1}$, $\tau^* = (kT/M)^{\frac{1}{2}}(\tau/\sigma)$ for translational motion and $\tau^* = (kT/I)^{\frac{1}{2}}(\tau/\sigma)$ for rotational motion where M is the total molecular mass and I is the molecular moment of inertia.

Caution should be used when looking at the correlation functions beyond approximately 1.2×10^{-12} seconds as the fluctuations and structure beyond this are generally less than the statistical fluctuations produced by averaging over a small number of particles (108) for a limited number of time steps ($\approx$ 5000). This can be seen from significant differences in runs with 256 particles at long times.

The essential features of the variation of $C_v(t)$ with T^*, ρ^* and L^* remain the same as that shown by Singer et al.(21) for the basic

2LJC systems. This is illustrated in Figures (VI-1) to (VI-7), from which the following general features are observed.

1) That for all densities and temperatures there is a strong initial decay of approximately gaussian shape.

2) For $T^* \approx 1$ and $p^* \approx 0$ the correlation functions have a negative lobe, which is seen to increase in magnitude with increasing quadrupole moment, followed by a long negative tail.

3) The depth of the minimum is weakly temperature dependent at constant density. However, the minimum is strongly dependent on ρ^*; decreasing as ρ^* decreases. The minimum is also dependent on Q^*, increasing with Q^*.

4) For any given values of ρ^*, T^* and Q^*, the magnitude of the minimum decreases with increasing L^*, such that for large values of L^* the minimum disappears completely.

5) An interesting secondary effect is that for low ρ^*, the initial decay rate increases as T^* increases, although the depth of the minimum is decreased.

However, for the dipolar systems no significant differences can be seen from the basic 2LJC systems of Singer et al. This is due to the dipolar perturbation being small (of order 0.5 Debye) and thus these systems will not be discussed further.

These features are reproduced for most liquid systems studied by molecular dynamics simulation methods. These effects are thought to be due to rapid loss of initial correlation with the negative lobe caused by "back-scattering" by a surrounding cage of nearest neighbour molecules, which is a type of oscillatory motion. At lower densities there are fewer nearest neighbours giving the particles longer mean free paths, and thus their momentum correlation decays at a slower rate. This does not however mean that there are no "back-scattering" events happening, but rather that these events have less statistical significance.

The long negative tail is usually explained as a form of cooperative motion between the molecule and its 'cage' of nearest neighbours, such that the 'cage' itself has movement and thus correlation of velocity over much larger mean free paths. The double minima structure shown in the $C_v(t)$'s computed by Singer et al. for $L^* = 0.505$, $L^* = 0.608$ and $L^* = 0.632$, was first noticed in nitrogen systems by Barojas et al.(23). The systems of 2LJC liquids when perturbed by a quadrupolar interaction gradually lose this feature with increasing quadrupole moment. The feature was interpreted as coming from the different correlation loss rates for motion parallel and perpendicular to the molecular axis. This is shown by evaluating the parallel and perpendicular velocity correlation functions. These functions are more fully discussed in section (VI-9).

These results may also be compared with the work on nitrogen, with and without quadrupolar interactions by Cheung and Powles(24,25) and other simulations of purely model systems by Steele and Streett(27). Simulation of the 2LJC system by Quentrec(28) uses the same parameters as the present simulation and is thus most suitable for comparative purposes. However, the results of Cheung and Powles for $C_v(t)$ are in close agreement with those of Quentrec.

The comparison shows that the strong double minima feature observed by Quentrec has become a single minimum of slightly greater depth, due to the motion becoming more isotropic in the quadrupolar case. The reasons for this change are probably that despite the highly anisotropic nature of the quadrupole potential, the potential itself has become more cohesive. The effects of this would be to increase 'local' (i.e. nearest-neighbour) ordering in the system, and thus increase the cooperative motion effects. This would mean that the molecules tend to translate as a loosely bound complex rather than individual molecules. In this way the differences in isotropy

are minimized.

The results at the lower density $\rho^* = 0.626$ show that the effect of the quadrupole moment is to produce a negative lobe even at high temperatures, which is not shown in the 2LJC system results. Thus the statement by Cheung and Powles(25) that "the quadrupolar interaction appears to have little effect on translational motion", can only be valid of small quadrupolar perturbations. As the nitrogen quadrupole is not small, the explanation may be that the point-quadrupole potential used by Cheung and Powles, while adequately representing the averaged interaction potential, fails to represent close respulsive site-site interactions which will strongly influence the dynamics of the system. The difference in the two forms of potential used is also discussed by Streett and Tildesley(26) who conclude that there are significant differences in the calculated potential for the two models at small distances, for some orientations.

Comparison with the chlorine and carbon-dioxide like 2LJC systems of Singer et al. show the same general effects, i.e. the disappearance of the double negative lobe of $C_V(t)$ and an increase in the depth of the minima, as well as $C_V^{II}(t)$ and $C_V^{\perp}(t)$ becoming more like $C_V(t)$ with increasing quadrupole moment. Thus the motion of the system becomes more isotropic. Again the point-quadrupole results of Steele and Streett(27) show little difference from the basis 2LJC results except at large $Q^* \approx 2$. These authors also point out that differences exist in the dynamical properties of point-quadrupole and discrete charge models, but only for large values of Q^*. This also applies to the nitrogen case ($Q^* = 1.16$) which may be regarded as having a medium quadrupole moment.

From the various $C_V(t)$ and $C_V^{II}(t)$; $C_V^{\perp}(t)$ the diffusion constants were calculated by

$$D = (3kT/M)\int_0^{T'} C_v(t)\,dt \qquad \text{(VI-38)}$$

using Trapezoid rule with $T' = 600\Delta t$. The results are given in Table (VI-1). The accuracy is reduced by fluctuations in the correlation functions for $T' > 300\Delta t$ due to statistical noise. Comparison of correlation times evaluated up to $T' = 200\Delta t$ and $600\Delta t$ show differences of 20%, however, this could be due to the persistance of long negative tails.

(VI-4) Force Correlation Functions.

These correlation functions evaluated from and defined by equation (VI-37) are illustrated in Figures (VI-8) to (VI-10). The main features of $C_F(t)$ are very rapid initial decay to a strong negative lobe. This is similar to a highly damped oscillator behaviour. This shows that the sign of the force acting on a molecules changes approximately twice as quickly as the sign of the velocity. If the motion of the molecule was perfectly harmonic then the force and velocity would change sign with equal periodicity, thus the observation that the force changes sign twice as often shows that the molecule is undergoing highly anharmonic motion.

Force correlation times evaluated from

$$\tau_F = \int_0^{T'} C_F(t)\,dt \qquad \text{(VI-39)}$$

were found to be zero within statistical error, as would be expected for a function that is the second derivative of some other function. The similarity between the curves shown for nitrogen, chlorine and carbon dioxide is striking. The curves for the different quadrupole moments in chlorine were found to be almost indistinguishable, as were the functions evaluated at the same density but different

TABLE (VI-1).

T*	ρ*	Q* or μ	L*	$\int_0^{600\Delta t}$ $D\times10^{-9}(200\Delta t)$	$D^*\times10^{-2}$	$D_{\parallel}\times10^{-9}$	$D^*_{\parallel}\times10^{-2}$	$D_{\perp}\times10^{-9}$	$D^*_{\perp}\times10^{-2}$	$D_{\parallel}/D_{\perp}$
1.14	0.541			1.65(2.18)	3.25	3.06	6.04	1.80	3.55	1.70
1.45	0.485	0.739	0.608	3.94(4.68)	7.78	5.81	11.46	3.60	7.10	1.61
1.74	0.485			4.67(5.09)	9.22	6.69	13.20	3.87	7.63	1.73
1.21	0.546			1.26(1.87)	2.54					
1.55	0.546	1.321	0.608	2.04(2.63)	4.12					
1.55	0.490			3.49(4.13)	7.04	4.93	9.95	3.50	7.07	1.41
1.81	0.490			4.32(4.93)	8.71					
1.50	0.551			0.80(1.48)	1.77					
1.85	0.551	2.073	0.608	1.48(2.00)	1.85	2.37	5.25	2.00	4.43	1.18
1.86	0.494			3.27(3.42)	7.26	3.72	8.24	3.23	7.15	1.15
2.19	0.494			3.93(4.27)	8.70	4.51	9.98	3.87	8.58	1.16
1.61	0.700			0.73(1.32)	1.96	1.80	4.84	1.41	3.79	1.28
2.66	0.700	1.159	0.328	1.99(2.30)	5.34					
2.27	0.626			3.80(4.22)	10.23	4.40		3.52		1.25
3.60	0.626			5.93(5.61)	15.95					
1.61	0.423			4.00(4.28)	8.38	4.65		3.80		1.23
2.14	0.423	2.039	0.793	5.81(5.82)	12.17	6.34		5.05		1.26
1.83	0.381			7.21(6.95)	15.10					
2.39	0.381			8.83(9.00)	18.49	8.63		7.73		1.12
1.13	0.541			2.10(2.53)	4.07					
1.39	0.541	0.5Debye	0.608	2.48(3.11)	4.80					
1.42	0.485			4.79(5.02)	9.30					
N=256										
1.13	0.541	0.739	0.608	1.64(2.28)	3.24					
1.42	0.551	2.073	0.608	0.95(1.40)	2.10					

temperatures, for all systems. Thus the force auto-correlation functions are found to be highly damped and oscillatory, with little variation in shape, except with density. This is probably due to the change in the gradients of the effective potential well formed by the particles nearest neighbours.

(VI-5) Rotational Motion.

The rotational motion of the system is most usefully described in terms of the orientational self-correlation functions given as the Legendre polynomial expansion of the vector product of the molecular orientation $\underset{\sim}{1}_i(t)$ at time t, where $\underset{\sim}{1}_i(t)$ is the unit vector along the molecular axis. These are

$$C_1(t) = \langle \underset{\sim}{1}_i(0).\underset{\sim}{1}_i(t) \rangle \qquad \text{(VI-40)}$$

$$C_2(t) = 3/2\langle |\underset{\sim}{1}_i(0).\underset{\sim}{1}_i(t)|^2 \rangle - \tfrac{1}{2} \qquad \text{(VI-41)}$$

$C_1(t)$ is related to the broadening of infra-red adsorption hands in dipolar systems whereas $C_2(t)$ is related to the corresponding Raman phenomena(6,19). Plots of these functions are shown in Figures (VI-11) to (VI-14). All these curves show the same features.

1) Initial gaussian like decay.

2) Exponential decay after a time roughly corresponding to the minimum of the angular momentum correlation function discussed later.

The gradient of $C_2(t)$ is less consistent as the function decays faster and is thus more affected by statistical fluctuations.

The correlation times are given by

$$\tau_n = \int_0^{T'} C_n(t)\,dt \qquad \text{(VI-42)}$$

where $T' = 600\Delta t$, and extrapolated to $t = \infty$ by assuming an expontial tail whose decay constant is approximated by least-squares fitting to $\ln|C_n(t)|$ in the range $200 \rightarrow 500\Delta t$. The results are given in Table (VI-2). Direct comparison with the results of Quentrec(28) show that there is good agreement with the basic 2LJC system results, the quadrupole causing a 10 to 20% increase in τ_1 and τ_2 and a smaller decrease in τ_w.

The same effects are observed for the chlorine and carbon dioxide systems, whereby the quadrupole results in an increase in the orientational correlation times and a decrease in the angular momentum correlation times. It is interesting that the ratio τ_1/τ_2 remains unchanged, which means that the quadrupole effects τ_1 and τ_2 equally. The simple explanation of these effects is that the quadrupole potential is more cohesive and thus maintains orientations for longer periods, by libration about the orientational position. Thus it is reasonable that the molecules are more strongly bound to their nearest neighbours in particular orientations. This suggests that the motion in quadrupolar fluids is on a more cooperative basis which the long range nature of the quadrupolar interactions must also encourage.

The values of the relaxation time τ_2 for 2LJC chlorine systems were compared to the experimental values by Singer et al. who found that the values predicted by the molecular dynamics were consistantly too small. The values calculated for quadrupolar systems are

T(K)	Q*	$\tau_2 \times 10^{-12}$s
227.5	0.739	0.89
230.5	1.321	1.15
236.1	2.073	1.97

TABLE (VI-2).

T^*	ρ^*	Q^* or μ	L^*	τ_1^*	τ_2^*	τ_ω^*	τ_1/τ_2	$2\tau_1^*\tau_\omega^*$	$6\tau_2^*\tau_\omega^*$
1.14	0.541			4.01	1.45	0.127	2.78	1.02	1.10
1.45	0.485	0.739	0.608	2.46	0.95	0.227	2.60	1.12	1.29
1.74	0.485			2.29	0.91	0.238	2.50	1.09	1.31
1.21	0.546			5.19	1.87	0.106	2.78	1.10	1.19
1.55	0.546	1.321	0.608	4.07	1.48	0.137	2.76	1.12	1.22
1.55	0.490			2.62	1.04	0.201	2.52	1.05	1.25
1.81	0.490			2.46	0.93	0.222	2.65	1.09	1.24
1.50	0.551			8.99	3.25	0.062	2.77	1.12	1.22
1.85	0.551	2.073	0.608	6.17	2.25	0.089	2.74	1.10	1.21
1.86	0.494			4.30	1.53	0.126	2.81	1.08	1.15
2.19	0.494			3.23	1.20	0.171	2.70	1.10	1.23
1.61	0.700			2.25	0.96	0.270	2.33	1.21	1.56
2.66	0.700	1.159	0.328	1.32	0.66	0.400	1.98	1.05	1.60
2.27	0.626			1.52	0.69	0.569	2.20	1.73	2.36
3.60	0.626			1.08	0.59	0.778	1.83	1.68	2.75
1.61	0.423			4.47	1.62	0.120	2.76	1.07	1.17
2.14	0.423	2.039	0.793	3.36	1.26	0.160	2.66	1.08	1.21
1.83	0.381			3.06	1.19	0.178	2.57	1.09	1.27
2.39	0.381			2.52	0.96	0.211	2.62	1.07	1.22
1.13	0.541			4.35	1.55	0.124	2.81	1.08	1.15
1.39	0.541	0.5Debye	0.608	3.78	1.41	0.147	2.67	1.11	1.25
1.42	0.485			2.47	1.00	0.242	2.46	1.19	1.45
N=256									
1.13	0.541	0.739	0.608	3.73	1.39	0.142	2.68	1.06	1.18
1.42	0.551	2.073	0.608	2.52	0.96	0.211	2.79	1.03	1.11

Comparison with Figure 5 of reference(21) shows that the quadrupole does indeed improve agreement with experiment for the two lower values of Q^*, which seem to be equally close to the experimental values. The relaxation time for $Q^* = 2.073$ is however far too high, but the comparison may not be strictly valid as the large quadrupole may well be a significant perturbation to the equation of state of the system. The difference between the 2LJC and quadrupolar relaxation times would appear to be very roughly proportional to Q^{*2}.

A study of the correlation times for molecular reorientation, calculated for various types of diffusion models has been given by Powles and Rickayzen(29), who plot the predictions of various models as a function of the reduced variables τ_1^*, τ_2^* and τ_w^*. It can be seen from Table (VI-2) that for all systems, except nitrogen at high temperatures, that the product $2\tau_1^*\tau_w^*$ is very close to unity. The same is true for the product $6\tau_2^*\tau_w^*$ but with rather greater deviations from unity. This shows that there is little deviation from the Hubbard relations(30) for $\tau_w^* << 1$ i.e.

$$\tau_n^*\tau_w^* = [n(n+1)]^{-1} \qquad \text{(VI-43)}$$

This corresponds to the Debye limit, which is obtained for highly viscous liquids. Deviation from this limiting case shows increasing amounts of free rotor like behaviour, with the strongest deviation being for nitrogen at high temperatures, as would be expected. The ratio τ_1/τ_2, as found by Singer et al., is weakly dependent on T^*, with values of the order of 2.5 and approaches 3 at low T^* and high ρ^*, which is as would be predicted for systems whose rotation is becoming increasingly hindered. This shows that the behaviour of the orientational correlation functions is complex and strongly dependent on the exact form of the potential used.

Comparison with the models discussed by Powles and Rickayzen, show that none really satisfactorily represents all aspects of molecular rotational motion. Thus the perturbation type treatment of Snook and Watts(31,32), which they applied to translational motion would seem a much more valid type of approach then rather artificial model calculations.

(VI-6) Angular Momentum Correlation Functions.

These correlation functions are given by

$$C_w(t) = \langle \underset{\sim}{J}_i(0).\underset{\sim}{J}_i(t)\rangle / \langle |\underset{\sim}{J}_i(0)|^2\rangle \qquad \text{(VI-44)}$$

where $\underset{\sim}{J}_i(t) = \mu \underset{\sim}{l}_i(t) x \dot{\underset{\sim}{l}}_i(t)$. The variation of $C_w(t)$ with density and temperature is shown in Figures (VI-15) to (VI-20). From these it is seen that

1) At all densities and temperatures there is rapid gaussian-like initial decay of the correlation function.

2) For all densities and temperatures, with the exception of nitrogen at high temperature and/or low density, the correlation functions have a negative lobe.

3) The magnitude of the negative lobe increases with increasing quadrupole moment and is strongly density dependent, but varies less strongly with temperature.

4) The initial decay of the function is density dependent, but not significantly temperature dependent.

5) The correlation functions do not exhibit any significant "tail" or long-time effects.

6) The magnitude of the negative lobes does not increase with L*.

The correlation times τ_w^* calculated from equation (IV-42) are given in Table (VI-2). They increase with decreasing density but increase less strongly with increasing temperature. In comparison with the 2LJC results of Singer et al., the increasing quadrupole

moment can be seen to progressively decrease τ_w^*, up to 40% for $Q^* = 2.073$. For nitrogen the quadrupole moment produces faster initial decay, and a negative lobe at high densities and/or low temperatures which was not present in the basic 2LJC system simulated by Quentrec(28).

The shape of $C_w(t)$ is attributed to quasi-librations of the molecule within the cage of its nearest neighbours. The quadrupole moment increases the anisotropy of the molecule, which increased the specification of energetically preferred orientations, about which the molecule will tend to librate rather than rotate through heightened rotational barriers.

(VI-7) Torque Correlation Functions.

The torque correlation functions are given by

$$C_T(t) = \langle \underset{\sim}{T}_i(0).\underset{\sim}{T}_i(t)\rangle / \langle \underset{\sim}{T}_i(0).\underset{\sim}{T}_i(0)\rangle \qquad \text{(VI-45)}$$

where $\underset{\sim}{T}_i(t) = \mu \underset{\sim}{l}_i(t) \times \ddot{\underset{\sim}{l}}_i(t)$. The correlation functions are illustrated in Figures (VI-21) to (VI-24). They are similar to the translational force correlation functions are are characterized by

1) Very rapid initial decay.

2) A deep negative lobe which is weakly dependent on temperature, density and quadrupole moment. This shows that the torques acting on a molecule change approximately twice as rapidly as the angular momentum vector, which as explained for the force correlation functions, shows that the motion is that of a highly damped oscillator which is also strongly anharmonic.

(VI-8) Quasi-Oscillation and Librational Analysis.

Given that the translational force and torque correlation times are much smaller than the correlation times for the corresponding velocities, and that the strong negative lobes of the correlation

functions indicates some type of oscillatory behaviour, (even if strongly damped), then it was suggested by Singer et al.(21) that the correlation functions should be analysed in terms of this oscillatory behaviour, rather than the physically unrealistic discrete-jump or collision models.

If a given correlation function C(t) changes sign for the first time in τ_o, then $2\tau_o$ in an estimate of the time between successive zeros of C(t). Thus $4\tau_o$ is the period of oscillation. Let τ_f be the time at which the integral of C(t) has reached its asymptotic value (i.e. correlation has ceased; $\lim_{t\to\infty} C(t)=0$) then the number of oscillations before complete loss of correlation is $\tau_f/4\tau_o$. Successive displacements of length $\Delta x(\tau)$ can be regarded as a random walk, which taken to τ_f gives the diffusion constant

$$D = \langle \Delta x^2(\tau_f) \rangle / 2\tau_f \qquad \text{for translational motion}$$

$$D_R = \langle \Delta\Theta^2(\tau) \rangle / 2\tau_f \qquad \text{for rotation, where } \Delta\Theta$$

is an angular displacement.

The amplitude of oscillation is defined as the interval x between successive zeros of the function. For the n and (n+1) turning points of the velocity this is given by

$$\xi(1;n) \equiv x(\dot{x}=0;n+1) - x(\dot{x}=0;n) \qquad \text{(VI-46)}$$

which corresponds to a time interval of $2\tau_o$. Now using $\langle \dot{x}^2 \rangle = RT/M$, one obtains

$$\langle \xi(1;n)^2 \rangle = 4\tau_o^2 RT/M \equiv \langle \xi(1)^2 \rangle \qquad \text{(VI-47)}$$

which is the mean-square interval between successive turning points. The same may be applied to a complete cycle, between the n and (n+2) turning points.

$$\xi(2;n) = x(\dot{x}=0;\ n+2) - x\ (\dot{x}=0;n) \qquad \text{(VI-48)}$$

This can now be used to estimate the mean-square displacement per cycle $\langle\xi(2;n)^2\rangle \equiv \langle\xi(2)^2\rangle$ where $\langle\Delta x^2(\tau_f)\rangle$ is modified to correspond to the displacement in τ_f', which is defined by $(\tau_f'/4\tau_o) = m$, being the nearest integer ratio to (τ_f/τ_o). Thus for m=1

$$\langle\Delta x^2(\tau_f')\rangle = \langle\xi(2;n)^2\rangle = \langle(\xi(1;n+1) + \xi(1-n))^2\rangle \qquad \text{(VI-49)}$$

$$= 2\langle\xi(1)^2\rangle + 2\langle\xi(1;n)\,\xi(1;n+1)\rangle$$

It is found in all cases that m=0 or 1 only, so that the higher order expressions given by Singer were not required.

Rewriting equation (VI-49) to isolate the correlation term gives

$$-\frac{\langle\xi(1;1)\,\xi(1;2)\rangle}{\langle\xi(1)^2\rangle} = 1 - \tfrac{1}{2}\left[\frac{\langle\xi(2)^2\rangle}{\langle\xi(1)^2\rangle}\right] \qquad \text{(VI-50)}$$

From this it can be seen that if $\langle\xi(2)^2\rangle = 4\langle\xi(1)^2\rangle$ (i.e. $\xi(2) = 2\xi(1)$), then $\langle\xi(1;1)\xi^*1;2)\rangle/\langle\xi(1)^2\rangle = 1$, which corresponds to a particle translating with no forces acting on it, whereas if $\langle\xi(2)^2\rangle = 0$, then $\langle\xi(1;1)\xi(1;2)\rangle/\langle\xi(1)^2\rangle = -1$, which corresponds to a particle returning to exactly its original position, which is a stationary oscillation about a point. Thus the quasi-oscillation analysis gives the degree of asymmetry of an oscillation about a point; that is the amount of diffusion associated with each oscillation, when the amplitude of oscillation is taken into account. However, the analysis cannot give any information about the character of the oscillation (i.e. the degree

of anharmonicity).

The results of this quasi-oscillation analysis are given in Table (VI-III). As in the case of the diffusion constants, the correlation functions were only studied in the range $0 \rightarrow 200\Delta t$, which must neglect the presence of any long range negative tails of $C_v(t)$. This results in almost identical values for τ_f, reflecting the correlation range considered (0.8×10^{-12}s). The values for τ_o are also remarkably constant with variation of temperature and show slight decrease with increasing quadrupole moment. The strongest effect is the increase in τ_o with decreasing density. The values for chlorine, nitrogen and carbon dioxide are all of the same order despite widely differing bond lengths, although this may just be fortuitous. The subsequent analysis reflects the truncation of $C_v(t)$ at $200\Delta t$, but still shows relationship between $\langle \dot{\xi}(1)^2 \rangle$ and $\langle \dot{\xi}(2)^2 \rangle$ within one complete quasi-cycle. The difference between them is shown by the correlation term $\langle \dot{\xi}(1;1)\, \dot{\xi}(1;2) \rangle / \langle \dot{\xi}(1)^2 \rangle$ which can be seen to be remarkably consistant over the entire range of cases considered. At high density the correlation coefficient becomes less negative with temperature but becomes more negative with quadrupole moment. However, at lower density the trend with changing quadrupole moment is reversed. This means that the effect of density changes cannot be assessed from the present small sample of P.V.T. points.

For rotation, the angular momentum correlation functions do not have long range negative tails, and thus the truncation at $200\Delta t$ does not have any effect as the asymptotic limit has already been reached. The results of the librational analysis are given in Table (VI-IV). The variation of τ_o obeys the same criterion as in the case of translational motion, although the variation is stronger with

T^*	ρ^*	Q^*	L^*	$\tau_f/10^{-12}_s$	$\tau_o/10^{-12}_s$	$\tau_f/4\tau_o$	$\langle\Delta x^2(\tau_f)\rangle/\sigma^2$	$\langle\xi(1)^2\rangle/\sigma^2$	$\langle\xi(2)^2\rangle/\sigma^2$	$\langle\xi(1;1)\xi(1;2)\rangle/\langle\xi(1)^2\rangle$
1.14	0.541	0.739	0.608	0.79	0.22	0.91	0.031	0.046	0.034	-0.624
1.45	0.485			0.78	0.59	0.33	0.066	0.424	(0.198)	(-0.766)
1.21	0.546	1.321	0.608	0.79	0.21	0.95	0.027	0.042	0.028	-0.667
1.55	0.546			0.78	0.21	0.92	0.037	0.056	0.040	-0.638
1.55	0.490			0.78	0.38	0.51	0.058	0.181	0.114	-0.686
1.50	0.551	2.073	0.608	0.79	0.20	0.99	0.021	0.039	0.021	-0.731
1.85	0.551			0.79	0.20	1.00	0.029	0.048	0.029	-0.702
1.86	0.494			0.78	0.28	0.70	0.049	0.098	0.070	-0.646
1.61	0.700	1.159	0.328	0.79	0.23	0.87	0.019	0.037	0.021	-0.710
1.61	0.423	2.039	0.793	0.78	0.33	0.60	0.075	0.196	0.125	-0.681

TABLE (VI-3).

T^*	ρ^*	Q^*	L^*	$\tau_f/10^{-12}s$	$\tau_o/10^{-12}s$	$\tau_f/4\tau_o$	$\langle\Delta O^2(\tau_f)\rangle$	$\langle\eta(1)^2\rangle$	$\langle\eta(2)^2\rangle$	$\langle\eta(1;1)\eta(1;2)\rangle/\langle\eta(1)^2\rangle$
1.14	0.541			0.73	0.20	0.90	0.31	0.44	0.35	-0.600
1.41	0.541	0.739	0.608	0.58	0.20	0.71	0.32	0.54	0.45	-0.584
1.45	0.485			0.48	0.29	0.41	0.38	1.12	(0.93)	(-0.582)
1.21	0.546			0.71	0.18	1.00	0.26	0.34	0.26	-0.618
1.55	0.546	1.321	0.608	0.56	0.18	0.78	0.28	0.44	0.36	-0.583
1.55	0.490			0.75	0.26	0.71	0.56	0.94	0.79	-0.580
1.50	0.551			0.76	0.14	1.31	0.16	0.23	0.12	-0.729
1.85	0.551	2.073	0.608	0.71	0.15	1.20	0.24	0.30	0.20	-0.668
1.86	0.494			0.76	0.18	1.07	0.36	0.44	0.34	-0.611
1.61	0.700	1.159	0.328	0.74	0.23	0.81	1.01	1.37	1.26	-0.541
1.61	0.423	2.039	0.793	0.70	0.14	1.22	0.33	0.33	0.27	-0.589

TABLE (VI-4.

quadrupole moment, but weaker with density. Again the values for chlorine, nitrogen and carbon dioxide are all of the same order. The analysis in terms of the librational correlation coefficient $\langle\eta(1;1)\eta(1;2)\rangle/\langle\eta(1)^2\rangle$ shows that the coefficient becomes less negative with temperature, but more negative with quadrupole moment. This trend remains constant at both densities and it can be seen that the coefficient becomes less negative with decreasing density. Again the coefficient shows little variation with bond length. These values reflect the ability of the molecule to break from the surrounding particles, as a function of temperature, density and interaction potential.

(VI-9) Parallel and Perpendicular Translational Motion.

In order to further study the translational motion of the system, it is possible to examine the velocity correlation function $C_v(t)$ parallel and perpendicular to the molecular axis. This was originally proposed by Quentrec(28) for the case of nitrogen. These correlations are simply defined by

$$C_{11}(t) = \langle \underset{\sim}{A}_{11}(0).\underset{\sim}{A}_{11}(t)\rangle/\langle|\underset{\sim}{A}_{11}(0)|^2\rangle \qquad \text{(VI-51)}$$

where $\underset{\sim}{A}_{11}(t) = (\dot{\underset{\sim}{R}}(t).\underset{\sim}{\ell}(t))\hat{\underset{\sim}{\ell}}(t)$ and $\underset{\sim}{A}_{\perp}(t) = \dot{\underset{\sim}{R}}(t)-\underset{\sim}{A}_{11}(t)$

$$C_{\perp}(t) = \langle \underset{\sim}{A}_{\perp}(0).\underset{\sim}{A}_{\perp}(t)\rangle/\langle|\underset{\sim}{A}_{\perp}(0)|^2\rangle \qquad \text{(VI-52)}$$

These functions are illustrated in Figures (VI-25) to (VI-28). Comparing these with those calculated for the corresponding 2LJC systems by Singer et al.(21), it can be seen that the effect of the quadrupole moment is to severely reduce the translational anisotropy of the system. The values of the diffusion constants for the correlation functions transcribed at $200\Delta t$ are given in Table (VI-1),

as well as their ratios

$$D_{11}/D_{\perp} = \left[\int_0^{\infty} C_{11}(t)dt\right]/\left[\int_0^{\infty} C_{\perp}(t)dt\right] \qquad \text{(VI-53)}$$

These ratios for the systems illustrated are 1.18, 1.70, 1.23 and 1.28 respectively. On comparison with the results of Singer, it can be seen that the only similar value is that of the low quadrupole moment chlorine system. The other cases show very much less translational anisotropy, particularly for chlorine and carbon dioxide where the two correlation functions are remarkably alike.

These correlation functions may now be analysed using the quasi-oscillation method for translational motion as before. The correlation functions were again truncated at $200\Delta t$, and then the subsequenty analysis can only apply to one complete quasi-cycle.

The results of this analysis are given in Table (VI-V). The values for τ_o are divided either side of those for $C_v(t)$ given earlier in Table (VI-III) with $\tau_o^{\perp} < \tau_o < \tau_o^{11}$. The deviation of these from τ_o decreases with increasing quadrupole moment.

The values of the correlation coefficients give the degree of asymmetry of the oscillations about a point. The less negative values for the perpendicular coefficient in the case of nitrogen and low-quadrupole chlorine indicate that the motion perpendicular to the molecular axis is slightly less symmetric than in the parallel direction, although the diffusion constant ratios indicate that diffusion is strongly preferred in the parallel direction. However, for high-quadrupole chlorine and carbon dioxide the parallel correlation coefficient is slightly less negative, showing that the degree of asymmetry is almost identical in each direction, with a small preference towards the parallel case. It should be remembered

T^*		1.14	1.45	1.55	1.85	1.86	1.61	1.61
ρ^*		0.541	0.485	0.490	0.551	0.494	0.700	0.423
Q^*		0.739	0.739	1.321	2.073	2.073	1.159	2.039
L^*		0.608	0.608	0.608	0.608	0.608	0.329	0.793
$\tau_f/10^{-12}s$	∥	0.79	0.77	0.78	0.77	0.74	0.78	0.77
	⊥	0.78	0.76	0.75	0.78	0.78	0.78	0.78
$\tau_o/10^{-12}s$	∥	0.33	0.56	0.40	0.22	0.28	0.27	0.31
	⊥	0.18	0.24	0.24	0.18	0.26	0.20	0.30
$\tau_f/4\tau_o$	∥	0.60	0.34	0.49	0.88	0.66	0.71	0.63
	⊥	1.11	0.79	0.79	1.08	0.75	0.98	0.65
$\langle\Delta x^2(\tau_f)\rangle/\sigma^2$	∥	0.044	0.081	0.069	0.033	0.050	0.025	0.080
	⊥	0.025	0.049	0.048	0.028	0.046	0.020	0.066
$\langle\xi(1)^2\rangle/\sigma^2$	∥	0.106	0.388	0.197	0.059	0.099	0.054	0.172
	⊥	0.030	0.071	0.071	0.041	0.084	0.029	0.163
$\langle\xi(2)^2\rangle/\sigma^2$	∥	0.073	(0.235)	(0.142)	0.038	0.076	0.035	0.127
	⊥	0.023	0.063	0.061	0.026	0.061	0.020	0.101
$\frac{\langle\xi(1;1)\xi(1;2)\rangle}{\langle\xi(1)^2\rangle}$	∥	-0.653	(-0.696)	(-0.640)	-0.683	-0.616	-0.670	-0.630
	⊥	-0.617	-0.561	-0.574	-0.676	-0.639	-0.648	-0.690

TABLE (VI-5).

that the correlation coefficient only shows the degree of asymmetry of the oscillation, while the diffusion rate in a given direction is a product of the degree of asymmetry and the amplitude of oscillation, which is proportional to $\langle \xi(2)^2 \rangle$ which in all cases is larger in the parallel direction, particularly for the low-quadrupole cases. Thus although the asymmetry can be greater in the perpendicular direction, diffusion is still preferred along the parallel axis.

(VI-10) Conclusion.

The effect of a quadrupole moment on the interactions within a molecular fluid is to increase the cohesiveness of the potential, particularly with respect to certain favoured configurations. This leads to a form of dynamics in which the molecules can translate and rotate while remaining clustered to some nearest neighbours, so forming a type of cooperative motion. In this type of motion differences in mobilities parallel and perpendicular to the molecular axis caused by the anisotropy of the bond vector are likely to be minimized as the potential becomes increasingly cohesive. This can be seen in the translational velocity correlation functions where the negative double minimum associated with strongly anisotropic translational motion becomes a single minimum with increasing quadrupole moment. This is also shown by the decrease in difference between the parallel and perpendicular correlation functions.

The orientational correlation functions decay more slowly for quadrupolar systems than the corresponding 2LJC systems, giving correlation times in better agreement with the experimental values. This again suggests that the molecules are more strongly bound to their nearest neighbours. The increase in depth of the angular momentum correlation function minimum indicates that rotational oscillation about given configurations has become more likely.

The effects of a quadrupole on any cross-correlation functions, between two or more particles, from this type of cooperative motion is probably significant. This has not been investigated, however, as they require approximately an order of magnitude more statistics for their evaluation.

References.

(1) H.N.V. Temperley, J.S. Rowlinson and G.S. Rushbrooke, "Physics of Simple Liquids" (North-Holland-Amsterdam-1968).

(2) P.A. Egelstaff, "Introduction to the Liquid State" (Academic Press - London - 1967).

(3) B.J. Berne and G.D. Harp, Adv.Chem.Phys., 1970, 17, 63.

(4) B.J. Berne and R. Pecora, "Dynamic Light Scattering" (Wiley and Sons - New York - 1976).

(5) G Williams, Chem.Soc.Rev., 1978, 1, 89.

(6) B.J. Berne, "Physical Chemistry: An Advanced Treatise" Vol.VIIIB (Ed: D. Henderson - Academic Press - New York - 1971).

(7) G.D. Harp and B.J. Berne, J.Chem.Phys., 1968, 49, 1249.

(8) R. Zwanzig, Ann.Rev.Phys.Chem., 1965, 16, 67.

(9) K.E. Gubbins, Chem.Soc.S.P.R. - "Statistical Mechancis" 1973, 1, 194.

(10) P. Schofield, Chem.Soc.S.P.R., "Statistical Mechanics", 1975, 2, 1.

(11) S.A. Rice and P. Gray, "The Statistical Mechanics of Simple Liquids", (Interscience - New York - 1965).

(12) J.P. Hansen and I.R. McDonald, "Theory of Simple Liquids" (Academic Press - London - 1976).

(13) W.A. Steele, "Transport Phenomena in Fluids", (Ed: H.J.M. Hanley - Marcel Dekker - New York 1969).

(14) W.A. Steele, Adv.Chem.Phys., 1976, 34, 1.

(15) R. Kubo, Prog.Phys., 1966, 29, 255.

(16) G.H. Weiss, "Transport Phenomena in Fluids" (Ed: H.J.M. Hanley - Marcel Dekker - New York - 1969).

(17) J.R.D. Copley and S.W. Lovesey, Rep.Prog.Phys., 1975, 38, 461.

(18) J.M. Haile, K.E. Gubbins and W.B. Streett, Private Communication, Unpublished Review.

(19) Faraday Symposium 1976, No.11 (Chemical Society).

(20) H. Goldstein, "Classical Mechanics" (Addison-Wesley, Cambridge, Mass. 1958).

(21) K. Singer, J.V.L. Singer and A.J. Taylor, Mol.Phys., 1979, 37, 1239.

(22) E.M. Gosling, Royal Holloway College (University of London), Private communication.

(23) J. Barojas, D. Levesque and B. Quantrec, Phys.Rev., 1973, A2, 1092.

(24) P.S.Y. Cheung and J.G. Powles, Mol.Phys., 1975, 30, 921.

(25) P.S.Y. Cheung and J.G. Powles, Mol.Phys., 1976, 32, 1383.

(26) W.B. Streett and D.J. Tildesley, Proc.R.Soc.Lond., 1977, A355, 239.

(27) W. Steele and W. Streett, Mol. Phys., 1980, 39, 279.

(28) B. Quentrec, Ph.D. Thesis, 1971, Orsay, France.

(29) J.G. Powles and G. Rickayzen, Mol.Phys., 1977, 33, 1207.

(30) P.S. Hubbard, Phys.Rev., 1963, 131, 1155.

(31) I.K. Snook and R.O. Watts, Mol.Phys., 1977, 33, 431.

(32) I.K. Snook and R.O. Watts, Mol.Phys., 1977, 33, 443.

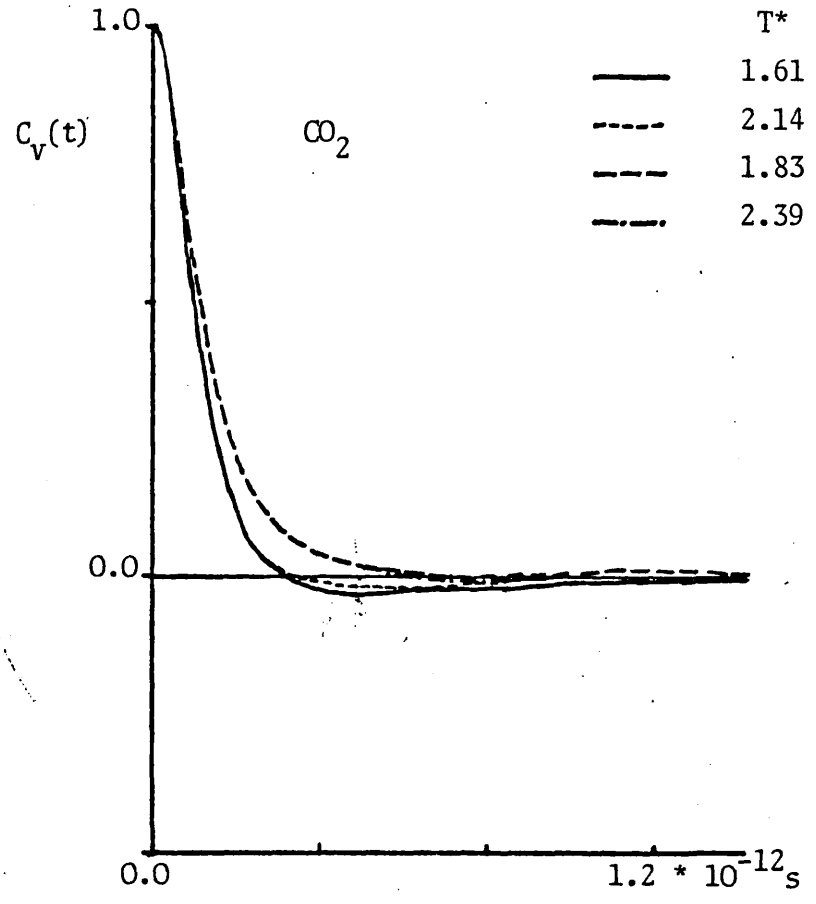

FIGURE (VI-1)

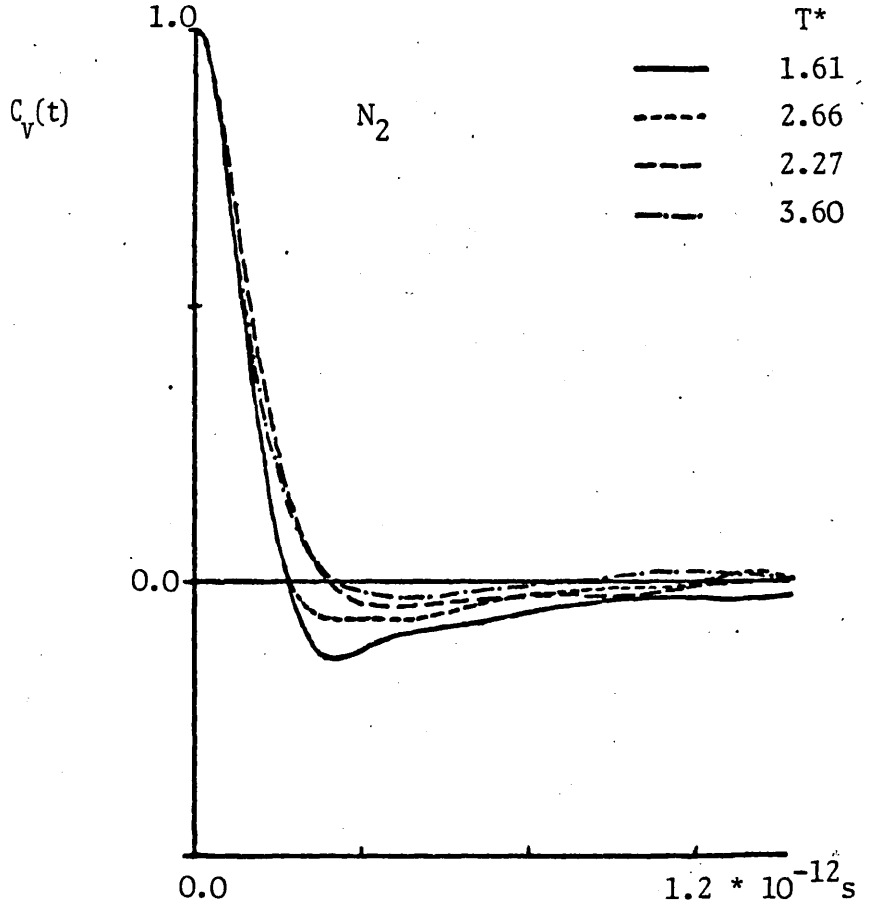

FIGURE (VI-2)

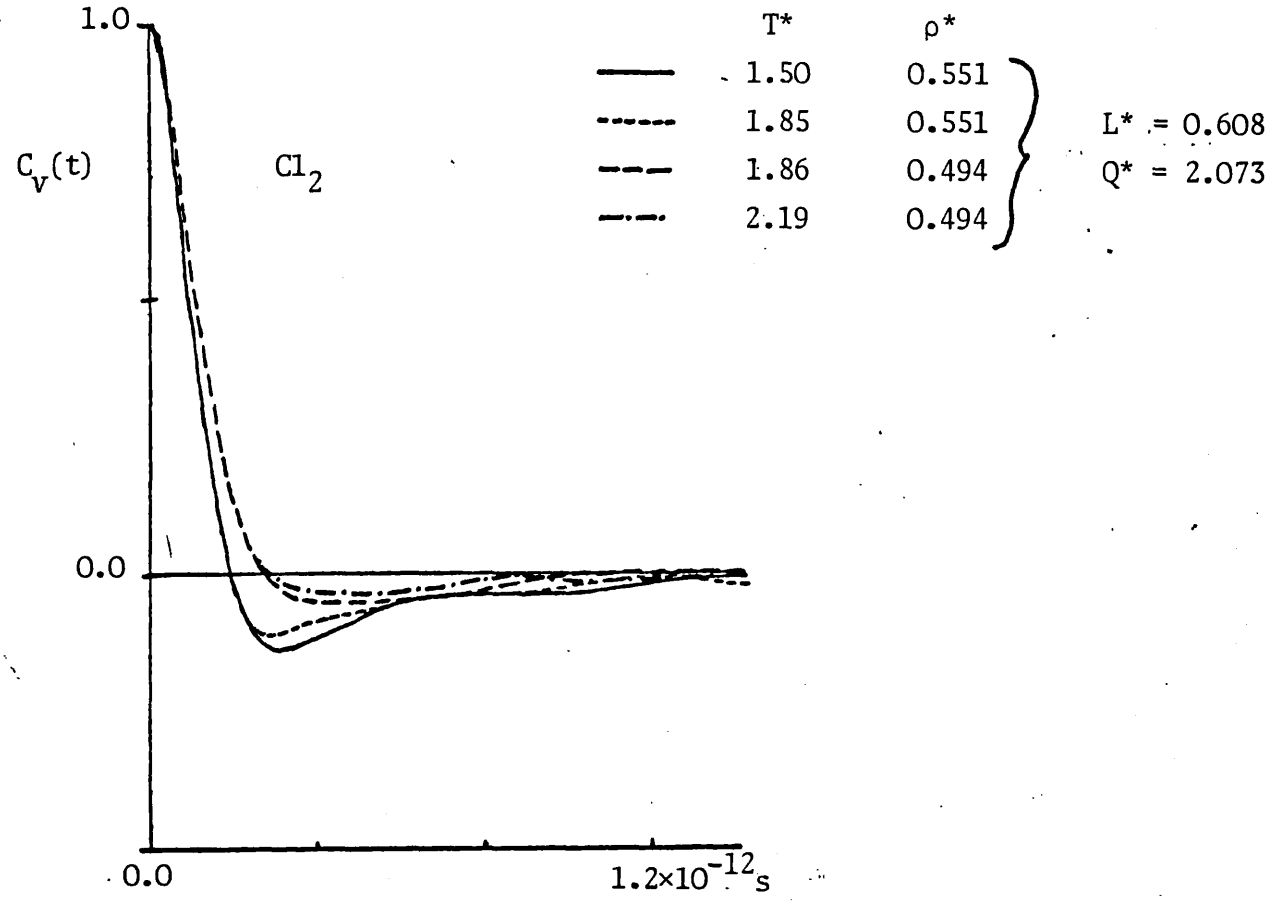

FIGURE (VI-3)

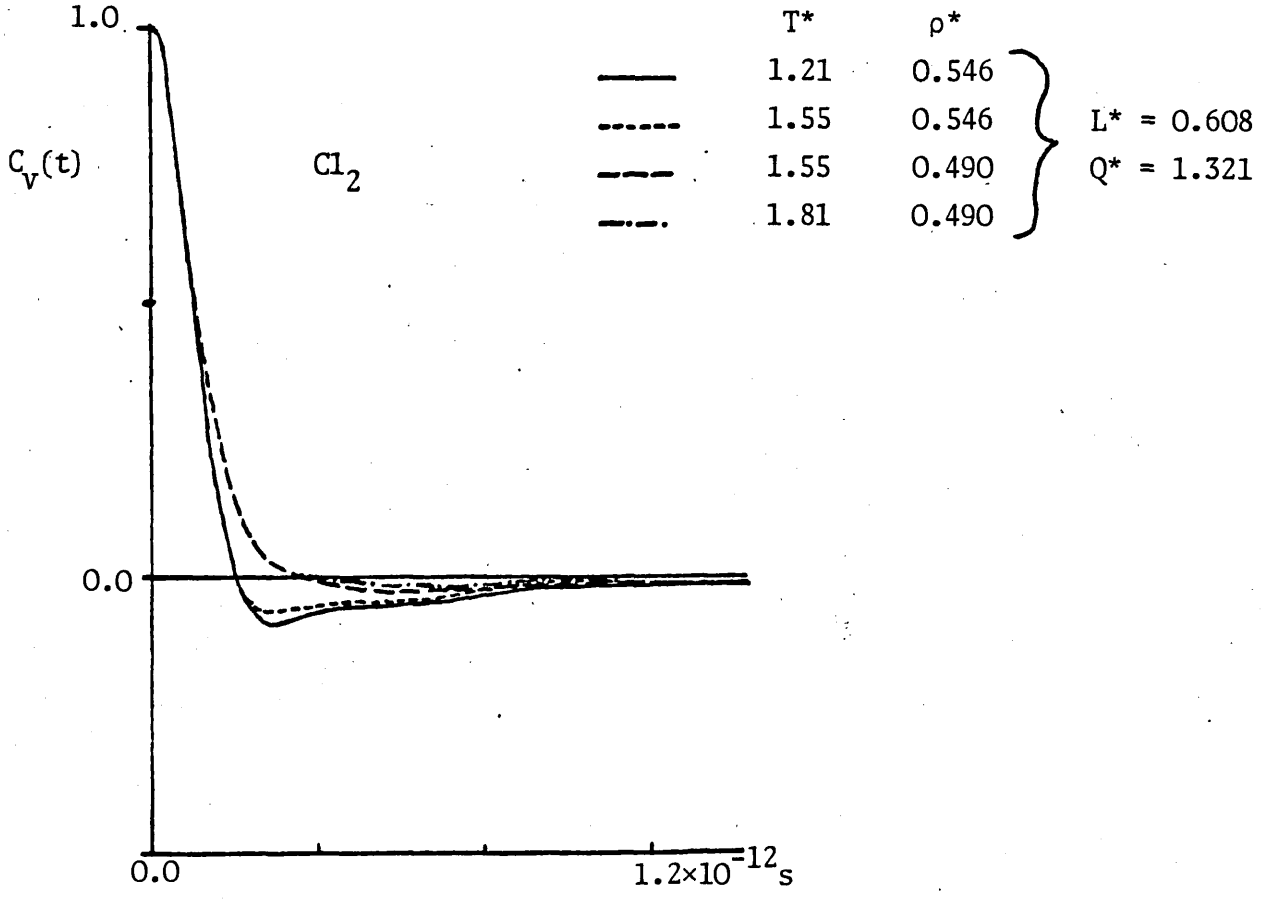

FIGURE (VI-4)

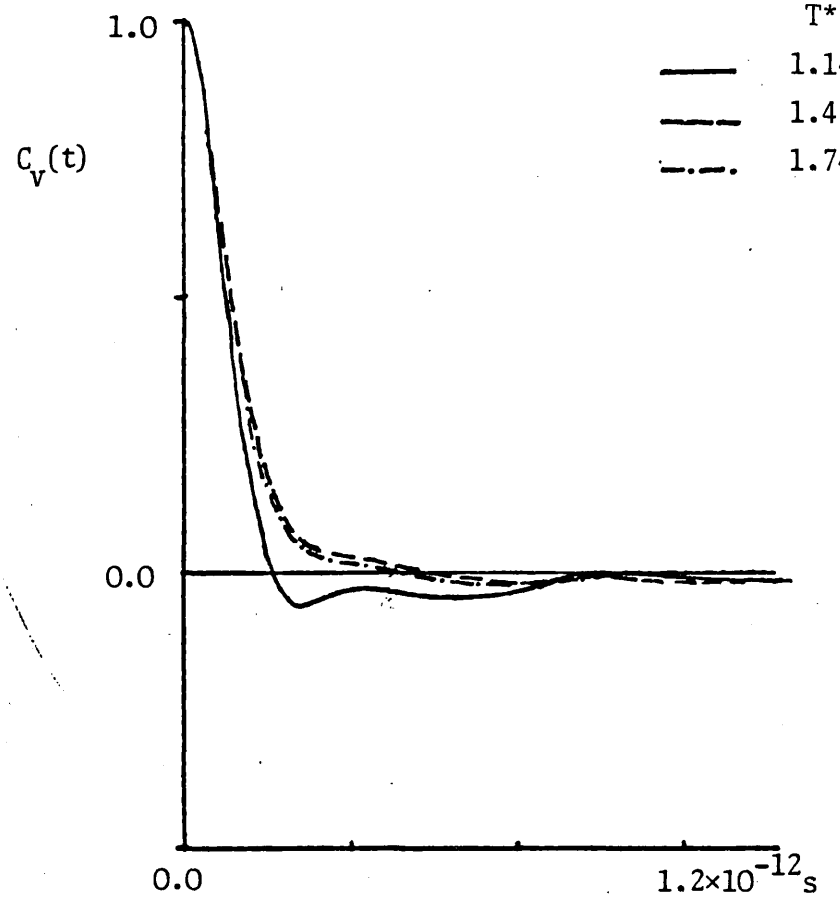

FIGURE (VI-5)

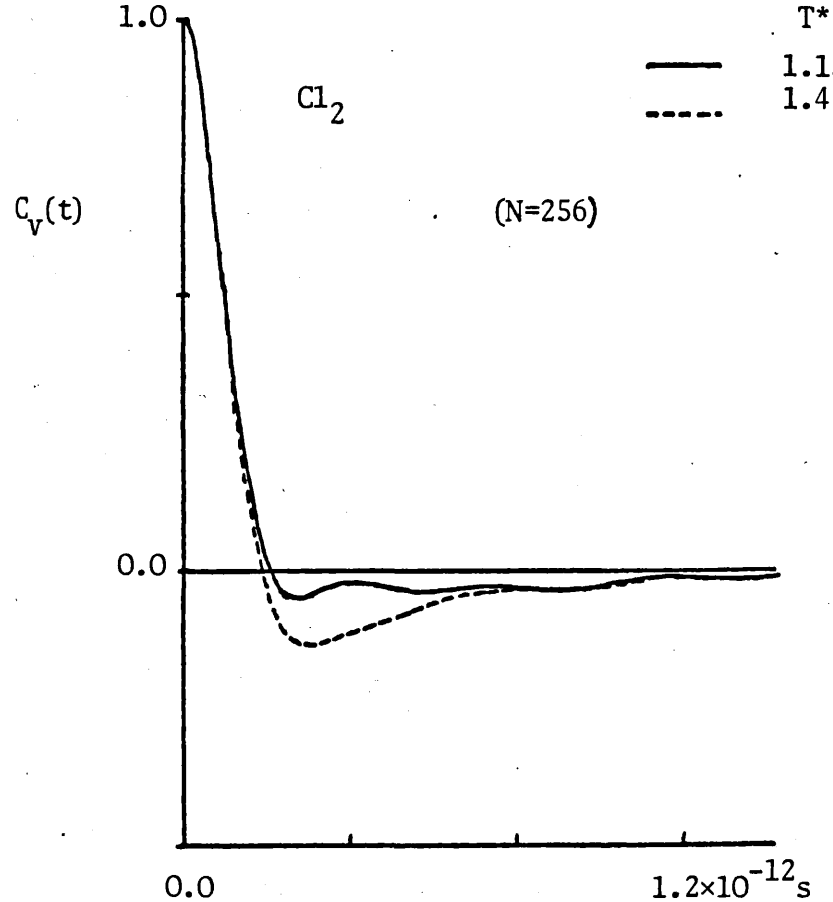

FIGURE (VI-6)

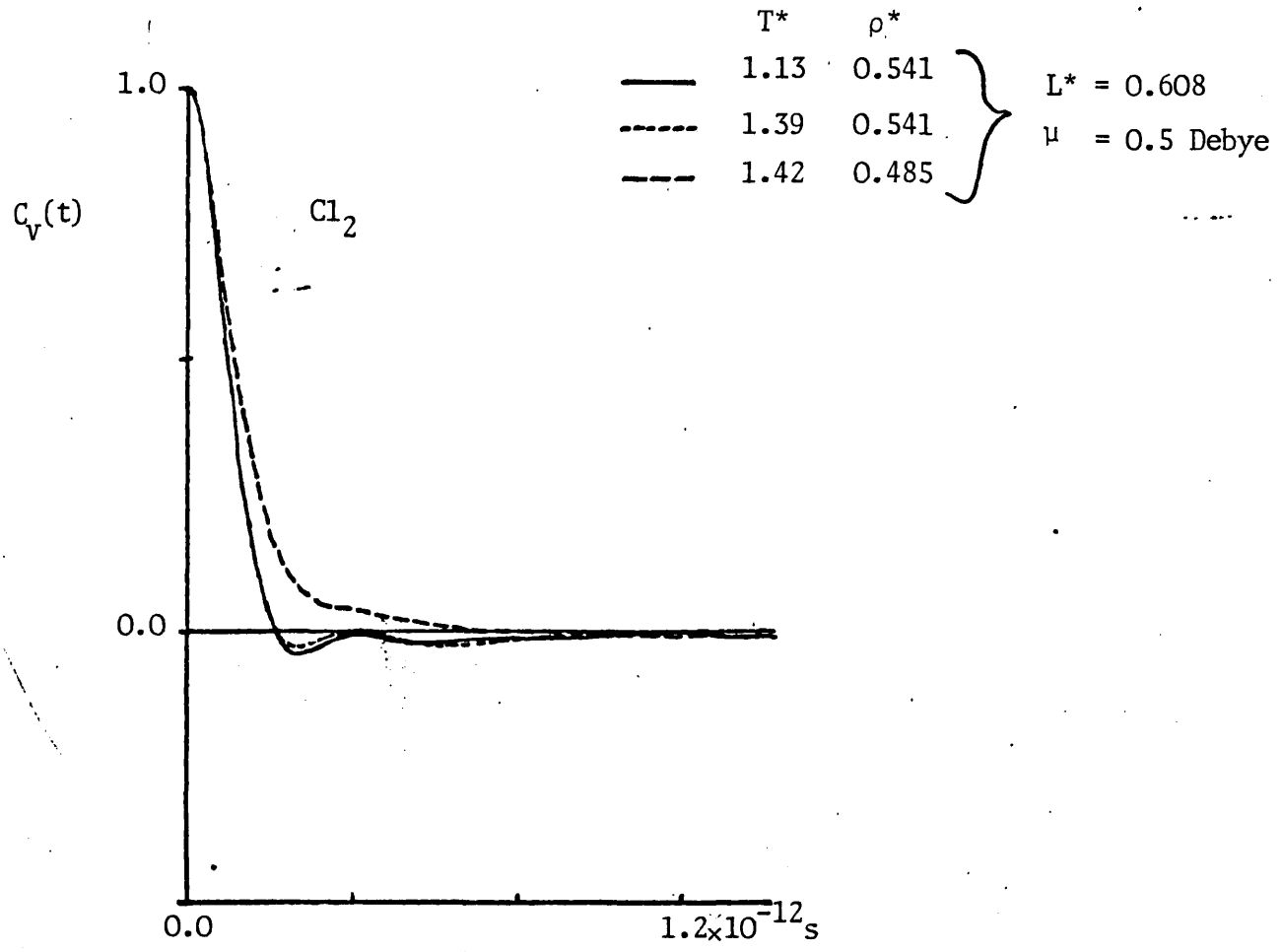

FIGURE (VI-7)

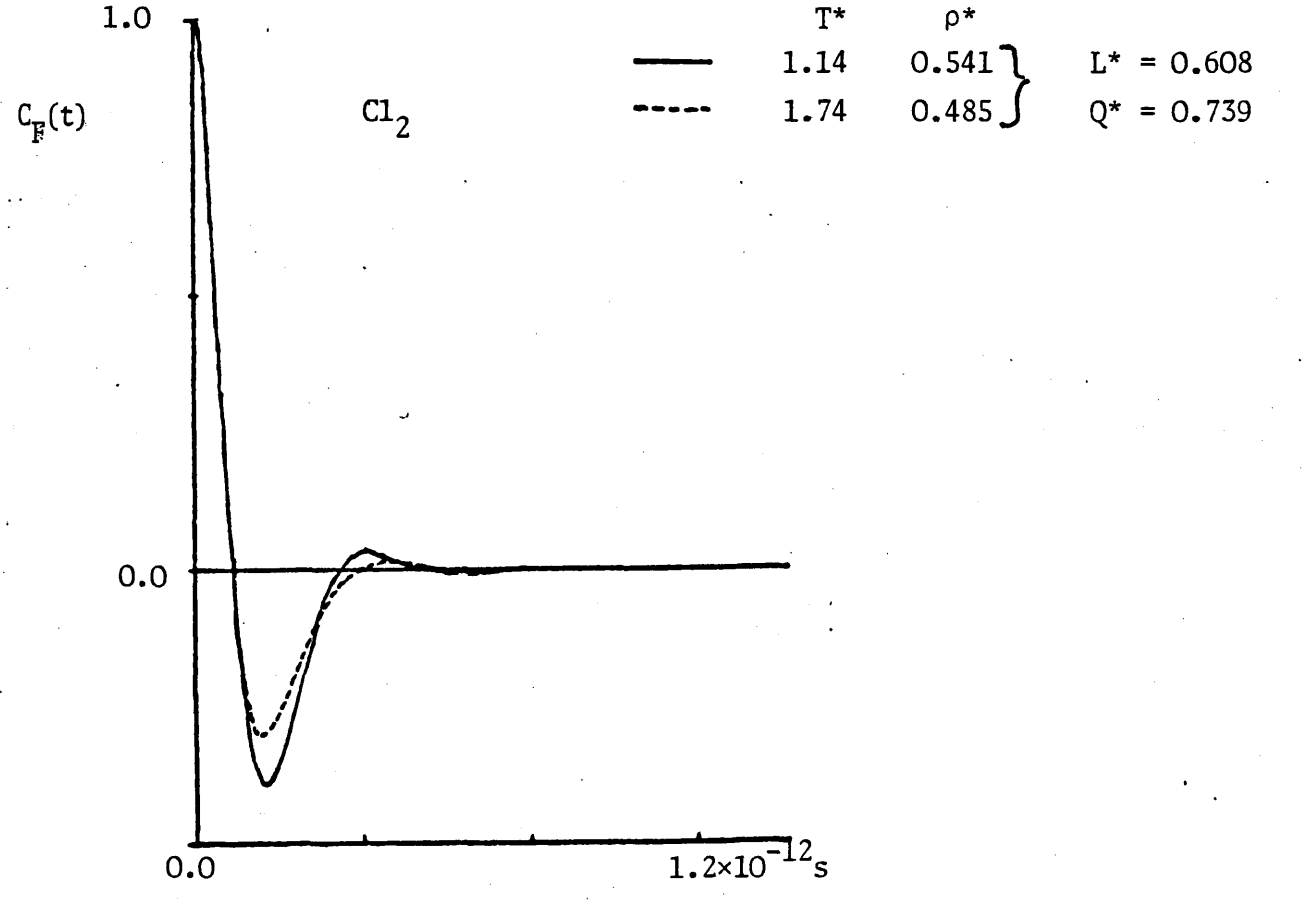

FIGURE (VI-8)

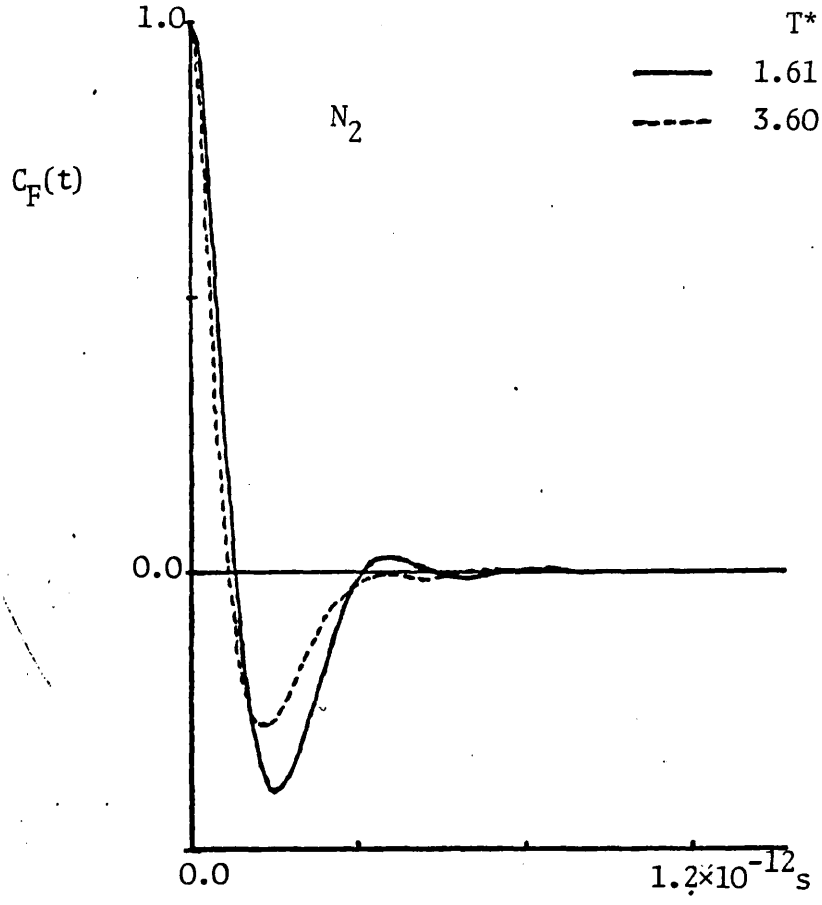

FIGURE (VI-9)

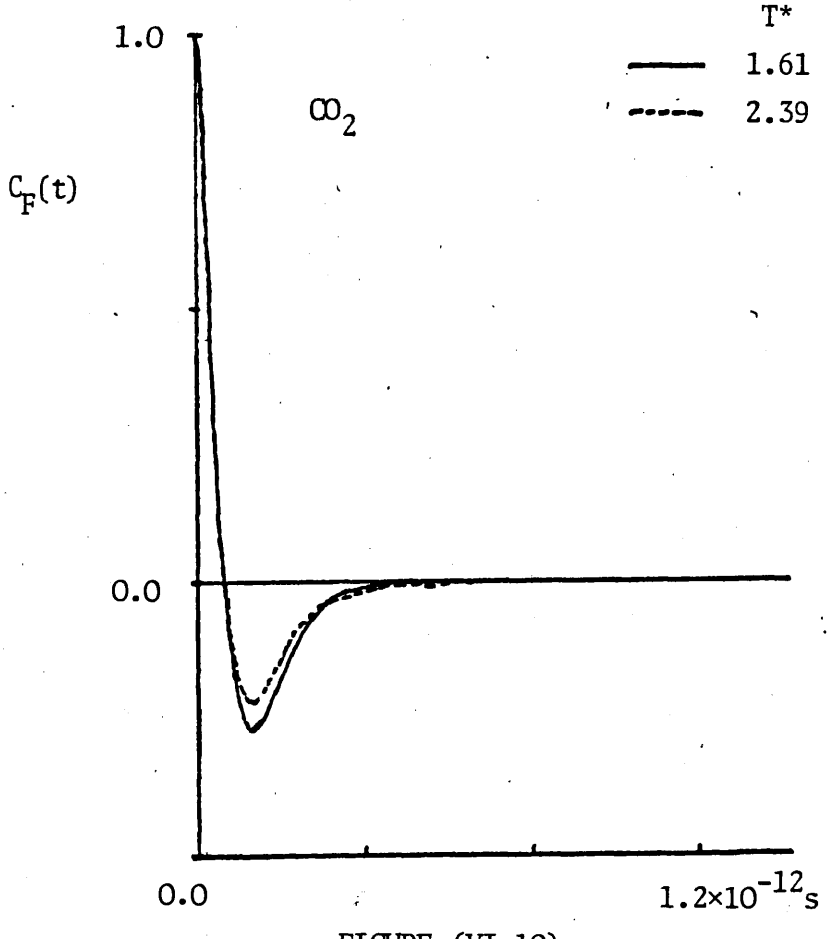

FIGURE (VI-10)

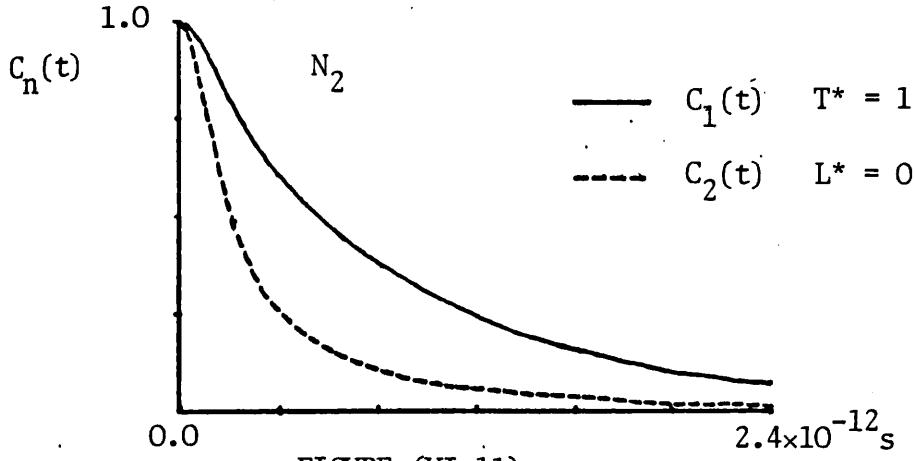

FIGURE (VI-11)

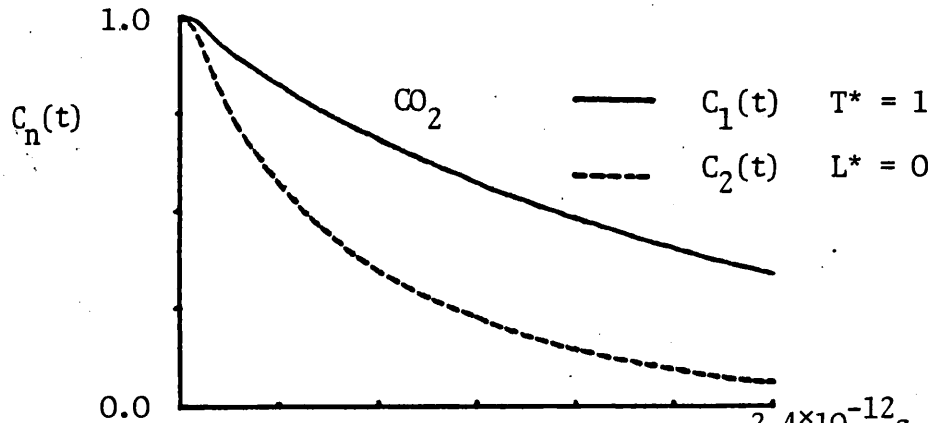

FIGURE (VI-12)

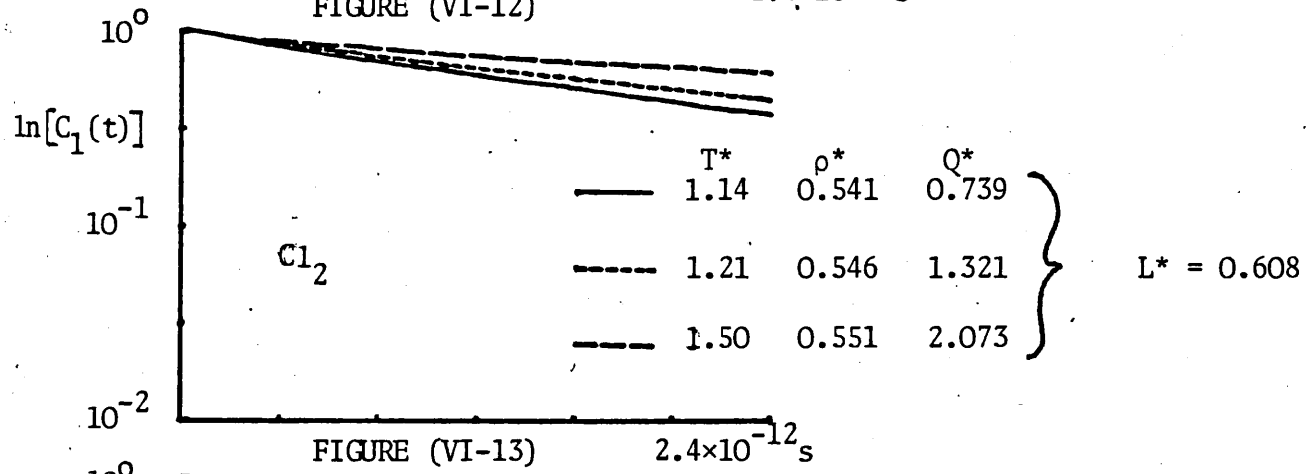

FIGURE (VI-13)

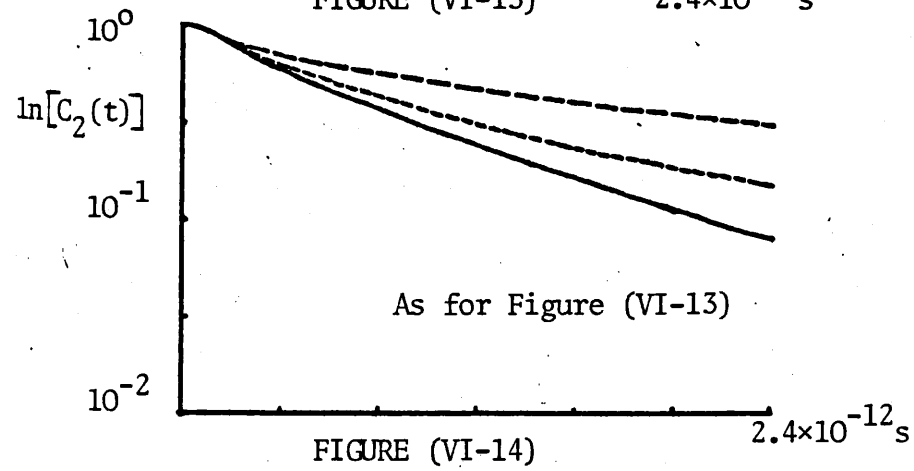

FIGURE (VI-14)

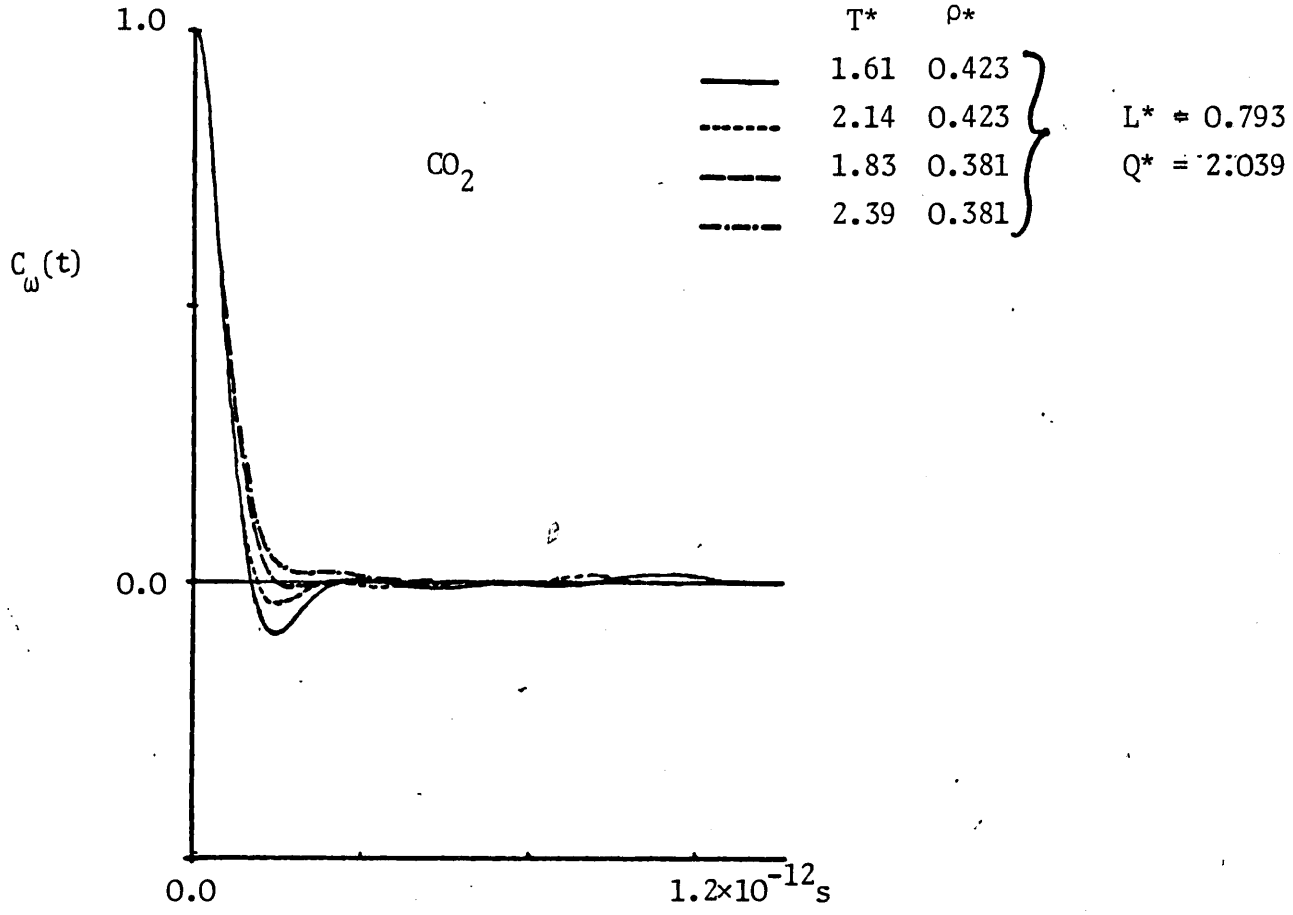

FIGURE (VI-15)

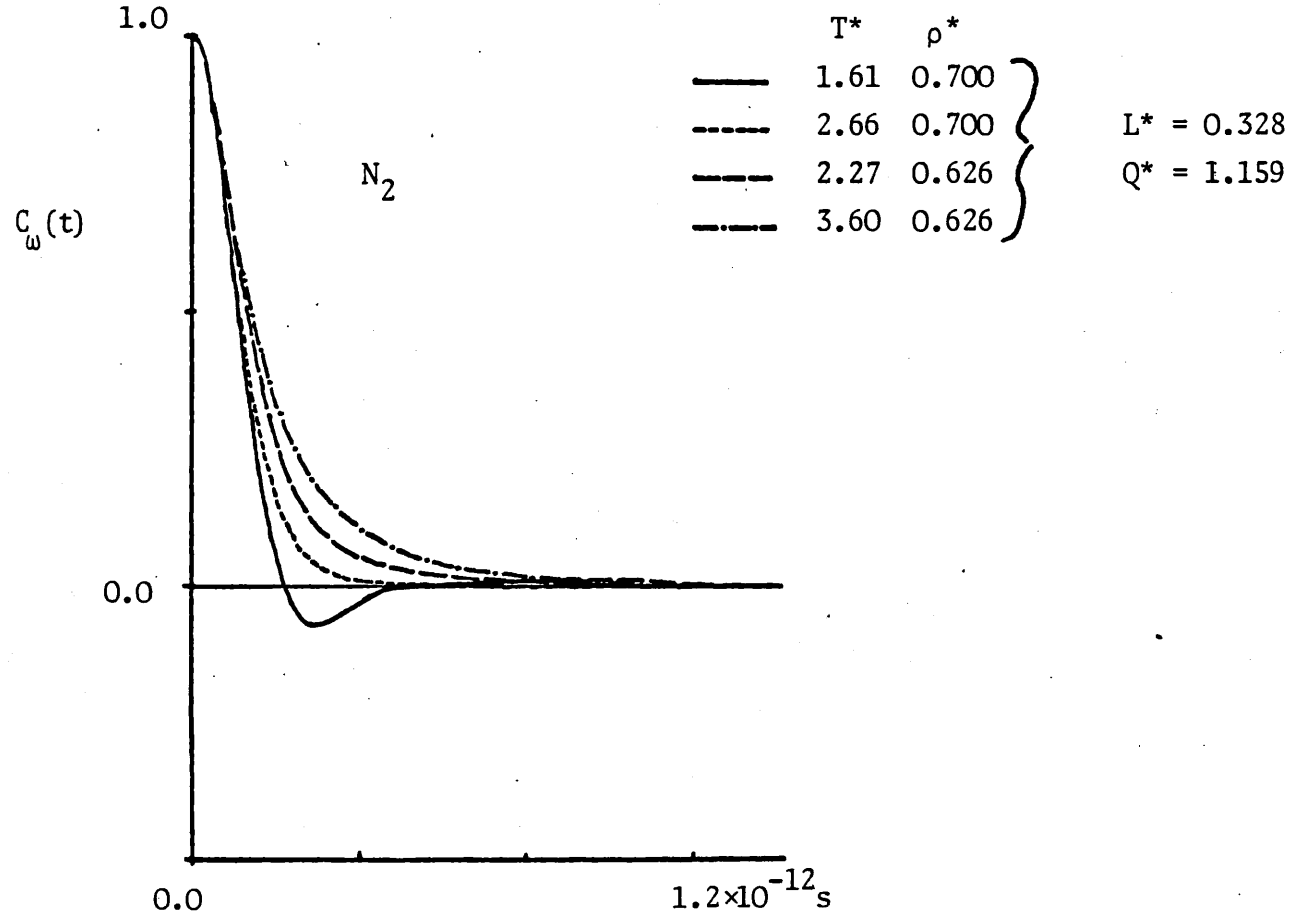

FIGURE (VI-16)

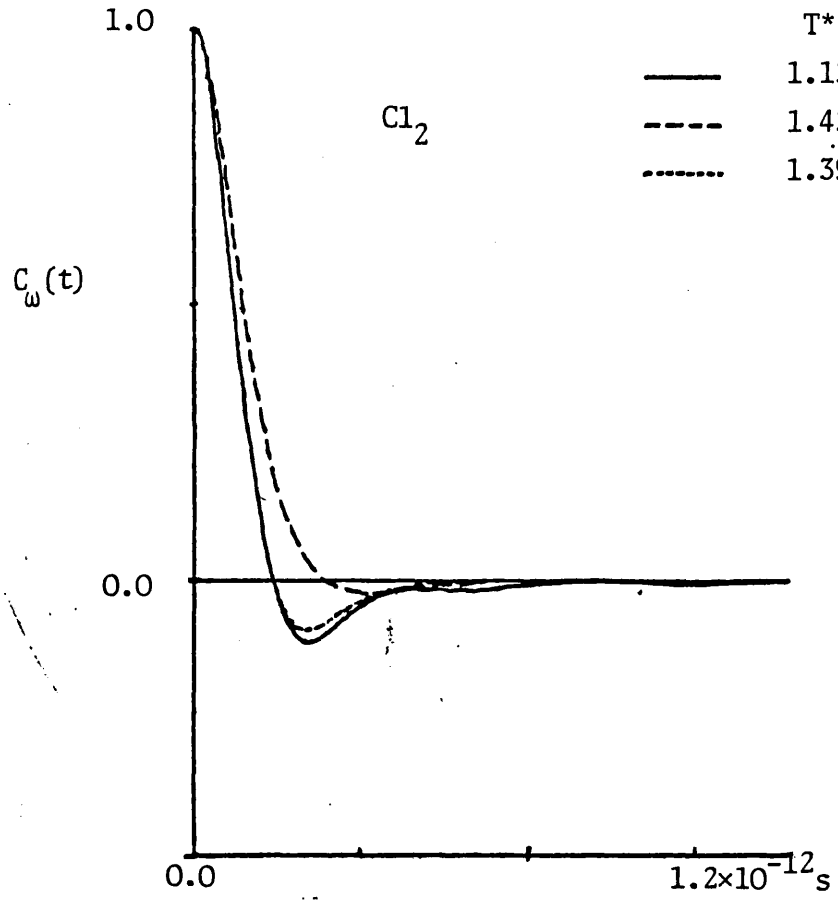

FIGURE (VI-17)

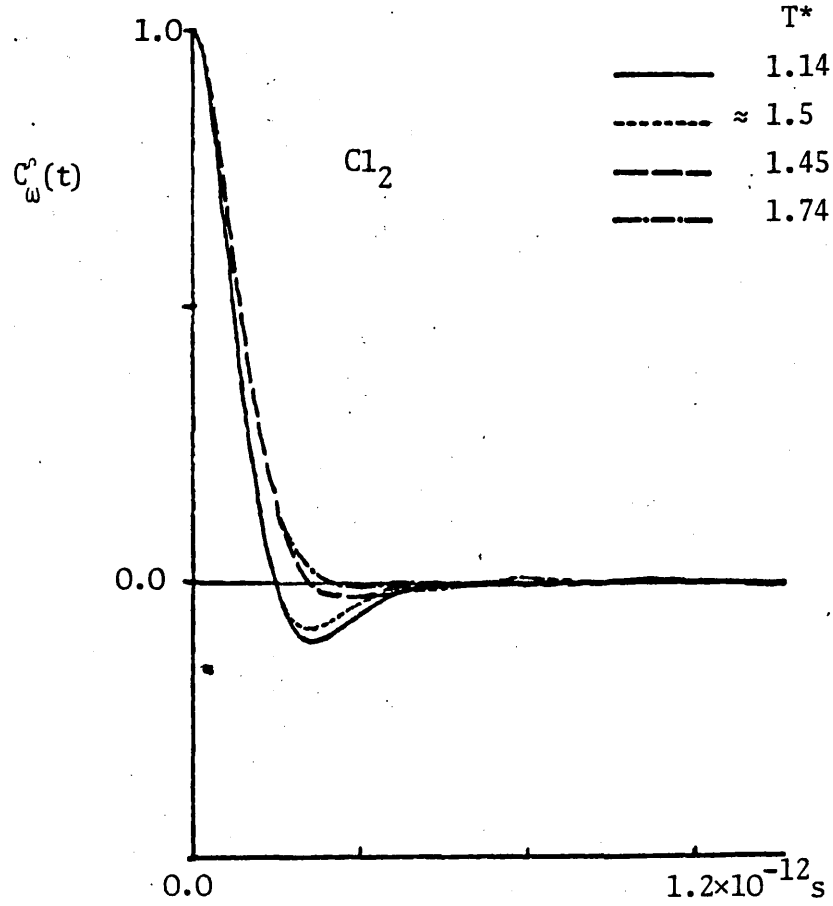

FIGURE (VI-18)

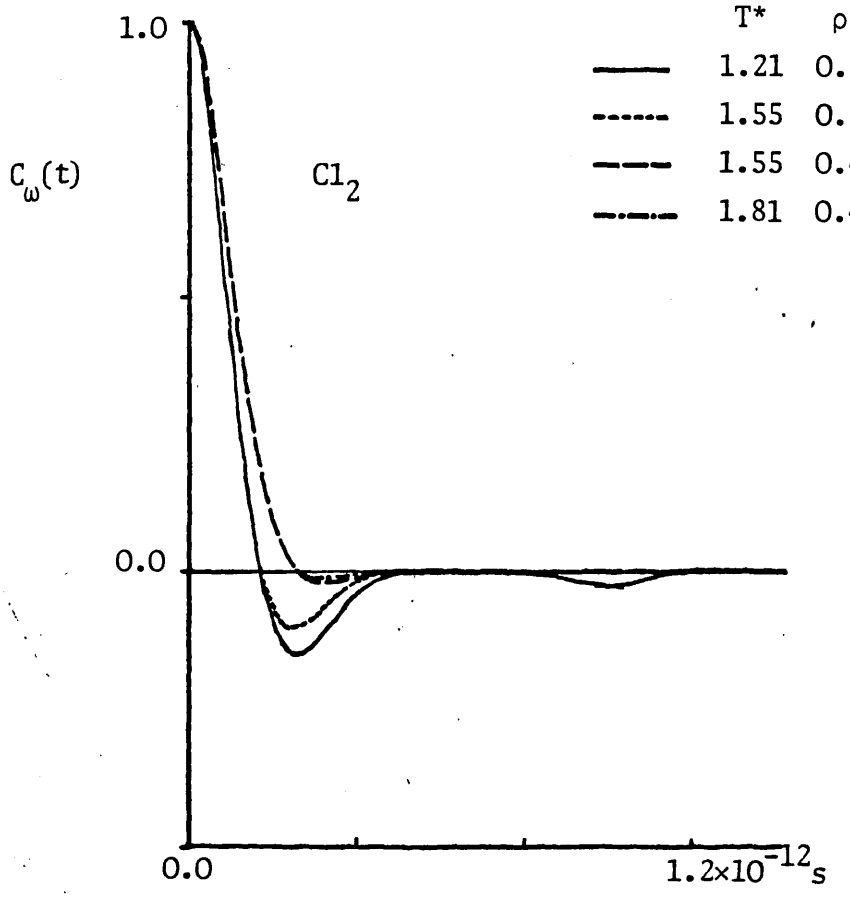

FIGURE (VI-19)

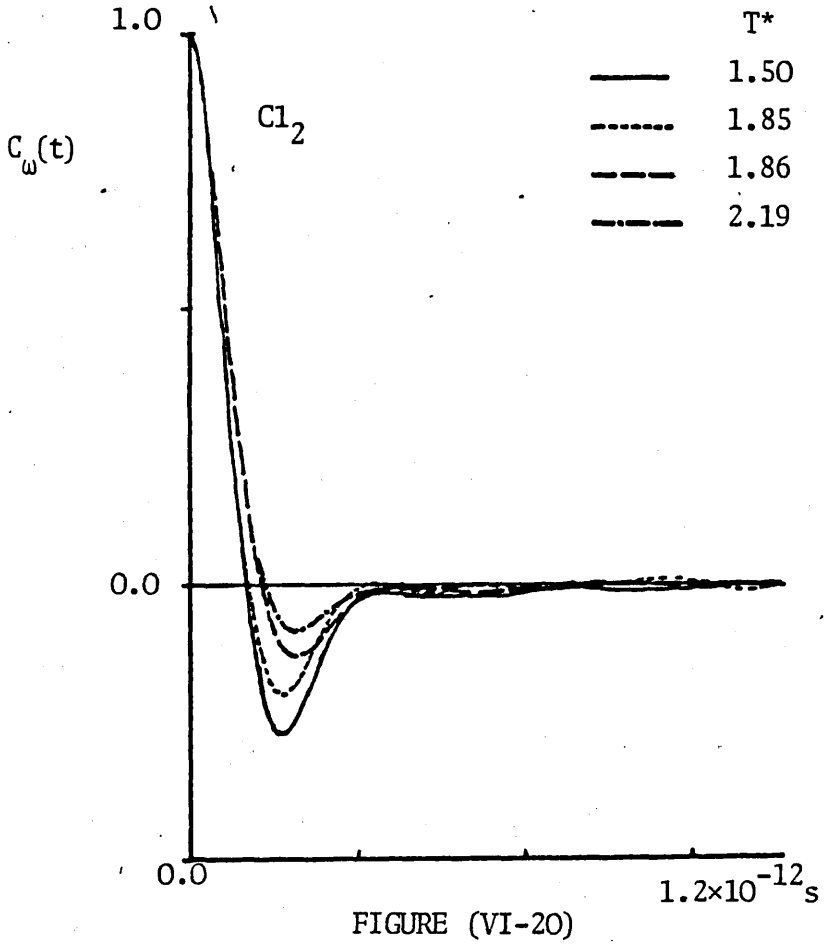

FIGURE (VI-20)

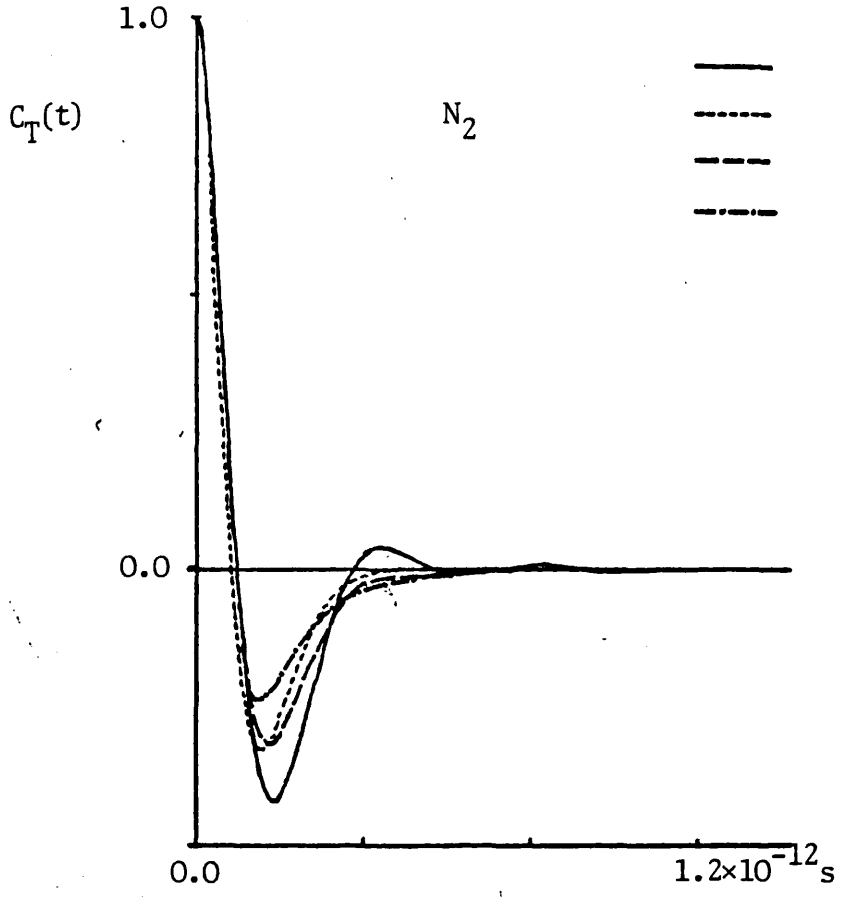

FIGURE (VI-21)

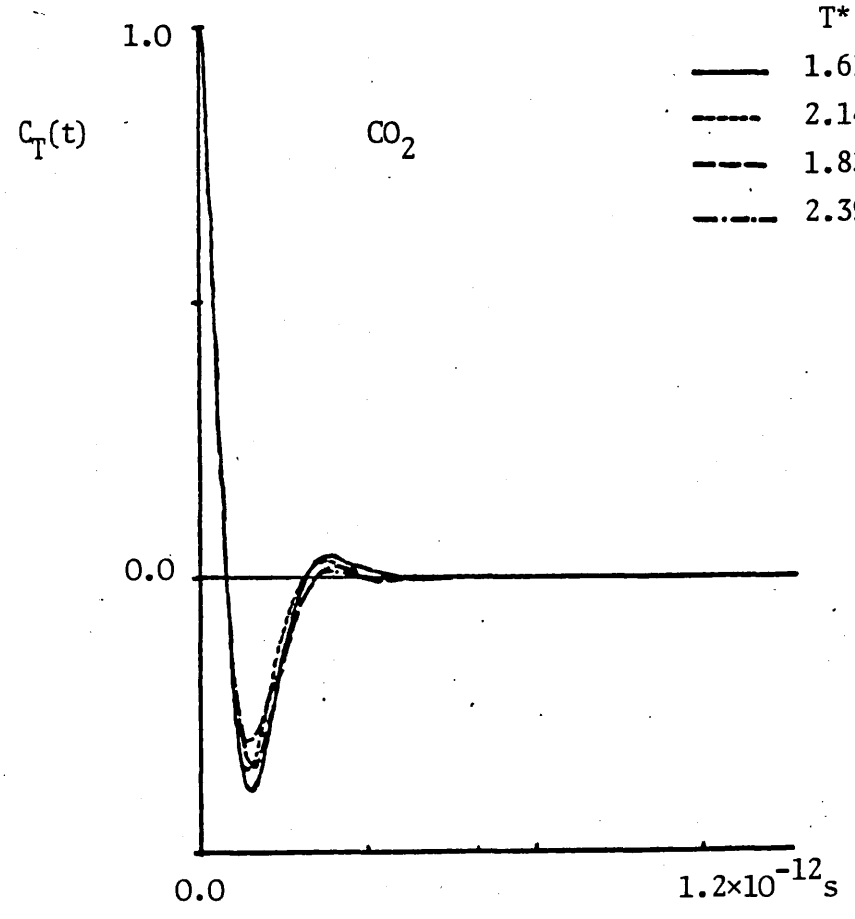

FIGURE (VI-22)

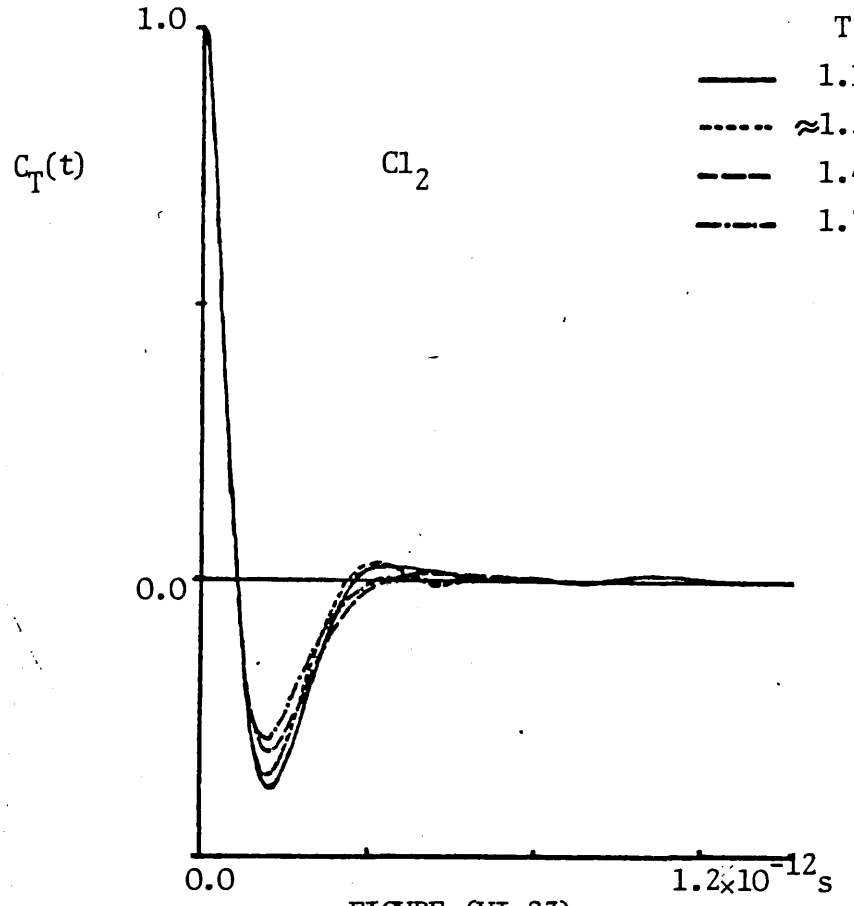

FIGURE (VI-23)

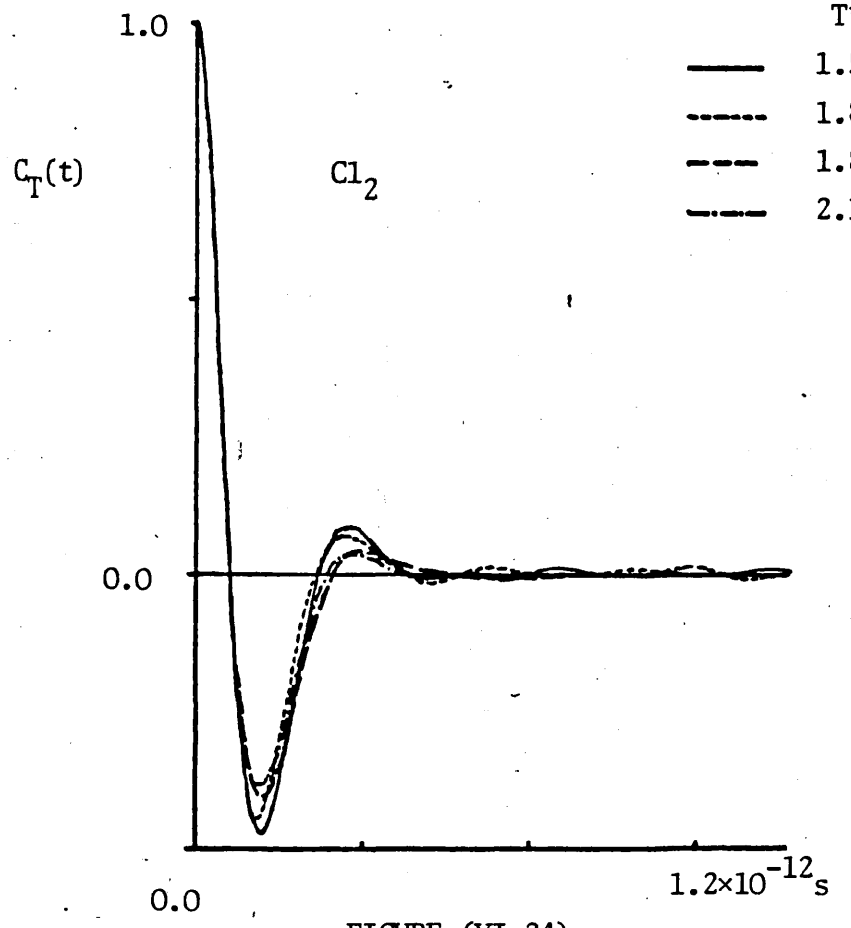

FIGURE (VI-24)

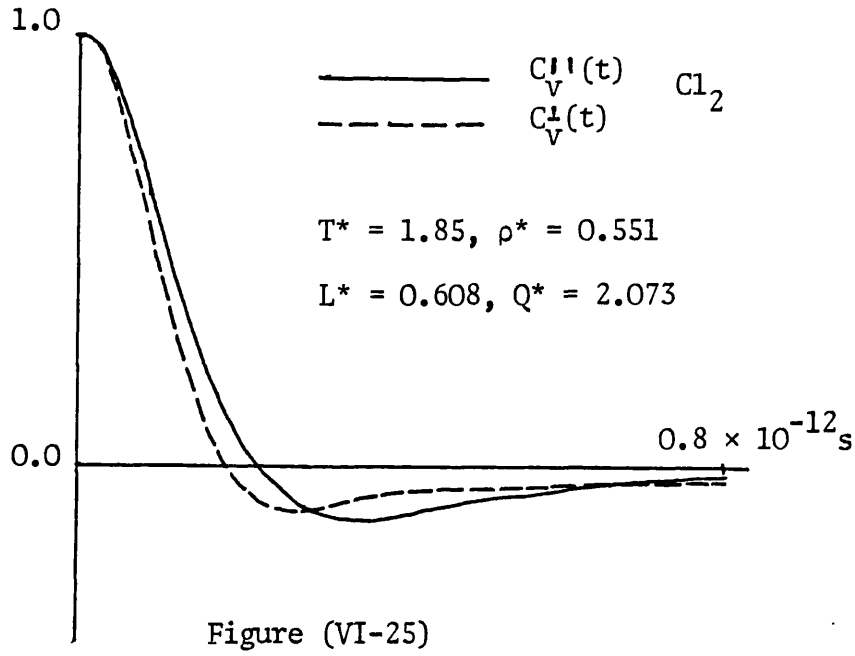

Figure (VI-25)

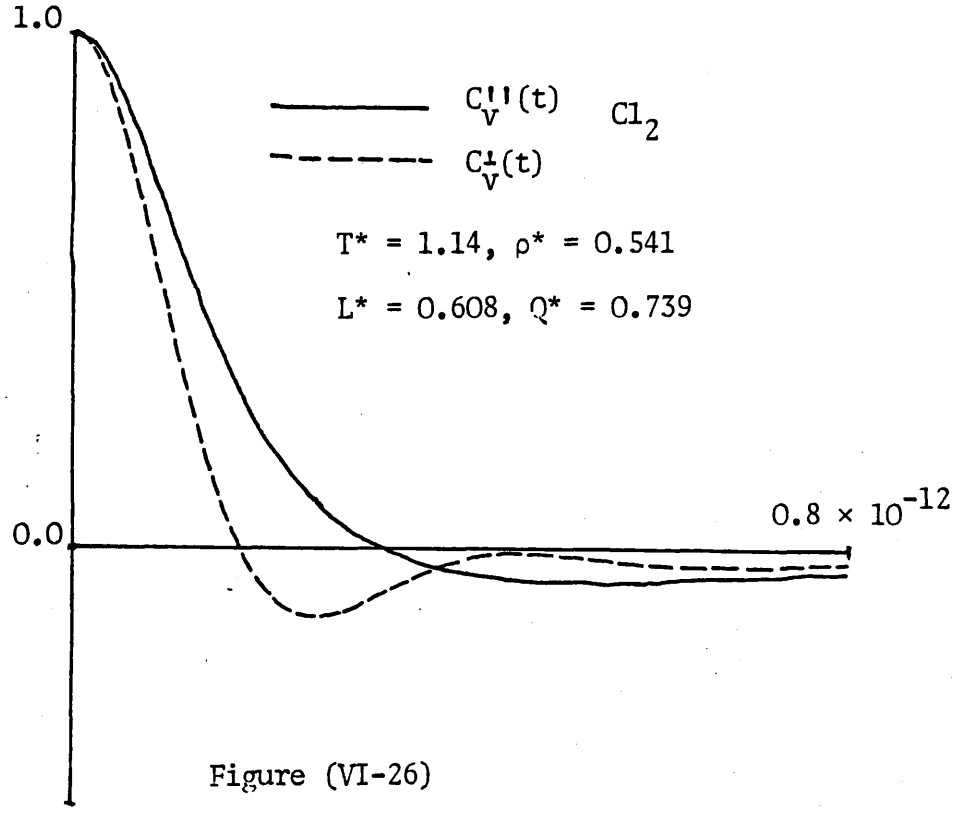

Figure (VI-26)

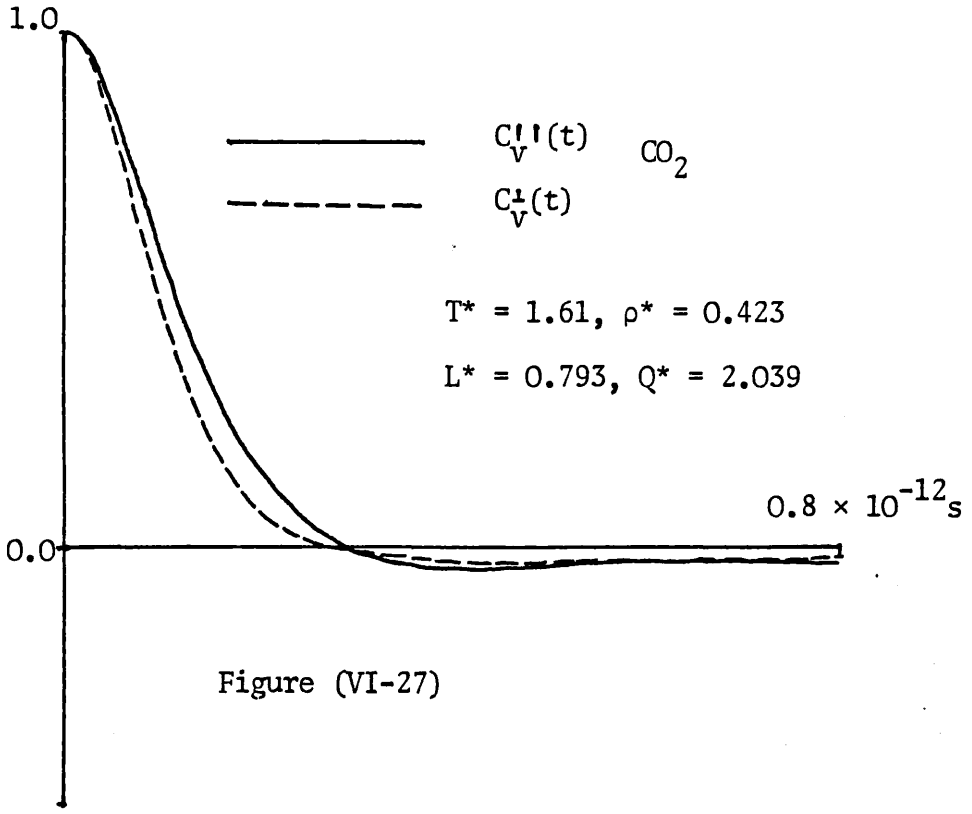

Figure (VI-27)

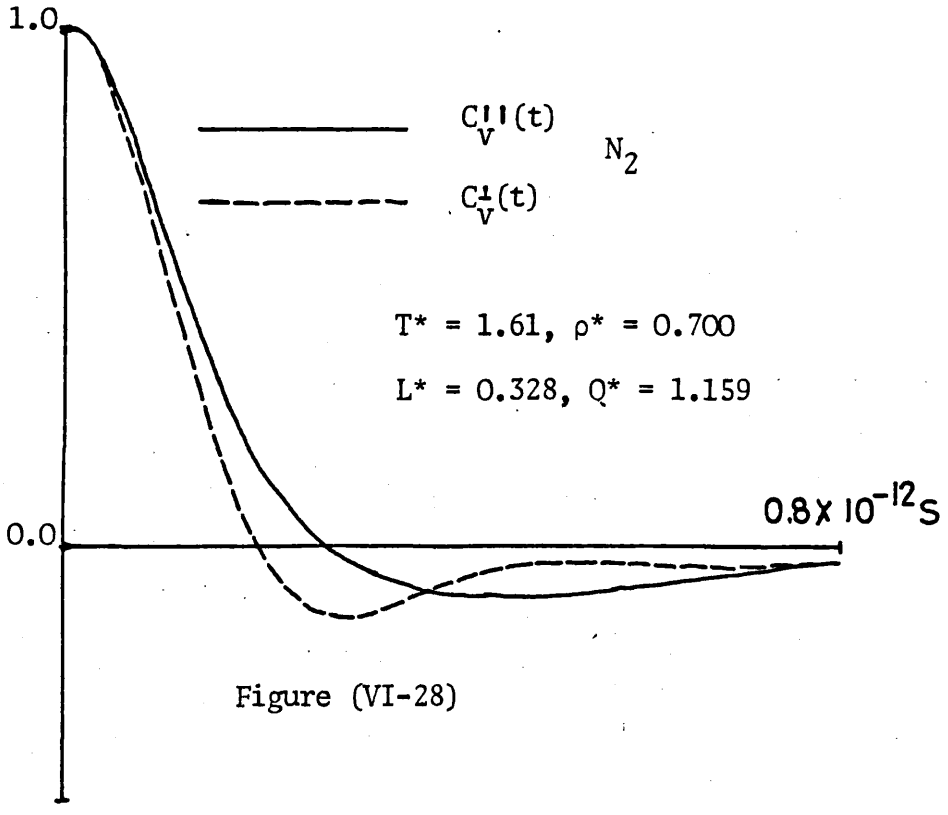

Figure (VI-28)

CHAPTER VII.

Dynamics - Analysis.

1. Introduction.

In order to analyse the time dependent behaviour of a system which obeys Hamilton's equations of motion

$$\dot{\underset{\sim}{r}}_i = \frac{\partial H_N}{\partial \underset{\sim}{p}_i} \quad : \quad \dot{\underset{\sim}{p}}_i = - \frac{\partial H_N}{\partial \underset{\sim}{r}_i} \quad i = 1,2...N \tag{VII-1}$$

it is first necessary to study the time evolution of the distribution function $f^N(\underset{\sim}{p}^N, \underset{\sim}{r}^N, t)$ (1,2). This function, when normalized gives the probability of finding a phase point in volume element $d\underset{\sim}{p}^N d\underset{\sim}{r}^N$ about point $(\underset{\sim}{p}^N, \underset{\sim}{r}^N)$ at time t as $f^N(\underset{\sim}{p}^N, \underset{\sim}{r}^N, t) d\underset{\sim}{p}^N d\underset{\sim}{r}^N$. If the system is closed and there are no external forces acting, then the dynamics of the system vary adiabatically and must be conservative, which can be expressed as

$$\frac{\partial f^N}{\partial t} + \text{div } \underset{\sim}{j} = 0 \tag{VII-2}$$

where $\underset{\sim}{j}$ is the current vector defined by

$$\underset{\sim}{j} = (f^N \dot{\underset{\sim}{p}}_1, f^N \dot{\underset{\sim}{p}}_2, \ldots f^N \dot{\underset{\sim}{r}}_N) \tag{VII-3}$$

Thus equation (VII-2) can be rewritten as

$$\frac{\partial f^N}{\partial t} + \sum_i \{ \frac{\partial}{\partial \underset{\sim}{p}_i} \cdot (f^N \dot{\underset{\sim}{p}}_i) + \frac{\partial}{\partial \underset{\sim}{r}_i} \cdot (p^N \dot{\underset{\sim}{r}}_i) \} = 0 \tag{VII-4}$$

which is equivalent to

$$\frac{\partial f^N}{\partial t} + \sum_i \{\frac{\partial f^N}{\partial \underset{\sim}{p}_i} \cdot \dot{\underset{\sim}{p}}_i + \frac{\partial f^N}{\partial \underset{\sim}{r}_i} \cdot \dot{\underset{\sim}{r}}_i\} + f^N \sum_i \{\frac{\partial}{\partial \underset{\sim}{p}_i} \cdot \dot{\underset{\sim}{p}}_i + \frac{\partial}{\partial \underset{\sim}{r}_i} \cdot \dot{\underset{\sim}{r}}_i\} = 0 \quad \text{(VII-5)}$$

Here the last term can be shown to be zero using Hamilton's equations of motion. Thus equation (VII-2) can be written as

$$\frac{\partial f^N}{\partial t} + [f^N, H_N] = 0 \quad \text{(VII-6)}$$

where the Poisson bracket is given by

$$[f^N, H_N] = \sum_i \{\frac{\partial f^N}{\partial \underset{\sim}{r}_i} \cdot \frac{\partial H_N}{\partial \underset{\sim}{p}_i} - \frac{\partial f^N}{\partial \underset{\sim}{p}_i} \cdot \frac{\partial H_N}{\partial \underset{\sim}{r}_i}\} \quad \text{(VII-7)}$$

The solution to equation (VII-6) can then be written

$$\frac{\partial f^N}{\partial t} = i\mathcal{L} f^N \quad \text{(VII-8)}$$

where $\mathcal{L}$ is the Lionville operator defined by

$$\mathcal{L} = -i \sum_i \{\frac{\partial H_N}{\partial \underset{\sim}{p}_k} \cdot \frac{\partial}{\partial \underset{\sim}{r}_k} - \frac{\partial H_N}{\partial \underset{\sim}{r}_k} \cdot \frac{\partial}{\partial \underset{\sim}{p}_k}\} \quad \text{(VII-9)}$$

Equation (VII-6) may now be integrated to give

$$f^N(\underset{\sim}{p}^N, \underset{\sim}{r}^N, (t) = \exp[i\mathcal{L}t] f^N(\underset{\sim}{p}^N, \underset{\sim}{r}^N, t) \quad \text{(VII-10)}$$

This equation is then valid for any dynamical variable $A(\underset{\sim}{p}^N, \underset{\sim}{r}^N, t)$ t) whose time evolution is governed by Hamilton's equations of motion, and is a function of the coordinates and momenta only.

The time dependence of $A(\underset{\sim}{p}^N, \underset{\sim}{r}^N, t)$ may now be studied by two distinct methods of analysis. These methods are both based on the separation of the dynamics into a systematic part and a stochastic part.

However the nature of the stochastic part is not equivalent in the two methods. The difference between the two methods can be shown by the use of projection operators.

2. Memory Function Analysis.

The memory function equations were proposed by Mori(3,4) and Zwanzig(13) as a method of rewriting the equations of motion of the system in such a way that the systematic parts are separated from any stochastically varying parts by the use of projection operators in the following way.

Consider a Hilbert space of dynamical variables whose invariant parts are set to zero, in which the inner product of two variables F and G is given by (F,G^*), corresponding to the correlation function for classical systems, where the asterisk denotes the Hermitian conjugate. The time evolution of the system is then given by the Liouville equation (VII-10) for which it is required that the Liouville operator be Hermitian

$$(\mathcal{L}F,G^*) = (F,[\mathcal{L}G]^*) \qquad \text{(VII-11)}$$

Now defining a pair of linear Hermitian projection operators P_o and Q_o, satisfying $P_o+Q_o=1$, such that the projection of the vector G onto the A axis is given by

$$P_oG = (G,A^*)(A,A^*)^{-1}.A \qquad \text{(VII-12)}$$

Then the dynamical variable A(t) may be separated into components projected onto the A axis and orthogonal to it giving

$$A(t) = \Xi_o(t).A + A'(t) \qquad \text{(VII-13)}$$

where

$$\Xi_o(t) = (A(t),A^*)(A,A^*)^{-1} \tag{VII-14}$$

$$A'(t) = Q_o A(t) \tag{VII-15}$$

Similarly the quantity $i\mathcal{L}A$ may be separated

$$\dot{A} = i\mathcal{L}A = i\omega_o A + f_1 \tag{VII-16}$$

where

$$f_1 = Q_o\, i\mathcal{L}A = Q_o\dot{A} \tag{VII-17}$$

$$i\omega_o = (\dot{A},A^*)(A,A^*)^{-1} = \left[\frac{d}{dt}\Xi_o(t)\right]_{t=o} \tag{VII-18}$$

It now follows from equation (VII-11) that

$$(A,A^*)\omega_o^* = \omega_o\cdot(A,A^*)$$

$$(A,A^*)\,\Xi_o^*(t) = \Xi_o(-t)(A,A^*) \tag{VII-19}$$

where the asterisks denote Hermitian conjugates. Thus the equation of motion for the dynamical variable A(t)

$$\frac{d}{dt}A(t) = i\mathcal{L}A \tag{VII-20}$$

may be transformed by operating Q_o throughout and then using equations (VII-15), (VII-13) and (VII-17) to obtain

$$\frac{d}{dt} A'(t) - Q_o \, i\mathcal{L} A'(t) = \Xi_o(t).f_1 \qquad \text{(VII-21)}$$

This can now be integrated to give

$$A'(t) = \int_o^t \Xi_1^o(t) f_1(t-s)ds \qquad \text{(VII-22)}$$

where

$$f_1(t) = \exp[Q_o \, i\mathcal{L}t] f_1 \qquad \text{(VII-23)}$$

Now it can be shown that $[Q_o\mathcal{L}]$ is Hermitian in the subspace orthogonal to the A subspace. Differentiating equation (VII-14) and using equation (VII-16) gives

$$\frac{d}{dt} \Xi_o(t) = i\omega_o \Xi_o(t) + (f_1(t), A^*)(A, A^*)^{-1} \qquad \text{(VII-24)}$$

The second term can now be rearranged by noting that f_1 is orthogonal to A, and using equations (VII-13), (VII-19) and (VII-22) the expression for $\Xi_o(t)$ becomes

$$\frac{d}{dt} \Xi_o(t) = i\omega_o \Xi_o(t) - \int_o^t \phi_A^1(s) \Xi_o(t-s)ds \qquad \text{(VII-25)}$$

where

$$\phi_A^1(t) = (f_1(t), f_1^*)(A, A^*)^{-1} \qquad \text{(VII-26)}$$

Equation (VII-25) may now be Laplace transformed to give

$$\hat{\Xi}_o(z) = \frac{1}{z - i\omega_o + \hat{\phi}_1(z)} \qquad \text{(VII-27)}$$

This analysis corresponds to an exact equation of motion for A(t), in which the time evolution is determined by $i\omega_o$ and the function $\phi_1(t)$

$$\frac{d}{dt} A(t) = i\omega_o A(t) - \int_o^t \phi_1(t-s)A(s)ds + f_1(t) \qquad \text{(VII-28)}$$

Thus $f_1(t)$ is a generalized random force acting on A(t), which by the orthogonality condition is statistically independent of the variable A(t)

$$(f_1(t),A^*) = 0 \qquad \text{(VII-29)}$$

However, the time evolution of the variable $f_1(t)$ will also be governed by an equation of motion similar to (VII-20), in which the Lionville operator $\mathcal{L}$ is replaced by $\mathcal{L}_1 = Q_o\mathcal{L}$. This may then itself be separated into components along the f_1 axis and orthogonal to it, as before using the projection operators Q_1 and P_1 which satisfy $Q_1+P_1=1$. The analysis then proceeds exactly as before with A(t) replaced by $f_1(t)$. This process can then be repeated indefinitely, leading to an expression for the inter-relation of successive correlation functions

$$\frac{d}{dt} \Xi_j(t) = i\omega_j\Xi_j(t) - \int_o^t \Xi_{(j+1)}(t-s)\Delta^2_{(j+1)}\Xi_j(s)ds \qquad \text{(VII-30)}$$

where

$$\Xi_j(t) = (f_j(t),f_j^*)(f_j,f_j^*)^{-1} \qquad \text{(VII-31)}$$

$$\Delta^2_{(j+1)} = (f_{(j+1)},f^*_{(j+1)})(f_j,f_j^*)^{-1} \qquad \text{(VII-32)}$$

Using the Laplace transform relationship (VII-27) and making successive substitutions, a continued fraction form can be obtained for the correlation function, involving only $\Xi_n(t)$ and $2(n-\ell)$ constants Δ_j^2 and ω_j to completely specify a given $\Xi_\ell(t)$

$$\hat{\Xi}_\ell(t) = \cfrac{1}{z-i\omega_\ell + \cfrac{\Delta^2_{(\ell+1)}}{z-i\omega_{(\ell+1)} + \ddots \cfrac{\Delta^2_{(n-1)}}{z-i\omega_{(n-1)} + \Delta_n^2 \hat{\Xi}_n(z)}}} \qquad \text{(VII-33)}$$

The continual fraction form enables $\Xi_\ell(t)$ to have complex structure even when a very simple approximation is used for $\Xi_n(t)$, the structure of the fraction itself partially determining the form of $\Xi_\ell(t)$. However, the basic relation (VII-25) is a transformation rather than any simplification as the function $\phi(t)$ must contain all the information that was present in the initial function $\Xi_o(t)$. The functions $\phi(t)$ are known as "memory" functions. The basic theory of linear projection operators in Hilbert space is discussed by Schmeidler(5) and Wall(6) has written a useful text on continued fractions.

3. Random Frequency Modulation Analysis.

The theory of the analysis of stochastic Liouville equations was first proposed by Kubo(7,8,9), in the context of oscillators whose natural frequency was modulated randomly by a certain disturbance. This theory was later re-examined by Tokuyama and Mori(10) with the projection operator techniques used for the memory function analysis. Considering the dynamical variable A(t) whose true dependence is governed by the Liouville equation (VII-20), the formal solution of which is governed by the exponential operator $\exp[Mt]$ where $M=i\mathcal{L}$. This may be separated into components along and orthorgonal to the A axis, as before, by introducing the projection operators P and Q which satisfy $P+Q=1$, giving

$$\exp[\bar{M}t] = \exp[\bar{M}t]P + \exp[\bar{M}t]Q \tag{VII-33}$$

$$= \exp[QMt] + \exp[\bar{M}t]\tilde{S}(t) \tag{VII-34}$$

where

$$\tilde{S}(t) = 1-\exp[-Mt]\exp[QMt] \tag{VII-35}$$

this enables equation (VII-34) to be rewritten with the use of P and Q giving

$$\exp[\bar{M}t] = \exp[QMt] + \exp[\bar{M}t]P\tilde{S}(t) + \exp[\bar{M}t]Q\tilde{S}(t) \tag{VII-36}$$

$$= \exp[\bar{M}t]PT(t) + V(t) \tag{VII-37}$$

where

$$T(t) = \tilde{S}(t)[1-Q\tilde{S}(t)]^{-1}, \quad \{T(0) = 0\} \tag{VII-38}$$

$$V(t) = \exp[QMt][1-Q\tilde{S}(t)]^{-1}, \quad \{V(0) = 1\} \tag{VII-39}$$

This may now be used to obtain a new operator identity by substituting equation (VII-37) into the term $\exp[\bar{M}t]Q$ in equation (VII-33) and multiplying through by M to give

$$\frac{d}{dt}\exp[\bar{M}t] = \exp[\bar{M}t]\bar{M}$$

$$= \exp[\bar{M}t]PM + \exp[\bar{M}t]PT(t)QM + V(t)QM \tag{VII-40}$$

This may now be transformed into an equation of motion for A(t) by operating on A(0) throughout to obtain

$$\frac{d}{dt} A(t) = [i\omega - \Psi(t)].A(t) + g(t) \qquad \text{(VII-41)}$$

where

$$\Psi(t) = -(T(t)QMA,A^*).(A,A^*)^{-1} \qquad \text{(VII-42)}$$

$$g(t) = V(t)QMA \qquad \text{(VII-43)}$$

$i\omega$ is defined as in the case of memory functions as

$$i\omega = (MA,A^*)(A,A^*)^{-1} \qquad \text{(VII-44)}$$

Now as the projection operators are the same as those in the memory function case, such that $PQ = 0$, giving the analogue of equation (VII-29), that is

$$(g(t),A^*) = 0 \qquad \text{(VII-45)}$$

thus g(t) is a randomly fluctuating force, but whose definition is very different from $f_1(t)$. From equation (VII-41), using equation (VII-45) it is simply shown that

$$[i\omega - \Psi(t)] = (\dot{A}(t),A^*)(A(t),A^*)^{-1} \qquad \text{(VII-46)}$$

where

$$\Psi(t) = \int_0^t \Psi(s)ds \qquad \text{(VII-47)}$$

Since $\Psi(0)$, it can be shown from equation (VII-46) that

$$\Psi(t) = \frac{d\Psi(t)}{dt} \qquad \text{(VII-48)}$$

$$= [(\dot{A}(t),\dot{A}^*)-(\dot{A}(t),A^*)(A(t),\dot{A}^*)(A(t),A^*)^{-1}](A(t),A^*)^{-1}$$

$$\equiv (g(t),g^*)(A(t),A^*)^{-1} \qquad \text{(VII-49)}$$

The time evolution of $\Xi_o(t)$, defined by equation (VII-14), is now obtained using equations (VII-41) and (VI-45) to give

$$\Xi_o(t) = \exp_+ \left[i\omega t - \int_0^t (t-s)\Psi(s)ds\right] \qquad \text{(VII-50)}$$

where $\exp_+$ denotes a time-ordered exponential. Again this analysis leads to a transform type relation between $\Xi_o(t)$ and $\Psi(s)$. It should also be noted that this type of analysis is restricted to well behaved functions which are always positive. It can be seen from equation (VII-49) that if $(A(t),A^*)=0$ then $\Psi(t)$ is infinite. It is also doubtful if this method of analysis is meaningful for systems in which $\Xi_o(t)$ is negative.

4. Relation between Analysis Methods.

It has been shown by Mori(10) that the two methods of analysis may be related by using the projection operator formalism. In particular the relation between the two types of fluctuating force can be expressed as

$$f_1(t) = g(t) + \Delta g(t) \qquad \text{(VII-51)}$$

where

$$\Delta g(t) \equiv - \int_0^t d\tau \Psi(\tau) \int_0^\tau ds \Xi_0(s) f_1(t-s) \qquad \text{(VII-52)}$$

From this the relation between $\phi_1(t)$ and $\Psi(t)$ is given by

$$\phi_1(t) = \Psi(t)\Xi_0(t) - \int_0^t d\tau \Psi(\tau) \int_0^\tau ds \Xi_0(s) \phi_1(t-s) \qquad \text{(VII-53)}$$

which in the classical limit can be simplified using equation (VII-25). It is evident that while $f_1(t)$ and $g(t)$ are not equivalent, nevertheless they both obey the same limiting conditions.

5. Continued Fraction Form.

In the case of classical motion, for which $i\omega=0$, it is possible to establish relations between successive memory functions and the derivatives of the corresponding correlation function at $t=0$, by the differentiation and rearrangement of equation (VII-30) giving

$$\frac{d^2}{dt^2} \Xi_j(t) = -\Delta^2_{(j+1)} \Xi_j(0) \Xi_{(j+1)}(t)$$

$$- \int_0^t \left[\frac{d}{dt} \Xi_j(t-s)\right] \Delta^2_{(j+1)} \Xi_{(j+1)}(s) ds \qquad \text{(VII-54)}$$

which in the limit of $t=0$ reduces to

$$\frac{d^2}{dt^2} \Xi_j(0) = - \Delta^2_{(j+1)} \Xi_j(0) . \Xi_{(j+1)}(0) \qquad \text{(VII-55)}$$

Denoting the correlation function by $C(t)$ and its n^{th} memory function by $M_n(t)$, the following $t=0$ relations may be obtained

$$M_1(0) = \Delta_1^2 = - C^{II}(0)/C(0) \qquad \text{(VII-56)}$$

$$M_2(0) = \Delta_2^2 = - C^{IV}(0)/C^{II}(0) + C^{II}(0)/C(0) \qquad \text{(VII-57)}$$

$$M_3(0) = \Delta_3^2 = \frac{[-C^{VI}(0)/C^{IV}(0) + C^{IV}(0)/C^{II}(0)]}{[1 - (C^{II}(0)/C^{IV}(0))^2]} \qquad \text{(VII-58)}$$

where the Roman numeral superscripts denote derivatives. Using these relations and assuming suitable functional forms for $M_n(t)$, analytic expressions for C(t) may be obtained. In the limit of short memory, $M_n(t)$ is assumed to be a δ-function, then by the continued fraction form, equation (VII-33), the Laplace transform of the correlation function is given by the ratio of two polynomials P(z) and Q(z), where the order of P is at least by one greater than the order of Q. The polynomial coefficients are determined from the variables Δ_n^2

$$\hat{C}(z) = \frac{\hat{Q}(z)}{P(z)} \qquad \text{(VII-59)}$$

Taking the inverse transform gives an analytic form for C(t), in terms of a sum of exponentials

$$C(t) = \sum_{i=\ell}^{n} Q(s_i)\exp(s_i t)/P'(s_i) \qquad \text{(VII-60)}$$

where

$$P'(s_i) = \left|\frac{dP(s)}{ds}\right|_{s=s_i} \qquad \text{(VII-61)}$$

and the polynomial P has n simple roots. In the case n=1, the form of C(t) simplifies to

$$C(t) = \exp[-\Delta_1^2 t] \qquad \text{(VII-62)}$$

However if $M_1(t)$ is supposed to decay exponentially

$$M_1(t) = \Delta_1^2 \exp[-\alpha t] \qquad \text{(VII-63)}$$

then this leads to the continued fraction expression for $\hat{C}(z)$

$$\hat{C}(z) = \cfrac{1}{z + \cfrac{\Delta_1^2}{z + \alpha}} \qquad \text{(VII-64)}$$

which is equivalent to $M_2(t) = \alpha\delta(t)$. Thus the assumption of an exponential form for $M_n(t)$ is the same as assuming $M_{(n+1)}(t)$ is a δ-function. Other functional forms also exhibit this property

$$M_n(t) = \Delta_n^2[1-(a_1-a)]\exp[-at] <=> \hat{M}_n(z) = \Delta_n^2\left[\frac{z+a_1}{(z+a)^2}\right] \qquad \text{(VII-65)}$$

$$M_n(t) = \Delta_n^2\exp[-bt]\cos[at] <=> \hat{M}_n(z) = \Delta_n^2\left[\frac{(z+b)}{(z+b)^2+a^2}\right] \qquad \text{(VII-66)}$$

both of which are the same as terminating the continued fraction after two extra terms with the δ-function approximation. In general where the Laplace transform of $M_n(t)$ is expressible as the ratio of two polynomials, where μ is the degree of the denominator, then this is the same as extending the continued fraction to $(n+\mu)$ terms, truncated with a δ-function. However the Laplace transform of a gaussian memory function involves the error function and so cannot easily provide any analytic forms for the corresponding correlation functions.

6. Time Ordered Exponentials.

The random frequency modulation analysis corresponds to a generalized evolution equation for $\Xi(t)$, given $\Xi(0)=1$, defined by

$$\frac{d}{dt}\Xi(t) = B(t)\Xi(t) \qquad \text{(VII-67)}$$

the solution of this can be shown to be given by

$$\Xi(t) = 1 + \int_o^t dt_1 B(t_1) + \int_o^t dt_1 \int_o^{t_1} dt_2 B(t_1)B(t_2) + \ldots$$

$$= \sum_{n=o}^{\infty} \int_o^t dt_1 \int_o^{t_1} dt_2 \ldots \int_o^{t_{n-1}} dt_n B(t_1)B(t_2)\ldots B(t_n) \qquad \text{(VII-68)}$$

However even when the $B(t_i)$ do not commute this may still be rewritten as

$$\Xi(t) = \sum_{t=o}^{\infty} \frac{1}{n!} \int_o^t dt_1 \int_o^t dt_2 \ldots \int_o^t dt_n \left[B(t_1)B(t_2)\ldots B(t_n) \right] \qquad \text{(VII-69)}$$

where $\left[\ldots . \right]$ denotes that the operators have been reordered in sequence of decreasing time arguments as discussed by Dyson(11). This can be written in the usual notation

$$\Xi(t) = \exp + \left[\int_o^t B(t')dt' \right] \qquad \text{(VII-70)}$$

where the time ordering symbol means explicitly: First expand the exponenential <u>then</u> order operators chronologically in each term. An alternative method of evaluation of the time ordered exponential is given by Van Kampen(12) in a full discussion of these types of stochastic differential equations. The method is to subdivide the interval (0,t) into N intervals of length t/N such that

$$t_o = 0; \quad t_1 = t/N; \quad t_2 = 2t/N; \ldots .; \quad t_N = t$$

In this case equation (VII-70) may be interpreted as

$$\lim_{N\to\infty} \exp\{\tfrac{t}{N} B(t_{N-1})\}\exp\{\tfrac{t}{N} B(t_{N-2})\}\ldots\exp\{\tfrac{t}{N} B(t_o)\} \qquad \text{(VII-71)}$$

$$= \lim_{N\to\infty}\{1 + \frac{t}{N} B(t_{n-1})\}\{1 + \frac{t}{N} B(t_{N-2})\}\ldots\{1 + \frac{t}{N} B(t_o)\} \qquad \text{(VII-72)}$$

This provides a simple numerical method for the evaluation of the time ordered exponential. However this time ordering does not facilitate obtaining analytic correlation functions for specific simple forms of $\Psi(t)$. However where $\Xi(t)$ is well behaved, having a decay time τ_c and the corresponding frequency modulation function $\Psi(t)$, has a decay time τ_ψ, then approximate behaviour in some special cases has been deduced by Mori et al.(10). The two limiting cases are firstly the static case where $t \lesssim \tau_c << \tau_\psi$, thus

$$\Psi(t) \approx \Delta_1^2 \equiv \Psi(0) \qquad \text{(VII-73)}$$

which leads to gaussian decay of $\Xi(t)$

$$\Xi(t) \approx \exp[i\Omega t - (\tfrac{1}{2})\Delta_1^2 t^2] \qquad \text{(VII-74)}$$

whereas, at the other extreme when $\tau_\psi << \tau_c$

$$\Psi(t) \approx 2\Gamma\delta(t) \qquad \text{(VII-73)}$$

the constant Γ being given by

$$\Gamma = \int_0^\infty dt(g(t).g^*)(A,A^*)^{-1} \exp[-i\Omega t] \qquad \text{(VII-76)}$$

then this gives exponential decay of $\Xi(t)$

$$\Xi(t) \approx \exp[i\Omega t - \Gamma t] \qquad \text{(VII-77)}$$

Unfortunately there are many other cases which do not satisfy either of these limits, for which approximate forms are not derivable.

7. Gaussian Memory Function Decay.

Returning to memory function analysis, the fluctuating force $f_j(t)$ corresponding to each successive memory function $\Xi_j(t)$ in the heirachy can be seen to obey an equation of motion of the form of equation (VII-20) with a Liouville operator $Q_j\mathcal{L}_j \equiv M_j$ which is unitary in the subspace orthogonal to the subspaces corresponding to all other $f_i(t)|i\neq j|$. Random frequency modulation analysis may now be applied directly as before to give

$$\Xi_j(t) = \exp + \left[i\omega_j t - \int_0^t (t-s)\Psi_j(s)ds\right] \qquad \text{(VII-78)}$$

However, if $\Xi_j(t)$ has gaussian decay them this corresponds to the static case $t \lesssim \tau_c << \tau_\Psi$ for which $\Psi_j(t) \approx \Delta_j^2$, as was discussed in the previous section. This then leads to the separation of $\Psi_j(t)$ into gaussian and non-gaussian terms

$$\Psi_j(t) = \Delta_j^2 + \Delta\Psi_j(t) \qquad \text{(VII-79)}$$

It has been shown by Mori at al.(10) that this can be used to rewrite the argument of the time ordered exponential giving

$$\Xi_j(t) = \exp + \left[i\omega_j t - \tfrac{1}{2}\Delta_j^2 t^2 - \nu(t)\right] \qquad \text{(VII-80)}$$

where

$$\nu(t) = \int_0^t (t-s)\ \Delta\Psi_j(s)ds \qquad \text{(VII-81)}$$

The function $\nu(t)$ may now be expanded as a Taylor series about t=o

$$\nu(t) = ({}_jC_3/3!)t^3 + ({}_jC_4/4!)t^4 + \ldots \qquad \text{(VII-82)}$$

where the expansion coefficients are given by

$${}_jC_{n+2} = [d^n\Delta\Psi_j(t)/dt^n]_{t=o} \qquad \text{(VII-83)}$$

The constants $i\omega_j$, $-\Delta_j^2$ and $-{}_jC_m$ are just equal to the cumulants of $\Xi_j(t)$ and can thus be evaluated. This method allows the magnitude of the deviation from gaussian decay for a given memory function to be assessed. However as the method relies on finding the numerical derivatives of $\Delta\Psi_j(t)$ generated from the memory function $\Xi_j(t)$, it is prone to numerical inaccuracy.

8. Memory Function Heirarchy.

Using the t=o relations given in equations (VII-56) to (VII-58), it is possible to obtain values for the physical constants associated with the system, both for translational and rotational motion. These values may then be compared with those obtained by Detyna, Singer and Singer(14) for systems of two-centre Lennard-Jones diatomics. In this way the effects of quadrupolar interactions on the dynamics of the system can be investigated.

For translational motion the following relations may be obtained for the first two memory functions, of the centre of mass velocity auto-correlation function $C_v(t)$ by considering the appropriate ensemble averages of the correlation function and its derivatives at t=o. This results in

$$M_1^V(0) = \langle F^2\rangle/3MkT \qquad \text{(VII-84)}$$

$$M_2^V(0) = \frac{\langle \dot{F}^2 \rangle}{\langle F^2 \rangle} - \frac{\langle F^2 \rangle}{3MkT} \qquad \text{(VII-85)}$$

where $\langle F^2 \rangle$ is the mean square force and $\langle \dot{F}^2 \rangle$ is the second derivative of the mean square force.

In the rotational case, these relations have been deduced by Detyna et al.(14). For the angular momentum auto-correlation function $C_J(t)$ these are

$$M_1^J(0) = \frac{\langle \tau^2 \rangle}{2IkT} \qquad \text{(VII-86)}$$

$$M_2^J(0) = \frac{\langle \dot{\tau}^2 \rangle}{\langle \tau^2 \rangle} - \frac{\langle \tau^2 \rangle}{2IkT} \qquad \text{(VII-87)}$$

where $\langle \tau^2 \rangle$ is the mean square torque, $\langle \dot{\tau}^2 \rangle$ is the second derivative of the mean square torque and I is the moment of inertia of the molecule. The first harmonic of the orientational autocorrelation function $C_1(t)$ gives

$$M_1^1(0) = \frac{2kT}{I} \qquad \text{(VII-88)}$$

$$M_2^1(0) = \frac{\langle \tau^2 \rangle}{2IkT} + \frac{2kT}{I} \qquad \text{(VII-89)}$$

$$M_3^1(0) = \frac{\left[\frac{\langle \dot{\tau}^2 \rangle}{\langle \tau^2 \rangle} - \frac{\langle \tau^2 \rangle}{2IkT} + \frac{2kT}{I} \left(4 + \frac{2(2kT)^2}{\langle \tau^2 \rangle} \right) \right]}{\left[1 + \frac{(2kT)^2}{\langle \tau^2 \rangle} \right]} \qquad \text{(VII-90)}$$

Similar relations are obtained for the second harmonic of the orientational auro-correlation function $C_2(t)$

$$M_1^2(0) = \frac{6kT}{I} \qquad \text{(VII-91)}$$

$$M_2^2(0) = \frac{\langle \tau^2 \rangle}{2IkT} + \frac{10kT}{I} \qquad \text{(VII-92)}$$

$$M_3^2(0) = \frac{\left[\frac{\langle \dot{\tau}^2 \rangle}{\langle \tau^2 \rangle} - \frac{\langle \tau^2 \rangle}{2IkT} + \frac{2kT}{I}\left(22 + \frac{32(2kT)^2}{\langle \tau^2 \rangle}\right)\right]}{\left[1 + \frac{5(2kT)^2}{2}\right]} \qquad \text{(VII-93)}$$

In the case of the torque autocorrelation function $C_{TQ}(t)$, the first memory function at t=o is given by

$$M_1^{TQ}(0) = \frac{\langle \dot{\tau}^2 \rangle}{\langle \tau^2 \rangle} \qquad \text{(VII-94)}$$

However as $C_{TQ}(t)$ is the normalized second derivative of $C_J(t)$, then it can be shown that the memory function $M_1^{TQ}(t)$ is equivalent to $M_2^J(t)$ plus a constant $\ddot{C}_J(0)$, which is negative.

$$M_2^J(t) = M_1^{TQ}(t) + \ddot{C}_J(0) \qquad \text{(VII-95)}$$

The numerical accuracy of those rotational constants calculated from $M_n^J(0)$ and $M_1^{TQ}(0)$ can be expected to be greater as they involve lower order derivatives to obtain the same information.

The values of $\langle F^2 \rangle$ and $\langle \dot{F}^2 \rangle$ calculated from equations (VII-84) and (VII-85) are given in Table (VII-1). However the values for $\langle \dot{F}^2 \rangle$ are liable to numerical inaccuracy, which in some cases has given negative values which are unphysical and have been omitted. The values for $\langle F^2 \rangle$ are in good agreement with those calculated directly, and given in Chapter III. $\langle F^2 \rangle$ can be seen to increase with increasing temperature and/or decreasing density. There is only a small increase in $\langle F^2 \rangle$ with increasing quadrupole moment in the chlorine-like systems. This suggests that quadrupolar interactions play a secondary role in

TABLE (VII-1).

T^*	ρ^*	Q^*	L^*	$\langle F^2 \rangle$ $N^2 \times 10^{-20}$	$\langle \dot{F}^2 \rangle$ $\times 10^6$
1.14	.541	.739	.608	14.6	100.0
1.45	.485			15.0	90.2
1.74	.485			20.4	165.4
1.21	.546	1.321	.608	15.2	62.7
1.55				22.0	183.1
1.55	.490			15.9	-
1.81				20.0	-
1.50	.551	2.073	.608	15.7	15.9
1.85				21.3	40.7
1.86	.494			16.2	76.1
2.19				20.5	-
1.61	.700	1.159	.328	1.2	2.5
2.66				1.8	16.4
2.27	.626			2.2	12.0
3.60				3.1	37.0
1.61	.423	2.039	.793	10.5	160.6
2.14				15.4	130.3
1.83	.381			10.1	140.6
2.39				14.6	208.6
1.13(R)	.541	0.5D	.608	15.2	91.0
1.39				20.4	238.3
1.42	.485			15.3	111.1
1.13	.541	..739	.608	14.5	63.0
1.42	.551	2.073	.608	14.5	-

determining the single particle translational motion, although they can be expected to be significant for collective translations, where the quadrupole increases the cohesiveness of the potential. The values of $\langle \dot{F}^2 \rangle$ increase strongly with increasing temperature, however numerical inaccuracy makes further correlations with density or quadrupole moment variation impossible.

For rotational motion the values of $\langle \tau^2 \rangle$ and $\langle \dot{\tau}^2 \rangle$ calculated from equations (VII-86) and (VII-87) are given in Table (VII-2). Again the values for $\langle \tau^2 \rangle$ are in close agreement with those of Chapter III. Both $\langle \tau^2 \rangle$ and $\langle \dot{\tau}^2 \rangle$ increase with increasing temperature and/or increasing density. In contrast to the case of $\langle \dot{F}^2 \rangle$, there is a strong increase in $\langle \tau^2 \rangle$ and $\langle \dot{\tau}^2 \rangle$ with increasing quadrupole moment. This is caused by increasing anisotropy of the quadrupolar potential. Similarly $\langle \tau^2 \rangle$ and $\langle \dot{\tau}^2 \rangle$ increase with increasing bond length, the effect of which is to further increase the anisotropy of the potential.

9. Trial Memory Functions.

It is useful to attempt to describe the molecular motion of a system by a few simple parameters, which may be given by the static properties of the system. In the present case of single-particle correlation functions the parameters are related to quantities such as $\langle \tau^2 \rangle$ and $\langle F^2 \rangle$. These parameters together with the use of the memory function heirarchy can determine the shape of a given correlation function, within a certain error which must correspond to the effect of any terms that have been neglected.

Numerical calculation of the memory functions of correlation functions has been carried out using the method of Detyna(14) and described in the Appendix. The first memory functions of various translational velocity autocorrelation functions are shown in Figures (VII-1) to (VII-5). It can be seen that the initial decay of the

TABLE (VII-2).

T^*	ρ^*	Q^*	L^*	$\langle\tau^2\rangle$ $\times 10^{-40}$	$\langle\dot{\tau}^2\rangle$ $\times 10^{-14}$
1.14	.541	.739	.608	10.1	44.2
1.41				13.5	70.6
1.45	.485			10.7	51.4
1.74				14.2	82.3
1.21	.546	1.321	.608	11.8	56.2
1.55				16.5	91.7
1.55	.490			12.2	66.6
1.81				15.4	88.1
1.50	.551	2.073	.608	15.2	74.7
1.85				19.9	117.0
1.86	.494			15.3	77.6
2.19				19.0	107.7
1.61	.700	1.159	.328	.28	.95
2.66				.48	2.32
2.27	.626			.31	1.22
3.60				.51	3.21
1.61	.423	2.039	.793	12.1	106.1
2.14				17.2	201.9
1.83	.381			11.7	102.3
2.39				16.1	214.8
1.13(R)	.541	0.5D	.608	10.4	47.6
1.39				13.9	74.2
1.42	.485			10.4	52.1
1.13	.541	.739	.608	10.1	46.5
1.42	.551	2.073	.608	14.7	68.5

memory function is considerably faster than that of the correlation function, however where the correlation function has a long negative tail, the memory function also has a slowly decaying positive tail. As the memory function equation (VII-25) may be considered as a type of transform relation, then the memory function must contain all the information within the correlation function. Thus although the memory function may exhibit considerably more rapid decay, its shape cannot be considered to be any simpler.

The rotational memory function for the same systems are illustrated in Figures (VII-6) to (VII-15). The correspondence of the first memory function of the orientational correlation functions, with the angular momentum correlation function is clearly shown. The numerical accuracy of the method is demonstrated by the spurious oscillations of the orientational second memory functions, which can be seen to correspond to the angular momentum first memory function. Also illustrated is the torque first memory function from which the constant part has been subtracted. The initial decay is approximately gaussian with a very small negative lobe at intermediate times in some cases, the magnitude of which seems to vary with the amount of damping of the oscillations of the torque correlation function. The torque memory function decays more rapidly than the angular momentum first memory function. In the limit of very rapid decay the gaussian function may be approximated by a δ-function for which the shape of the correlation function can be expressed analytically as discussed in Section (VII-5). However the rate of decay of the torque memory function is sufficiently fast that simple trial functions may be used to approximate its shape, while the decay is slow enough that the routines used are able to calculate the regenerated correlation functions with very little numerical error. The method of numerical regeneration of functions from their memory functions, due to Detyna(14), is given in

the Appendix. Thus the torque memory function was chosen as the basis function for the heirarchy, a schematic representation of which is given in Figure (VII-16)

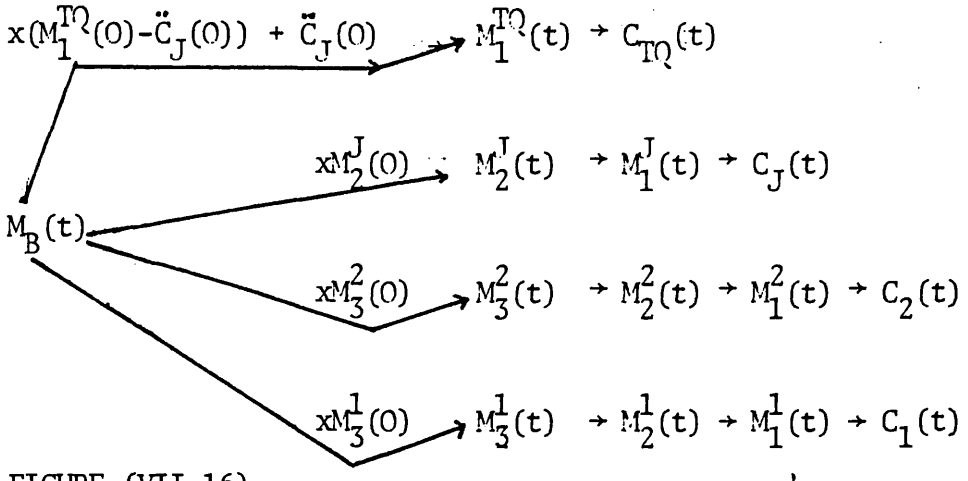

FIGURE (VII-16)

It can be seen that, with the exception of the torque, these functions at any given level are all equivalent within a simple scale factor. In the case of the torque, the addition of the constant $\ddot{C}_J(0)$ has a dramatic effect on the shape of the regenerated function. For translation the heirarchy for the centre of mass velocity is equivalent to that of the angular momentum and is illustrated in Figure (VII-17).

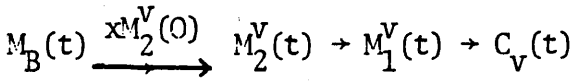

FIGURE (VII-17).

Trial functions may now be used to parameterize the normalized basis function $M_B(t)$. A number of functional forms were investigated by Detyna et al.(14), however in the present study, only the $(E+t^2E)$ approximation has been used, which is given by

$$(E + t^2E) \qquad \exp(-t/\tau_1) + \alpha t^2 \exp(-t/\tau_2)$$

This enables the systems to be parameterized in terms of simple

functions, which correspond to the first two terms of an exponential expansion of the memory function. The success of this approximation for a given system is found by using the form for $M_B(t)$, and calculating the resultant error in regeneration of the hierarchy of functions, when the best fit parameters τ_1, α and τ_2 are used. The error is calculated using

$$\Delta C = 100 \left[\int_0^{t_{max}} (C_{MD}-C_{MF})^2 \, dt\right]^{\frac{1}{2}} \qquad \text{(VII-96)}$$

the resultant C being averaged over the four correlation functions for rotational motion

$$\Delta C_R = \left[\Delta C_1 + \Delta C_2 + \Delta C_J + \Delta C_{TQ}\right]/4 \qquad \text{(VII-97)}$$

The fitted parameters for translational motion are given in Table (VII-3) and for rotational motion in Table (VII-4).

The results of the fitting show that in the translational case, there is very little variation in the parameters with increase in temperature only, apart from a small increase in τ_1. The changing of density however has a marked effect, with τ_1 and τ_2 substantially reduced, as the density is decreased. The opposite effect is observed with increasing quadrupole moment. Bond length changes alone do not seem to have any strong effect on the translational parameters. It should be remembered that these fitted parameters only determine the secondary characteristics of the regenerated correlation functions. The primary characteristics are determined by the memory function first values, which as shown before are related to $\langle F^2 \rangle$ and $\langle \dot{F}^2 \rangle$.

In the rotational case the results are rather more complete. Increase of temperature at constant density produces a strong decrease

TABLE (VII-3).

T^*	ρ^*	Q^*	L^*	τ_1 $\times 10^{-14}$s	τ_2 $\times 10^{-14}$s	α $\times 10^{-3}$	ΔC
1.45	.485	.739	.608	4.40	5.42	-.30	1.13
1.21	.546	1.321	.608	5.21	7.25	-.44	1.94
1.55				5.28	7.30	-.40	2.57
1.50	.551	2.073	.608	5.49	9.94	-.24	4.33
1.85				5.73	9.93	-.25	6.58
1.86	.494			4.68	6.58	-.45	1.35
2.27	.626	1.159	.328	4.76	6.82	-.45	1.10
3.60				4.79	6.21	-.41	1.56
1.61	.423	2.039	.793	4.46	5.96	-.50	2.07
1.83	.381			7.94	4.11	-.49	1.09
1.42	.551	2.073	.608	5.70	13.33	-.11	6.16

TABLE (VII-4).

T^*	ρ^*	Q^*	L^*	τ_1 $\times 10^{-14}$s	τ_2 $\times 10^{-14}$s	α $\times 10^{-3}$	ΔC_R
1.14	.541	.739	.608	4.77	6.58	-.34	2.02
1.41				4.21	5.35	-.50	1.57
1.45	.485			4.45	5.48	-.40	1.82
1.74				4.04	4.79	-.50	1.69
1.21	.546	1.321	.608	4.29	5.73	-.50	1.32
1.55				4.12	5.42	-.50	1.63
1.55	.490			3.92	4.62	-.50	1.11
1.81				4.05	4.77	-.50	1.63
1.50	.551	2.073	.608	4.29	6.59	-.50	1.62
1.85				3.65	5.66	-.50	1.35
1.86	.494			4.11	5.54	-.50	1.32
2.19				3.96	5.17	-.50	1.32
3.60	.626	1.159	.328	3.84	4.37	-.50	1.82
1.61	.423	2.039	.793	3.29	4.75	-.50	1.83
2.14				2.54	3.81	-.50	1.05
1.83	.381			3.34	4.45	-.50	1.76
2.39				2.07	3.97	-.50	0.88
1.13	.541	0.5D	.608	4.57	5.81	-.50	1.54
1.42	.485			4.21	5.22	-.50	1.26
1.13	.541	.739	.608	5.34	4.77	-1.25	1.22
1.42	.551	2.073	.608	4.59	7.13	-.50	1.96

in τ_1 and τ_2, as does a decrease in density at constant temperature. The variation with increasing quadrupole moment does not seem to be consistant for the three chlorine-like systems studied, and thus it is not possible to identify any quadrupolar effects. Similarly the effects of changing bond length are also not distinguishable. The values of α in both cases are remarkably constant and seem to play little part in determining the best fit.

An alternative gaussian approximation to the memory function $M_B(t)$ has also been investigated. This form was suggested by Martin and Yip(15) and has been fully discussed by Berne and Harp(16). In this approximation the basis memory function is simply given by

$$M_n(t) = M_n(0)\exp[-t^2/\tau_G^2] \qquad \text{(VII-98)}$$

where the decay time τ_G is determined by requiring compatability with the initial curvature such that

$$-2/\tau_G^2 = \ddot{M}_n(0)/M_n(0) = -M_{n+1}(0) \qquad \text{IVII-99)}$$

In this case the values of τ_G correspond to $M_3^V(0)$ and $M_3^J(0)$, which have been calculated from the derivatives of $M_1^V(t)$ and $M_1^J(t)$ respectively. The accuracy of τ_G calculated in this way is not high, but sufficiently good to give a reasonable estimate of the accuracy of the gaussian approximation.

It is found that in many cases this approximation gives a good estimate of the initial curvature of the regenerated correlation functions. However the approximation is seriously deficient at intermediate times failing to adequately represent the negative lobes of the momentum correlation functions. For comparison the gaussian correlation times τ_G have been given in Tables (VII-5) and (VII-6), together with their respective numerical errors ΔC_G, calculated as before. Illustrations

TABLE (VII-5).

TRANSLATIONAL.

T^*	ρ^*	Q^*	L^*	τ_G $\times 10^{-14}$s	ΔC_G
1.14	.541	.739	.608	5.76	3.61
1.45	.485			6.22	8.84
1.74	.485			5.18	7.08
1.21	.546	1.321	.608	8.64	16.06
1.55				5.21	3.81
1.55	.490				
1.81					
1.50	.551	2.073	.608		
1.85					
1.86	.494			7.54	16.12
2.19					
1.61	.700	1.159	.328	15.56	26.66
2.66				4.36	2.52
2.27	.626			6.61	12.29
3.60				4.03	2.61
1.61	.423	2.039	.793	3.63	3.18
2.14				5.50	12.71
1.83	.381			3.83	1.87
2.39				3.79	12.58
1.13(R)	.541	0.5D	.608	6.37	7.69
1.39				4.19	3.92
1.42	.485			5.50	1.32
1.13	.541	.739	.608	8.18	12.78
1.42	.551	2.073	.608		

TABLE (VII-6).

ROTATIONAL.

T*	ρ*	Q*	L*	τ_G $\times 10^{-14}$s	ΔC_G
1.14	.541	..739	.608		
1.41				12.62	26.23
1.45	.485				
1.74					
1.21	.546	1.321	.608	2.70	6.37
1.55					
1.55	.490			1.98	13.02
1.81				3.76	9.63
1.50	.551	2.073	.608	4.71	4.67
1.85				2.07	8.00
1.86	.494			3.39	2.27
2.19				2.93	4.93
1.61	.700	1.159	.328	3.56	8.90
2.66					
2.27	.626			4.86	1.76
3.60				2.11	15.88
1.61	.423	2.039	.793		
2.14				2.18	3.26
1.83	.381				
2.39				1.63	7.70
1.13(R)	.541	0.5D	.608		
1.39				4.75	5.09
1.42	.485			2.92	6.25
1.13	.541	..739	.608	14.07	25.32
1.42	.551	2.073	.608	5.31	5.95

of the accuracy of these fits to particular correlation functions are given in Figures (VII-18) to (VII-22) for translational motion and Figures (VII-23) to (VII-27) for rotational motion.

10. Binary Collision Approximation.

This approximation was suggested by Chandler(17,18), as a method of estimating self-correlation functions of hard sphere fluids, however the technique may be applied to the self-correlation functions of any general system. As seen in Section (VII-2) the time evolution of a given memory function $\Xi_j(t)$ may be expressed as

$$\Xi_j(t) = (\exp(Q_{(j-1)} i\mathcal{L} t) f_j, f_j^*)(f_j, f_j^*)^{-1} \qquad \text{(VII-100)}$$

and as the ensemble average of a dynamical variable A may be expressed as

$$\langle A \rangle_{fj} = (Af_j, f_j^*)(f_j, f_j^*)^{-1} \qquad \text{(VII-101)}$$

then the memory function $M_j(t)$ is given by

$$M_j(t) = (|f_j|^2)\langle \exp(Q_{(j-1)} i\mathcal{L} t) \rangle_{fj} \qquad \text{(VII-102)}$$

The averaged exponential operator can now be rewritten as a cummulant expansion using the technique of Kubo(19)

$$\langle \exp(Q_{(j-1)} i\mathcal{L} t) \rangle_{fj} = \exp\left[\sum_{n=1}^{\infty} K_n t^n / n!\right] \qquad \text{(VII-103)}$$

where K_n is the n^{th} cumulant in the series, which must be convergent.

This expansion method can now be used to study the deviation from ideal gas behaviour. Thus if $\Xi_j^{(0)}(t)$ is the corresponding ideal gas self-correlation function then the above arguments apply as before giving

a corresponding expression to equation (VII-103), where $K_n^{(0)}$ is the n^{th} cumulant. The memory function of the non-ideal system may now be written as

$$\Xi_j(t) = \Xi_j^{(0)}(t)\exp\left[\sum_{n=1}^{\infty}(K_n - K_n^{(0)})t^n/n!\right] \qquad \text{(VII-104)}$$

The ideal gas system is one in which successive collisions between particles are completely uncorrelated, and thus represents the binary collision limit.

11. Approximate Analytic Correlation Functions.

Approximate analytic forms for correlation functions may be obtained using the continued fraction approximation. This is accomplished by assuming a given form for the basis memory function, which has a Laplace transform that can be written in terms of powers of the transform variable z. Thus the $(E+t^2D)$ form used for the trial memory functions has an analytic Laplace transform.

$$\hat{M}_B(z) = M_B(0)\left\{\frac{(z+\tau_2)^3 + 2\alpha(z+\tau_1)}{(z+\tau_1)(z+\tau_2)^3}\right\} \qquad \text{(VII-105)}$$

The continued fraction approximation together with the appropriate first values in the heirarchy are now used to construct the Laplace transform of the correlation function as a ratio of two polynomials. The inverse transform is a standard form. If N(z) and D(z) are polynomials in z, the order of D being at least one greater than the order of N then

$$\hat{C}(z) = \frac{N(z)}{D(z)} \qquad \text{(VII-106)}$$

whose inverse transform is

$$C(t) = \sum_{i=1}^{N} \frac{N(z_i)e^{z_i t}}{D'(z_i)} \qquad \text{(VII-107)}$$

where D has N simple roots Z_i and

$$D'(z_i) = \left(\frac{dD(z)}{dz}\right)_{z=z_i} \qquad \text{(VII-108)}$$

The resultant exponential polynomial for C(t) may be expressed in terms of sine and cosine functions where complex roots are present.

The parameters used were obtained from the $(E+t^2E)$ trial memory functions determined by the best fit proceedure described in Section (VII-9). The error in the regenerated functions compared with those calculated numerically is typically of the order of 0.3% with a maximum error in any single point always being less than 1%. This is a vindication of the accuracy of the numerical methods of regeneration proposed by Detyna(14) and described in the Appendix.

The resultant approximate correlation functions may be expressed in the following forms, which for $C_1(t)$ and $C_2(t)$ is given by

$$A_{exp}(-\alpha) + 2exp(-\beta)\left[B\cos(\omega_A) + C\sin(\omega_A)\right] \qquad \text{(VII-109)}$$

and for $C_\omega(t)$, $C_{TQ}(t)$ and $C_v(t)$ as

$$2exp(-\beta)\left[B\cos(\omega_A) + C\sin(\omega_A)\right]$$

$$+ 2exp(-\gamma)\left[D\cos(\omega_B) + E\sin(\omega_B)\right] \qquad \text{(VII-110)}$$

The parameters calculated for $C_v(t)$, $C_{TQ}(t)$, $C_\omega(t)$, $C_2(t)$ and $C_1(t)$ are given in Tables(VII-7) to (VII-11) respectively. Only those cases for which the resultant polynomial approximation could be reduced to the simplified forms above to within 1%. have been included. However, as can be seen from the tables this criteria eliminated only a very few cases indeed, most notably $C_{TQ}(t)$ for CO_2.

TABLE (VII-7).

$C_v(t)$

	T*	ρ*	Q*	L*	$\beta\times10^{-1}$	$\gamma\times10^{-1}$	B	C	$\omega_A\times10^{-1}$	D	E	$\omega_B\times10^{-1}$
	1.45	.485	..739	.608	.300	.369	.479	.183	.155	.0217	.167	.736
	1.21	.546	1.321	.608	.192	.278	.412	-.151	.200	.0900	.177	.755
	1.55				.205	.266	.391	-.136	.193	.111	.170	.798
	1.50	.551	2.073	.608	.160	.215	.336	-.244	.169	.161	.197	.685
	1.85				.153	.216	.343	-.216	.163	.154	.167	.752
	1.86	.494			.190	.341	.462	-.054	.193	.039	.144	.772
	2.27	.626	1.159	.328	.188	.323	.452	-.107	.202	.049	.163	.748
	3.60				.220	.342	.468	.023	.179	.033	.146	.751
	1.61	.423	2.039	.793	.228	.356	.439	-.007	.192	.062	.131	.936
†	1.42	.551	2.073	.608	.141	.181	.265	-.259	.130	.217	.198	.643

† 256 particles - β, γ, ω_A, ω_B all * 4.0×10^{-15}s.

TABLE (VII-8).

				$C_{TQ}(t)$							
T*	ρ*	Q*	L*	β $\times 10^{-1}\Delta t$	γ $\times 10^{-1}\Delta t$	B	C	ω_A $\times 10^{-1}\Delta t$	D	E	ω_B $\times 10^{-1}\Delta t$
1.14	.541	.739	.608	.293	.252	.607	.265	.709	-.104	-.193	.211
1.41				.362	.295	.602	.334	.763	-.106	-.272	.241
1.45	.485			.365	.280	.573	.337	.734	-.077	-.299	.191
1.74				.417	.314	.560	.351	.808	-.066	-.341	.189
1.21	.546	1.321	.608	.328	.284	.639	.332	.717	-.141	-.260	.262
1.55				.346	.306	.623	.300	.788	-.124	-.232	.255
1.55	.490			.424	.340	.602	.424	.746	-.108	-.416	.219
1.81				.405	.331	.587	.355	.796	-.094	-.335	.206
1.50	.551	2.073	.608	.269	.267	.642	.220	.748	-.135	-.146	.261
1.86	.494			.348	.293	.635	.339	.737	-.135	-.269	.265
2.19				.375	.313	.620	.337	.784	-.120	-.275	.255
1.83	.381	2.039	.793	.442	.387	.609	.283	.991	-.104	-.232	.251
1.13	.541	0.5D	.608	.327	.267	.600	.323	.720	-.106	-.255	.238
1.42	.485			.409	.262	.527	.365	.754	-.032	-.324	.197
† 1.42	.551	2.073	.608	.232	.255	.627	.179	.734	-.077	-.299	.191

† 256 particles

TABLE (VII-9)

$C_\omega(t)$

T*	ρ*	Q*	L*	A	α $\times 10^{-1}\Delta t$	β $\times 10^{-1}\Delta t$	γ $\times 10^{-1}\Delta t$	B	C	ω_A $\times 10^{-1}\Delta t$	D	E	ω_B $\times 10^{-1}\Delta t$
1.14	.541	.793	.608	-	-	.252	.293	.413	-.133	.211	.088	.223	.709
1.41				-	-	.295	.362	.461	-.078	.240	.040	.220	.763
1.45	.485			-	-	.279	.366	.481	.062	.190	.020	.175	.734
1.74				-	-	.313	.420	.493	..159	.187	.008	.157	.808
1.21	.546	1.321	.608	-	-	.285	.327	.435	-.196	.263	.066	.274	.717
1.55				-	-	.306	.347	.428	-.136	.255	.073	.241	.788
1.55	.490			-	-	.341	.424	.516	.089	.219	-.015	.199	.746
1.81				-	-	.330	.406	.486	.094	.205	.015	.183	.797
1.50	.551	2.073	.608	-	-	.267	.269	.329	-.292	.261	.172	.282	.748
1.85				-	-	.310	.338	.384	-.272	.293	.115	.308	.780
1.86	.494			-	-	.294	.347	.446	-.173	.265	.055	.265	.737
2.19				-	-	.314	.375	.458	-.099	.256	.043	.235	.783
3.60	.626	1.159	.328	.456	.836	.356	-	.273	.583	.487	-	-	-
1.61	.423	2.039	.793	-	-	.387	.400	.388	-.136	.287	.111	.240	.985
2.14				-	-	.463	.571	.473	-.027	.315	.023	.232	1.066
1.83	.381			-	-	.387	.442	.439	-.001	.251	.061	.200	.991
1.13	.431	0.5D	.608	-	-	.268	.327	.448	-.131	.239	.054	.234	.719
1.42	.485			-	-	.263	.408	.505	.087	.199	-.004	.150	.753
† 1.13	.541	.739	.608	-	-	.300	.354	.483	-.056	.252	.020	.216	.750
† 1.42	.551	2.073	.608	-	-	.252	.236	.292	-.301	.247	.211	.265	.745

† 256 particles

TABLE (VII-10).

$C_{D2}(t)$

T*	ρ*	Q*	L*	A	α $\times 10^{-2}\Delta t$	β $\times 10^{-1}\Delta t$	γ $\times 10^{-1}\Delta t$	B	C	ω_A $\times 10^{-1}\Delta t$	D	E	ω_B $\times 10^{-1}\Delta t$
1.14	.541	.739	.608	.942	.460	.247		.031	.092	.235			
1.41				.971	.583	.294		.019	.093	.270			
1.45	.485			1.024	.813	.276		-.007	.132	.233			
1.74				1.080	1.014	.307		-.034	.145	.243			
1.21	.546	1.321	.608	.941	.391	.285		.033	.068	.282			
1.55				.955	.526	.302		.025	.083	.279			
1.55	.490			1.056	.790	.345		-.020	.096	.261			
1.81				1.066	.929	.326		-.028	.123	.249			
1.50	.551	2.073	.608	.895	.238	.259		.052	.055	.280			
1.85				.915	.358	.308		.045	.061	.313			
1.86	.494			.934	.498	.294		.037	.081	.290			
2.19				.957	.680	.313	.341	.026	.101	.289	-.004	.012	.867
3.60	.626	1.159	.328	1.693	1.98	.427	.393	-.325		0.0	-.022	.026	.793
1.61	.423	2.039	.793	.981	.526	.378		.011	.067	.309			
2.14				1.022	.796	.467		-.005	.075	.354			
1.83	.381			1.038	.810	.377		-.016	.094	.283			
2.39				1.157	1.16	.611	.606	-.063	.043	.232	-.014	.009	.977
1.13	.541	0.5D	.608	.949	.449	.267		.029	.081	.262			
1.42	.385			.986	.794	.265		.013	.135	.257			
† 1.13	.431	.739	.608	.992	.506	.298		.008	.076	.272			
† 1.42	.551	2.073	.608	.882	.183	.241		.057	.052	.266			

† 256 particles

TABLE (VII-11).

$C_{P1}(t)$

T*	ρ*	Q*	L*	A	α $\times 10^{-2}\Delta t$	β $\times 10^{-1}\Delta t$	B	C	A $\times 10^{-1}\Delta t$
1.14	.541	.739	.608	.985	.156	.257	.009	.031	.227
1.41				.998	.201	.300	.005	.031	.262
1.45	.485			1.026	.290	.280	-.010	.045	.216
1.74				1.052	.366	.311	-.023	.043	.218
1.21	.546	1.321	.608	.981	.132	.293	.012	.023	.280
1.55				.988	.178	.313	.008	.028	.274
1.55	.490			1.029	.279	.344	-.011	.032	.250
1.81				1.035	.325	.332	-.015	.038	.235
1.50	.551	2.073	.608	.965	.0777	.276	.018	.018	.273
1.85				.972	.120	.322	.016	.020	.310
1.86	.494			.980	.170	.304	.013	.028	.287
2.19				.991	.234	.322	.007	.034	.282
3.60	.626	1.159	.328	1.012	.455	.258	-.004	0.39	.514
1.61	.423	2.039	.793	.995	.175	.392	.003	.021	.303
2.14				1.013	.277	.470	-.004	.025	.341
1.83	.381			1.017	.274	.389	-.007	.029	.272
2.39				1.063	.417	.597	-.026	.009	.206
1.13	.541	0.5D	.608	.986	.153	.274	.009	.028	.257
1.42	.485			1.021	.301	.261	-.008	.049	.229
† 1.13	.541	.739	.608	.999	.169	.305	.003	.025	.273
† 1.42	.551	2.073		.961	.0587	.259	.019	.017	.257

† 256 particles

From the tables, the constants B,C,D and E are a functions of both temperature and density, while the decay and frequency coefficients α, β, γ, ω_A and ω_B are to a first approximation, only a function of density. The variation of these parameters is very consistent and regular for $C_\omega(t)$, $C_2(t)$ and $C_1(t)$, suggesting that the parameters might vary in the form of a simple one or two term polynomial, in temperature and density for a given fixed quadrupole moment and bond length.

The inverse correlation times α, β and γ, and the frequency coefficients ω_A and ω_B all show the same type of behaviour; all increasing with increasing T^* and also increasing with increasing ρ^* for all the correlation functions studied, as was the case for previous estimates made earlier in this chapter. Thus in general a correlation function will decay more rapidly with the period of the damped oscillations becoming smaller as the temperature and/or density is increased. These gross effects can be simply predicted by mean kinetic energy versus free volume per particle arguments. The variation of these coefficients with bond length and quadrupole moment for $C_v(t)$, $C_{TQ}(t)$ and $C_\omega(t)$ is not simple, the coefficients β/ω_A and γ/ω_B being closely inter-related, preventing prediction of the way these parameters change individually. For $C_2(t)$ and $C_1(t)$, ω_A increases with increasing quadrupole moment, while the inverse correlation time decreases, which is not consistant with the variation with T^* and ρ^*. This might be explained by supposing that as the quadrupole moment increases, giving a more cohesive potential, the molecule is bound in a particular orientation longer, although to maintain its rotational energy it must oscillate about that position more rapidly.

The coefficients B, C, D and E do not consistantly vary with T^*, ρ^* or Q^*, and are possibly subject to significant changes for a very small change in correlation function shape. It can be seen that the

principle cosine character of the oscillation is determined by B, with the parameters C, D and E acting as correction terms. The same coefficients C and E tend to have opposite sign, acting as two interferring sine-waves which have very high damping.

12. Conclusion.

The analysis of the correlation functions in this chapter has shown the same effects on molecular motion as was seen in Chapter VI. The use of memory function analysis has enabled the correlation function to be analysed in terms of a relatively few parameters, which can be fitted, together with moments of the correlation function itself. These moments can be expressed as time-independent quantities such as $\langle r^2 \rangle$ and $\langle \tau^2 \rangle$ which theoretically may be obtained by integration over the spherical harmonics of the radial distribution function g(r). This time-independent function may then be approximately calculated from knowledge of the interaction potential, temperature and density only by a number of methods.

Random frequency modulation analysis is equivalent to memory function analysis, however in this case the correlation function is analysed in terms of its own cumulants. Again these cumulants are theoretically obtainable from the radial distribution function. This analysis can then be truncated after sufficient cumulants have been calculated for convergence. This method may also be used to test the gaussian character of calculated memory functions.

The two methods of analysis are equivalent. The memory function analysis must assume the final memory function to be a delta function for the method to be completely estimable from the radial distribution function, while the random frequency modulation analysis must assume that all cumulants beyond the truncation order are zero. The two methods should thus converge at the same rate, having an equivalent amount of information at any given level.

REFERENCES.

1. A. Isihara, "Statistical Physics", (Academic Press, New York, 1971).
2. A.I. Khinchin, "Mathematical Foundations of Statistical Mechanics" (Dover, New York, 1949).
3. H. Mori, Prog.Theor.Phys., 1965, 33, 423.
4. H. Mori, Prog.Theor.Phys., 1965, 34, 399.
5. W. Schmeidler, "Linear Operators in Hilbert Space", (Academic Press, New York, 1965).
6. H. Wall, "The Analytic Theory of Continued Fractions", (Van Nostrand, Princeton, 1948).
7. R. Kubo, J.Math.Phys., 1963, 4, 174.
8. R. Kubo, in "Fluctuation, Relaxation and Resonance in Magnetic Systems", (Ed: D. ter Hoar, Oliver & Boyd, Edinburgh, 1962).
9. R. Kubo, in "Lectures in Theoretical Physics" Vol.1 (Ed: W.E. Britten and L.G. Dunham) (Interscience, New York, 1959).
10. M. Tokuyama and H. Mori, Prog.Theor.Phys., 1976, 55, 411.
11. F.J. Dyson, Phys.Rev., 1949, 75, 486.
12. N.G. Van Kampen, Phys.Rep., 1976, 24C, 171.
13. R.W. Zwanzig, in "Lectures in Theoretical Physics" Vol.3, (Ed: W.E. Britten and L.G. Dunham) (Interscience, New York, 1961).
14. E. Detyna, K. Singer and J.V.L. Singer, Mol.Phys., 1980, 41, 31.
15. P. Martin and S. Yip, Phys.Rev., 1968, 170, 151.
16. B.J. Berne and G.D. Harp, Adv.Chem.Phys., 1970, 17, 63.
17. D. Chandler, J.Chem.Phys., 1974, 60, 3500.
18. D. Chandler, J.Chem.Phys., 1974, 60, 3508.
19. R. Kubo, J.Phys.Soc.Japan, 1962, 17, 1100.

APPENDIX (V11A).

Memory Function Numerical Solution Methods.

(V11A-1) Generation of Memory functions.

The numerical methods for the solution of the memory function equation given by (A-1) are due

$$\dot{F}(t) = -\int_0^t M(s)F(t-s)\,ds \qquad (A\text{-}1)$$

to Detyna (1,2). The solution for M(t) from any given F(t) is found by differentiating equation (A-1) giving

$$\ddot{F}(t) = -F(0)M(t) - \int_0^t \dot{F}(t-s)M(s)\,ds \qquad (A\text{-}2)$$

which can then be rearranged to give

$$M(t) = -\frac{1}{F(0)}\left[\ddot{F}(t) + \int_0^t M(s)\dot{F}(t-s)\,ds\right] \qquad (A\text{-}3)$$

In the t=0 limit equation (A-3) becomes

$$M(0) = -\frac{\ddot{F}(0)}{F(0)} \qquad (A\text{-}4)$$

For a numerical solution to be obtainable, F(t) is assumed to be continuous and single valued. The first two derivatives are also assumed to be continuous, however odd derivatives may posess a single discontinuity at t=0. Further $\Delta = \dot{F}(0)$ must be known, before a solution can be found. If F(t) is an even function then all odd order derivatives at t=0 are zero, thus $\Delta = 0$.

Noting the identity (A-5) it is now possible to

$$\frac{d}{dt} F(t) = - \frac{d}{ds} F(t-s) \qquad \text{(A-5)}$$

solve equation (A-3) assuming $\Delta = 0$.

Let F(t) be an equidistantly tabulated function of (N+1) points at 0, Δt, $2\Delta t$,...., $N\Delta t$. Then the ith value of the memory function is given by

$$M_i = \frac{1}{F(0)} \left| \ddot{F}_i + \int_0^i d_j M_j \dot{F}_{(i-j)} \right| \qquad \text{(A-6)}$$

Where the notation

$$\int_k^1 dm \equiv \Delta t \int_{k\Delta t}^{1\Delta t} dm \equiv \int_a^b ds$$

is used to denote numerical integration between points k and 1, over index m, in such a way that the error in evaluating the integral is minimized, i.e. Trapezoid rule used for two points and Simpson's rule for higher number of points. The numerical second derivative in equation (A-6) can be evaluated using interpolation formulae or polynominal methods. Increased accuracy for small t can be obtained by noting that F is an even function to supply extra points. The integral sum in equation (A-6) is evaluated over i points $\dot{F}_o M_i$, $\dot{F}_1 M_{(i-1)}$,....,$\dot{F}_i M_o$, using $\dot{F}_o = 0$, and is thus dependent on only the preceeding (i-1) values of M(t). The accuracy of this method is dependent on the spacing Δt of the values of F(t), determining the accuracy of the second derivative and integral in equation (A-6). The details and relative accuracy of these methods is discussed by Hamming (3) and Margenau and Murphy (4).

The method is simply extended to non-zero first derivatives of F(t). Suppose

$$\dot{F}(0) = - \Theta F(0) \tag{A-7}$$

then equation (A-1) becomes

$$\dot{F}(t) = - \int_0^t [M(s) + \Theta\delta(s)] F(t-s) \, ds \tag{A-8}$$

which on differentiation and rearrangement becomes

$$M(t) = - \frac{1}{F(0)} [\ddot{F}(t) + \Theta\dot{F}(t) + \int_0^t M(s)\dot{F}(t-s) \, ds] \tag{A-9}$$

whose solution is as before with the additional $\Theta\dot{F}(t)$ term added.

The solution method can be further generalized to equations of the form

$$\dot{F}(t) = - \Theta F(t) - \int_0^t M(s)F(t-s) \, ds + B(t) \tag{A-10}$$

where B(t) is any single valued continuous function which is differentiable. Again on differentiation and rearrangement equation (A-10) yields

$$M(t) = \frac{-1}{F(0)} [\ddot{F}(0) + \Theta\dot{F}(t) + \int_0^t M(s)\dot{F}(t-s) \, ds - \dot{B}(t)] \tag{A-11}$$

which is solved as before with the term $(-\dot{B}(t))$ added.

(VIIA-11). Regeneration of Relaxation Functions.

The method for regenerating F(t) from a specified M(t) is also due to Detyna (1). This involves expanding equation (A-1) into a system of interdependent equations (A-12), (A-13), (A-14)

and (A-15). For these equations to be soluable the memory function M(t) and its first derivative must be supplied together with values for F(0) and $\Delta = \dot{F}(0)$ as before.

$$F(t) = \int_0^t F(t)\,dt + F(0) \tag{A-12}$$

$$\dot{F}(t) = -\int_0^t F(t-s)M(s)\,ds \tag{A-13}$$

$$\ddot{F}(t) = -F(0)M(t) - \int_0^t \dot{F}(t-s)M(s)\,ds \tag{A-14}$$

$$\dddot{F}(t) = -\dot{M}(t)F(0) - \dot{F}(0)M(t) - \int_0^t \ddot{F}(t-s)M(s)\,ds \tag{A-15}$$

From this, noting that $\dot{F}(0)M(t) = 0$ for even functions

$$\begin{aligned} \ddot{F}(0) &= -F(0)M(0) \\ \dddot{F}(0) &= -F(0)\dot{M}(t) \end{aligned} \tag{A-16}$$

The equations are then solved as four simultaneous equations in four unknowns $F(t)$, $\dot{F}(t)$, $\ddot{F}(t)$ and $\dddot{F}(t)$.

This is done using matrix methods, and approximating the convolution integrals over (i-1) points, as before, since the values of F(i-1) have been previously calculated. Now the value of the integral between limits a and b of g(x) can be numerically approximated by

$$\int_a^b g(x)dx = \frac{h}{2}(g_b+g_a) + \frac{h^2}{10}(\dot{g}_a-\dot{g}_b) + \frac{h^3}{120}(\ddot{g}_b+\ddot{g}_a) \tag{A-17}$$

This form may now be used to approximate the convolution integrals in the range between the (i-1) and i^{th} points, where h is the distance between points in this case taken to be 1. Also full use of the equivalence is made

$$\int_o^i d_j F_{(i-j)} M_j \equiv \int_o^i d_j F_j M_{(i-j)} \equiv \int_o^{(i-1)} d_j F_j M_{(i-j)} + \int_{(i-1)}^i F_j M_{(i-j)} \tag{A-18}$$

Putting $\Delta t=1$, this now gives

$$F_i = F_o + \int_o^{(i-1)} d_j F_j + \tfrac{1}{2}(F_i + F_{(i-1)}) + \frac{1}{10}(\dot{F}_i + \dot{F}_{(i-1)})$$

$$+ \frac{1}{120}(\ddot{F}_i + \ddot{F}_{(i-1)}) \tag{A-19}$$

$$\dot{F}_i = - \int_o^{(i-1)} d_j F_j M_{(i-j)} - \tfrac{1}{2}(F_i M_o + M_1 F_{(i-1)})$$

$$- \frac{1}{10}(\dot{F}_i M_o + \dot{M}_o F_i + M_1 \dot{F}_{(i-1)} + \dot{M}_1 (F_{(i-1)})$$

$$- \frac{1}{120}(\ddot{F}_i M_o + 2\dot{F}_i \dot{M}_o + \ddot{M}_o F_i$$

$$+ M_1 \ddot{F}_{(i-1)} + \dot{M}_1 \dot{F}_{(i-1)} + \ddot{M}_1 F_{(i-1)}) \tag{A-20}$$

$$\ddot{F}_i = - F_o M_i - \int_o^{(i-1)} d_j \dot{F}_j M_{(i-j)} - \tfrac{1}{2}(\dot{F}_i M_o + M_1 \dot{F}_{(i-1)})$$

$$- \frac{1}{10}(\ddot{F}_i M_o + \dot{F}_i \dot{M}_o + \ddot{M}_1 F_{(i-1)} + M_1 \ddot{F}_{(i-1)} + \dot{M}_1 \dot{F}_{(i-1)})$$

$$- \frac{1}{120}(\dddot{F}_i M_o + 2\ddot{F}_i \dot{M}_o + \dot{F}_i \ddot{M}_o$$

$$+ \dot{M}_1 \ddot{F}_{(i-1)} + 2\dot{M}_1 \dot{F}_{(i-1)} + \ddot{M}_1 \dot{F}_{(i-1)}) \tag{A-21}$$

$$\dddot{F}_i = - F_o\dot{M}_i - \dot{F}_o M_i - \int_o^{(i-1)} d_j \ddot{F}_j M_{(i-j)} - \tfrac{1}{2}(\ddot{F}_i M_o + M_1 \ddot{F}_{(i-1)})$$

$$- \frac{1}{12}(\dddot{F}_i M_o + \ddot{F}_i \dot{M}_o + M_1 \dddot{F}_{(i-1)} + \dot{M}_1 \ddot{F}_{(i-1)}) \qquad \text{(A-22)}$$

where the values of $\ddot{M}_o$ and $\ddot{M}_1$ are accurately estimated from the values of the supplied memory function and its first derivative, by interpolation or polynomial methods of reconstruction. Collecting up the terms these equations may now be recast in the form

$$\begin{aligned}
F_i &= \alpha_1 + \beta_1 F_1 + \gamma_1 \dot{F}_1 + \delta_1 \ddot{F}_i \\
\dot{F}_i &= \alpha_2 + \beta_2 F_i + \gamma_2 \dot{F}_i + \delta_2 \ddot{F}_i \\
\ddot{F}_i &= \alpha_3 + \gamma_3 \dot{F}_i + \delta_3 \ddot{F}_i + \varepsilon_3 \dddot{F}_i \\
\dddot{F}_i &= \alpha_4 + \delta_4 \ddot{F}_i + \varepsilon_4 \dddot{F}_i
\end{aligned} \qquad \text{(A-23)}$$

which can be put in matrix form

$$\begin{bmatrix} \beta_1 & \gamma_1 & \delta_1 & 0 \\ \beta_2 & \gamma_2 & \delta_2 & 0 \\ 0 & \gamma_3 & \delta_3 & \varepsilon_3 \\ 0 & 0 & \delta_4 & \varepsilon_4 \end{bmatrix} \begin{bmatrix} F_i \\ \dot{F}_i \\ \ddot{F}_i \\ \dddot{F}_i \end{bmatrix} = \begin{bmatrix} \alpha_1 \\ \alpha_2 \\ \alpha_3 \\ \alpha_4 \end{bmatrix}$$

or

$$\underset{\approx}{C}.\underset{\sim}{F} = \underset{\sim}{\alpha} \tag{A-25}$$

whose solution is given by

$$\underset{\sim}{F} = \underset{\approx}{C}^{-1}.\alpha \tag{A-26}$$

or, if the determinant is non-zero, applying Cramer's rule

$$F_i^{\,k} = \frac{D_k}{|C|} \tag{A-27}$$

where $|C|$ is the determinant of the matrix C, and D_k is the determinant formed by replacing the elements of the r^{th} column of C by $(\alpha_1 \ldots . \alpha_k)$.

The method may again be generalized to regenerate F(t) from equations of the type of (A-10). This is accomplished by the simple addition of these terms in equations (A-12) to (A-15) to give

$$F(t) = \int_o^t \dot{F}(t)\, dt + F(0) \tag{A-28}$$

$$\dot{F}(t) = -\Theta F(t) - \int_o^t M(s)F(t-s)ds + B(t) \tag{A-29}$$

$$\ddot{F}(t) = -\Theta\dot{F}(t) - F(0)M(t) - \int_o^t M(s)\dot{F}(t-s)ds + \dot{B}(t) \tag{A-30}$$

$$\dddot{F}(t) = -\Theta\ddot{F}(t) - \dot{M}(t)F(0) - \dot{F}(0)M(t) - \int_o^t M(s)\ddot{F}(t-s)ds + \ddot{B}(t) \tag{A-31}$$

which can simply be solved by the technique already outlined with the following substitutions

$$\alpha_2' = \alpha_2 + B_i \; ; \qquad \alpha_3' = \alpha_3 + \dot{B}_i$$

$$\alpha_4' = \alpha_4 + \ddot{B}_i \; ; \qquad \beta_2' = \beta_2 - \Theta$$

$$\gamma_3' = \gamma_3 - \Theta \; ; \qquad \delta_4' = \delta_4 - \Theta \qquad \text{(A-32)}$$

In this case B(t) is any twice differentiable continuous single-valued function.

The prime factor effecting the accuracy of the solution of the generation and regeneration, is the spacing of the equidistant points Δt, which should be as small as possible. The size of Δt should be small enough to allow accurate calculation of the second derivatives of functions, which also implies that for this method the functions themselves should be well behaved.

References.

1) E. Detyna - Private Communication.

2) E. Detyna, K. Singer, J.V.L. Singer and A.J. Taylor - Mol.Phys. 1980, 41, 31.

3) R.W. Hamming - "Numerical Methods for Scientists and Engineers" (2nd Ed. - McGraw-Hill - New York - 1973).

4) H. Margenau and G.M. Murphy - "The Mathematics of Physics and Chemistry", p.472ff. (2nd Ed. - Van Nostrand - New York 1964).

Figures.

(VII-1) Solid line $C_v(t)$: Broken line $\phi_1(t)$ of $C_v(t)$ - Horizontal axis - Time in seconds $\times 10^{-12}$ for L* = 0.608, Q* = 0.739, ρ* = 0.541, T* = 1.14.

(VII-2) As for (VII-1) at L* = 0.608, Q* = 1.321, ρ* = 546, T* = 1.21.

(VII-3) As for (VII-1) at L* = 0.608, Q* = 2.073, ρ* = 0.551, T* = 1.50

(VII-4) As for (VII-1) at L* = 0.328, Q* = 1.159, ρ* = 0.700, T* = 1.61

(VII-5) As for (VII-1) at L* = 0.793, Q* = 2.039, ρ* = 0.423, T* = 1.61

(VII-6) Solid line ($C_1(t)$: Horizontal axis - Time in seconds $\times 10^{-12}$

———— ———— $C_2(t)$

—— —— —— —— Normalized $\phi_1(t)$ of $C_1(t)$

———————— Normalized $\phi_2(t)$ of $C_1(t)$

as L* = 0.608, Q* = 0.739, ρ* = 0.541, T* = 1.14

(VII-7) As for (VII-6) at L* = 0.608, Q* = 1.321, ρ* = 0.546, T* = 1.21

(VII-8) As for (VII-6) at L* = 0.608, Q* = 2.073, ρ* = 0.551, T* = 1.50

(VII-9) As for (VII-6) at L* = 0.328, Q* = 1.159, ρ* = 0.700, T* = 1.61

(VII-10) As for (VII-6) at L* = 0.793, Q* = 2.039, ρ* = 0.423, T* = 1.61

(VII-11) Solid line $C_\omega(t)$: Solid line $C_T(t)$ - Faster initial decay Horizontal axis - Time in seconds $\times 10^{-12}$

—— —— —— —— $\phi_1(t)$ of $C_\omega(t)$

———————— $\phi_{basis}(t)$

at L* = 0.608, Q* = 0.739, ρ* = 0.541, T* = 1.14

(VII-12) As for (VII-11) at L* = 0.608, Q* = 1.321, ρ* = 0.546, T* = 1.21

(VII-13) As for (VII-11) at L* = 0.608, Q* = 2.073, ρ* = 0.551, T* = 1.50

(VII-14) As for (VII-11) at L* = 0.328, Q* = 1.159, ρ* = 0.700, T* = 1.61

(VII-15) As for (VII-11) at L* = 0.793, Q* = 2.039, ρ* = 0.423, T* = 1.61

(VII-16) Memory Function Heirarchy for Rotational Motion - See Text.

(VII-17) Memory Function Heirarchy for Translational Motion - See Text.

(VII-18) Solid line $C_v(t)$

Horizontal axis - Time in seconds $\times 10^{-12}$

——— ——— ——— Berne and Harp Gaussian II Memory function fit

— — — — — — — Best fit to $M(t) = e^{-t/\tau_1} + \alpha t^2 e^{-t/\tau_2}$

for L* = 0.608, Q* = 0.739, ρ* = 0.541, T* = 1.14

(VII-19) As for (VII-18) at L* = 0.608, Q* = 1.321, ρ* = 0.546, T* = 1.21

(VII-20) As for (VII-18) at L* = 0.608, Q* = 2.073, ρ* = 0.551, T* = 1.50

(VII-21) As for (VII-18) at L* = 0.328, Q* = 1.159, ρ* = 0.700, T* = 1.61

(VII-22) As for (VII-18) at L* = 0.793, Q* = 2.039, ρ* = 0.423, T* = 1.61

(VII-23) Solid lines $C_1(t)$ and $C_\omega(t) - C_\omega(t)$ has faster initial decay.

——— ——— ——— Berne and Harp Gaussian II Memory function fit

— — — — — — — Best fit to $M(t) = e^{-t/\tau_1} + \alpha t^2 e^{-t/\tau_2}$

for L* = 0.608, Q* = 0.739, ρ* = 0.541, T* = 1.14

(VII-24) As for (VII-23) at L* = 0.608, Q* = 1.321, ρ* = 0.546, T* = 1.21

(VII-25) As for (VII-23) at L* = 0.608, Q* = 2.073, ρ* = 0.551, T* = 1.50

(VII-26) As for (VII-23) at L* = 0.328, Q* = 1.159, ρ* = 0.700, T* = 1.61

(VII-27) As for (VII-23) at L* = 0.793, Q* = 2.039, ρ* = 0.423, T* = 1.61

(VII-28) Solid line $C_{||}(t)$: Horizontal Axis - Time in seconds $\times 10^{-12}$

——— ——— $C_\perp(t)$

——— ——— ——— $\phi_1(t)$ of $C_{||}(t)$

— — — — — — — — $\phi_1(t)$ of $C_\perp(t)$

for L* = 0.608, Q* = 0.739, ρ* = 0.541, T* = 1.14

(VII-29) As for (VII-28) at L* = 0.328, Q* = 1.159, ρ* = 0.700, T* = 1.61

(VII-30) As for (VII-29) at L* = 0.793, Q* = 2.039, ρ* = 0.423, T* = 1.61

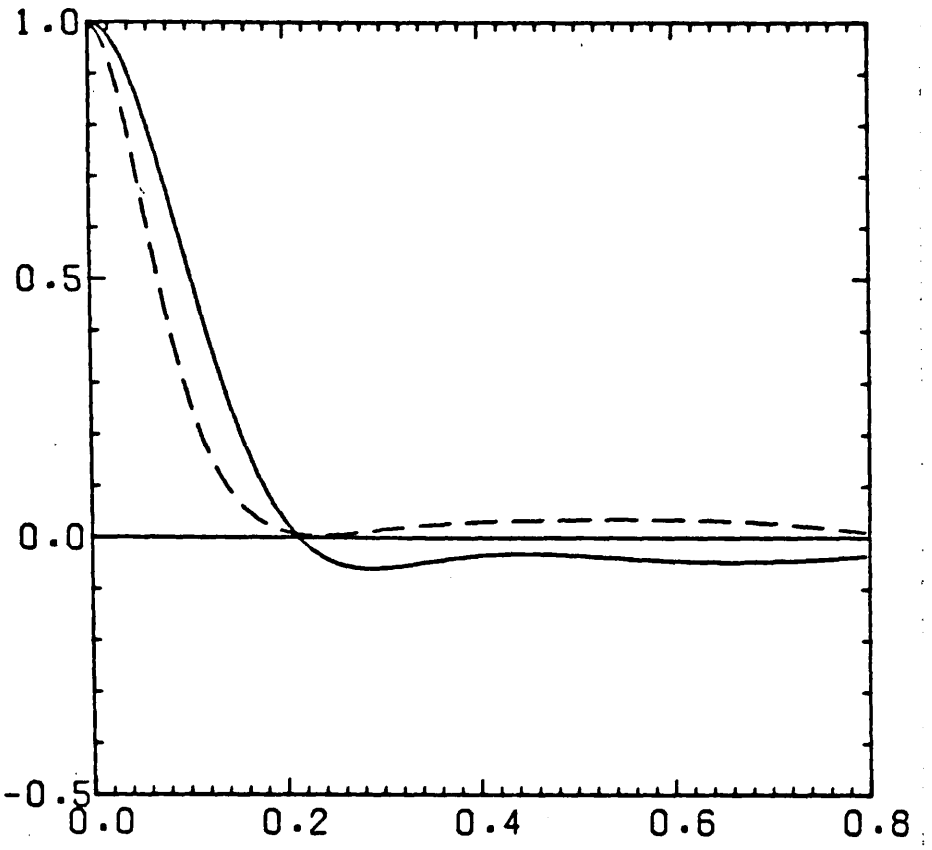

Figure (VII-1)

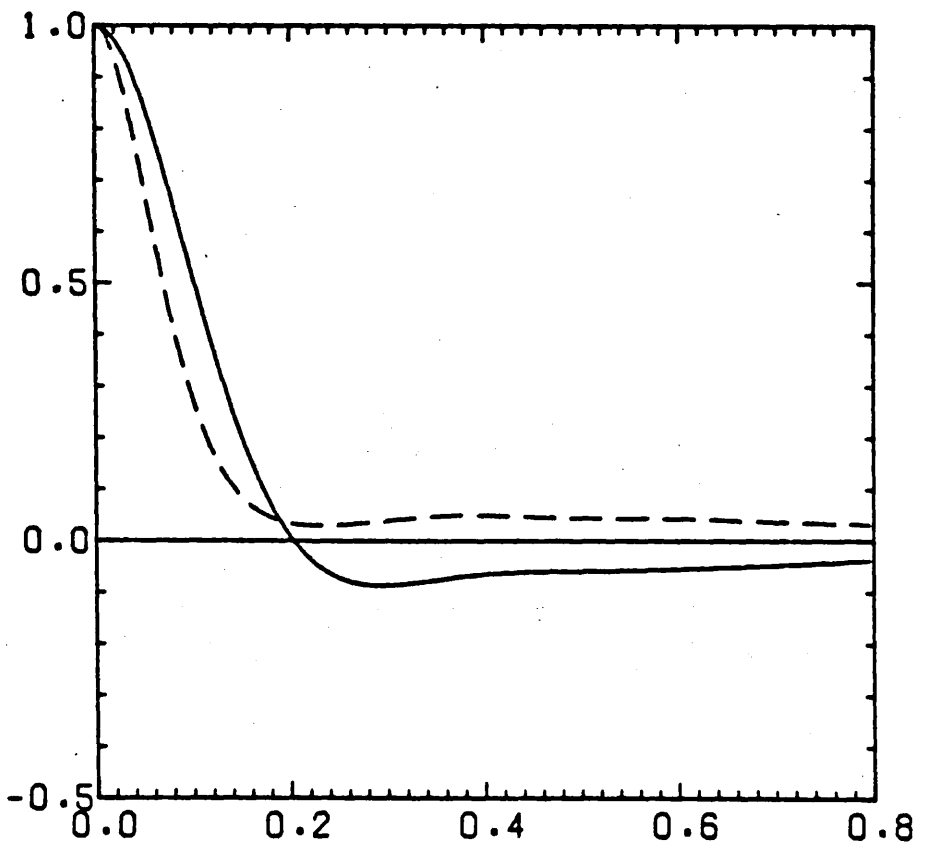

Figure (VII-2)

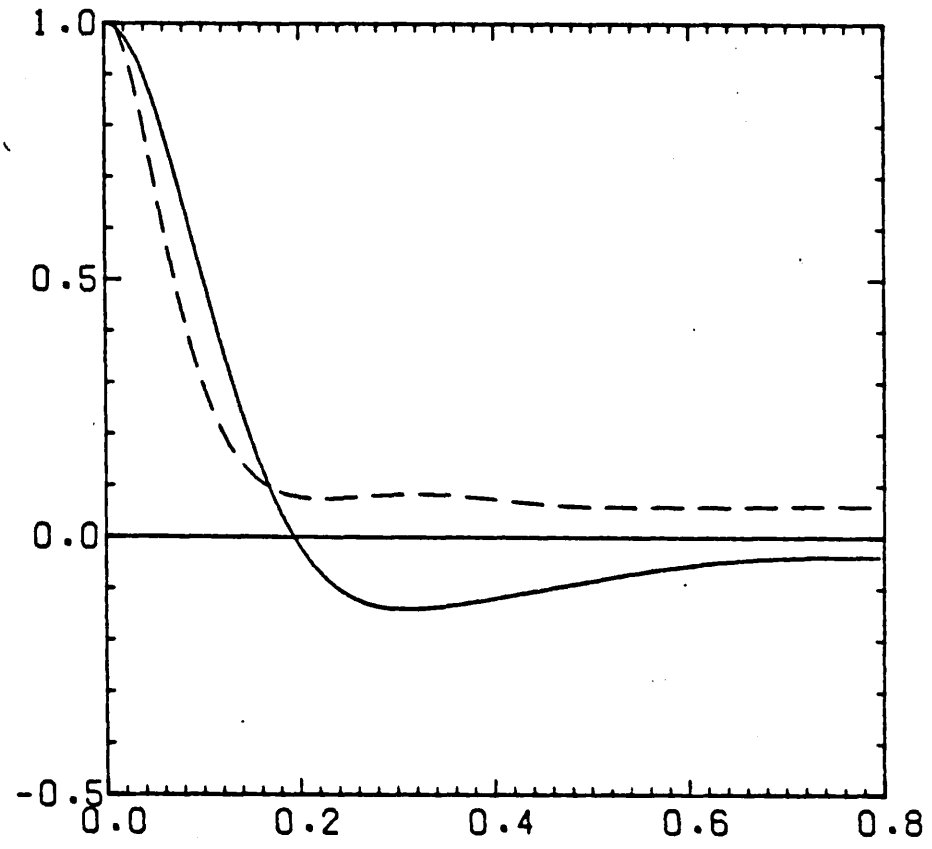

Figure (VII-3)

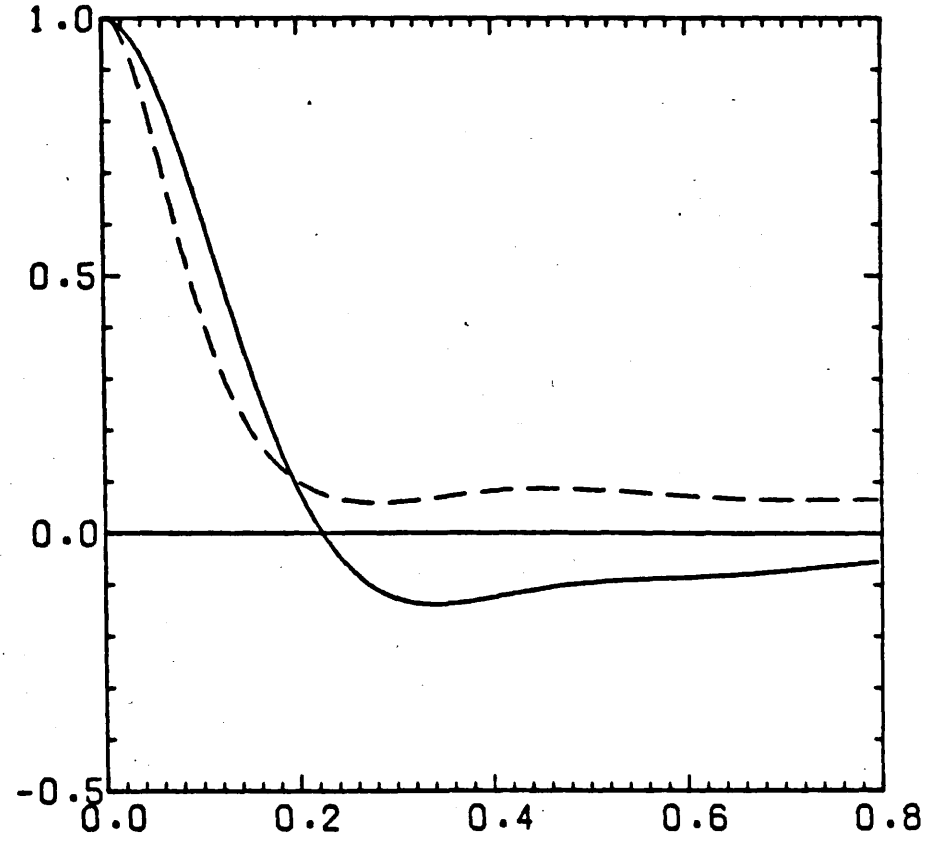

Figure (VII-4)

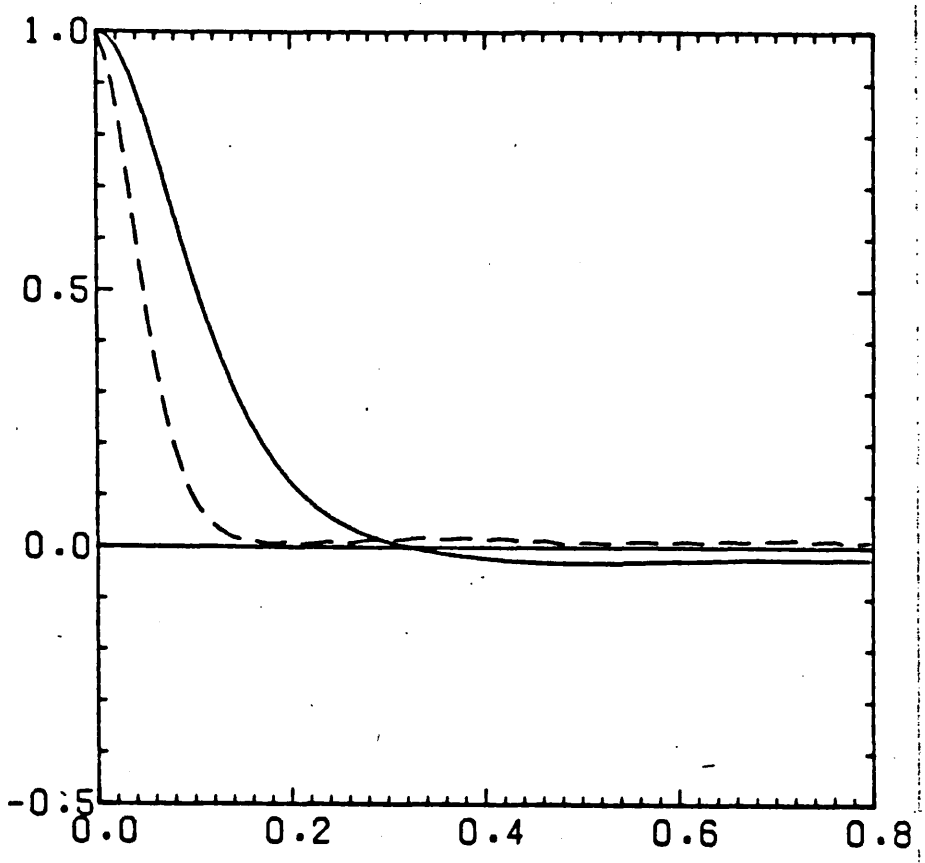

Figure (VII-5)

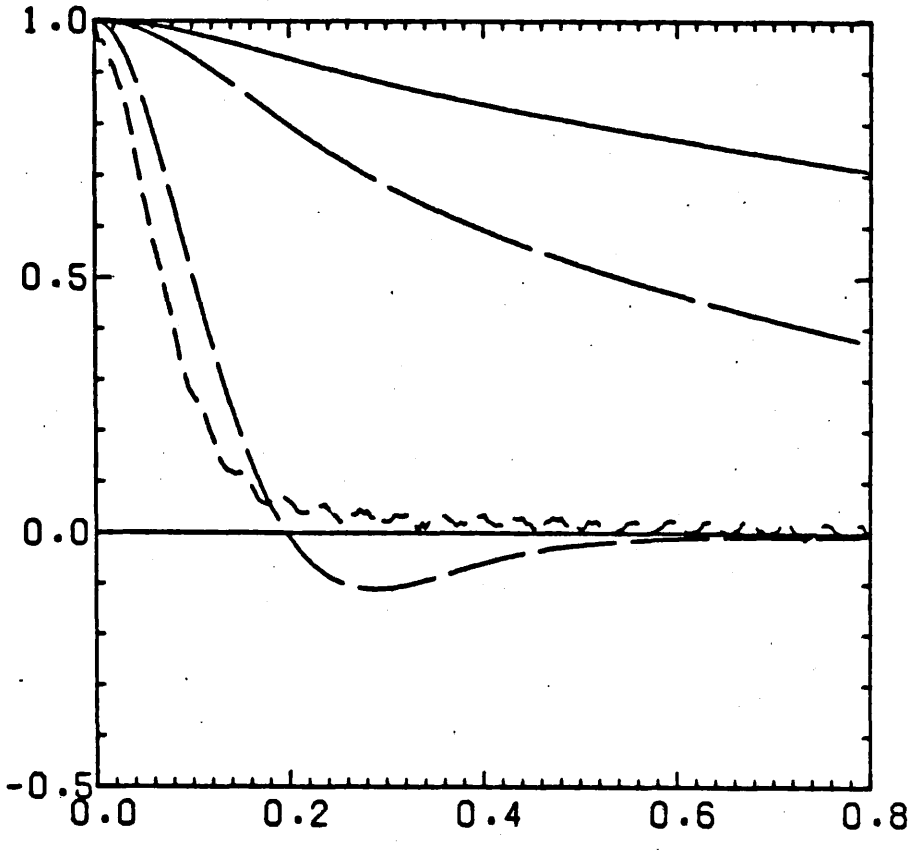

Figure (VII-6)

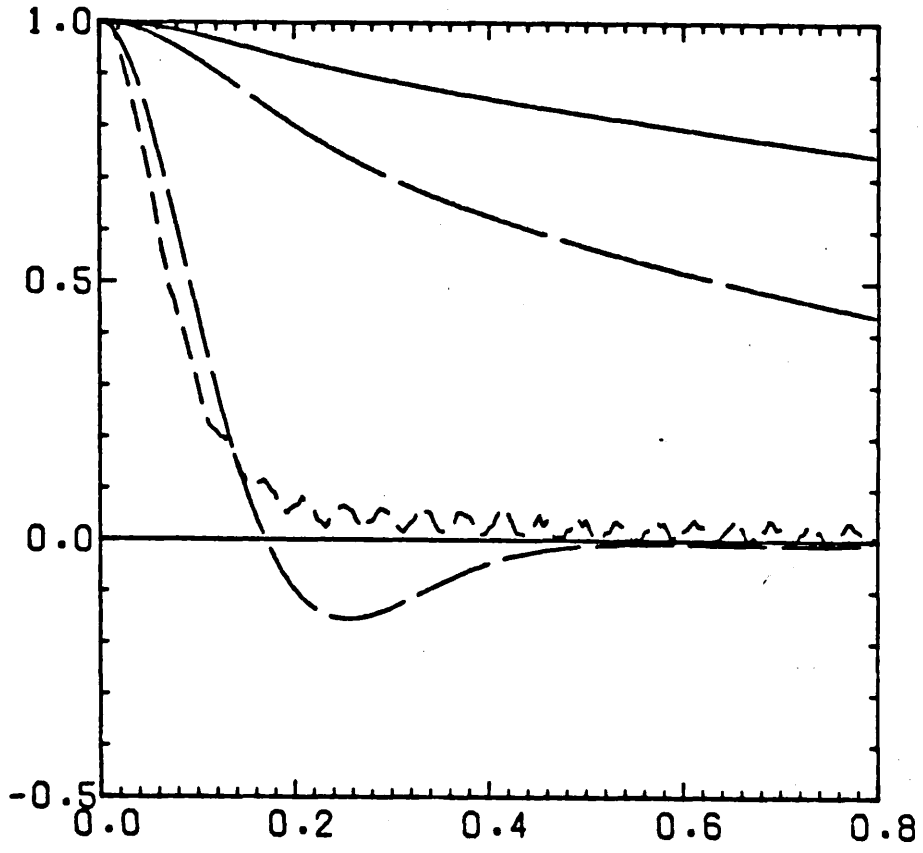

Figure (VII-7)

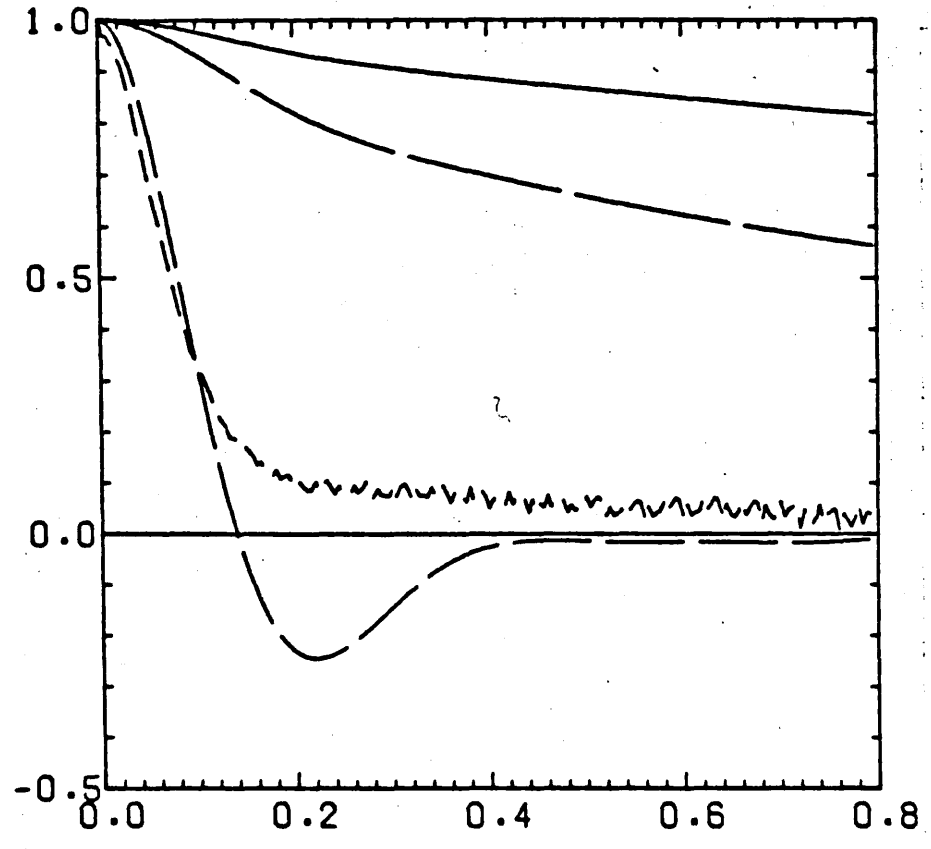

Figure (VII-8)

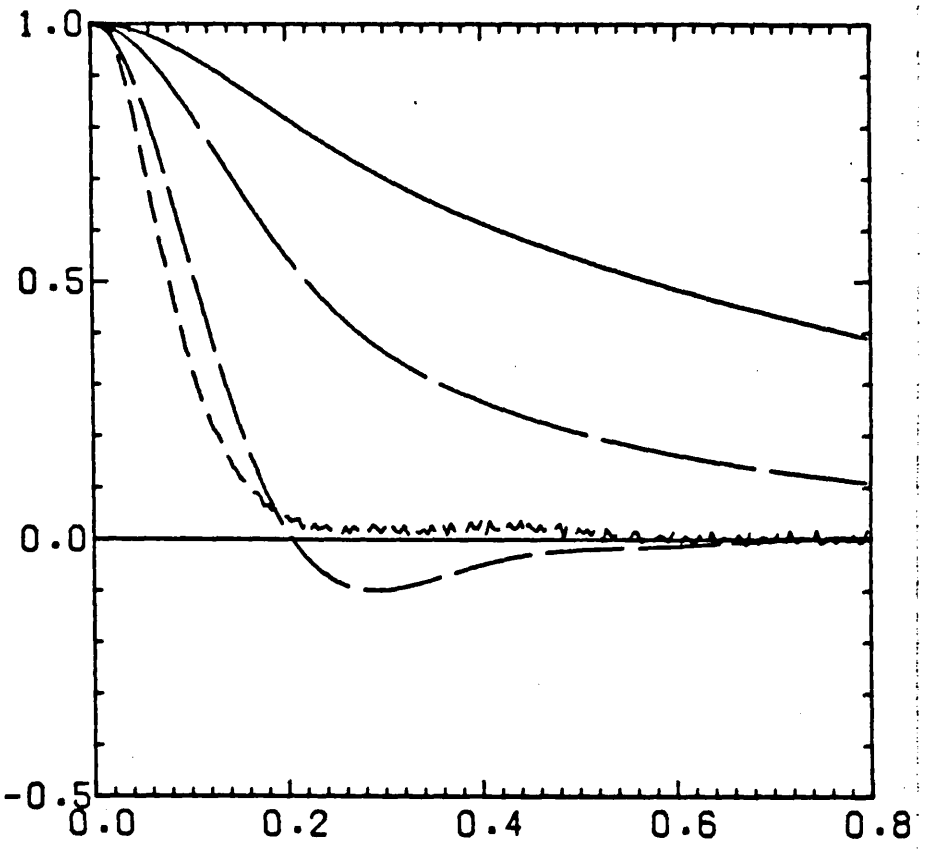

Figure (VII-9)

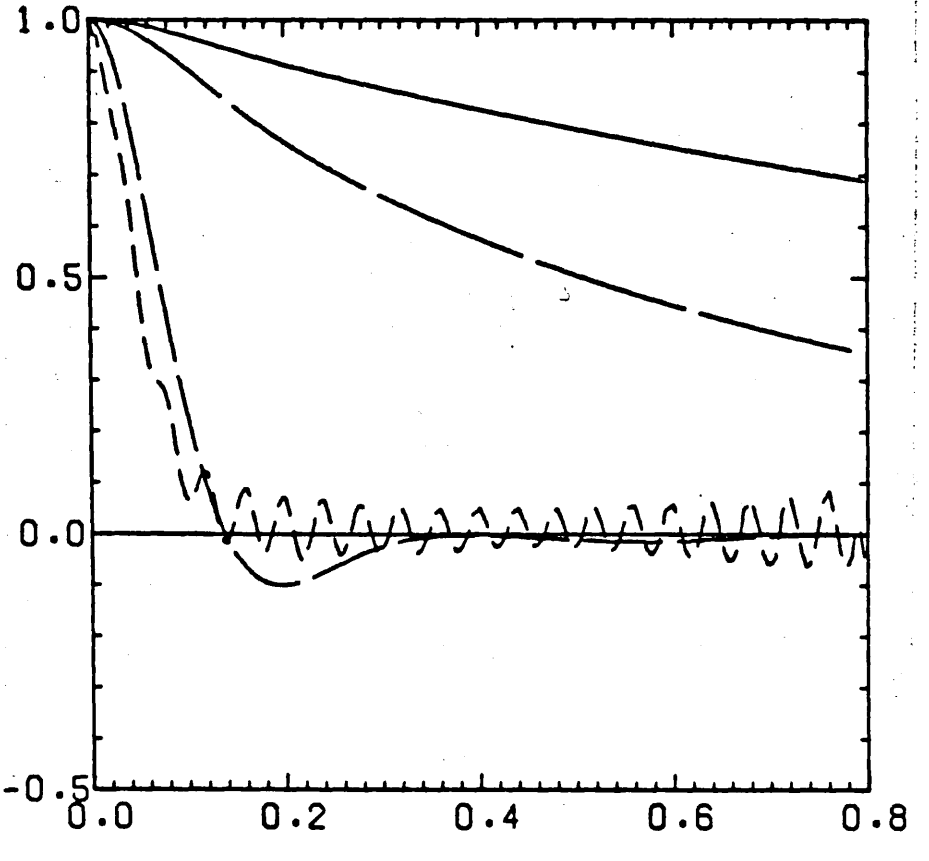

Figure (VII-10)

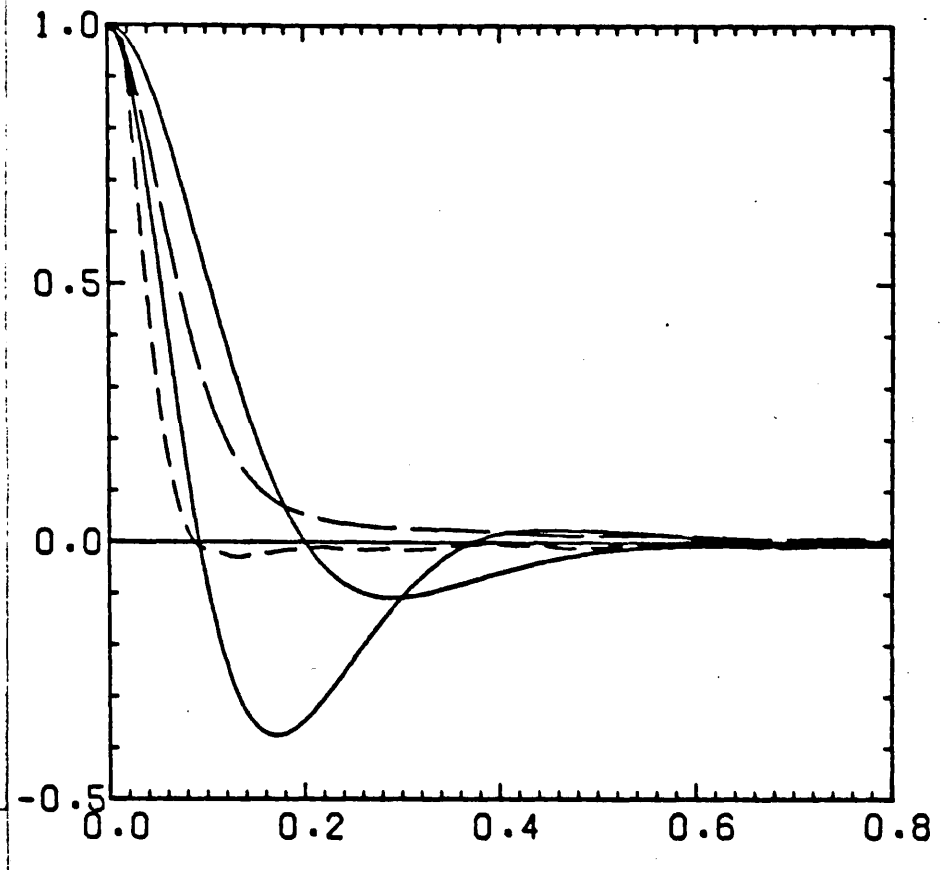

Figure (VII-11)

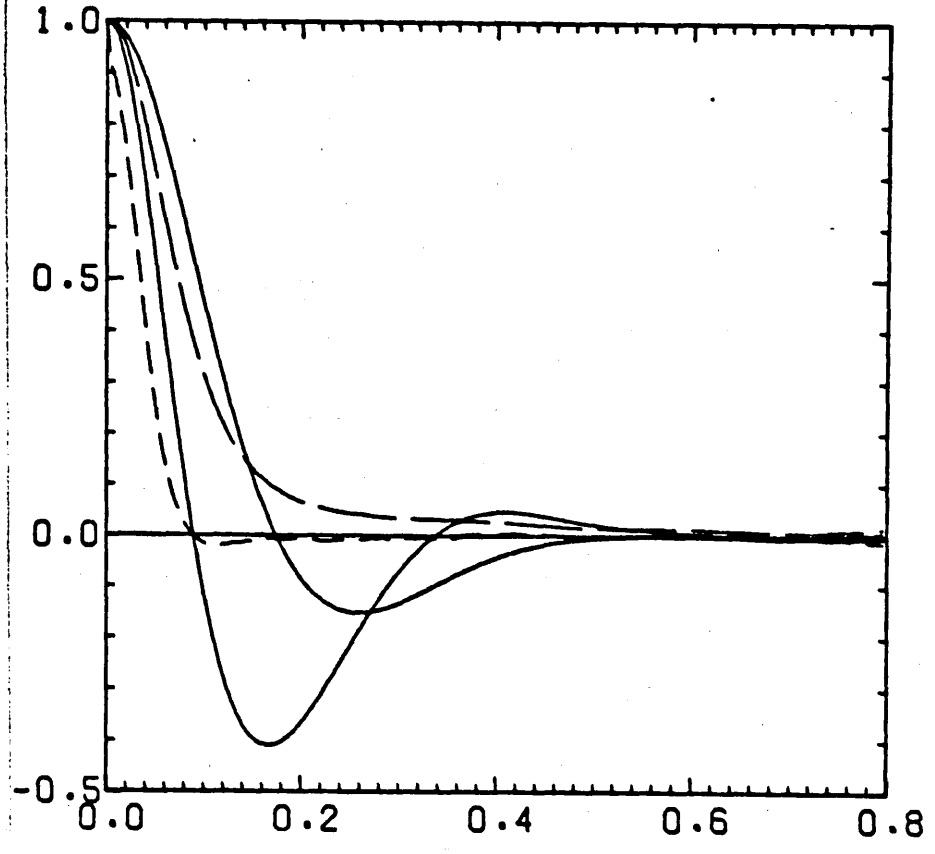

Figure (VII-12)

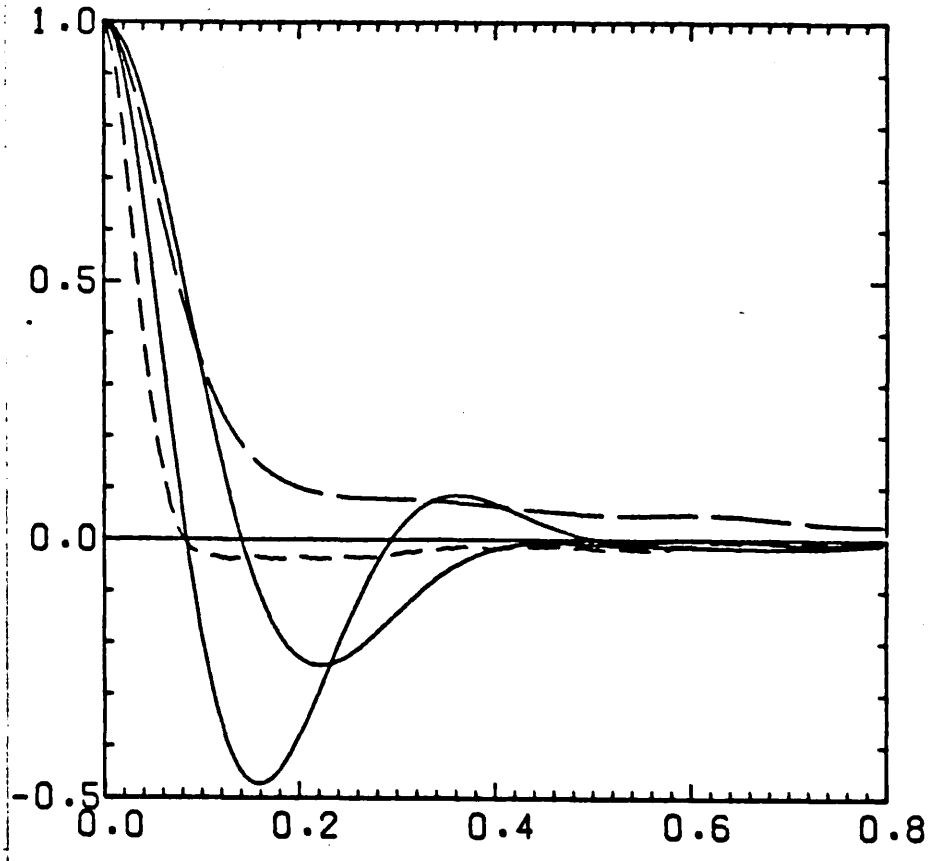

Figure (VII-13)

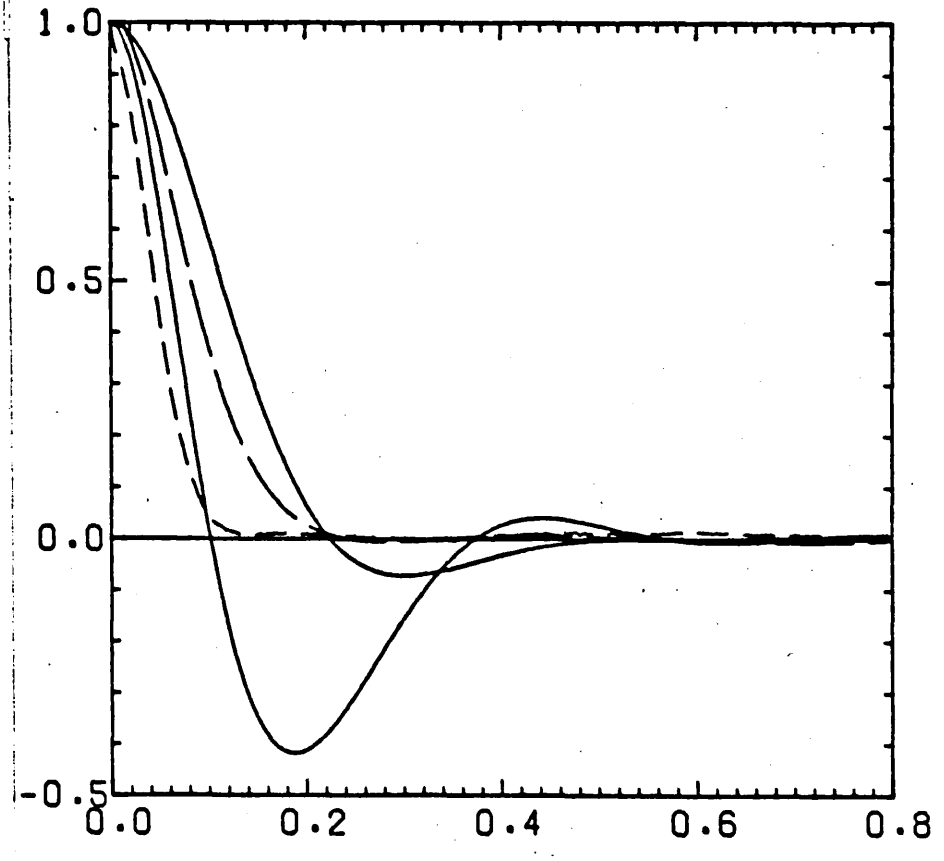

Figure (VII-14)

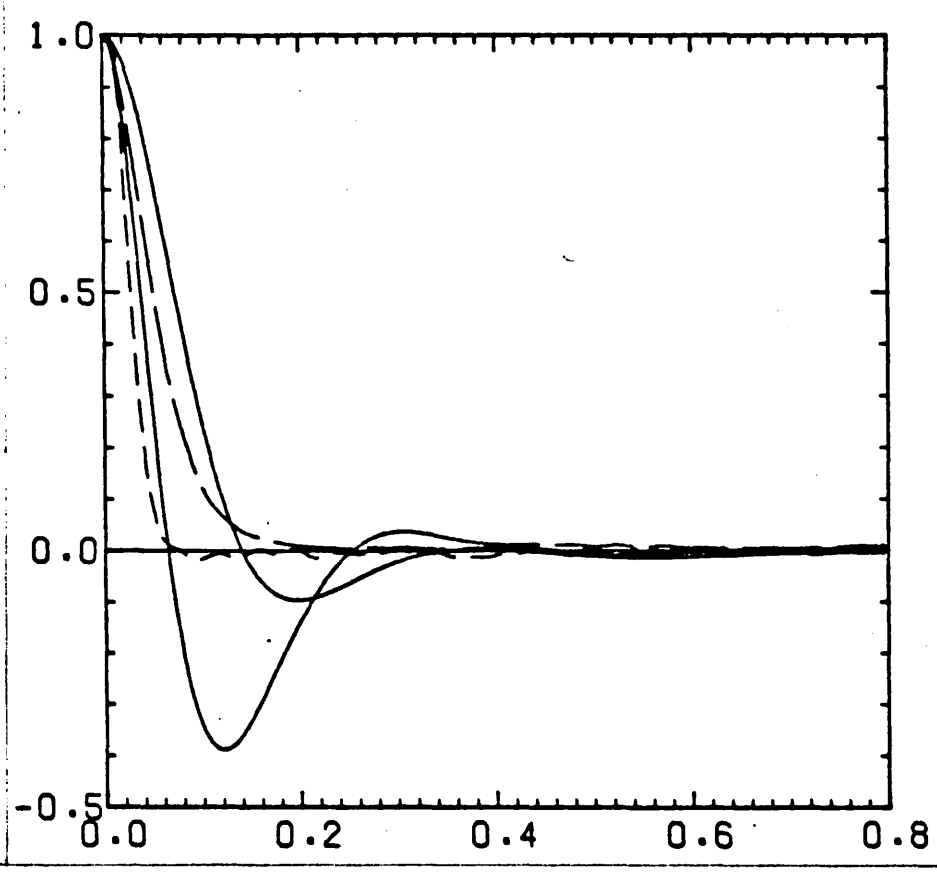

Figure (VII-15)

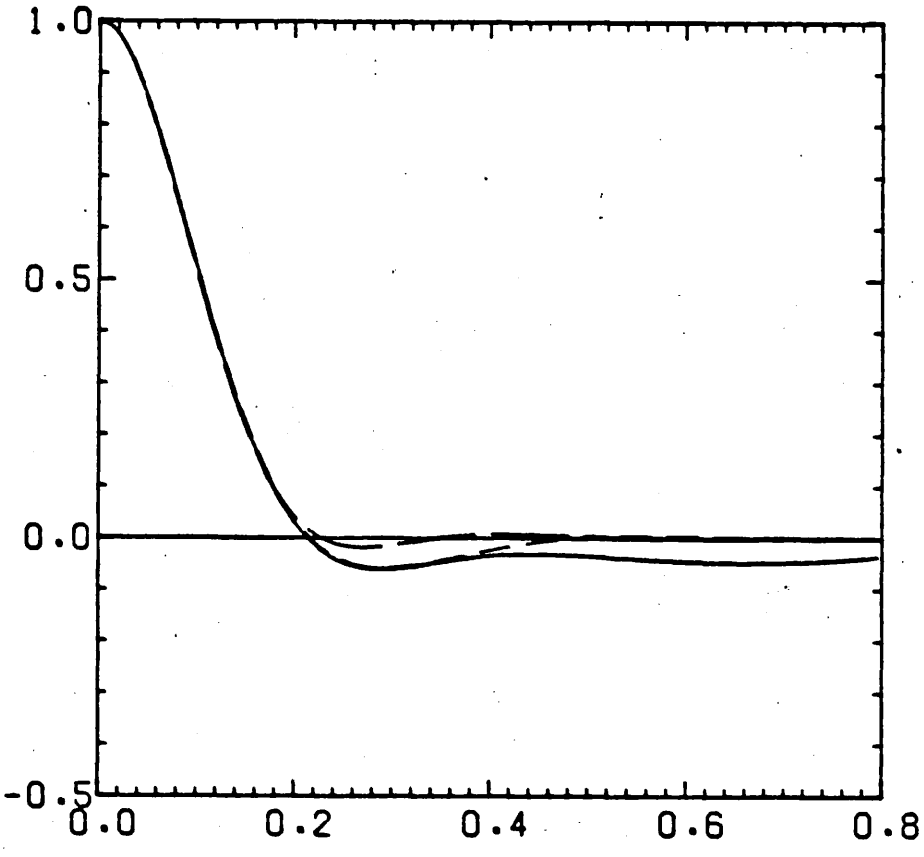

Figure (VII-18)

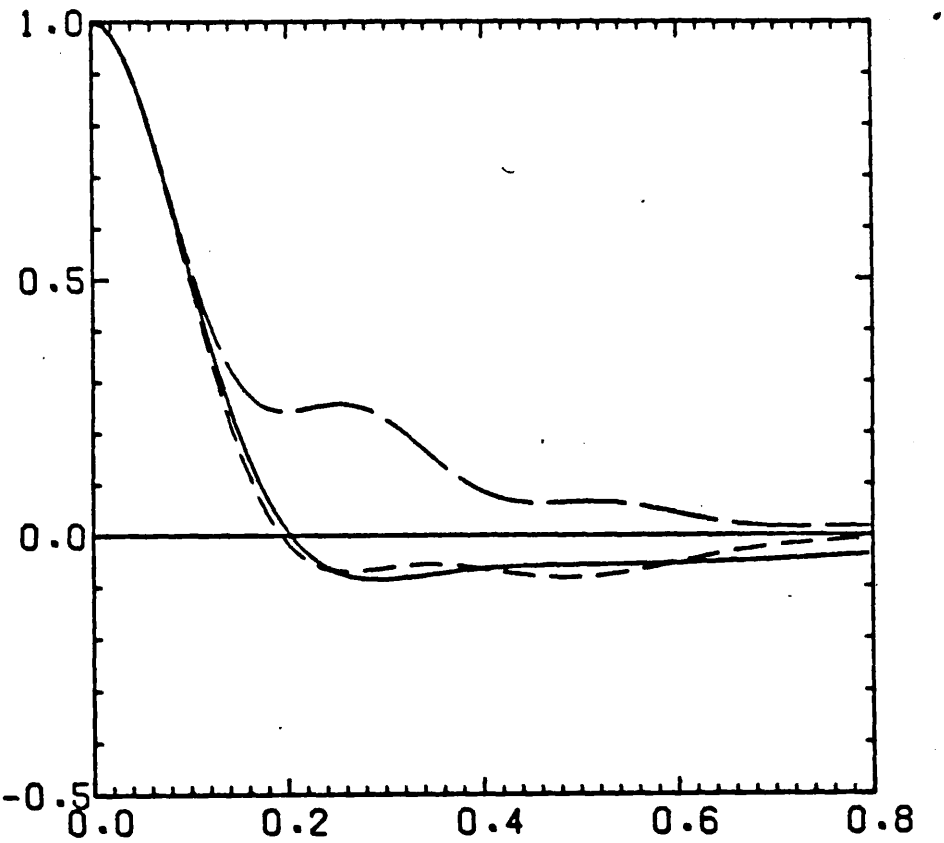

Figure (VII-19)

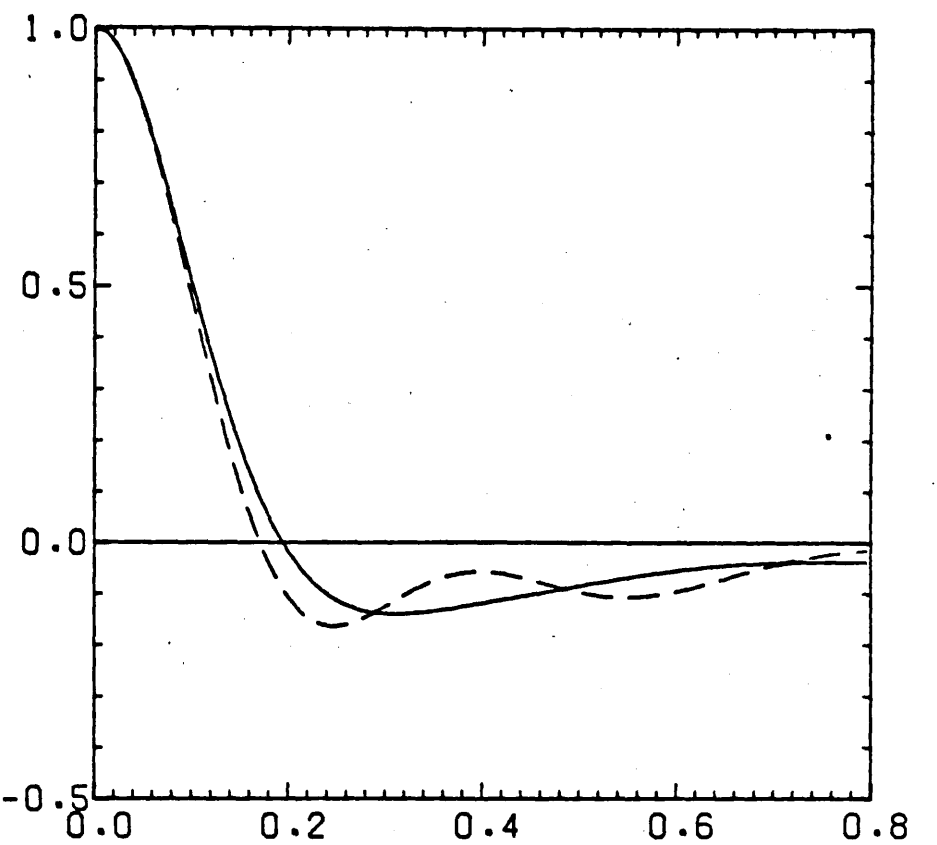

Figure (VII-20)

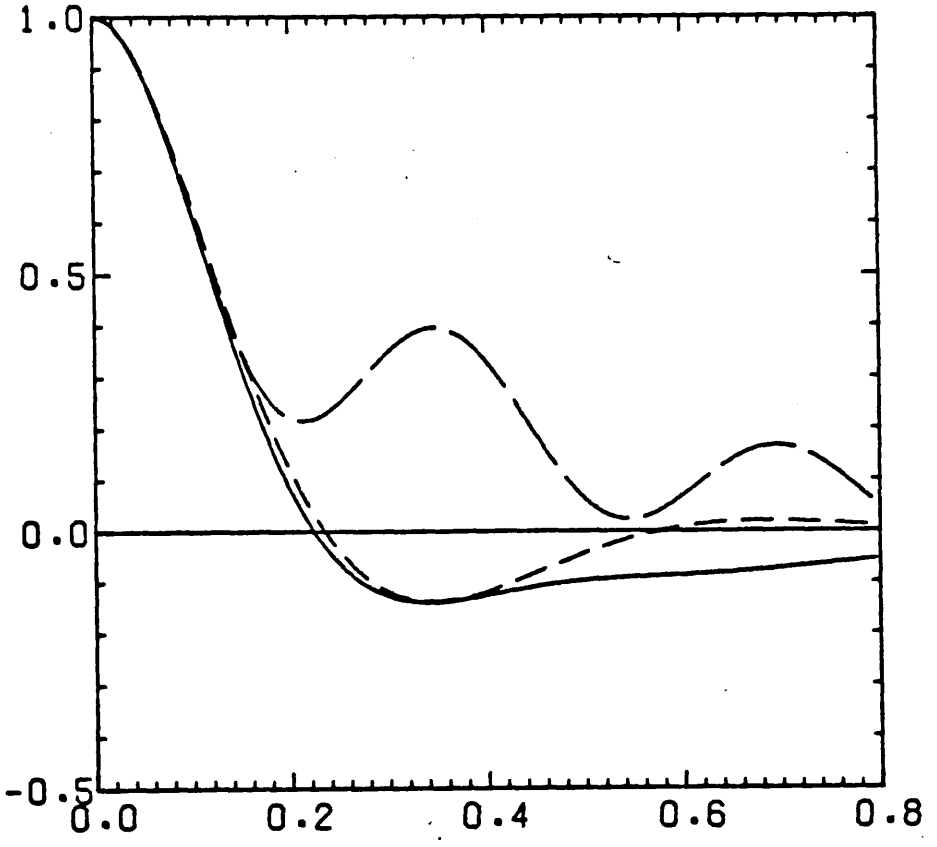

Figure (VII-21)

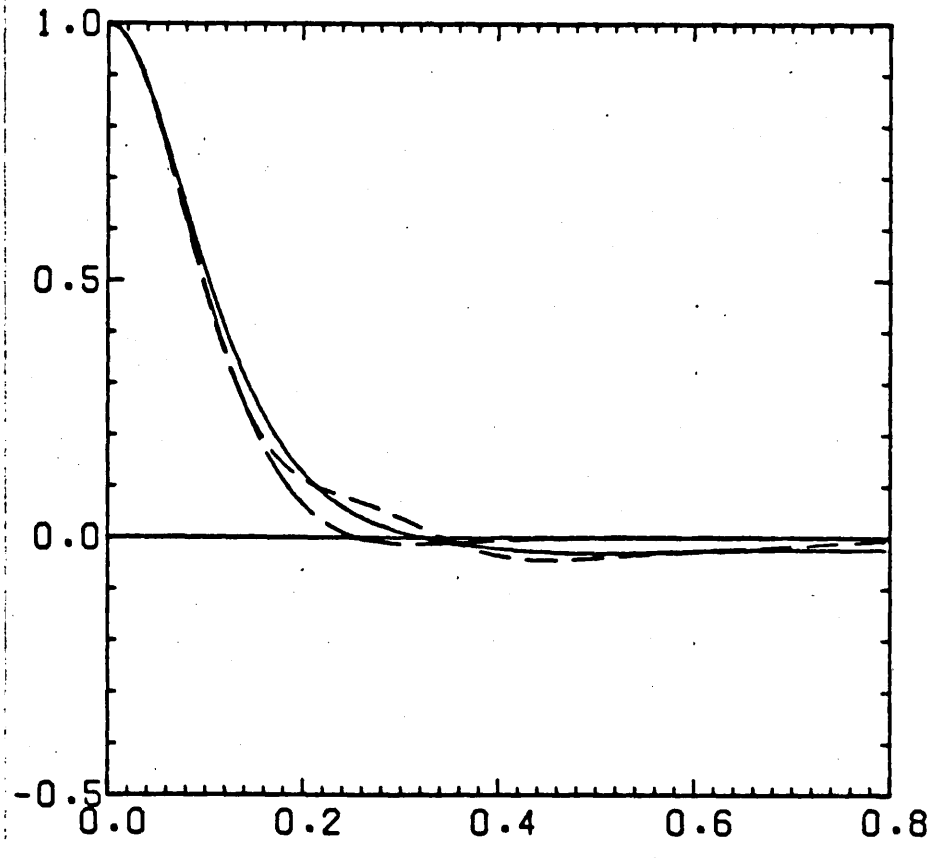

Figure (VII-22)

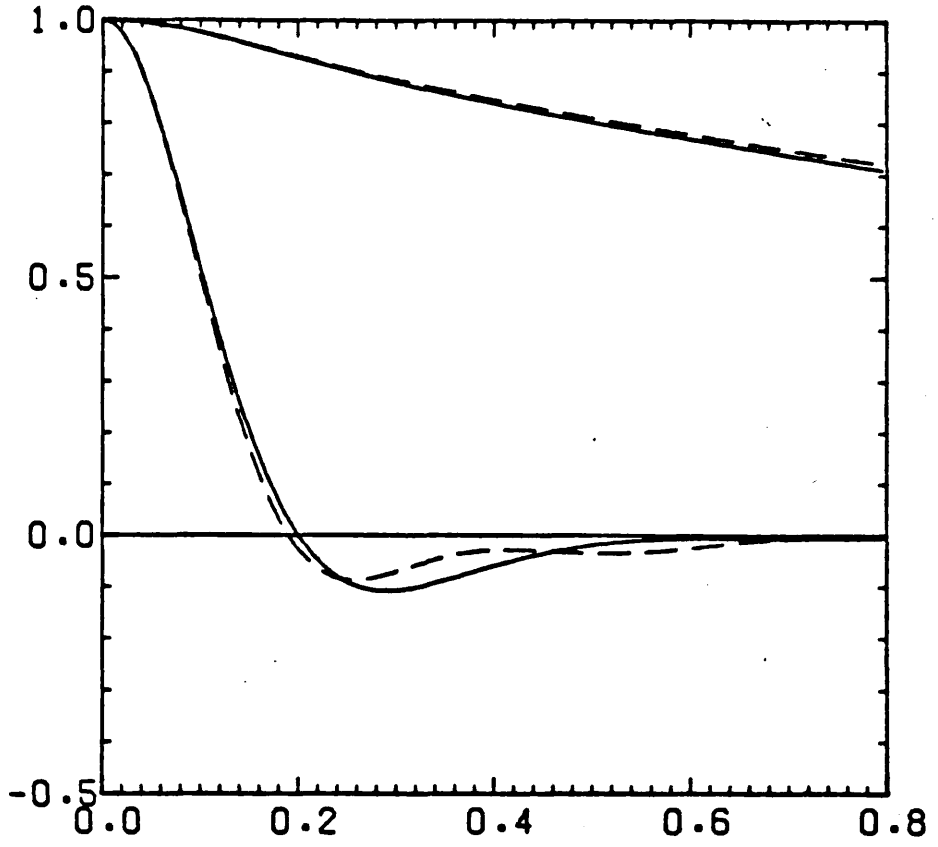

Figure (VII-23)

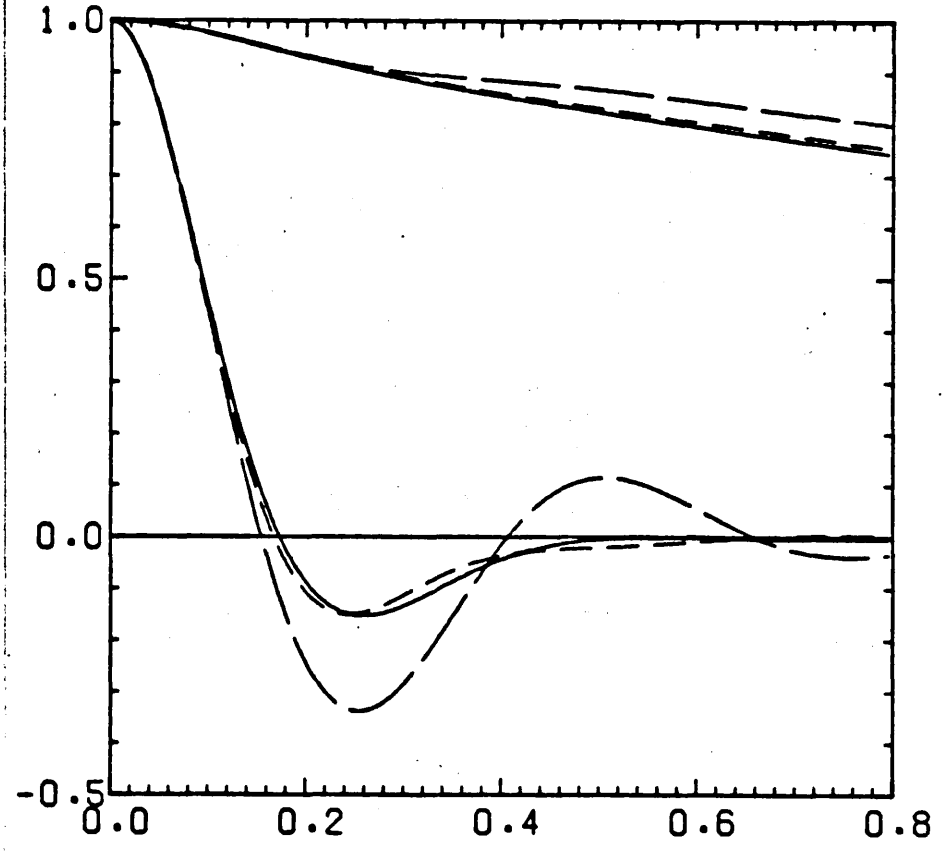

Figure (VII-24)

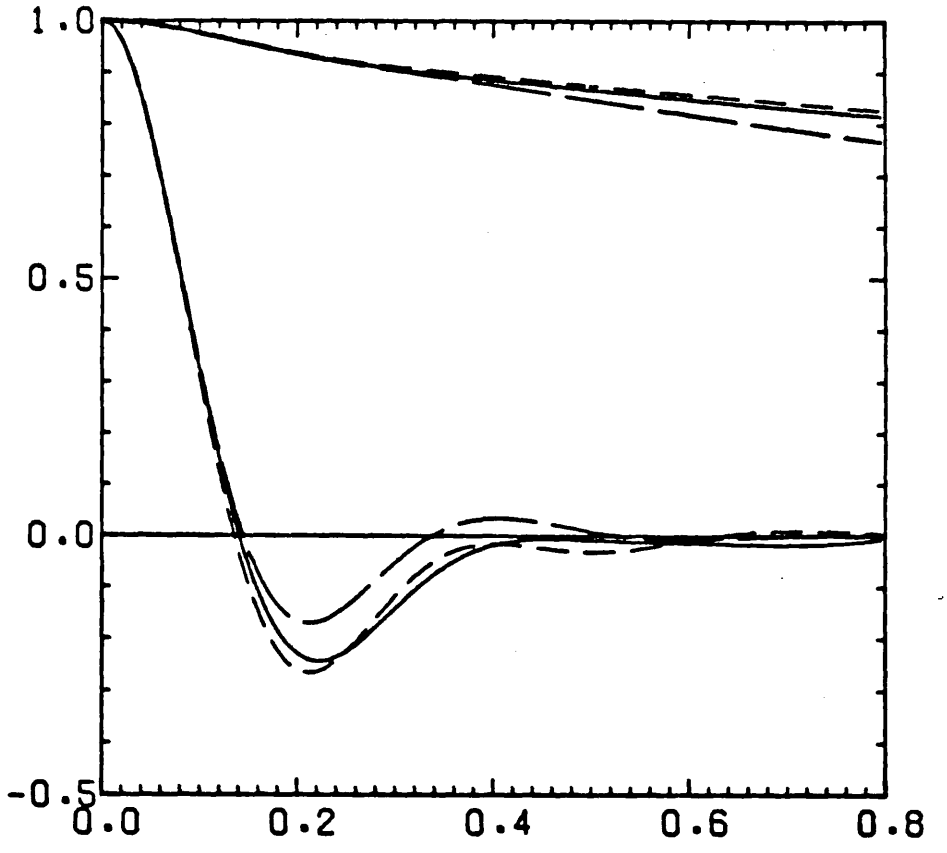

Figure (VII-25)

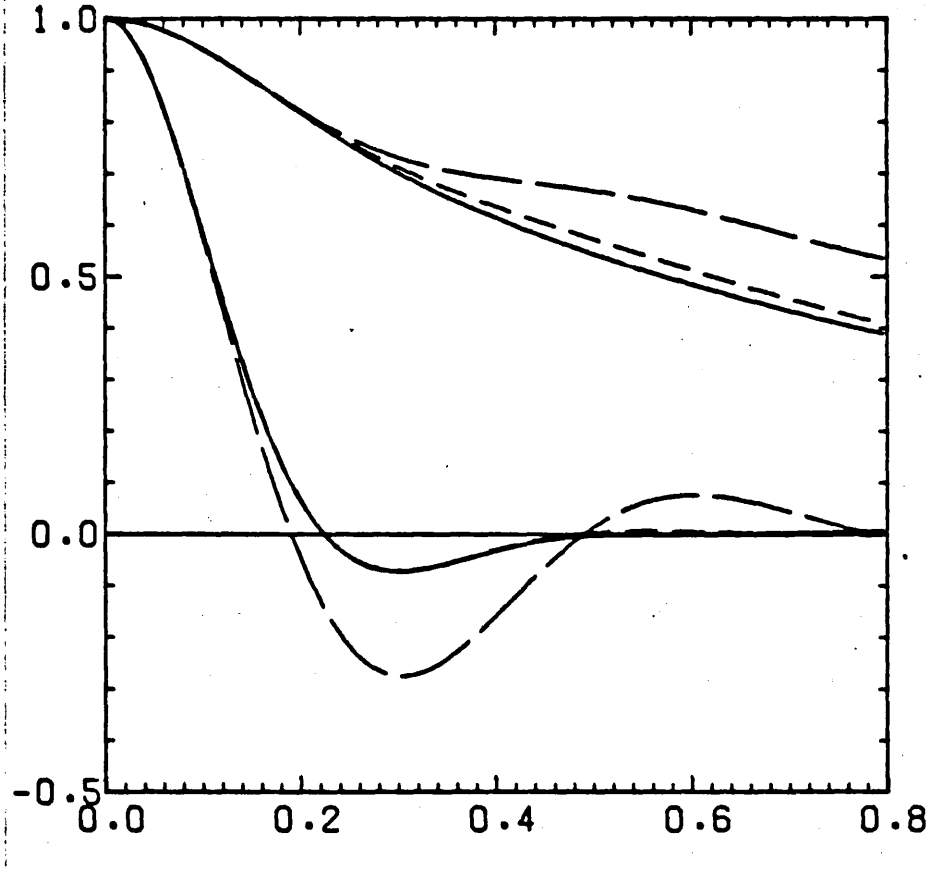

Figure (VII-26)

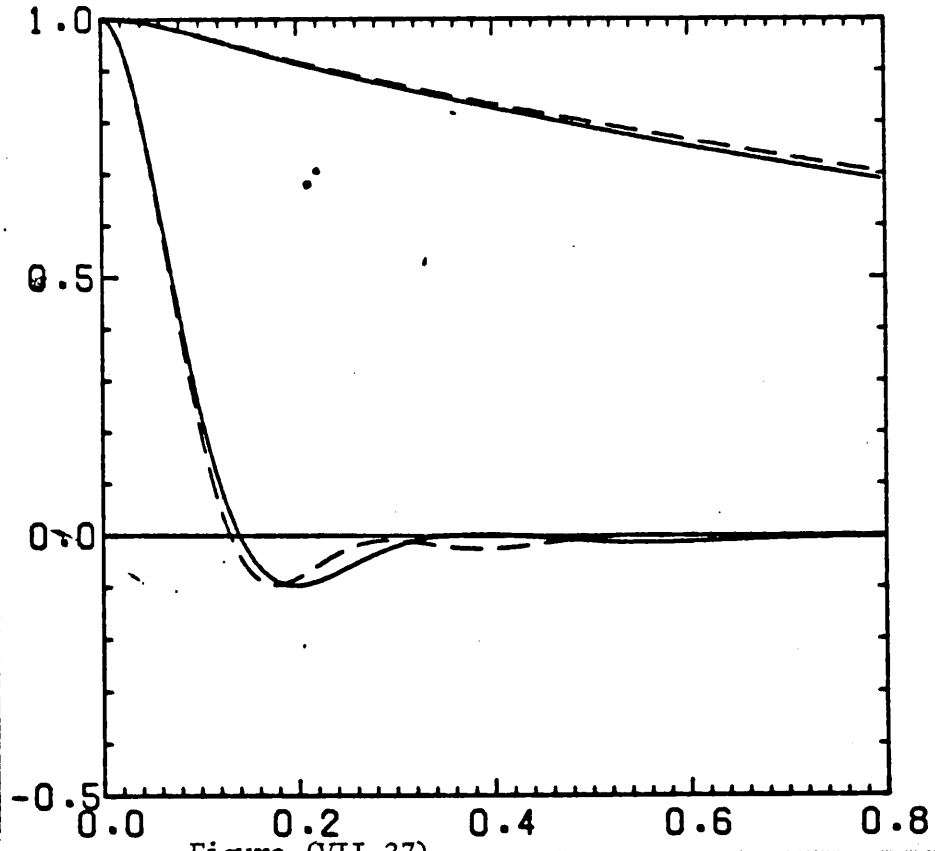

Figure (VII-27)

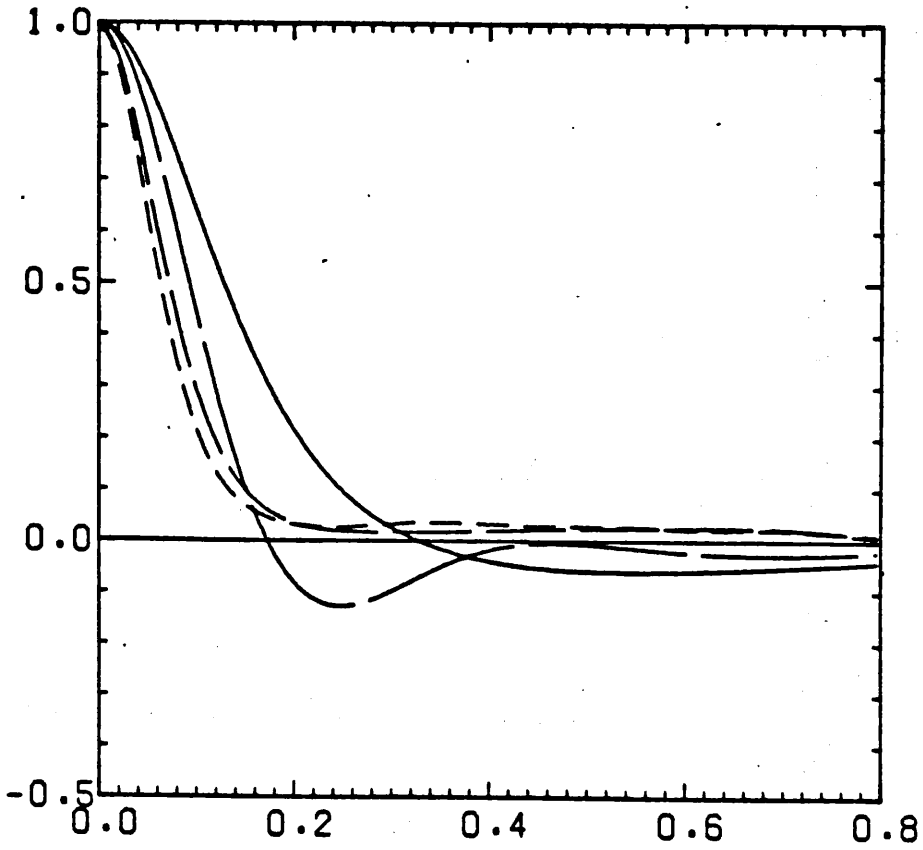

Figure (VII-28)

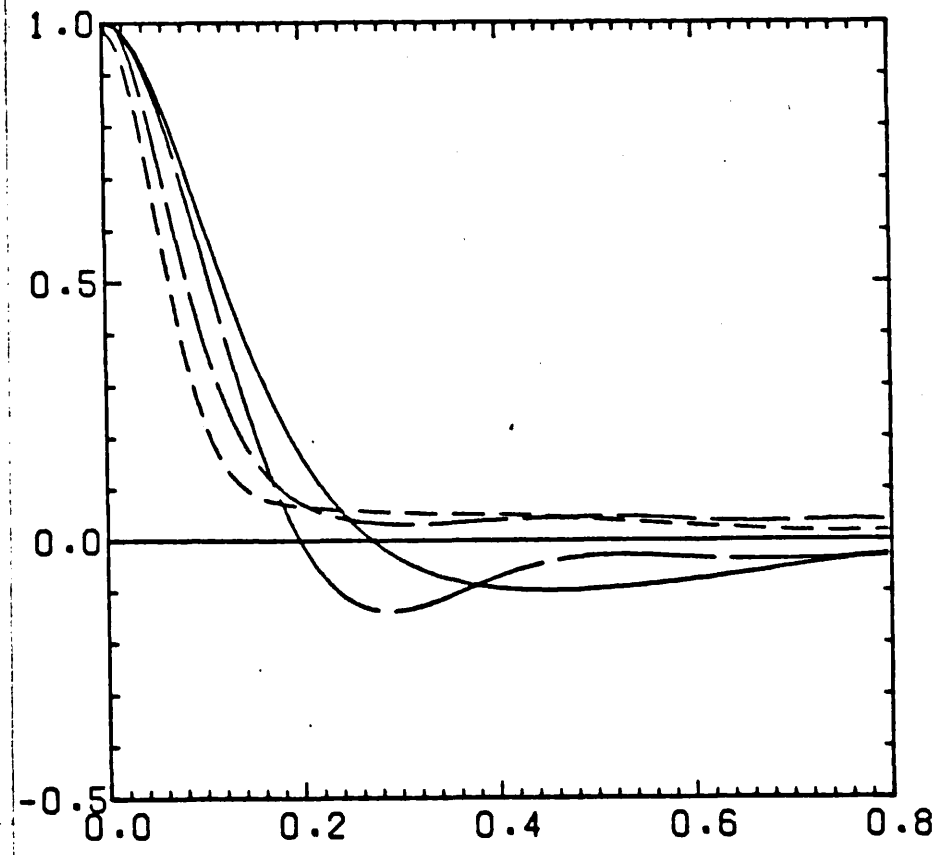

Figure (VII-29)

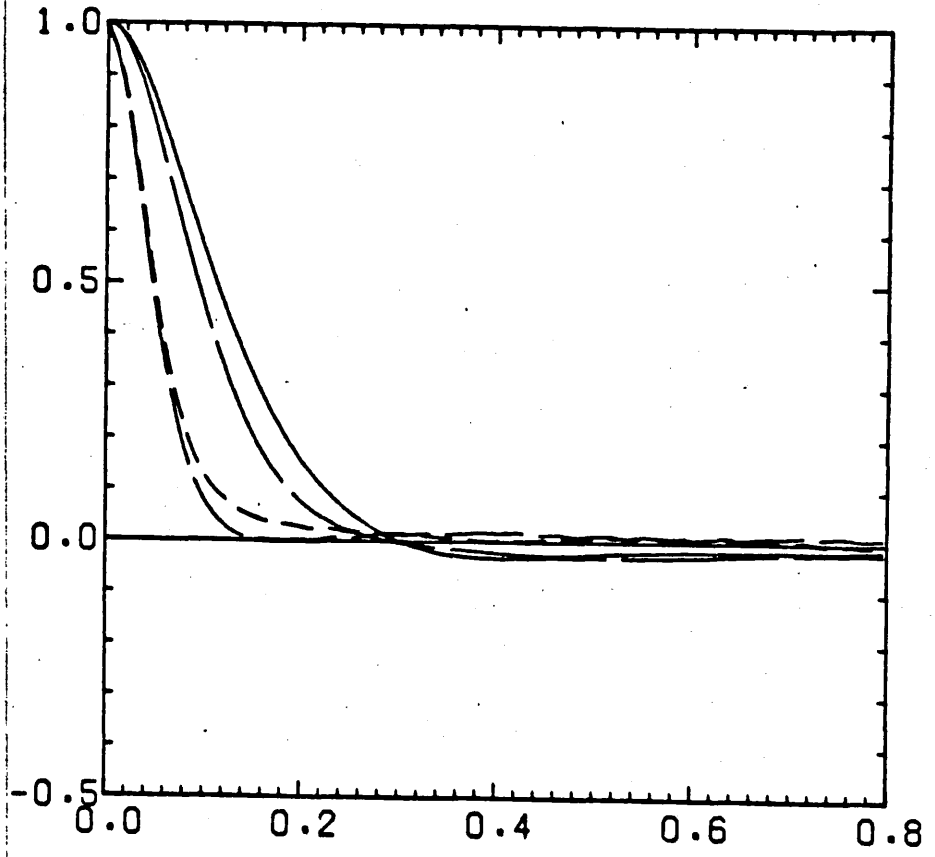

Figure (VII-30)

CHAPTER VIII.

Conclusion.

In the present study a large number of properties of the systems under investigation have been calculated. The quadrupolar interactions in these systems has been shown to make significant changes in the thermodynamic, static and dynamical properties.

In Chapter III the effect of the quadrupole on the thermodynamics was seen to produce increases in C_V and β_V for all values of the bond length, the comparison with the experimental data being improved over the two-centre Lennard-Jones only potential model, in the cases of nitrogen and carbon dioxide. The results for chlorine suggest that a quadrupole moment between $Q^* = 1.3$ and $Q^* = 2.0$ would produce the best agreement with experiment. The variation of the reduced thermodynamic quantities showed that the quadrupole produces a strongly non-linear perturbation which rapidly increases as the quadrupole becomes large. No analytic form could be found to describe this effect satisfactorily. The scaling of the thermodynamic variables using the principle of corresponding states was also discussed in the context of thermodynamic perturbation theory, using a simple model of the interaction potential. It was concluded that for quadrupolar fluids only small changes in the variables were consistent with the concept of equivalent fluids.

The static properties of these systems, investigated in Chapter IV, show qualitatively how the pair distribution functions are altered by changes in bond length and quadrupole moment. It is seen that for all values of the bond length, the effect of the quadrupole is to increase the incidence of the "T" configuration at the expense of the "Parallel" and "Cross" configurations within the constraints of packing considerations which reduce the effect at very large bond lengths. The

results of this are in the site-site distributions functions and the angular pair harmonics. Comparison with experimental data shows the shoulder on the right hand side of the first maximum of S(k) for chlorine systems is found to be a function of the quadrupole moment, going from weak, to strong, to a split peak as the quadrupole increases. However the position and magnitude of the first peak of the atom-atom distribution function seems independent of quadrupole strength.

The properties of the RISM method were studied in Chapter V both for hard-core and realistic two-centre Lennard-Jones potentials. Unfortunately it was not possible to incorporate potentials of multipolar symmetry into this method. However in the systems studied the RISM equations proved to give good first order results for the properties, but was found to have a systematic defect in the description of the angular dependence. This is probably due to the neglect of higher order terms in the method.

The dynamical properties of the quadrupolar systems, investigated in Chapter VI, shows the effects of the increased cohesiveness of the potential. This results in the onset of a more cooperative type of motion in which the molecules have a tendency to remain in a given configuration during translation and rotation by oscillation about that position. This gives rise to increased orientational correlation times, and decreases the difference between translation parallel and perpendicular to the bond vector.

The analysis of the dynamical functions performed in Chapter VII shows that the dynamics can be related to the first few moments of the function, involving quantities such as the mean square force or torque. These moments largely determine the behaviour of the function when used in the context of memory function analysis or random frequency modulation theory. The moments can then in principle be calculated directly from the static properties of the system for a given potential, provided that

it is possible to calculate the pair correlation function by some appropriate integral equation method such as RISM. Thus the prediction of the dynamical properties of a system at a given density and temperature can be made with knowledge of the interaction potential alone, provided that the pair distribution function can be calculated with sufficient accuracy.

In general the present study shows that the effect of the quadrupolar interaction is to increase the cohesiveness of the potential in such a way that particular orientations are strongly favoured. The properties of the systems are a direct result of this effect which is valid for all values of the bond length.